(2)

Advanced Optical Fiber Communication Systems

R&T Project Code: 4148130-01
ONR Status Report for the period 3/1/92 - 8/31/92
N00014-91-J-1857

Prof. Leonid Kazovsky, Principal Investigator
Optical Communications Research Laboratory
Stanford University

8-28-92

Our research is focused on three aspects of advanced optical fiber communication systems: dynamic wavelength division multiplexing (WDM) networks, linewidth-insensitive coherent optical analog links, and impact of fiber nonlinearities on optical communication systems. During the reporting period, we have been working in all three fields, as follows. In the area of WDM networks, we investigated, designed, and are currently implementing an experimental coherent WDM optical network with a throughput of 3 Gb/s/node. In the study of coherent optical analog links, we analyzed two linewidth-insensitive schemes that could overcome the impact of phase noise of semiconductor laser diodes. In the area of fiber nonlinearities, we evaluated the performance of optical WDM systems in the presence of four-wave mixing, and are analyzing the impact of stimulated Brillouin scattering on such systems. In addition, we have experimentally observed fiber-induced parasitic phase modulation, investigated its properties, and are beginning to investigate its impact on optical communication systems.

A more detailed summary of our work in the three fields is contained in the following sections.

Dynamic wavelength division multiplexing (WDM) networks

Routing and Reconfigurations Algorithms: A dynamically reconfigurable WDM optical network has the potential of achieving higher throughput, higher reliability and lower latency, when compared with a WDM optical network with fixed wavelength assignment. However, to realize such potential gains, dynamic WDM network has to employ a proper reconfiguration algorithm. This algorithm should dynamically decide on the allocation of channels based on the communication needs of the stations. Ideally, this should be a distributed algorithm (i.e., without central control) with low overhead.

DISCLAIMER NOTICE

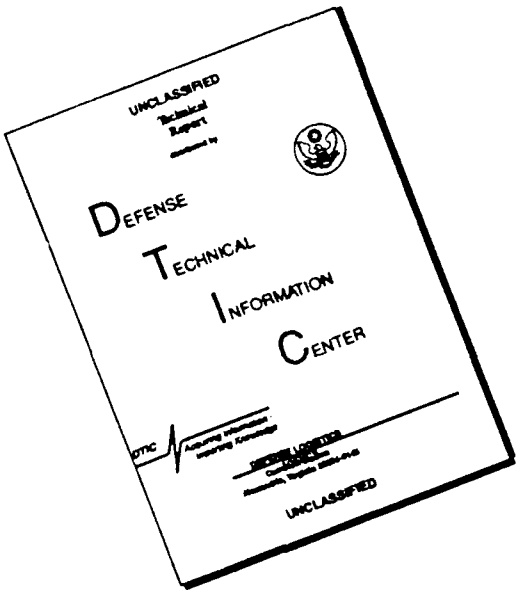

THIS DOCUMENT IS BEST QUALITY AVAILABLE. THE COPY FURNISHED TO DTIC CONTAINED A SIGNIFICANT NUMBER OF PAGES WHICH DO NOT REPRODUCE LEGIBLY.

We have formulated an optimum routing/reconfiguration algorithm as a non-linear integer programming problem and devised strategies to obtain approximate solutions to this problem. We are now adapting the algorithm to operate dynamically in the network, as requests are placed and terminate.

STARNET: An FDDI-Compatible WDM Local-Area Network: We proposed and investigated STARNET - a wavelength division multiplexed (WDM) optical broadband local area network based on a physical star topology. Over a single physical network, STARNET offers all users both a 125 Mb/s packet network and a high-speed (up to 3 Gb/s) circuit interconnect. Based on these two data transport facilities, several topological and protocol solutions are available to the users. As a result, STARNET supports traffic of widely different bandwidth and continuity characteristics. PSK modulation is used for data transmission over the high-speed circuit-switched network. The 125 Mb/s packet network is based on low modulation depth ASK modulation on top of the PSK modulated high-speed channel. Since one of the goals is to interface workstations over the STARNET, we have chosen the FDDI standard as the mode of operation over the ASK packet switched network. Figure 1 shows the logical topology of the STARNET architecture and Figure 2 is a more detailed block-diagram of the actual implementation that is currently under construction in our lab.

We have completed the construction and characterization of one high-speed receiver. We have been able to attain a bit error rate (BER) of 10^{-9} at a data rate of 2.488 Gb/s with a -38 dBm receiver sensitivity. We have also completed the construction and characterization of an ASK receiver. We have obtained a BER of 10^{-9} at a data rate of 125 Mb/s with a -49 dBm sensitivity. The increased sensitivity of the ASK receiver is primarily attributable to the lower data rate.

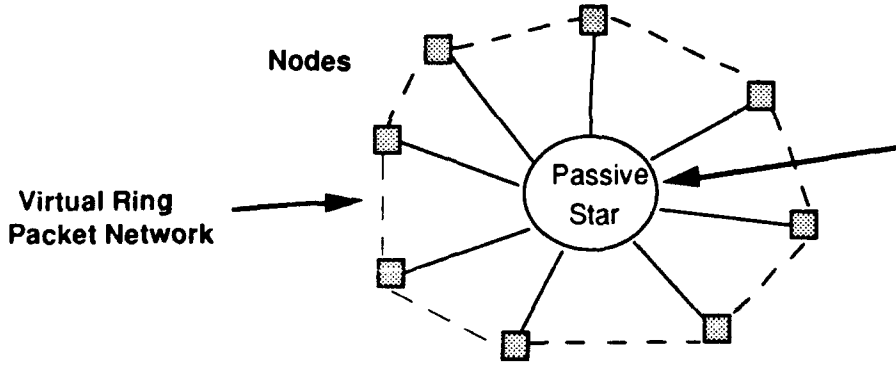

Figure 1. STARNET network topology.

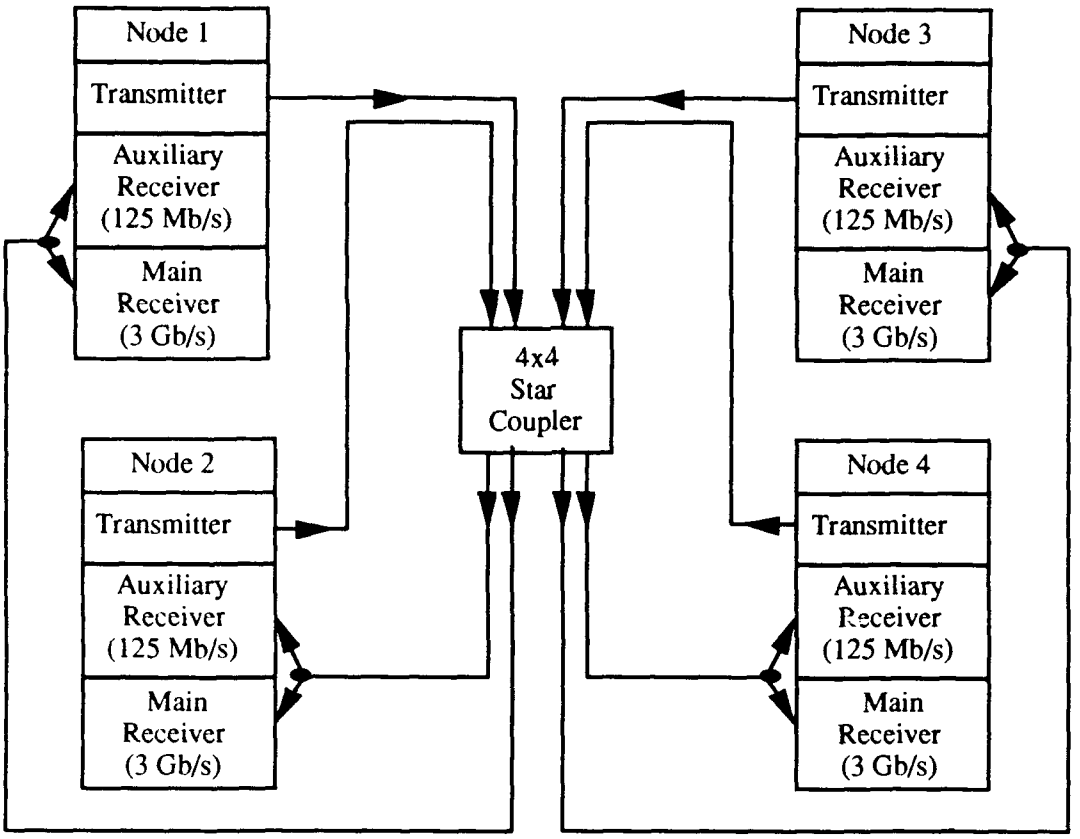

Figure 2. A block diagram of the 4 node STARNET experiment.

The STARNET ASK transmitter and receiver replace standard FDDI transmitter/receiver hardware in two DECstation 5000/240 workstations. Therefore, a two-node FDDI ring is formed by the two workstations with one FDDI link formed by the STARNET hardware , and the other link formed by the standard FDDI interconnect. We have written software to send pseudo random data, or large image files, using either the TCP or the UDP protocol over the FDDI link while measuring the BER at the FDDI receiver. Simultaneously, we transmit 2.488 Gb/s data over the PSK link and measure the BER at the PSK receiver. With this experimental setup we are examining the impact of the ASK modulated data on the performance of the PSK receiver and vice versa. In addition, we are investigating the optimum modulation depth/transmitter power that simultaneously optimizes both the ASK and PSK receiver BER's.

Optical Network Performance Evaluations: In the area of network performance, we have run simulations comparing the network throughput of an eight node extended STARNET (2 high-speed receivers per node) versus an eight node centralized active packet switch. The simulations compare the performance in virtual circuit operation of

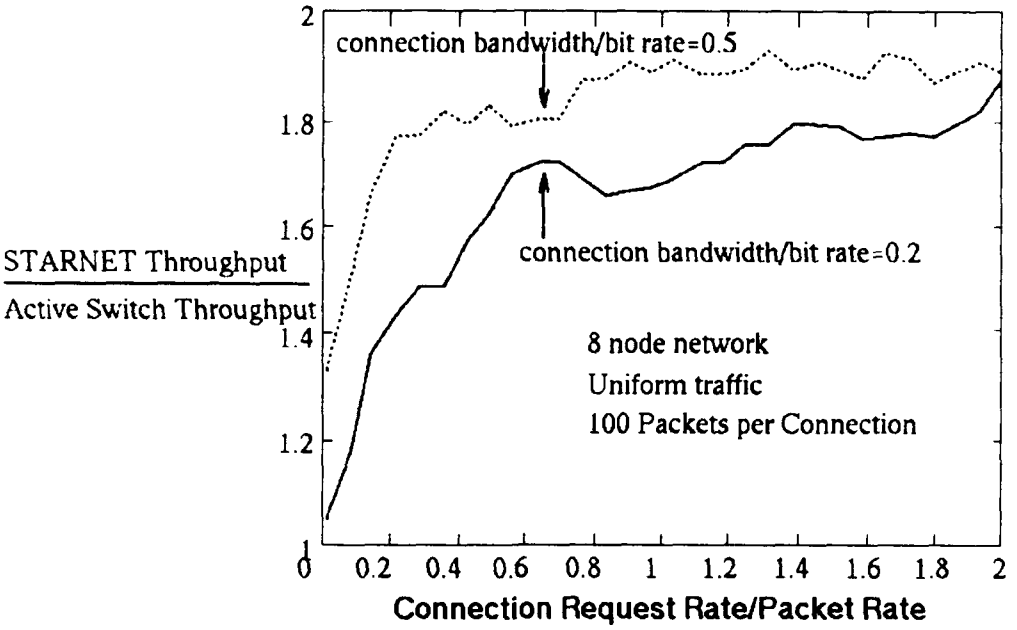

Figure 3. Network throughput comparison: STARNET vs. centralized switch.

the two network architectures under uniform and centralized destination traffic for high and low bandwidth connections for short and long duration connections. Uniform traffic is applicable in the case of peer-to-peer traffic. Centralized traffic is applicable in the case of a file server and its satellites. An example of low bandwidth long duration traffic is real-time voice; high bandwidth long duration traffic, real-time video. Simulation results such as those shown in Figure 3 indicate that for an eight node network the extended STARNET architecture provides a performance advantage over the centralized active switch. The performance advantage is greatest under uniform destination, high bandwidth traffic.

Polarization Modulations: We have also been working on a theoretical analysis and an experimental demonstration of digital transmission based on a coherent system utilizing polarization modulation (POLSK - POLarization Shift Keying).

Traditional transmission systems use either amplitude, phase or frequency as the modulating parameter to encode data. POLSK systems, instead, use the state of polarization of the lightwave carrier.

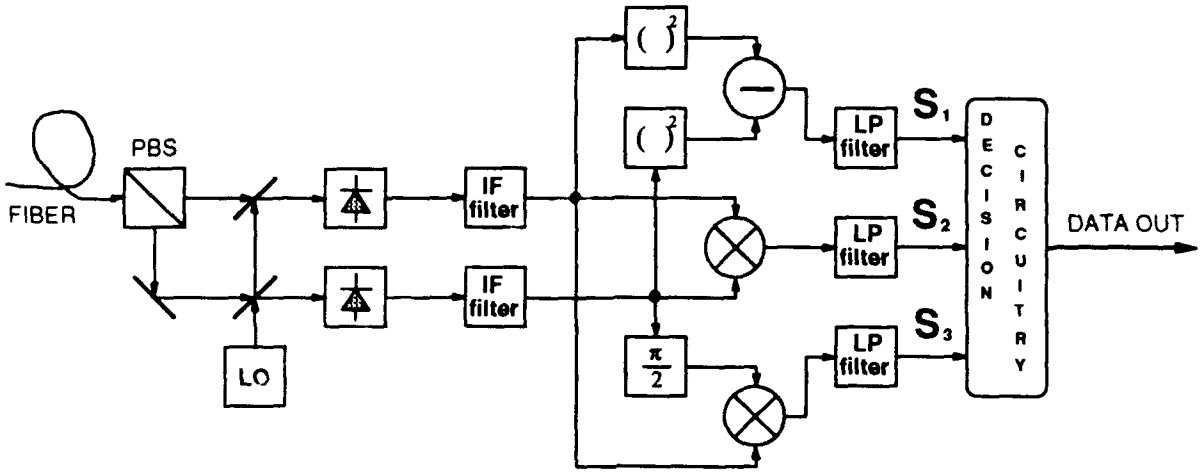

Figure 4. A typical block diagram of a POLSK receiver.

This new approach has numerous potential advantages. POLSK detection is insensitive to the laser linewidth (phase noise); polarization fluctuations along the fiber can be electronically suppressed in the decision baseband circuitry in the receiver; the power spectrum of POLSK signals is more compact than that of FSK or even PSK; multilevel transmission is feasible, allowing for significant optical and electrical bandwidth reduction, at constant bit rates.

As for sensitivity, an extensive theoretical analysis, mostly carried out by some of the investigators involved in this experiment, is available in the literature and shows that POLSK systems have a better performance than ASK and single-filter FSK binary coherent schemes (by approximately 3 dB). The sensitivity gain becomes more remarkable when multilevel modulation is addressed.

A typical block diagram of a POLSK receiver is shown in Figure 4. The receiver extracts information on the state of polarization of the incoming lightwave by analogically computing the Stokes Parameters. The Stokes Parameters are one of the possible set of parameters describing the state of polarization of a lightwave. They were found to be the most convenient means of accomplishing POLSK demodulation.

A $LiNbO_3$ Polarization modulator was built at Ericsson Telecom Research AB in Sweden specifically for this experiment (Dr. Bo Lagerstrom). Two monolithically integrated balanced optical photoreceivers are now being built at AT&T Bell Labs and

will be used in the set-up (Dr. Chandrasekhar). The laser sources used in the experiment come from AT&T Bell Labs (Dr. Bernard Glance and Dr. Uzi Koren).

Linewidth-insensitive coherent optical analog links

We continued both theoretical and experimental investigations of linewidth-insensitive coherent optical analog links.

Theoretical Work

We analyzed the signal-to-noise ratio (SNR) and the dynamic range of the amplitude-modulated (AM) WIRNA (which stands for WIdeband filter-Rectifier-NArrowband filter, and refers to the signal processing at the receiver) local reference system shown in Figure 5 and the frequency-modulated (FM) embedded reference system shown in Figure 6. Furthermore, we investigated the impact of the IF bandwidth, phase noise, shot noise, thermal noise, laser relative intensity noise (RIN) and device nonlinearities on the link performance.

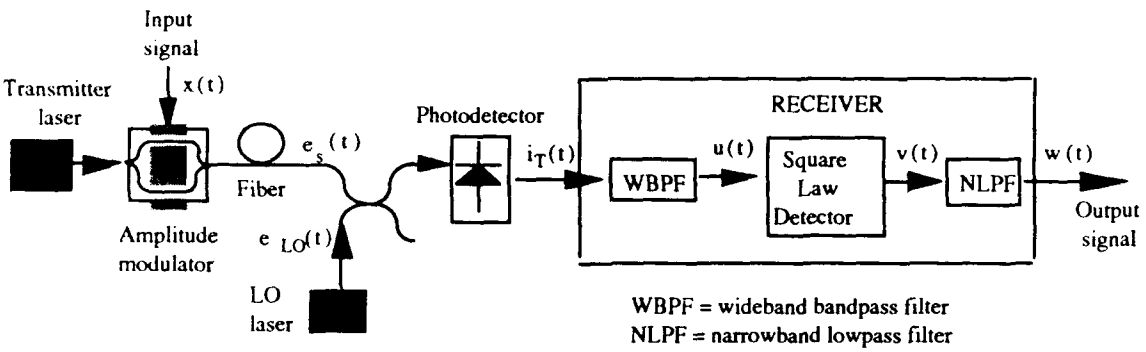

Figure 5. Block diagram of the AM-WIRNA heterodyne link.

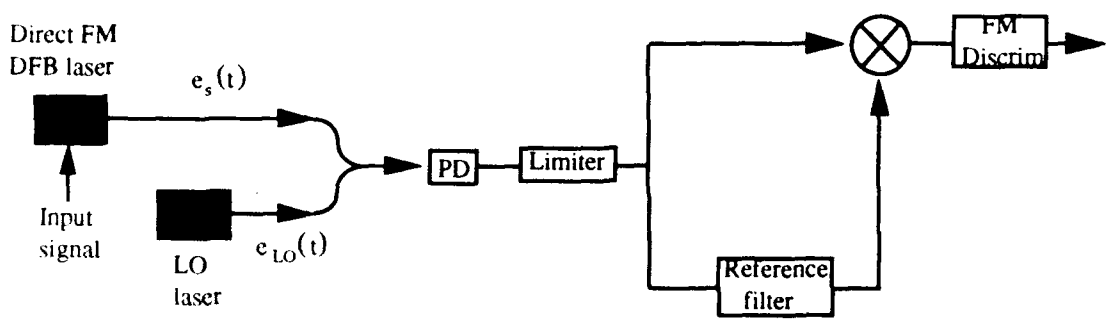

Figure 6. Embedded reference FM system.

AM Systems: For the AM-WIRNA coherent link, our analysis shows that there exists an optimum IF bandwidth which gives the best system performance. The optimum bandwidth is a strong function of the received optical signal power and the total laser linewidth. With the proper selection of the IF bandwidth (about 40 times or more the signal bandwidth), the AM-WIRNA receiver can be made insensitive to laser linewidths up to 100 MHz, with an SNR penalty of less than 0.5 dB.

Figure 7 shows the output SNR versus the received optical power P_S for the direct detection and for the AM-WIRNA heterodyne links. Inspection of Figure 7 shows that for received powers less than 1 mW (which applies to most semiconductor lasers used for distribution systems in CATV and long distance transmission of analog signals), the AM-WIRNA system has a better SNR (and therefore, a better dynamic range) than the direct detection system. For higher power levels, the performance of the AM-WIRNA coherent link is very similar to that of the direct detection system, with the difference being less than 3 dB for properly designed systems. The single photodiode coherent AM system was found to be highly susceptible to laser RIN. A balanced receiver improves the dynamic range by some 3 dB.

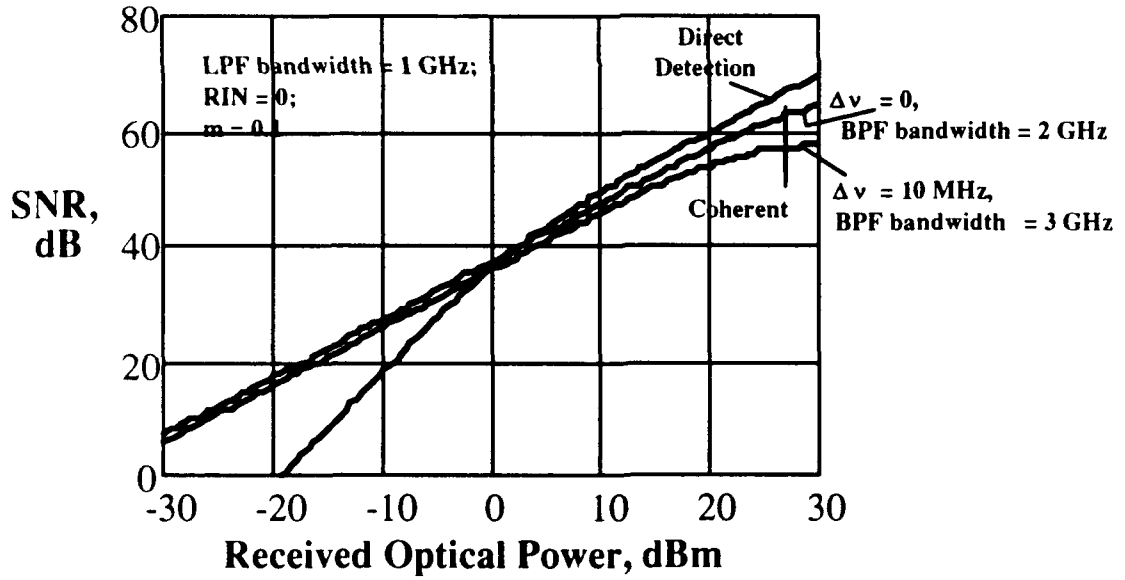

Figure 7. The SNR versus the received optical power for the AM-WIRNA receiver; r = 50Ω, R = 0.8 A/W, T = 300K, and P_{LO} = 30 dBm.

FM Systems: We have found that *under ideal conditions* coherent FM links have the potential to increase the SNR and the dynamic range by more than 10 dB as compared to direct detection and coherent AM links. Through frequency modulation, substantial

suppression of additive white Gaussian noise and RIN can be achieved. However, the FM link is sensitive to laser linewidth and requires elaborate phase noise cancellation techniques when semiconductor lasers are used. We are now in the process of investigating the performance of FM links with a novel phase noise cancellation circuit, and evaluating the linearity of the FM characteristics of semiconductor lasers and the FM receiver.

Experimental Work

We investigated the FM behavior of a two-section distributed Bragg reflector (DBR) laser. Dependence of the lasing wavelength on the Bragg reflector section current has been measured. Due to the presence of mode hops, the maximum usable frequency deviation is 18 GHz with the particular laser used in our experiment. From the theoretical results and the DBR laser experiments, we evaluated the components' requirements for the experimental AM-WIRNA heterodyne system and the FM embedded reference system we will investigate.

Impact of fiber nonlinearities on optical communication systems

Four-Wave Mixing

We evaluated theoretically the performance of optical WDM systems in the presence of four-wave mixing (FWM). The nonlinear FWM process limits the maximum optical power that can be launched into fibers, and the shot noise limits the minimum power at the receiver. We have evaluated the link budget defined as the ratio of the maximum transmitter power to the minimum optical power at the receiver, and derived the maximum transmission distance.

We have also proposed and investigated FWM noise reduction method using Manchester coding. The performance of NRZ (non-return-to-zero) and Manchester coding in both ASK (amplitude-shift keying) and DPSK (differential phase-shift keying) modulated systems was evaluated. The effect of fiber dispersion on FWM noise was also investigated. Our analysis shows that Manchester coding improves both ASK and DPSK systems, and that systems utilizing dispersion-shifted fiber are more seriously impaired by FWM noise than those utilizing nondispersion-shifted fibers.

Figure 8 shows the bit error rate versus transmitter power for a 16-channel ASK system with dispersion-shifted fiber. Channel separation for this particular system is 10 GHz. Bit rate is 1 Gb/s. Inspection of Figure 8 reveals that BER increases rapidly if the transmitter power exceeds a threshold power of about 1 mW. Figure 8(a) shows the results for NRZ coded system; Figure 8(b) shows the results for Manchester coded system. Figure 9 shows similar results for a 16-channel DPSK system with dispersion-

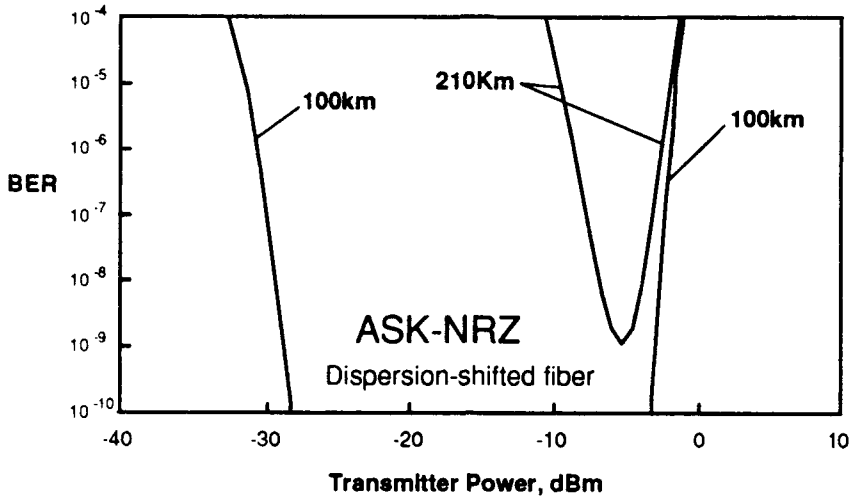

(a) ASK system with NRZ coding

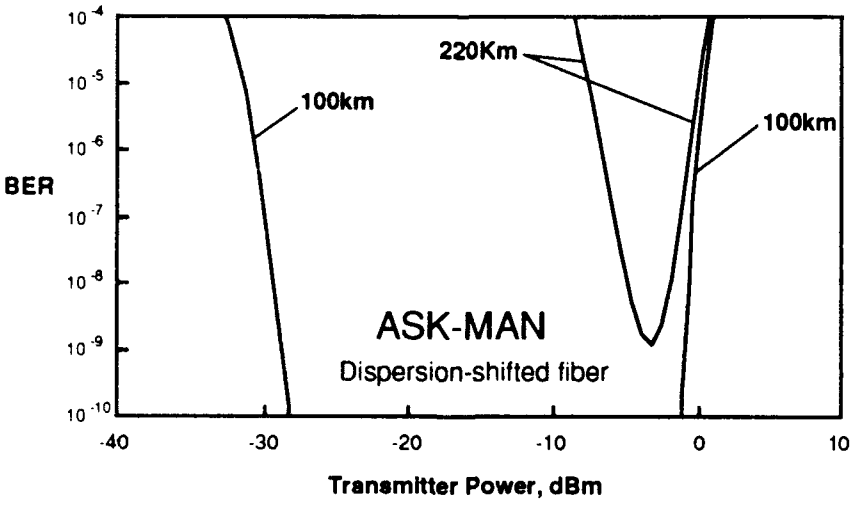

(b) ASK system with Manchester coding

Figure 8. Bit error rate of a 16-channel ASK system impaired by FWM.

shifted fiber. Analysis of Figures 8 and 9 shows that Manchester coding can suppress FWM by 2 dB, and extend the maximum transmission distance by about 10 km for both ASK and DPSK systems.

Fig. 10 shows the calculated maximum transmission distance of both ASK and DPSK

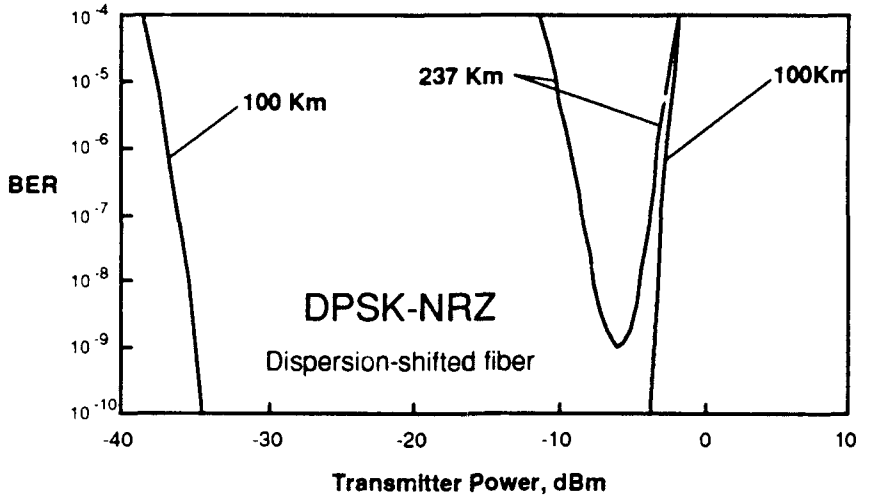

(a) DPSK system with NRZ coding

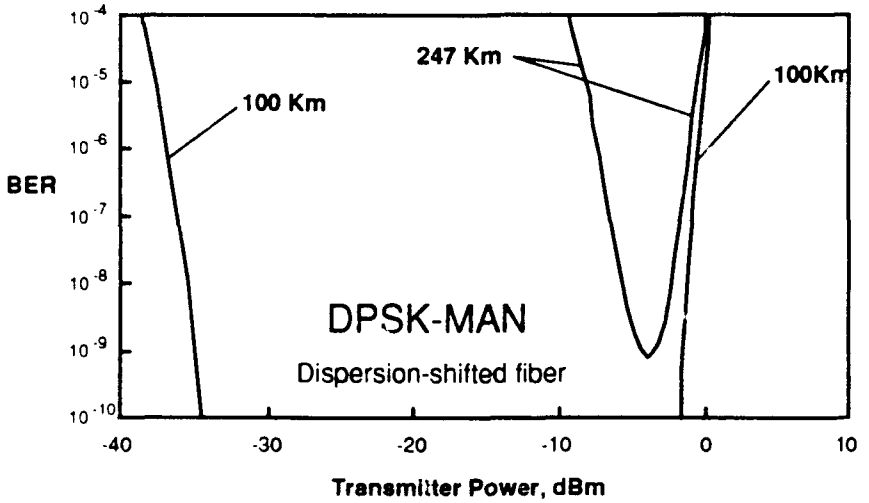

(b) DPSK system with Manchester coding

Figure 9. Bit error rate of a 16-channel DPSK system impaired by FWM.

systems using NRZ and/or Manchester codes. The results show that DPSK systems are less sensitive to FWM than ASK systems, and that systems employing dispersion-shifted fiber are inferior to those employing conventional single-mode fiber.

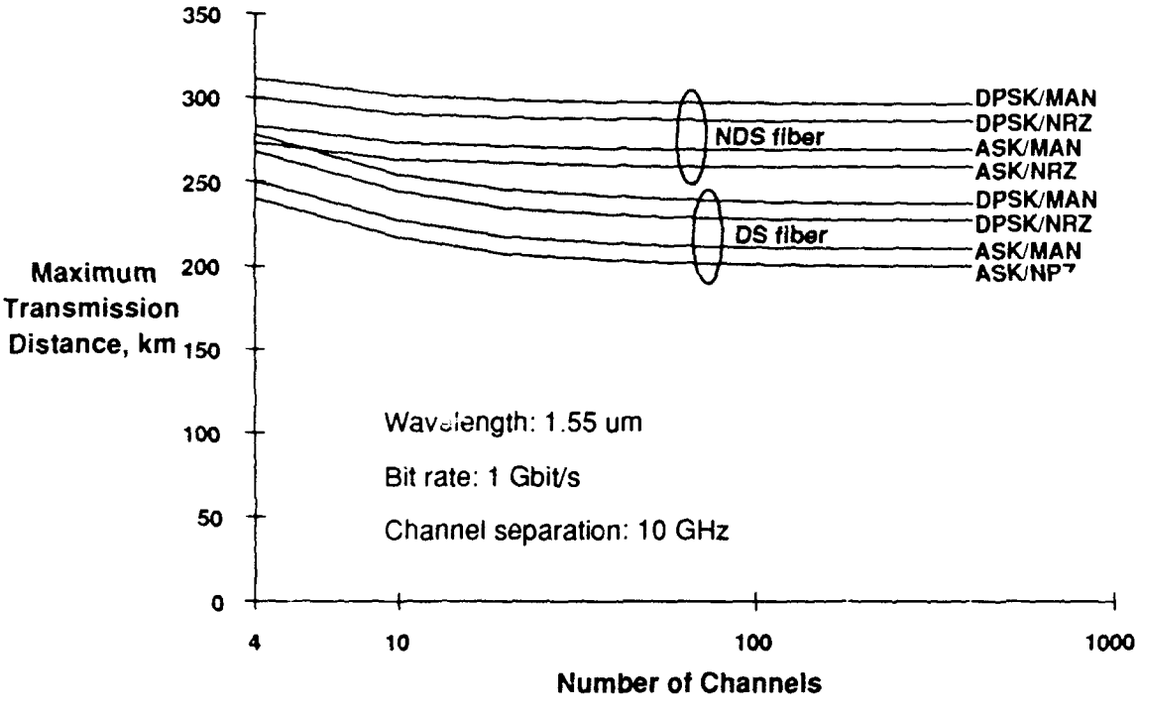

Figure 10. Maximum transmission distance of DPSK and ASK systems impaired by FWM.

Stimulated Brillouin Scattering

Another potentially limiting nonlinear effect is stimulated Brillouin scattering (SBS). SBS process tends to reflect back the launched optical power exceeding a certain threshold, and also induces excess noise in the transmitted signals. We are currently analyzing the impact of SBS process theoretically and experimentally. Figure 11 shows the experimental setup we used to measure the characteristics of transmitted signal under Brillouin scattering.

Two Nd:YAG lasers with very narrow linewidth are used in this experiment. By heterodyning the transmitted or back-scattered signal with the second laser, we can characterize the extra noise induced by Brillouin scattering effect.

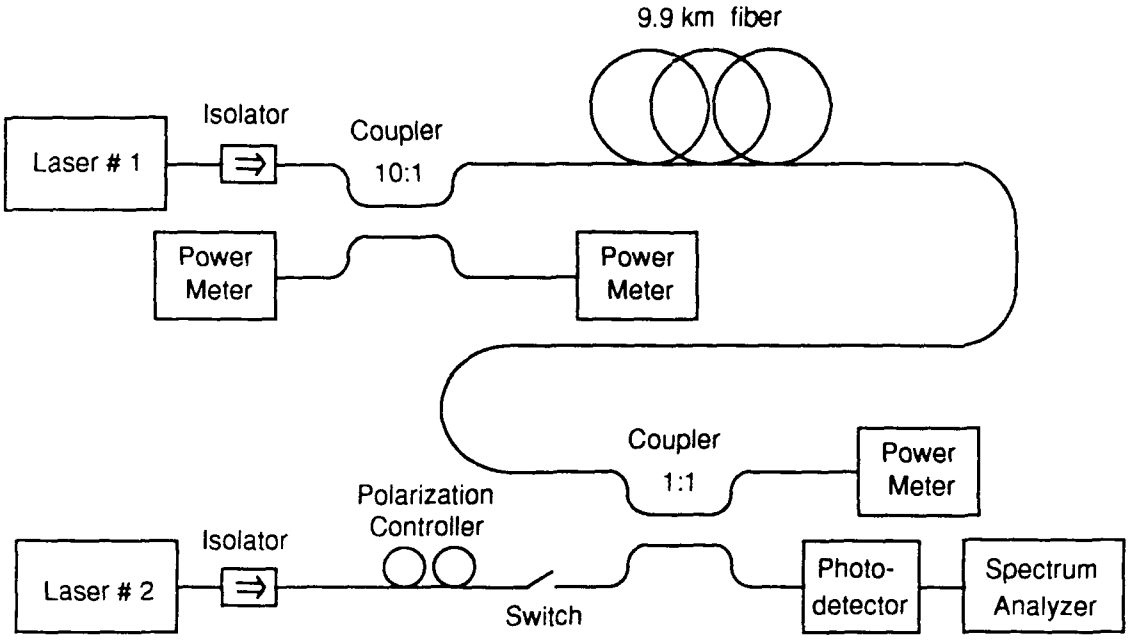

Figure 11. Experimental setup used to characterize signal under Brillouin scattering.

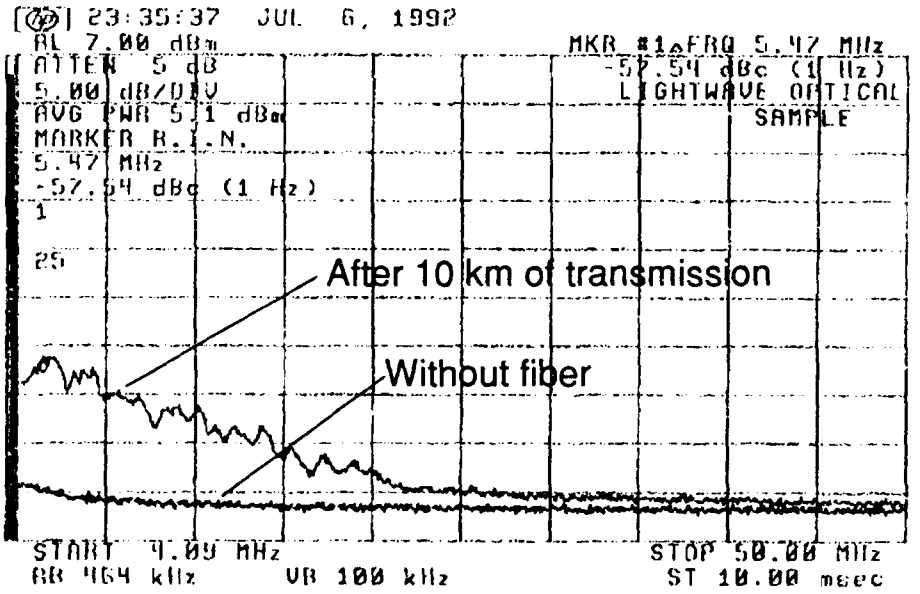

Figure 12. Spectrum of the transmitted light intensity.

The transmitted light has been found to be impaired by relaxation oscillation of stimulated Brillouin scattering once the launched power exceeded Brillouin threshold. As

shown in Figure 12, this effect causes low frequency intensity fluctuation of the transmitted signal. The influence of this intensity fluctuation on optical communication systems is currently analyzed.

Fiber-Induced Parasitic Phase Modulation

We experimentally observed a phase modulation caused by thermal acoustic vibrations in the fiber. The acoustic wave excited by thermal vibrations modulates the phase of the light propagating along the fiber. The acoustic wave in the fiber has several discrete modes with different resonant frequency associated with each mode. More than 30 spectral lines have been observed in the phase modulated spectrum, as shown in Figure 13. Spectral lines caused by the phase modulation are about 30 dB lower than the main spectral component, corresponding to a phase modulation index of 10^{-3} for 10 km of propagation. The strength of the effect grows proportionally to the square root of propagation distance.

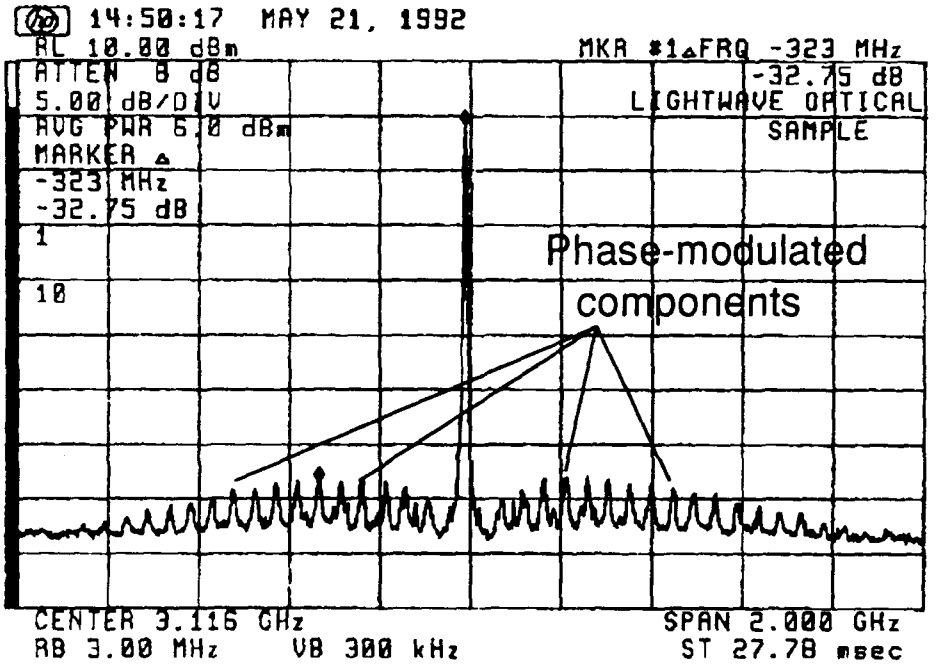

Figure 13. Heterodyned spectrum of the transmitted light modulated by thermal acoustic waves.

Based on these experimental observations, we performed a preliminary theoretical analysis of the impact of parasitic fiber-induced phase modulation on DPSK optical communication systems. Our results show that the performance of an optical DPSK

system can be impaired by thermal acoustic modulation. Figure 14 shows the calculated BER floor of a 1 Gb/s DPSK receiver versus laser linewidth for different fiber lengths in the presence of thermal acoustic phase noise. Inspection of Figure 13 reveals that the BER floor increases about 400 times at the transmission distance of 500 km when the laser linewidth is 10 MHz.

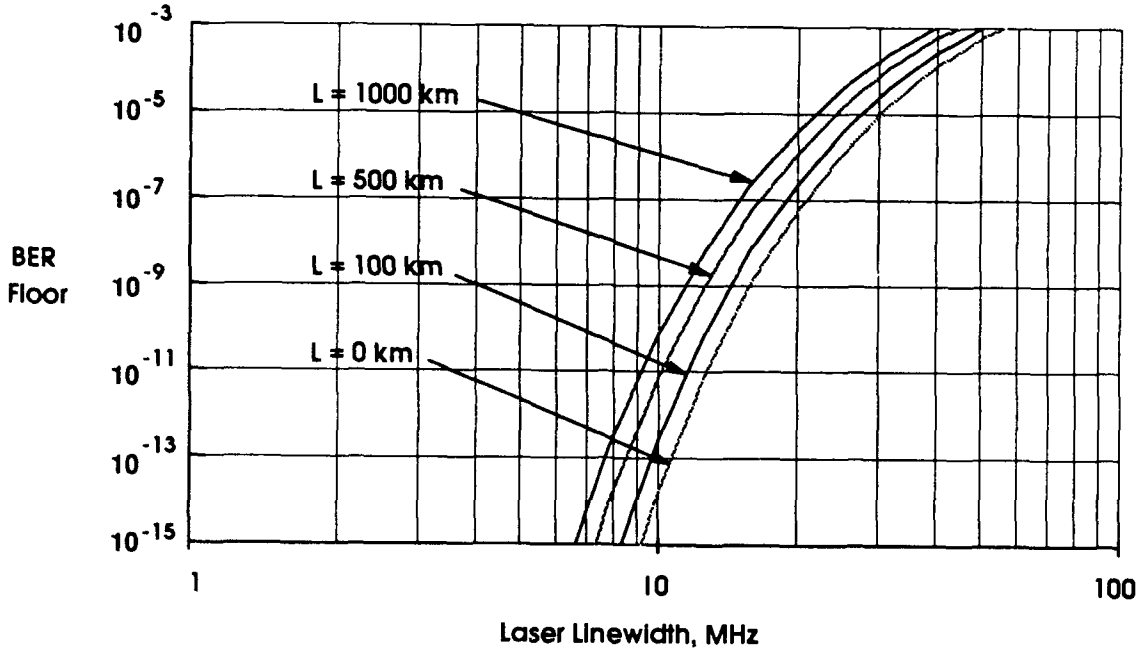

Figure 14. Calculated BER floor of a 1 Gb/s DPSK heterodyne receiver. Both laser phase noise and fiber-induced parasitic phase noise are included in our analysis.

IMPACT OF FINITE FREQUENCY DEVIATION ON THE PERFORMANCE OF DUAL-FILTER HETERODYNE FSK LIGHTWAVE SYSTEMS

Ozan K. Tonguz, *Member, IEEE,* and M. Okan Tanrikulu, *Student Member, IEEE*

Photonics Research Center

Department of Electrical and Computer Engineering

State University of New York at Buffalo

Buffalo, NY 14260

USA

Leonid G. Kazovsky[1], *Fellow, IEEE*

Department of Electrical Engineering

Stanford University

Stanford, CA 94305-4055

USA

[1]The work of Leonid Kazovsky was partially supported by ONR under grant number N00014-91-J-1857.

Abstract

A detailed theoretical analysis is given for the impact of finite frequency deviation on the sensitivity of dual-filter heterodyne Frequency Shift Keying (FSK) lightwave systems. Our analysis provides closed-form signal-to-noise ratio (SNR) results for estimating the bit-error-ratio (BER) performance of the system. These closed-form results provide an insight into the impact of finite frequency deviation $2\Delta f_d$, laser linewidth $\Delta\nu$, bit rate R_b, and IF filter bandwidths on the system performance. It is shown that there is a well-defined relationship between the choice of frequency deviation and the tolerable amount of laser phase noise. When there is no phase noise, a frequency deviation of $2\Delta f_d = 0.72R_b$ is sufficient for 1 dB sensitivity penalty with respect to infinite frequency deviation case; whereas for a linewidth of $\Delta\nu = 0.50R_b$ the required frequency deviation increases to $2\Delta f_d = 3.42R_b$ for the same sensitivity penalty. The sensitivity degradation can be very severe for a fixed linewidth as the frequency deviation gets smaller: for a linewidth of 20% the sensitivity penalty is only 0.54 dB when the frequency deviation is infinite whereas it is 3.48 dB when the frequency deviation is $2\Delta f_d = R_b$. We also quantify the impact of finite frequency deviation on optimum IF filter bandwidths. For a fixed linewidth, the optimum IF filter bandwidth decreases as frequency deviation becomes smaller: for $\Delta\nu = 0.5R_b$ the optimum IF filter bandwidth reduces from $7R_b$ to $3R_b$ when $2\Delta f_d$ reduces from very large values to $3R_b$.

I. INTRODUCTION

The FSK heterodyne dual filter and single filter detection systems are examples of asynchronous lightwave systems, whereby a relatively large laser diode (LD) spectral spread can be tolerated. That makes the use of conventional DFB LD's possible which in turn is important for achieving a simple and stable system [1]-[8]. The dual filter detection system is particularly attractive because it offers a 3-dB higher receiver sensitivity than the single filter detection system [1]. The ideal performance of dual filter heterodyne FSK lightwave systems were previously studied by several authors assuming ideal conditions for the intermediate frequency (IF) and the frequency deviation between the two frequencies of data transmission [2], [9], [10].

In particular, in [2], [9] and [10] the sensitivity degradation due to laser phase noise and shot noise was studied assuming that the IF and the frequency separation between the two tones are infinitely large. In practical systems, however, these assumptions are not valid [1], [3], [4], [11], [12]. In this paper, we study the impact of finite frequency deviation on the system performance. Our analysis also includes the impact of laser phase noise and additive shot noise.

We show that there is a well-defined relationship between the choice of frequency deviation and the tolerable amount of laser phase noise for a prescribed level of sensitivity degradation (e.g., 1 dB). Our results indicate that when there is no phase noise, a frequency deviation $2\Delta f_d = 0.72R_b$ is sufficient for 1 dB sensitivity penalty with respect to infinite frequency deviation case; whereas, for an IF linewidth of $\Delta\nu = 0.50R_b$ the required frequency deviation increases to $2\Delta f_d = 3.42R_b$ for the same sensitivity penalty. The influence of finite frequency deviation on the values of other important system parameters such as optimum IF filter bandwidth and bit-error-ratio (BER) is also quantified. It is demonstrated that for a fixed IF linewidth value, the optimum IF filter bandwidth decreases as the frequency separation between the two tones becomes smaller. As an example, for $\Delta\nu = 0.5R_b$ the optimum IF filter bandwidth required reduces from $7R_b$ to $3R_b$ when $2\Delta f_d$ reduces from very large

values to $3R_b$. Using the BER results computed, sensitivity penalty due to finite frequency deviation is quantified as a function of IF laser linewidth. Our results show that the sensitivity degradation can be very severe for a fixed linewidth as the frequency deviation gets smaller. As an example, for an IF linewidth of 20% the sensitivity penalty is only 0.54 dB when the frequency deviation is extremely large (infinite); whereas it is 3.48 dB when the frequency deviation is $2\Delta f_d = R_b$. In this paper, we also investigate practically important suboptimum cases which do not use optimum IF filter bandwidths. More specifically, we quantify the sensitivity degradation due to finite frequency deviation for a fixed linewidth value when the IF filter bandwidth used is not optimized for different frequency deviations.

The rest of this paper is organized as follows. In Section II we give a system description and problem statement. Section III contains basic receiver equations, the signal-to-noise ratio, the bit-error rate, and the main results of the paper. A physical interpretation of the main results obtained is presented in Section IV. Finally, Section V contains the conclusions of this study.

II. SYSTEM DESCRIPTION AND PROBLEM STATEMENT

The block diagram of the dual filter optical heterodyne FSK receiver is shown in Figure 1. It was shown in [9] that the total output current processed by such a receiver is

$$i_T(t) \equiv \begin{cases} A_S cos[(\omega + \Delta\omega)t + \phi(t)] + n(t), & \text{for } data = 1 \\ A_S cos[(\omega - \Delta\omega)t + \phi(t)] + n(t), & \text{for } data = 0 \end{cases} \tag{1}$$

where A_S is the signal amplitude; $n(t)$ is the total noise process at the output of the balanced receiver; $\omega = 2\pi f_{IF}$ is the intermediate frequency (IF) in radians per second; $\phi(t)$ is the total phase noise due to the transmitter and local oscillator (LO) lasers; and $\Delta\omega = 2\pi\Delta f_d$ is the frequency deviation in radians/sec. These quantities are given by the following expressions:

$$A_S \equiv 2R\sqrt{P_S P_{LO}} \qquad amperes \tag{2}$$

$$n(t) \equiv n_1(t) - n_2(t) \qquad amperes \tag{3}$$

$$\omega \equiv \omega_S - \omega_{LO} \qquad radians/second \tag{4}$$

$$\phi(t) \equiv \phi_S(t) - \phi_{LO}(t) \qquad radians \tag{5}$$

$$2\Delta\omega \equiv \omega_1 - \omega_0 \qquad radians/second \tag{6}$$

where R is the detector responsivity; $n_1(t)$ and $n_2(t)$ are the noises of the two photodiodes; ω_S and ω_{LO} are the frequencies of the signal and the LO, respectively; $\phi_S(t)$ and $\phi_{LO}(t)$ are the phase noises of the transmitter and LO lasers, respectively; and ω_1 and ω_0 are the frequencies of transmission for $data = 1$ and $data = 0$, respectively.

The total phase noise $\phi(t)$ is defined by expression (5). Its derivative $\dot{\phi}_{(t)}$ has a zero-mean Gaussian probability density function (pdf); the single-sided power spectral density (PSD) of $\dot{\phi}_{(t)}$ is given by

$$S_{\dot{\phi}(t)}(f) = 4\pi\Delta\nu \qquad 0 < f < \infty \tag{7}$$

where $\Delta\nu$ is the FWHM linewidth at the IF, i.e.,

$$\Delta\nu = \Delta\nu_T + \Delta\nu_{LO} \tag{8}$$

where $\Delta\nu_T$ and $\Delta\nu_{LO}$ are the linewidths of the transmitter and LO lasers, respectively. The PSD shape in (7) implies the Lorentzian laser lineshape.

The additive noise $n(t)$ is composed of both the shot noise and the thermal noise. The single-sided PSD of $n(t)$ is

$$S_n \equiv \eta \quad \text{for } 0 < f < \infty \qquad amperes^2 \text{ per hertz} \tag{9}$$

where

$$\eta \equiv 2eRP_{LO} + \eta_{TH} \quad amperes^2 \text{ per hertz.} \tag{10}$$

In (10), e is the electron charge and η_{TH} is the PSD of the thermal noise. Expression (9) implies that the additive noise is white; this assumption may be inaccurate in systems having wide laser linewidth or large bit rate. The autocorrelation function of $n(t)$ is given by

$$R_n(t_1, t_2) \equiv E[n(t_1)n(t_2)] = 0.5\eta\delta(t_1 - t_2) \tag{11}$$

In previous studies on dual filter heterodyne FSK lightwave systems, the frequency separation between the two FSK frequencies $2\Delta\omega$ was assumed to be sufficiently large, so that the crosstalk between the two filters was negligible [2], [9], [10]. For practical system design, however, such an assumption is not valid. Specifically, in multichannel lightwave systems employing dual-filter heterodyne FSK receivers, the frequency separation between the two tones is a significant system design parameter which influences the number of channels that can be received for a prescribed level of crosstalk [13]-[17].

The physical scenario under consideration is shown in Figure 2. Figure 2(a) illustrates the case when the two frequencies are sufficiently apart from each other so that there is negligible crosstalk. The information-bearing signal may also contain phase noise. As the frequency deviation becomes smaller the two information-bearing signals start overlapping (see Fig. 2(b)) and the performance of the system under investigation deteriorates. One of the objectives of this study is to quantify the required frequency deviation for a given linewidth and a fixed sensitivity penalty (e.g., 1 dB). Another important case is shown in Figure 2(c). For a fixed frequency deviation, assuming the two information-bearing signals have no phase noise, there is a certain performance level (and a corresponding BER) which depends on the frequency spacing between ω_1 and ω_0. Clearly, if the

frequency deviation is kept fixed, as the two signals are impaired by more and more phase noise, the crosstalk due to laser phase noise becomes more severe; and the system performance deteriorates sharply. This physical situation is illustrated in Fig. 2(d). Another objective of this paper is to quantify the laser linewidth which can be tolerated for a prescribed level of sensitivity penalty, such as 1 dB, and for a fixed value of frequency deviation.

The physical scenario described above can only be analyzed if certain other system parameters are also carefully engineered. Note in Figures 2(a) and 2(b), for example, that as the frequency deviation gets narrower the optimum IF filter bandwidth required becomes smaller. Thus, to optimize the system performance it is essential to evaluate the optimum IF filter bandwidth corresponding to a fixed (but finite) frequency deviation and a fixed linewidth in the physical situation depicted by Figures 2(a) and 2(b). Computation of optimum IF filter bandwidths is also a necessity for the optimum performance evaluation of the system described by Figures 2(c) and 2(d). Obviously, one can choose not to optimize the IF filter bandwidth; in that case, however, a certain sensitivity penalty must be paid and the system performance is no longer optimum.

III. SYSTEM PERFORMANCE EVALUATION

This section is organized as follows. First, the basic receiver equations are given in Section III-A. Then the SNR at the threshold comparator input is found in Section III-B. The BER is evaluated in Section III-C. Finally, in Section III-D numerical results are presented.

A. Basic Receiver Equations :

The dual filter optical FSK receiver under investigation is shown in Figure 1. Following [9] and [10], we assume the IF filters to be finite-time bandpass integrators, with impulse responses

$$h_{B1}(t) = \begin{cases} \frac{\alpha}{T}\cos[\omega_1 t] & \text{if } t \in [0, \frac{T}{\alpha}] \\ 0 & \text{if } t \notin [0, \frac{T}{\alpha}] \end{cases} \tag{12}$$

and

$$h_{B2}(t) = \begin{cases} \frac{\alpha}{T} cos[\omega_0 t] & \text{if } t \in [0, \frac{T}{\alpha}] \\ 0 & \text{if } t \notin [0, \frac{T}{\alpha}] \end{cases} \tag{13}$$

where $\alpha \geq 1$ is a positive integer. The square-law device (SLD) is an envelope detector modeled by [9]

$$\begin{aligned} v_F(t) &\equiv |U_1(t)|^2 - |U_2(t)|^2 \\ &= x_F(t) + y_F(t) + z_F(t) \end{aligned} \tag{14}$$

where $U_1(t)$ and $U_2(t)$ are the complex amplitudes of the outputs of the IF filter 1 and IF filter 2, respectively. In expression (14), $x_F(t), y_F(t)$, and $z_F(t)$ denote the signal-cross-signal, noise-cross-noise, and signal-cross-noise terms, respectively. The postdetection lowpass filter is assumed to have the following impulse response [9]:

$$h_L(t) = \sum_{i=1}^{\alpha} \delta(t - \frac{iT}{\alpha}) \tag{15}$$

The output current of the IF filters at time t is

$$\begin{aligned} u_1(t) &\equiv h_{B1}(t) * i_T(t) \\ &= s_{B1}(t) + n_{B1}(t) \qquad lT \leq t \leq (l+1)T \end{aligned} \tag{16}$$

and

$$\begin{aligned} u_2(t) &\equiv h_{B2}(t) * i_T(t) \\ &= s_{B2}(t) + n_{B2}(t) \qquad lT \leq t \leq (l+1)T \end{aligned} \tag{17}$$

where * denotes convolution; $n_{B1}(t)$ and $n_{B2}(t)$ are the filtered versions of the noise, and $s_{B1}(t)$ and $s_{B2}(t)$ are the filtered versions of the signal, respectively; i.e.,

$$n_{B1}(t) \equiv h_{B1}(t) * n(t) \qquad lT \leq t \leq (l+1)T \tag{18}$$

$$n_{B2}(t) \equiv h_{B2}(t) * n(t) \qquad lT \leq t \leq (l+1)T \tag{19}$$

and

$$s_{B1}(t) = h_{B1}(t) * A_S cos[\omega_d t + \phi(t)], \quad lT \leq t \leq (l+1)T \tag{20}$$

$$s_{B2}(t) = h_{B2}(t) * A_S cos[\omega_d t + \phi(t)], \quad lT \leq t \leq (l+1)T \tag{21}$$

where $\omega_d = \omega_1$ or $\omega_d = \omega_0$. Hence the output of the summer is

$$v_F(t) \equiv x_F(t) + y_F(t) + z_F(t) \tag{22}$$

where

$$x_F(t) = s_{B1}^2(t) + \hat{s}_{B1}^2(t) - s_{B2}^2(t) - \hat{s}_{B2}^2(t) \tag{23}$$

$$y_F(t) = n_{B1}^2(t) + \hat{n}_{B1}^2(t) - n_{B2}^2(t) - \hat{n}_{B2}^2(t) \tag{24}$$

$$z_F(t) = 2\left[s_{B1}(t)n_{B1}(t) + \hat{s}_{B1}(t)\hat{n}_{B1}(t) - s_{B2}(t)n_{B2}(t) - \hat{s}_{B2}(t)\hat{n}_{B2}(t)\right] \tag{25}$$

In expressions (23)-(25), $\hat{s}_{Bd}(t)$ is the Hilbert transform of $s_{Bd}(t)$, $\hat{n}_{Bd}(t)$ is the Hilbert transform of $n_{Bd}(t)$, and $d = 0$ or $d = 1$. Finally, the output signal of the lowpass filter (LPF) $w_F(t)$ is

$$w_F(t) = h_L(t) * v_F(t) \tag{26}$$

The signal $w_F(t)$ is sampled at $t = (l+1)T$ and sent to the decision gate. The value of $w_F(t)$ at $t = (l+1)T$ is denoted by w_{FT} (decision variable) in the remainder of this paper.

B. The Signal-to-Noise Ratio :

The SNR at the input of the decision gate (Figure 1) is defined as [9], [18]

$$\gamma \equiv \frac{m(when\ \ data = 1) - m(when\ \ data = 0)}{\sigma(when\ \ data = 1) + \sigma(when\ \ data = 0)} \tag{27}$$

where m and σ are the mean and the standard deviation of w_{FT}. We note that, strictly speaking, the signal-to-noise ratio γ is a meaningful performance measure for a Gaussian hypothesis test only, whereas the probability density function (PDF) of w_{FT} is non-Gaussian for both ONE and ZERO symbols even when the linewidth is zero and the frequency deviation is infinite. In the case of zero linewidth and infinite frequency deviation, the LPF is not needed, and the bandwidth of the BPF is taken to be equal to the bit rate R_b. Conceptually, in this case $w_F(t) = v_F(t)$. The probability density function of $v_F(t)$ in this case can be found exactly. When $\Delta\nu$ is not equal to zero, and $2\Delta f_d$ is finite, the impact of phase noise and crosstalk further complicates the PDF. Since the actual pdf of w_{FT} is non-Gaussian, it is clear that the value of γ does not contain all the information needed to evaluate the system BER exactly. Hence, using expression (27) for estimating the SNR at the decision gate is an approximation; see Subsection C and Ref.[9] for an analysis of the accuracy of this approximation.

Calculation of m and σ is a long and a very complicated process. Therefore, we omit the intermediate steps of our derivations. Our analysis indicates that a general closed-form result can be obtained for the signal-to-noise ratio at the decision gate:

$$\gamma = \frac{m_1}{\sigma_1} \tag{28}$$

where

$$m_1 = \frac{A_S^2}{4}(2\alpha)\left[\frac{1}{a} + \frac{b-1}{a^2} + \frac{1}{k_1}\left\{-a - \frac{(x^2 - a^2)}{k_1}(1 - bcosx) + \frac{2abxsinx}{k_1}\right\}\right] \tag{29}$$

and

$$\sigma_1^2 = \sigma_{XF}^2 + \sigma_{YF}^2 + \sigma_{ZF}^2 \tag{30}$$

In expression (30), σ_{XF}^2, σ_{YF}^2, and σ_{ZF}^2 are given by:

$$\sigma_{XF}^2 = 4\frac{A_S^4}{16}\frac{\alpha}{a^4}\left[a^2 - \frac{11}{2}a - \frac{16}{3}ab + \frac{80}{9}(1-b) + (1-b^2) - \frac{1}{72}(1-b^4)\right] s(2\Delta\omega T) \tag{31}$$

$$\sigma_{YF}^2 = \frac{A_S^4}{16}\frac{2\alpha^3}{\xi^2}\left[1 - \frac{sin^2x}{x^2}\right] \tag{32}$$

and

$$\begin{aligned}\sigma_{ZF}^2 \;=\; & \frac{A_S^4}{16}\frac{16\alpha^2}{\xi^2}\left[-\frac{sin^2x}{4ax^2} + \frac{sinx}{8xk_1}\left\{1 + cosx + (\frac{x}{a} - \frac{2a}{x})sinx + (1-2b)\frac{y}{a}\right\} + \right. \\ & \left. \frac{a}{4k_1} + \frac{1}{4k_1^2}\left\{[x^2 - a^2][1 - bcosx] - 2abxsinx\right\} + \frac{1}{4a}\left\{1 + \frac{1}{a}(b-1)\right\}\right]\end{aligned} \tag{33}$$

where

$$\tau = T/\alpha \tag{34}$$

$$a = \pi\Delta\nu\tau \tag{35}$$

$$b = exp(-a) \tag{36}$$

$$x = 2\Delta\omega\tau \tag{37}$$

$$y = (a + acosx - xsinx) \tag{38}$$

$$k_1 = (a^2 + x^2) \tag{39}$$

and

$$s(2\Delta\omega T) = \begin{cases} 1 - e^{-\beta\omega_n 2\Delta\omega T}\left[cos(q) + \frac{\beta}{\sqrt{1-\beta^2}}sin(q)\right] & \text{for } \beta \neq 1 \\ 1 - e^{-\omega_n 2\Delta\omega T} - \omega_n 2\Delta\omega T e^{-\omega_n 2\Delta\omega T} & \text{for } \beta = 1 \end{cases} \tag{40}$$

In expression (40), ω_n, β, and q are defined as follows:

$$\omega_n \approx -0.0155 - 0.263/\alpha^2 + 0.578/\alpha \tag{41}$$

$$\beta \approx 0.27 - 1.5/\alpha^2 + 2.22/\alpha \tag{42}$$

$$q = \omega_n 2\Delta\omega T\sqrt{1-\beta^2} \tag{43}$$

For the dual filter optical heterodyne FSK system under investigation, there is a simple relationship between the peak IF SNR ξ, peak normalized signal energy E_{pn}, and the average normalized signal energy per bit E_{an} defined as

$$\xi = E_{pn} = E_{an} = \frac{A_S^2 T}{2\eta} \tag{44}$$

The value of γ in expressions (28)-(43) can be considerably simplified in several important practical cases:

Case 1: If $\Delta\nu = 0$ (no phase noise), then γ reduces to

$$\gamma = \frac{\sqrt{2\alpha}\left(\frac{1}{2} - \frac{(1-cosx)}{x^2}\right)}{\left[\frac{\alpha^2}{\xi^2}(1 - \frac{sin^2x}{x^2}) + \frac{8}{\xi}(\frac{cos^2x - cosx}{4x^2} + \frac{1}{8})\right]^{0.5}} \tag{45}$$

Expression (45) predicts the performance of the FSK system under consideration when there is no phase noise. Note that in this simple expression $x = 2\Delta\omega T$ is a design parameter. Hence, to obtain a BER = 10^{-9} (which corresponds to $\gamma = 6$), the IF filter bandwidth expansion factor α can be optimized for fixed values of $2\Delta\omega T$. By using α_{opt} values in expression (45), the impact of reducing $2\Delta\omega T$ on the sensitivity (the value of average signal energy in photons/bit) can be easily computed. As a sanity check, we also note that as $2\Delta\omega T$ gets sufficiently large, expression (45) reduces for $\alpha_{opt} = 1$ to

$$\gamma = \frac{1}{\sqrt{2(\frac{1}{\xi^2} + \frac{1}{\xi})}} \tag{46}$$

which is the result given in [9].

Case 2: If $\frac{\Delta\nu T}{\alpha} \ll 1 \ll \frac{2\Delta\omega T}{\alpha}$, then γ becomes

$$\gamma \approx \frac{\sqrt{2\alpha}\left(\frac{1}{2} - \frac{\pi\Delta\nu T}{6\alpha} - \frac{(1+\frac{\pi\Delta\nu T}{\alpha} - cos(2\Delta\omega T/\alpha))}{(2\Delta\omega T/\alpha)^2}\right)}{\left[\frac{2}{45}(\pi\Delta\nu\frac{T}{\alpha})^2 s(2\Delta\omega T) + \frac{\alpha^2}{\xi^2} + \frac{2\alpha}{\xi}(\frac{1}{2} - \frac{\pi\Delta\nu T}{6\alpha} - \frac{(1+\frac{\pi\Delta\nu T}{\alpha} - cos(2\Delta\omega T/\alpha))}{(2\Delta\omega T/\alpha)^2})\right]^{0.5}} \tag{47}$$

Expression (47) predicts the SNR at the decision gate of a well-designed dual filter heterodyne FSK lightwave system in presence of laser phase noise and finite frequency deviation. We note that for a well-designed system, $\Delta\nu T \ll \alpha \ll 2\Delta\omega T$. Clearly, expression (47) is an approximation for the SNR at the decision gate. The inaccuracy of expression (47) compared to the exact SNR results given by expressions (28)-(43), however, is only 0.1 dB for a well-designed system. In Table I, simple guidelines are provided for the choice of α_{opt} and $2\Delta f_d T$ for a given $\Delta\nu$ in well-designed systems.

C. The Bit Error Rate

A simple estimate of the BER can be obtained by using the Gaussian approximation [9], [18]

$$BER \equiv Q(\gamma) = \frac{1}{\sqrt{2\pi}}\int_{\gamma}^{\infty} e^{-x^2/2}dx \tag{48}$$

We note that expression (48) gives the accurate value of BER for a Gaussian hypothesis test only and assumes that the decision threshold is selected optimally, i.e., at the intersection of the conditional pdf's of w_{FT} calculated for $data = 1$ and for $data = 0$. As mentioned before, in the problem investigated, the pdf of w_{FT} is generally non-Gaussian. It was shown in [9] that using Gaussian PDF's for BER evaluation leads to an inaccuracy of approximately 2.6 dB. This, however, is not a serious limitation in itself since it can be somewhat rectified using an empirical factor. Such an empirical factor was shown to be useful in estimating the BER; in particular, it was shown that the inaccuracy of the BER predictions of Gaussian approximation can be reduced to less than 1 dB over a wide range of linewidth values (up to 250%) when such an empirical correction factor is used. Hence, in this paper we estimate BER as

$$BER \equiv Q(\gamma') = \frac{k}{\sqrt{2\pi}} \int_{\gamma}^{\infty} e^{-x^2/2} dx \tag{49}$$

where $k = 1.36$ is the empirical factor used for reducing the inaccuracy of the Gaussian BER estimate to 0 dB at $\Delta\nu T = 0$.

It should be noted that though the absolute accuracy of the Gaussian approximation technique is not perfect, a modified Gaussian approximation does provide a very useful analytical tool for studying the impact of crucial system parameters such as finite frequency deviation and laser linewidth on system performance.

D. Numerical Results

Figure 3 shows the optimum IF filter bandwidth values α_{opt} versus normalized laser linewidth for fixed values of the frequency separation $2\Delta f_d T$. We observe that for a fixed linewidth, the required α_{opt} decreases as the frequency deviation becomes smaller. The physical reason of this phenomenon is the so-called crosstalk. As the frequency deviation gets narrower, the IF filter collects more crosstalk from the other signal. To maintain the same BER (let's say BER = 10^{-9}) as in the case of infinite frequency deviation, a narrower IF filter bandwidth must be used in order to reduce the influence of crosstalk. There is, however, a certain IF filter bandwidth value beyond which a further reduction in IF filter bandwidth is detrimental because the information-bearing signal gets substantially truncated and the loss in signal power becomes more than the loss in noise power. This tendency can easily be observed in Figure 4(a). Figure 4(b) shows α_{opt} versus normalized frequency deviation for several linewidths at BER = 10^{-9}. A careful inspection of Figure 4(b) reveals that, at each fixed linewidth there is a required α_{opt} and $2\Delta f_d T$ for maintaining a BER = 10^{-9}. We emphasize that Figure 4(b) does not necessarily correspond to a well-designed system. When $\Delta\nu T = 1.0$, for example, Figure 4(b) indicates that both α_{opt} and $2\Delta f_d T$ can be as small as 3 and a BER = 10^{-9} can still be maintained. Such a system, however, is not a well-designed system. It is clear from Table I that,

when $\Delta\nu T = 1.0$, $\alpha_{opt} = 6$ and $2\Delta f_d T \approx 5.46$ in a well-designed system.

Figures 5-9 show BER versus ξ for fixed linewidth values and for α_{opt} as the frequency deviation varies parametrically. As expected, for a fixed linewidth value, the sensitivity of the system deteriorates as frequency deviation becomes smaller. As an example, Figure 7 shows that, when $2\Delta f_d = 0.75R_b$ the sensitivity of the system is 3 dB worse than the ideal case ($2\Delta f_d = \infty$). Note that (see Figures 3 and 4(a)) $\alpha_{opt} = 1$ for $2\Delta f_d = 0.75R_b$ as opposed to $\alpha_{opt} = 4$ in the ideal case when $\Delta\nu T = 0.16$. The curves shown in Figures 5-9 are plotted using α values which are optimum only at BER $= 10^{-9}$. Hence, for BER $\neq 10^{-9}$ the curves are not optimum. This is the main reason for the better performance of the $2\Delta f_d = 0.75R_b$ curve compared to the $2\Delta f_d = 1.5R_d$ curve at BER values larger than 10^{-9} in Figure 8.

In Figures 10-14 the BER performance is shown versus ξ for a fixed frequency deviation value as the laser linewidth increases. It can be observed from these Figures that for a fixed frequency deviation, there is a finite degradation in sensitivity (or an increase in the required ξ for BER $= 10^{-9}$) as linewidth becomes larger. Figure 12, for instance, shows that there is approximately a 2.5 dB sensitivity penalty when the linewidth increases from 0 to 16%, for a fixed frequency deviation of $2\Delta f_d = 1.5R_b$. Another important result which should be observed from Figures 10-14 is that the aforementioned effect becomes stronger for decreasing values of frequency deviation.

In Figures 15-17 the sensitivity penalty (in dB) is plotted versus laser linewidth for fixed frequency deviation values. Figure 15, for example, clearly illustrates that for a fixed linewidth value the sensitivity penalty increases as the frequency separation between the two tones decreases. For a linewidth of 50%, Figure 15 shows that the sensitivity penalty becomes more than 5 dB for a frequency separation of $2\Delta f_d = R_b$ which is a drastic deterioration compared to 0.88 dB penalty in the ideal case.

Figure 16 shows the sensitivity penalty of the system under investigation versus frequency deviation $2\Delta f_d T$ for several laser linewidths when optimum IF filter bandwidth values are employed. It

can be observed from Figure 16 that, for a 1 dB sensitivity penalty the required frequency deviation is $\approx 2\Delta f_d = 0.72R_b$ for zero linewidth whereas this number goes up to $2\Delta f_d = 3.4R_b$ for 50% linewidth. We emphasize that in Figure 16 the α values used are always optimum. It is interesting to contrast the results of Figure 16 with those where α values are not optimum. This is illustrated in Figure 17. In Figure 17, each sensitivity penalty curve uses the α value which is optimum only for the ideal case ($\alpha_{inf-opt}$); i.e., when $2\Delta f_d T = \infty$. It can be easily seen that suboptimum α values will make the frequency deviation requirement for 1 dB penalty worse.

IV. PHYSICAL INTERPRETATION OF RESULTS

The performance of the dual-filter heterodyne FSK lightwave receiver under investigation depends on the IF laser linewidth, frequency deviation between the two frequencies of data transmission, IF, and the bandwidth of the two IF filters. In this study we assume that IF is sufficiently large so that the sensitivity penalty due to finite IF is negligible. This assumption also enables us to isolate the impact of finite frequency deviation on system performance in presence of phase noise and shot noise.

In this paper it is shown that the frequency deviation, laser linewidth, and the optimum IF filter bandwidths are interrelated system parameters. Furthermore, this relationship is quantified by the results of our analysis.

It is interesting to note that, though they stem from different physical origins, the net impact of finite frequency deviation on system performance is very similar to the impact of laser linewidth on system performance. For each linewidth and frequency deviation value, there is an optimum IF filter bandwidth. If for that fixed linewidth value the frequency deviation is decreased, more crosstalk power is collected by each IF filter. For maintaining the same BER, a smaller IF filter bandwidth is required. When the IF filter bandwidth is reduced, however, the information-bearing signal is also truncated. For each linewidth there is a critical value of the IF filter bandwidth beyond which a

further reduction in bandwidth implies more loss in signal power than noise power and, therefore, a severe BER floor. Hence, for optimum system performance the IF filter bandwidth should be optimized for each linewidth value and frequency deviation. If this is not done and the optimum IF filter bandwidth for the ideal case (i.e. if $\alpha = \alpha_{inf-opt}$) is used for all frequency deviation values, the sensitivity penalty paid rises sharply as the frequency deviation decreases. This result is illustrated in Figure 18 for a linewidth of 27%. In other words, larger-than-optimum IF filter bandwidth values may have a very profound adverse effect on system performance. The physical reason for this degradation is the excess crosstalk power in addition to the excess shot noise collected by the IF filters when the bandwidths used are larger-than-optimum.

Similarly, for a fixed frequency separation $2\Delta f_d T$, the optimum IF filter bandwidths required increase as the linewidth increases. In other words, in order to maintain a BER = 10^{-9} larger IF filter bandwidths are required for larger linewidth values. Therefore, if one wants to pay a 1 dB sensitivity penalty due to laser linewidth at a fixed value of frequency deviation, it is clear that there is a maximum permissible laser linewidth. Beyond this $\Delta\nu$ value, the sensitivity penalty is more than 1 dB. This phenomenon is a result of the interaction of the influence of crosstalk due to finite frequency deviation with the influence of phase noise. Specifically, for larger values of linewidth a larger value of α_{opt} is required. As α_{opt} gets larger, however, the IF filters collect more crosstalk and the sensitivity deteriorates.

The sensitivity penalty curves shown in Figures 16 and 17 also reveal an important physical phenomenon. When the linewidth is zero, for example, the sensitivity penalty is zero at different frequency deviation values; namely, at integer multiples of the bit rate. These values of frequency deviation which give equivalent performance with infinite frequency deviation are known as orthogonal values. Similarly, a dual filter FSK system which uses integer multiples of bit rate for the frequency deviation between the two information frequencies is known as an orthogonal FSK system. Figure 16 clearly shows that, in such a system the sensitivity penalty has an oscillatory behaviour

as frequency deviation becomes smaller, up to a certain frequency deviation (up to $2\Delta f_d = R_b$). Hence, surprisingly, the system performance for $2\Delta f_d = R_b$, for example, is actually better than the system performance at $2\Delta f_d = 2.5R_b$. Note that the sensitivity penalty increases uniformly and sharply for $2\Delta f_d < R_b$. A simple mathematical derivation for the performance of the dual-filter FSK system with zero linewidth is given in [21]. That derivation gives some insight into the reasons of the mentioned oscillatory behaviour. It can be shown that when f_1 and f_0 are orthogonal the two signals are uncorrelated in the signal-space constellation diagram. Therefore, as long as the system is orthogonal its performance is not affected by the actual value of the frequency deviation. For non-negligible linewidths, Figure 17 shows the same type of oscillatory behaviour for sensitivity penalty. Note, however, that the ideal performance is never reached at any finite frequency deviation value for non-negligible linewidths. In other words, the dual-filter FSK lightwave system is never orthogonal in the true sense for finite (non-negligible) linewidths.

The sensitivity penalty results shown in Figures 16 and 17 can be checked with the classical communication theory literature for zero linewidth [19]-[22]. In all these references, it is a well established fact that the crosstalk is negligible when $2\Delta f_d = R_b$. This gives us a certain confidence in the validity of the approach used in this paper. For non-negligible linewidths, however, it remains to be seen how close the results predicted by our approximate theory are to those which will be predicted by a much more exact approach such as [10].

Though in this paper a single channel dual-filter FSK lightwave system is studied, the results obtained can give very rough estimates about the electrical domain channel spacings required in a multichannel dual-filter FSK system. In such a system, clearly there will be adjacent channel interference in addition to the co-channel interference due to finite frequency deviation.

V. CONCLUSIONS

In this paper the impact of finite frequency deviation on the performance of dual-filter FSK lightwave systems in presence of laser phase noise and shot noise is studied and quantified. Our analysis shows that for zero linewidth, a frequency deviation of $2\Delta f_d = 0.72R_b$ is required for 1 dB penalty. When the linewidth is 50%, for 1 dB sensitivity penalty the required frequency deviation increases to $2\Delta f_d = 3.4R_b$. In this work we also show that for a fixed linewidth, the optimum IF filter bandwidth decreases as the frequency deviation becomes narrower. As an example, for $\Delta\nu = 0.5R_b$, α_{opt} reduces from 7 to 3 as $2\Delta f_d$ reduces from very large values to $1.5R_b$. The BER computations carried out in this paper enable us to estimate the largest permissible linewidth values for a fixed frequency deviation. One of the main strengths of this analysis is the fact that it leads to a simple closed-form SNR expression in terms of the main system parameters. This closed-form simple expression facilitates physical insight into the impact of finite frequency deviation on system performance and provides simple guidelines for practical system design.

The results obtained in this paper are based on the Gaussian assumption for the distributions of the two decision variables. We checked the results of our analysis for zero linewidth with the results given by classical communication theory and found a good match.

Factors not taken into account may change the results obtained in this paper. Receiver thermal noise and finite IF are among such factors. The ideal case of $f_{IF} \gg R_b$ was assumed in this study in order to isolate the impact of finite frequency deviation. Further study is needed, however, to quantify the impact of finite IF (in presence of laser phase noise, finite frequency deviation, and shot noise) on the system performance of the dual-filter FSK lightwave systems.

The obtained results should be conceived as essential first steps for computing the electrical domain and optical domain channel spacing required for a prescribed sensitivity penalty in multichannel dual-filter FSK lightwave systems.

References

[1] K. Emura, S. Yamazaki, M. Yamaguchi, M. Shikada, and K. Minemura, "An optical FSK heterodyne dual filter detection system for taking advantage of DFB LD applications", *IEEE/OSA Journal of Lightwave Technology*, Vol. 8, No. 2, pp. 243-250, February 1990.

[2] M. Azizoglu and P. A. Humblet, "Envelope detection of orthogonal signals with phase noise", *IEEE/OSA Journal of Lightwave Technology*, Vol. LT-9, No. 10, pp. 1398-1410, October 1991.

[3] K. Emura, S. Yamazaki, M. Shikada, S. Fujita, M. Yamaguchi, I. Mito and K. Minemura, "System design and long-span transmission experiments on an optical FSK heterodyne dual filter detection system", *IEEE/OSA Journal of Lightwave Technology*, Vol. LT-5, pp. 469-477, April 1987.

[4] K. Emura, S. Yamazaki, S. Fujita, M. Shikada, I. Mito, and K. Minemura, "Over 300 km transmission experiment on an optical FSK heterodyne dual filter detection system", *Electronics Letters*, Vol. 22, pp. 1096-1097, October 1986.

[5] T. Okoshi, "Ultimate performance of heterodyne/coherent optical fiber communications", *IEEE/OSA Journal of Lightwave Technology*, Vol. LT-4, No. 10, pp. 1556-1562, October 1986.

[6] Y. Yamamoto and T. Kimura, "Coherent optical fiber transmission systems", *IEEE Journal of Quantum Electronics*, Vol. QE-17, No. 6, pp. 919-935, June 1981.

[7] T. Okoshi, K. Emura, K. Kikuchi, and R. Th. Kersten, "Computation of bit-error rate of various heterodyne and coherent-type optical communication schemes", *Journal of Optical Communications*, Vol. 2, pp. 89-96, 1981.

[8] T. Okoshi and K. Kikuchi, *Coherent Optical Fiber Communications*. KTK Scientific Publishers, Tokyo, 1988.

[9] L. G. Kazovsky and O. K. Tonguz, "ASK and FSK coherent lightwave systems: a simplified approximate analysis", *IEEE/OSA Journal of Lightwave Technology*, Vol. LT-8, No. 3, pp. 338-352, March 1990.

[10] G. J. Foschini, L. J. Greenstein, and G. Vanucci, "Noncoherent detection of coherent lightwave signals corrupted by phase noise", *IEEE Transactions on Communications*, Vol. 36, No. 3, pp. 306-314, March 1988.

[11] M. C. Brain, M. J. Creaner, R. C. Steele, N. G. Walker, G. R. Walker, J. Mellis, S. Al-Chalabi, J. Davidson, M. Rutherford, and I. C. Sturgess, "Progress towards the field deployment of coherent optical fiber systems", *IEEE/OSA Journal of Lightwave Technology*, Vol. 8, No. 3, pp. 423-437, March 1990.

[12] I. Hardcastle, T. Large, F. Davis, A. Hadjifotiou, "High performance 140 Mbit/s FSK coherent system", *Electronics Letters*, Vol. 26, No. 18, pp. 1523-1525, August 1990.

[13] G. Jacobsen and I. Garrett, "The effect of crosstalk and phase noise in multichannel coherent optical ASK systems", *IEEE/OSA Journal of Lightwave Technology*, Vol. LT-9, No. 9, pp. 1006-1018, August 1991.

[14] L. G. Kazovsky and J. L. Gimlett, "Sensitivity penalty in multichannel coherent optical communications", *IEEE/OSA Journal of Lightwave Technology*, Vol. 6, pp. 1353-1365, 1988.

[15] P. Healey, "Effect of intermodulation in multichannel optical heterodyne systems", *Electronics Letters*, Vol. 21, pp. 101-103, 1985.

[16] G. Jacobsen and I. Garrett, "Crosstalk and phase-noise effects in multichannel coherent optical CP-FSK systems with tight IF filtering", *IEEE/OSA Journal of Lightwave Technology*, Vol. LT-9, No. 9, pp. 1168-1177, September 1991.

[17] L. G. Kazovsky, "Multichannel coherent optical Communication systems", *IEEE/OSA Journal of Lightwave Technology*, Vol. LT-5, No. 8, pp. 1095-1102, 1987.

[18] S. D. Personick, "Receiver design for digital fiber-optic communication systems, Part I", *Bell System Technical Journal*, Vol. 52, No. 6, pp. 843-874, July-August 1973.

[19] E. D. Sunde, *Communication Systems Engineering Theory*. New York: Wiley, 1969.

[20] W. R. Bennett and J. R. Davey, *Data Transmission*. McGraw-Hill, 1965.

[21] H. Taub and D. L. Schilling, *Principles of Communication Systems*. McGraw-Hill, 1986, Second Edition.

[22] F. G. Stremler, *Introduction to Communication Systems*. Addison-Wesley, 1982, Second Edition.

Table 1: Requirements for a well-designed receiver

$\Delta\nu T \ll \alpha$	$\Rightarrow$	$0.29 + 5.95(\Delta\nu T) - 0.68(\Delta\nu T)^2 \leq \lceil\alpha\rceil$
$\alpha \ll 2\Delta f_d T$	$\Rightarrow$	$\alpha \leq 1.073(2\Delta f_d T)$
$\Delta\nu T \ll 2\Delta f_d T$	$\Rightarrow$	$0.9 + 4.57(\Delta\nu T) + 1.9(\Delta\nu T)^2 - 1.91(\Delta\nu T)^3 \leq 2\Delta f_d T$

Figure Captions :

Fig. 1 Block diagram of the dual-filter heterodyne FSK system under investigation.

Fig. 2 Physical scenario under consideration :

(a) The frequency spectrum of the two information-bearing signals with infinitely large frequency separation.

(b) The same frequency spectrum with finite frequency separation.

(c) The frequency spectrum of the two information-bearing signals with finite frequency separation and zero phase noise.

(d) The spectrum in (c) with the same frequency separation and non-negligible phase noise.

Fig. 3 Optimum normalized IF filter bandwidth versus normalized linewidth for several values of frequency deviation at BER = 10^{-9}.

Fig. 4(a) Optimum normalized IF filter bandwidth versus normalized linewidth for several values of frequency deviation at BER = 10^{-9}.

Fig. 4(b) Optimum normalized IF filter bandwidth versus normalized frequency deviation for several linewidths at BER = 10^{-9}.

Fig. 5 BER versus IF SNR for several values of frequency deviation when the linewidth is zero.

Fig. 6 BER versus IF SNR for several values of frequency deviation when $\Delta\nu T = 0.04$.

Fig. 7 BER versus IF SNR for several values of frequency deviation when $\Delta\nu T = 0.16$.

Fig. 8 BER versus IF SNR for several values of frequency deviation and when $\Delta\nu T = 0.27$.

Fig. 9 BER versus IF SNR for several values of frequency deviation and $\Delta\nu T = 0.50$.

Fig. 10 BER versus IF SNR for several linewidths and infinite frequency separation between f_1 and f_0.

Fig. 11 BER versus IF SNR for several linewidths when $2\Delta f_d = 4.5R_b$.

Fig. 12 BER versus IF SNR for several linewidths when $2\Delta f_d = 1.5R_b$.

Fig. 13 BER versus IF SNR for several linewidths when $2\Delta f_d = 0.75R_b$.

Fig. 14 BER versus IF SNR for several linewidths when $2\Delta f_d = 0.3R_b$.

Fig. 15 Sensitivity penalty (in dB) versus normalized linewidth for several values of frequency deviation at BER = 10^{-9}.

Fig. 16 Sensitivity penalty (in dB) versus normalized frequency deviation for several linewidths at BER = 10^{-9}. All curves are computed using $\alpha = \alpha_{opt}$ at BER = 10^{-9}.

Fig. 17 Sensitivity penalty (in dB) versus normalized frequency deviation for several linewidths at BER = 10^{-9}. All curves are computed using the optimum α values for infinite frequency separation ($\alpha_{inf-opt}$).

Fig. 18 Impact of suboptimum α values on the sensitivity penalty for $\Delta\nu T = 0.27$ at BER = 10^{-9}. The solid line corresponds to the curve computed with α_{opt} for all frequency deviation values and the broken line corresponds to the curve computed with $\alpha_{inf-opt}$.

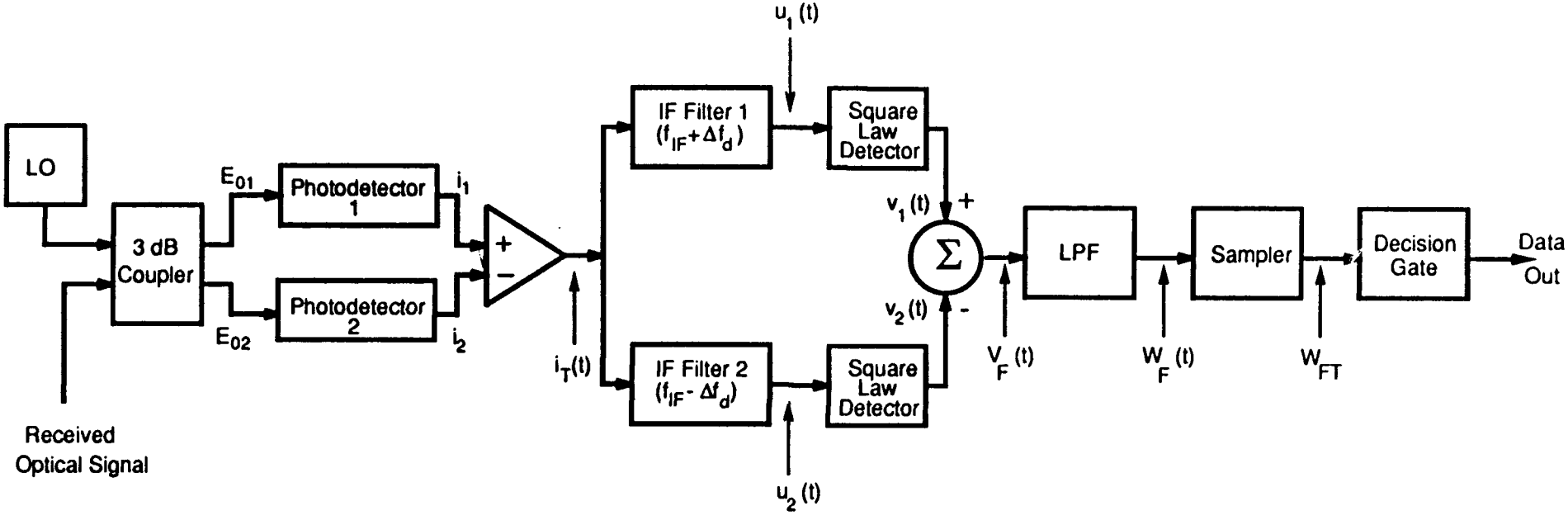
LO
3 dB Coupler
Received Optical Signal
E_{01}
E_{02}
Photodetector 1
Photodetector 2
i_1
i_2
+
−
$i_T(t)$
IF Filter 1 ($f_{IF}+\Delta f_d$)
IF Filter 2 ($f_{IF}-\Delta f_d$)
$u_1(t)$
$u_2(t)$
Square Law Detector
Square Law Detector
$v_1(t)$
$v_2(t)$
+
-
Σ
$V_F(t)$
LPF
$W_F(t)$
Sampler
W_{FT}
Decision Gate
Data Out

Figure 1

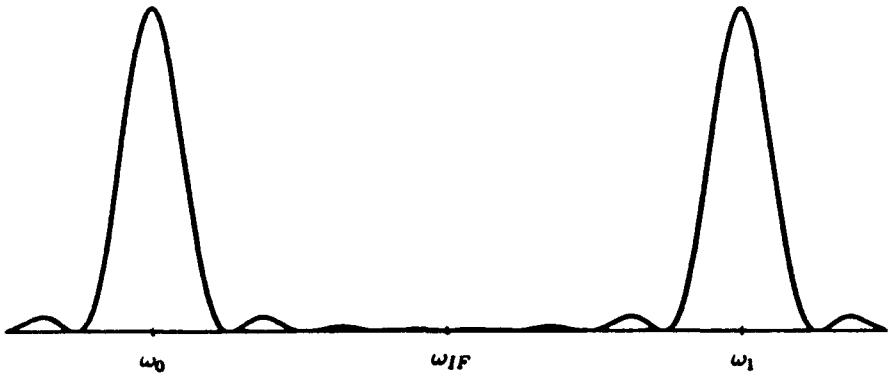

(a)

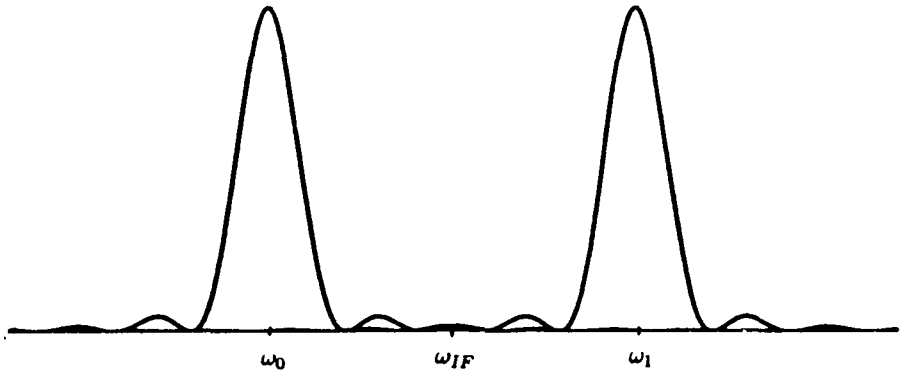

(c)

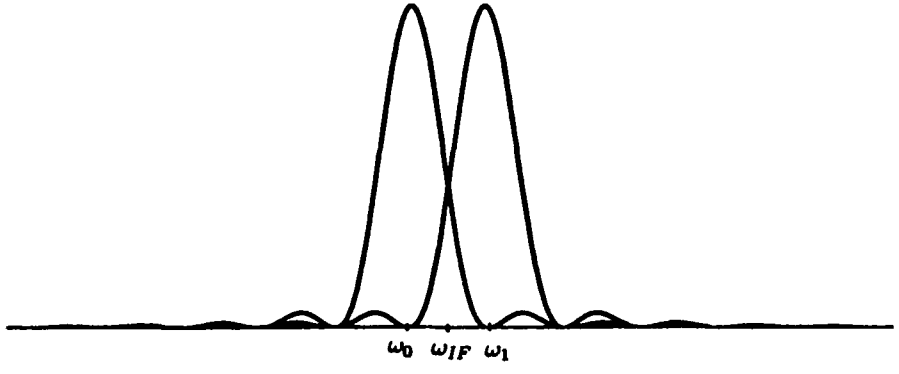

(b)

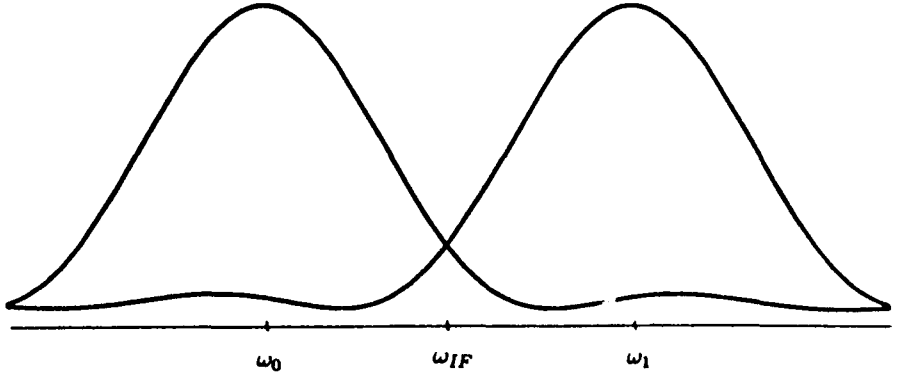

(d)

Figure 2

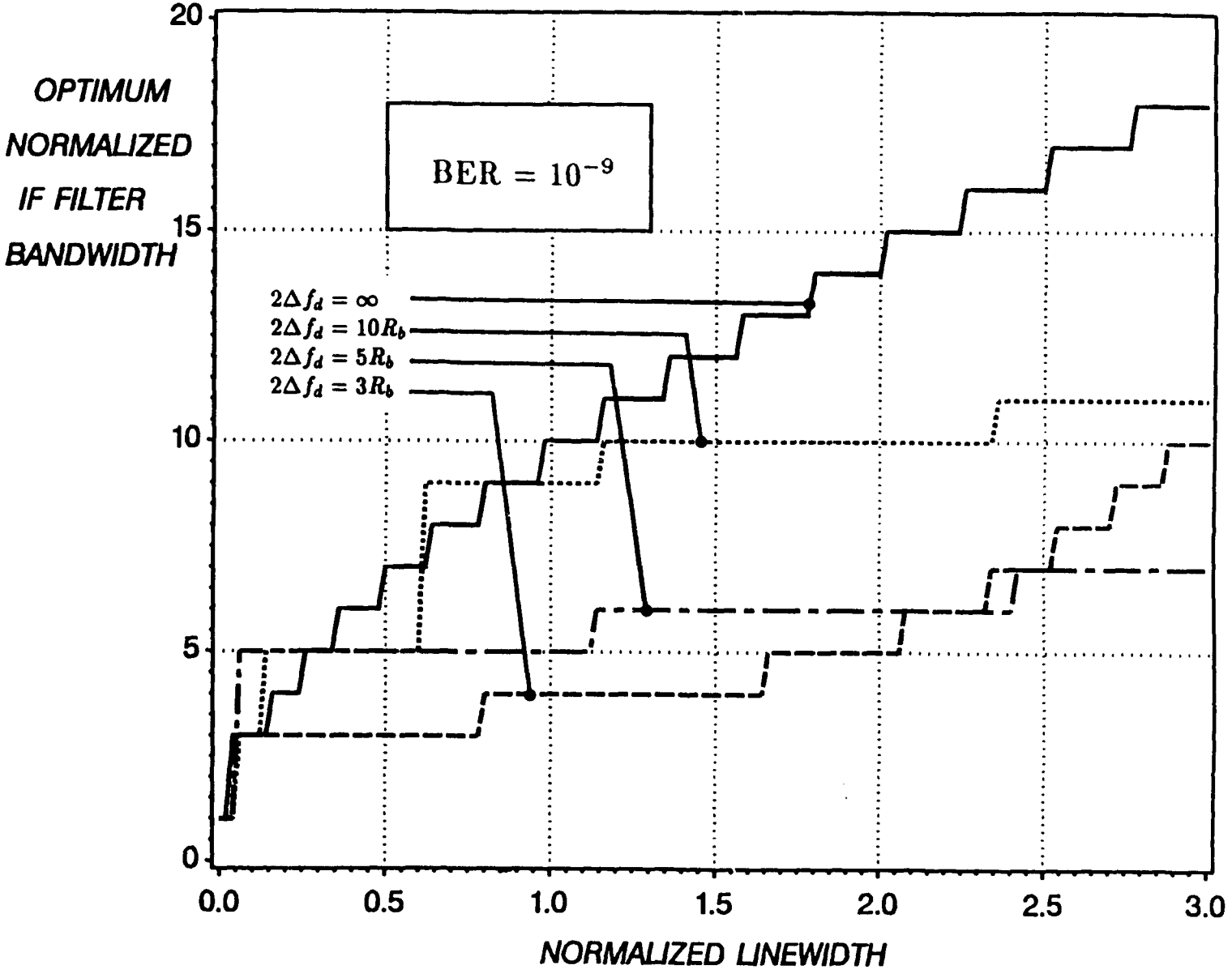
OPTIMUM
NORMALIZED
IF FILTER
BANDWIDTH
20
15
10
5
0
BER = 10^{-9}
$2\Delta f_d = \infty$
$2\Delta f_d = 10R_b$
$2\Delta f_d = 5R_b$
$2\Delta f_d = 3R_b$
0.0
0.5
1.0
1.5
2.0
2.5
3.0
NORMALIZED LINEWIDTH

Figure 3

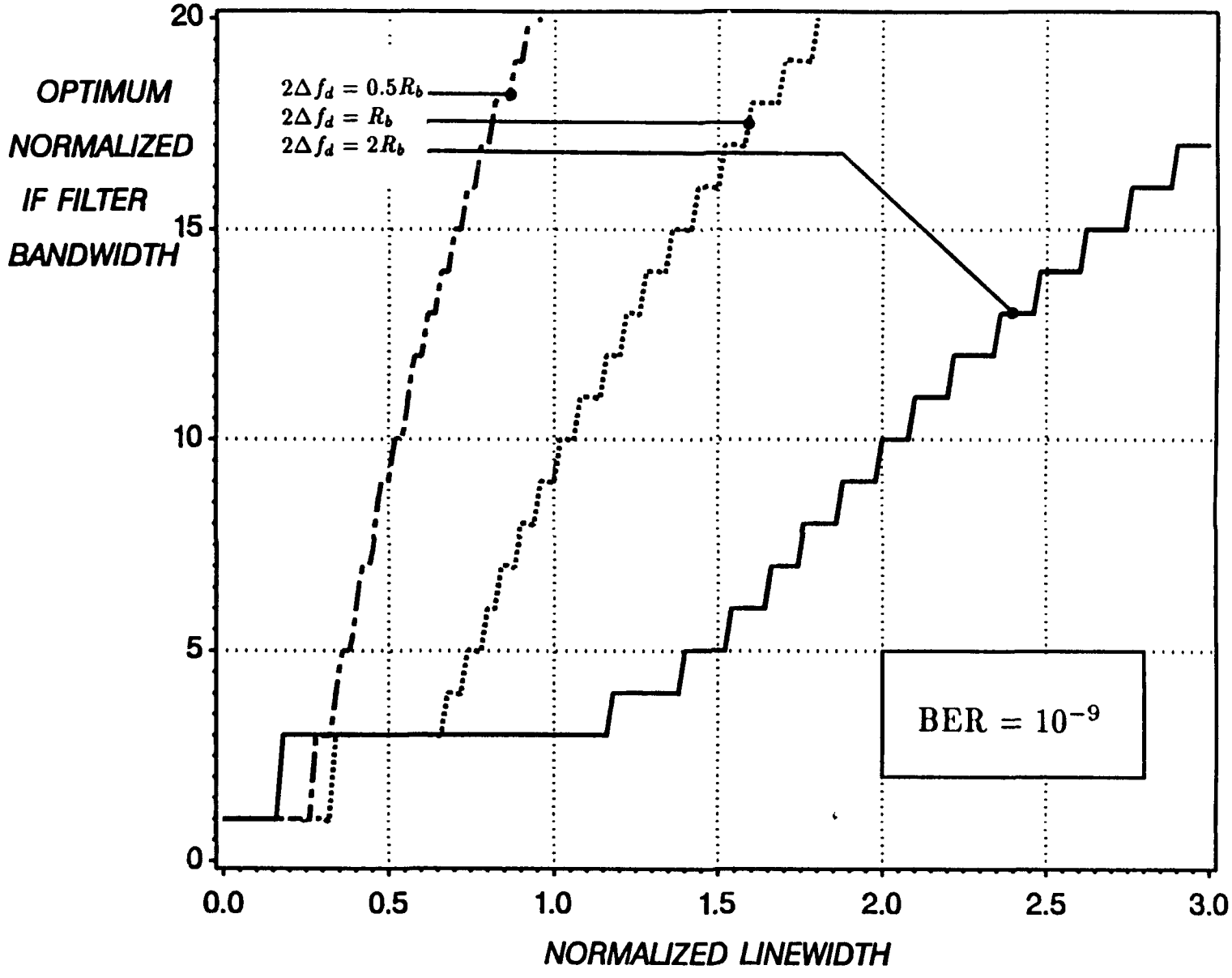
OPTIMUM
NORMALIZED
IF FILTER
BANDWIDTH
20
15
10
5
0
$2\Delta f_d = 0.5R_b$
$2\Delta f_d = R_b$
$2\Delta f_d = 2R_b$
BER = 10^{-9}
0.0
0.5
1.0
1.5
2.0
2.5
3.0
NORMALIZED LINEWIDTH

Figure 4(a)

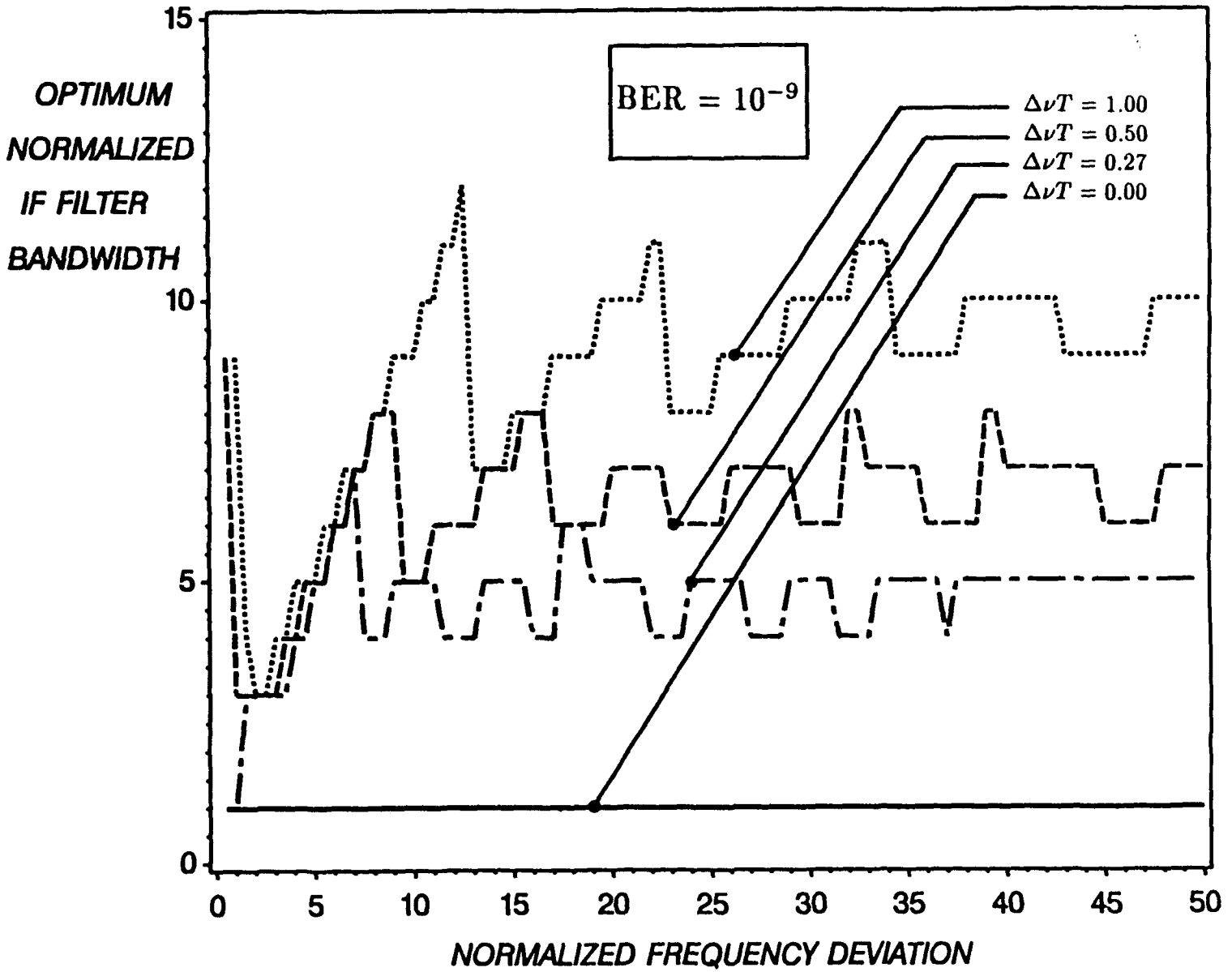
15
10
5
0
OPTIMUM
NORMALIZED
IF FILTER
BANDWIDTH
BER = 10^{-9}
$\Delta\nu T$ = 1.00
$\Delta\nu T$ = 0.50
$\Delta\nu T$ = 0.27
$\Delta\nu T$ = 0.00
0
5
10
15
20
25
30
35
40
45
50
NORMALIZED FREQUENCY DEVIATION

Figure 4(b)

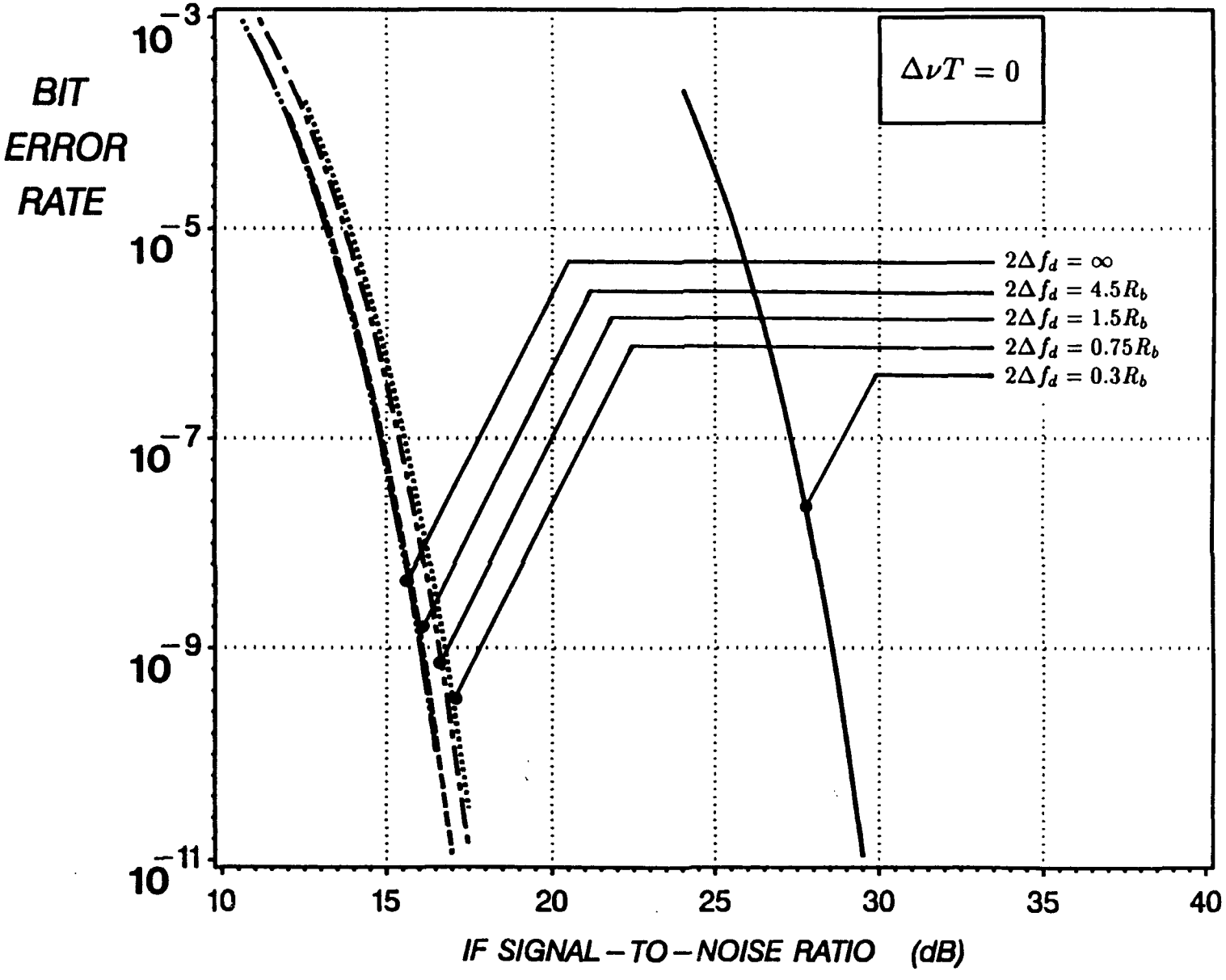
BIT ERROR RATE
10^{-3}
10^{-5}
10^{-7}
10^{-9}
10^{-11}
$\Delta\nu T = 0$
$2\Delta f_d = \infty$
$2\Delta f_d = 4.5R_b$
$2\Delta f_d = 1.5R_b$
$2\Delta f_d = 0.75R_b$
$2\Delta f_d = 0.3R_b$
10
15
20
25
30
35
40
IF SIGNAL – TO – NOISE RATIO (dB)

Figure 5

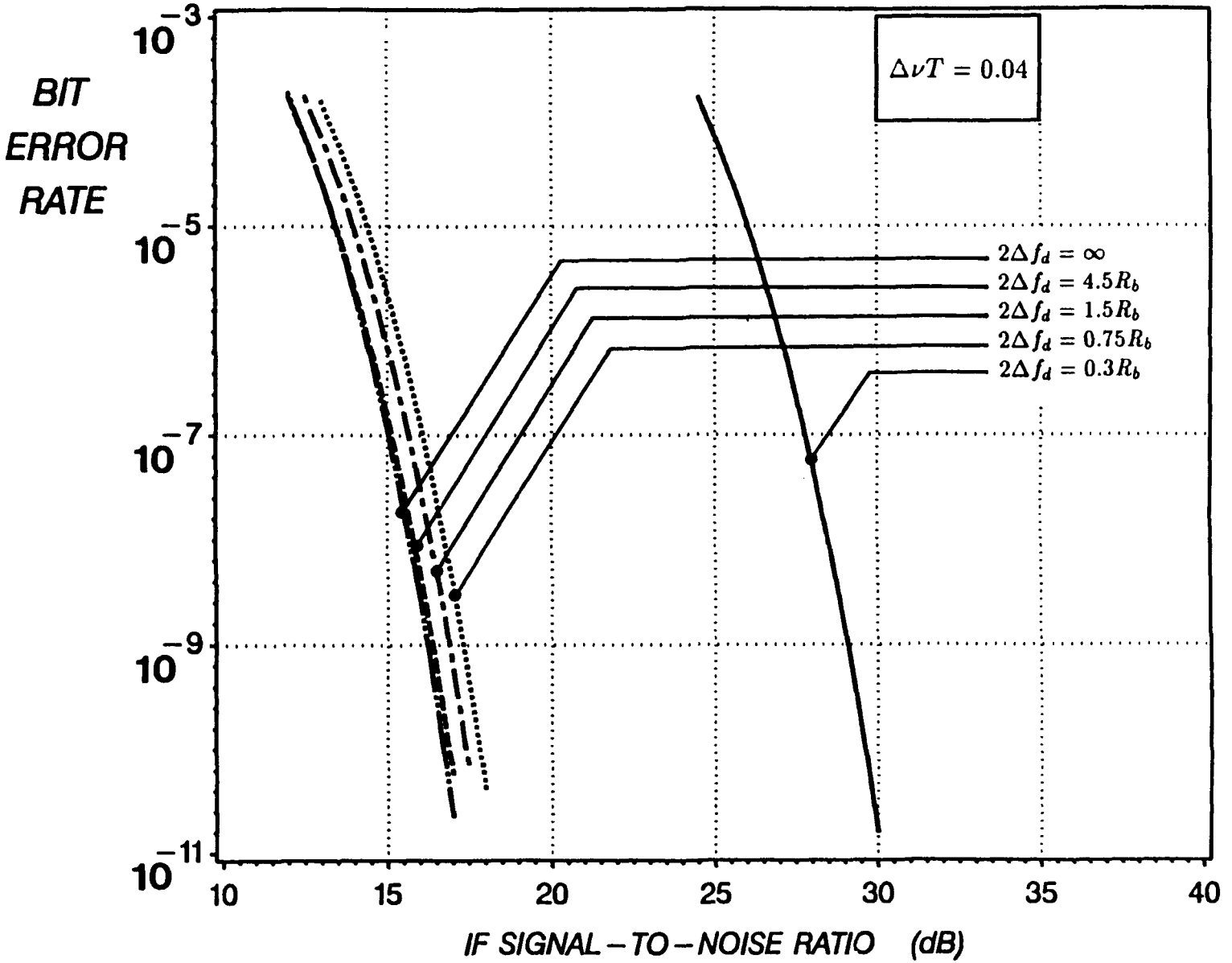
BIT ERROR RATE
10^{-3}
10^{-5}
10^{-7}
10^{-9}
10^{-11}
$\Delta\nu T = 0.04$
$2\Delta f_d = \infty$
$2\Delta f_d = 4.5R_b$
$2\Delta f_d = 1.5R_b$
$2\Delta f_d = 0.75R_b$
$2\Delta f_d = 0.3R_b$
10
15
20
25
30
35
40
IF SIGNAL – TO – NOISE RATIO (dB)

Figure 6

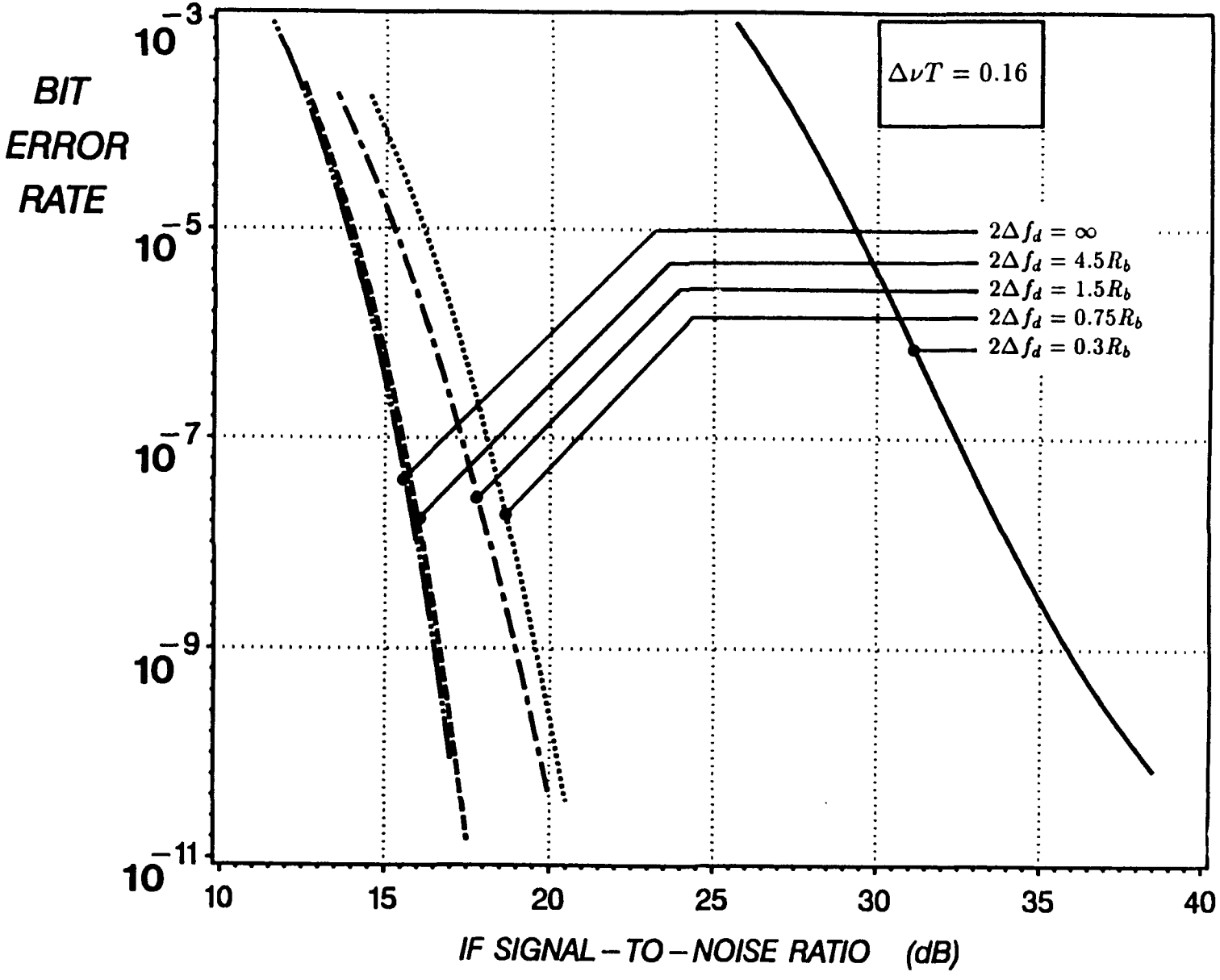
BIT ERROR RATE
10^{-3}
10^{-5}
10^{-7}
10^{-9}
10^{-11}
$\Delta\nu T = 0.16$
$2\Delta f_d = \infty$
$2\Delta f_d = 4.5R_b$
$2\Delta f_d = 1.5R_b$
$2\Delta f_d = 0.75R_b$
$2\Delta f_d = 0.3R_b$
10
15
20
25
30
35
40
IF SIGNAL – TO – NOISE RATIO (dB)

Figure 7

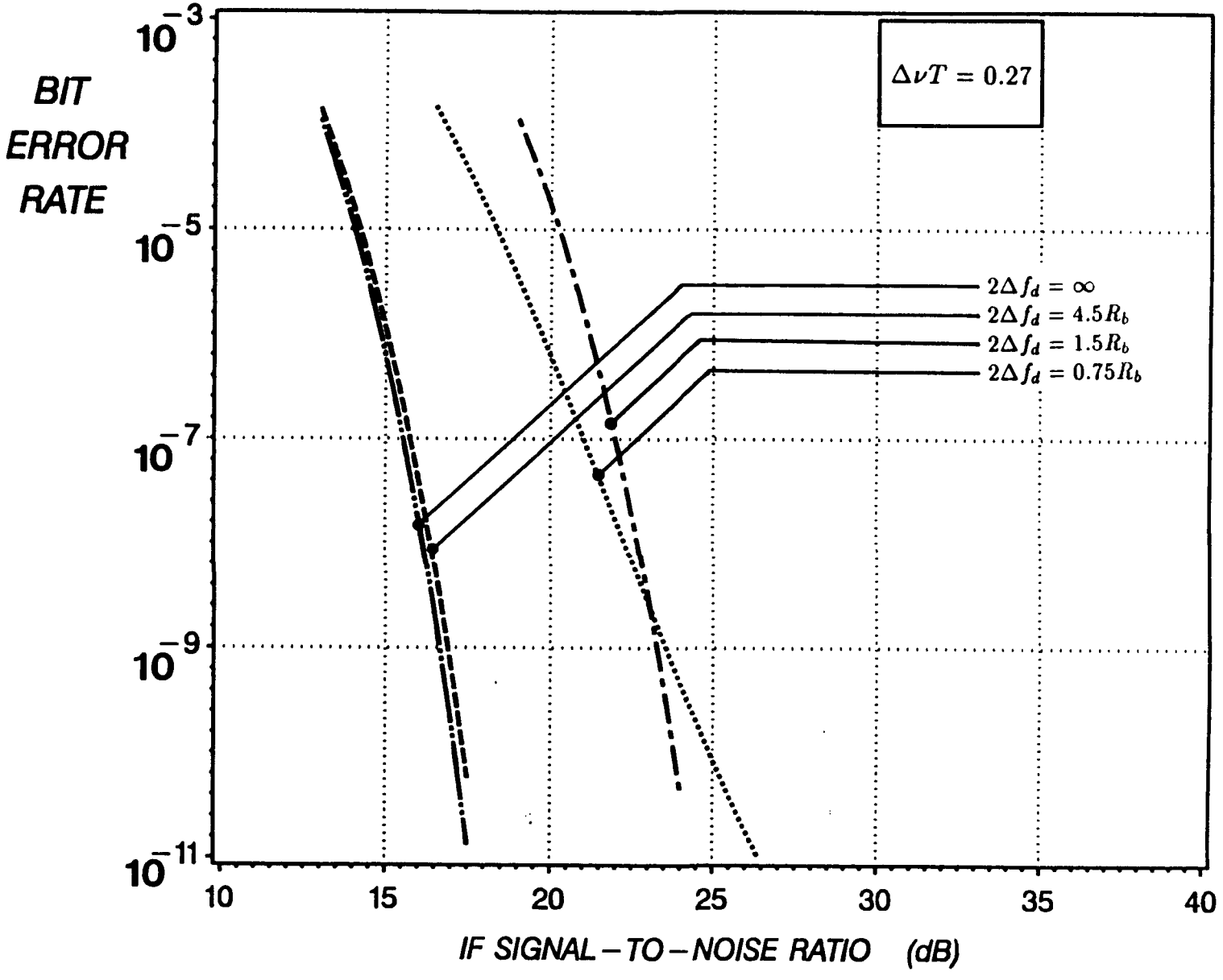
BIT ERROR RATE
10^{-3}
10^{-5}
10^{-7}
10^{-9}
10^{-11}
$\Delta\nu T = 0.27$
$2\Delta f_d = \infty$
$2\Delta f_d = 4.5R_b$
$2\Delta f_d = 1.5R_b$
$2\Delta f_d = 0.75R_b$
10
15
20
25
30
35
40
IF SIGNAL – TO – NOISE RATIO (dB)

Figure 8

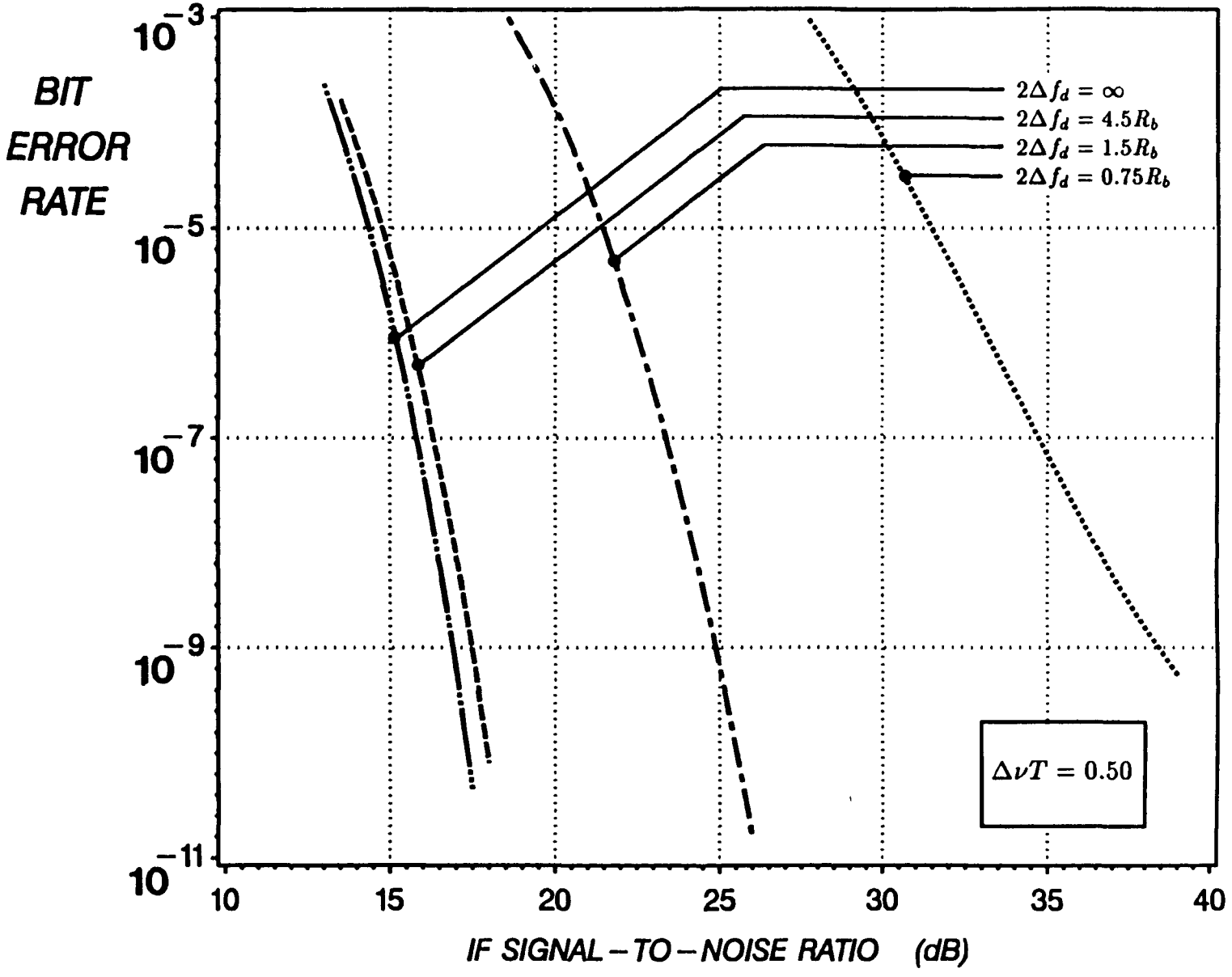
BIT ERROR RATE
10^{-3}
10^{-5}
10^{-7}
10^{-9}
10^{-11}
10
15
20
25
30
35
40
IF SIGNAL – TO – NOISE RATIO (dB)
$2\Delta f_d = \infty$
$2\Delta f_d = 4.5R_b$
$2\Delta f_d = 1.5R_b$
$2\Delta f_d = 0.75R_b$
$\Delta \nu T = 0.50$

Figure 9

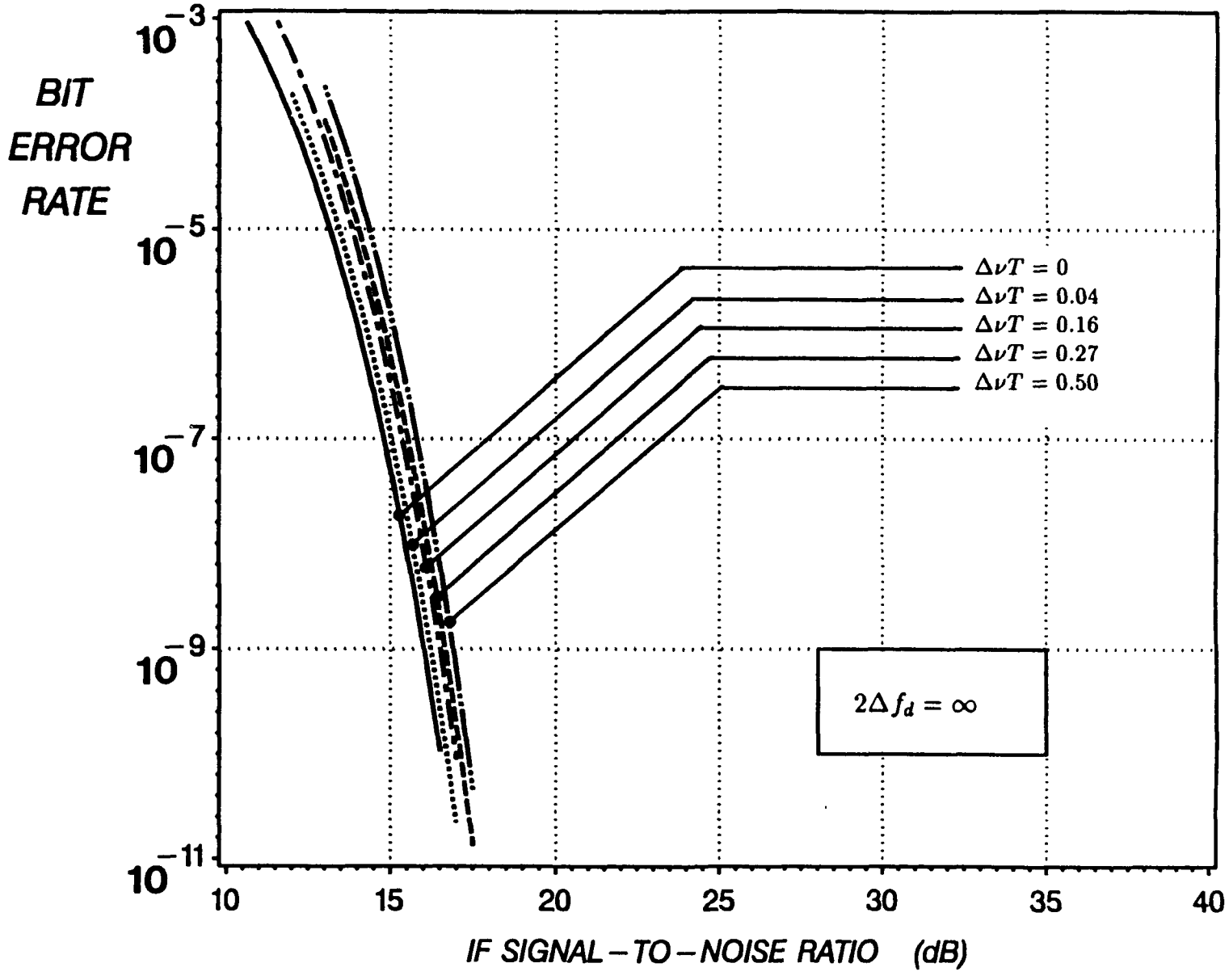
BIT ERROR RATE
10^{-3}
10^{-5}
10^{-7}
10^{-9}
10^{-11}
10
15
20
25
30
35
40
IF SIGNAL – TO – NOISE RATIO (dB)
$\Delta\nu T = 0$
$\Delta\nu T = 0.04$
$\Delta\nu T = 0.16$
$\Delta\nu T = 0.27$
$\Delta\nu T = 0.50$
$2\Delta f_d = \infty$

Figure 10

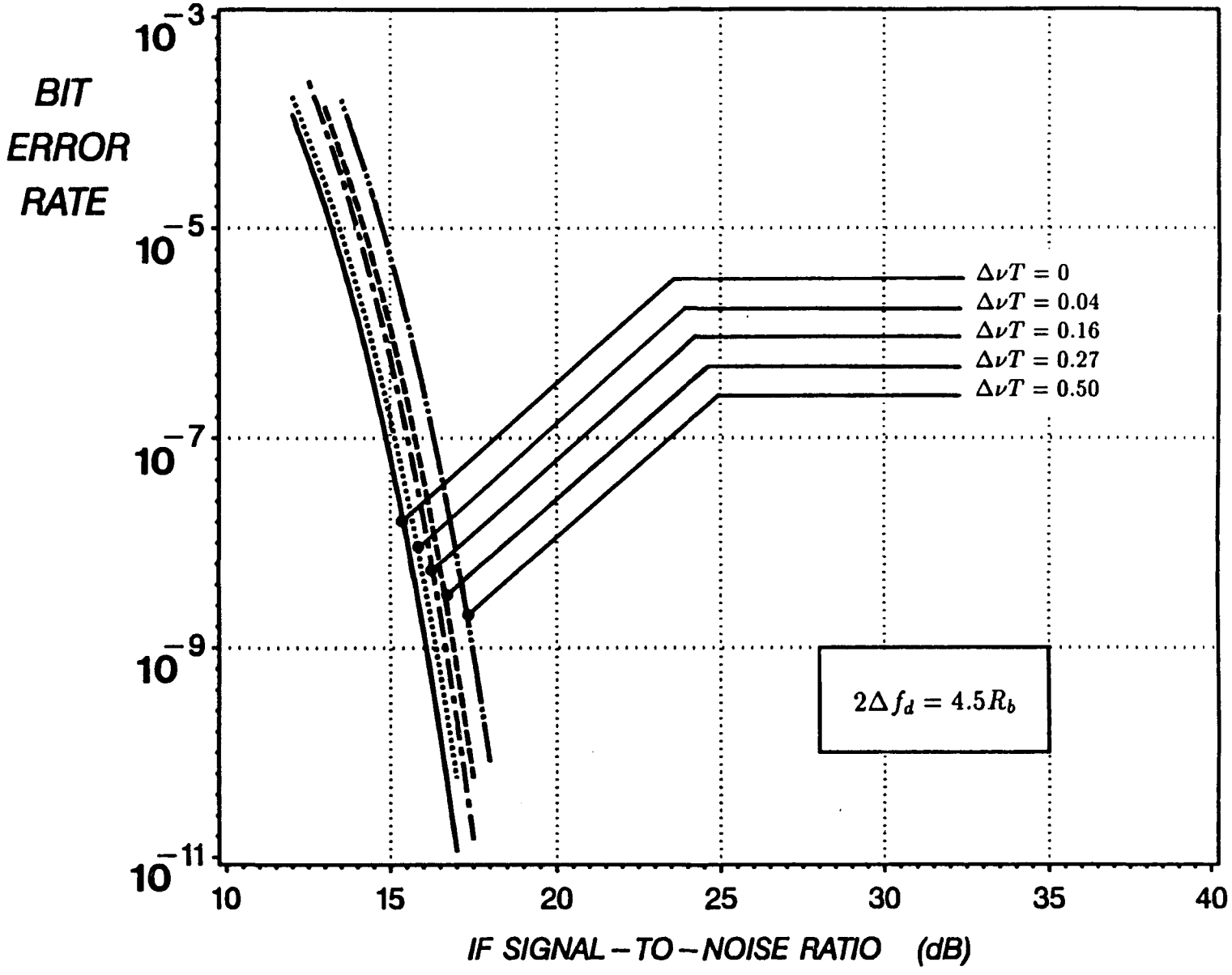
BIT ERROR RATE
10^{-3}
10^{-5}
10^{-7}
10^{-9}
10^{-11}
10
15
20
25
30
35
40
IF SIGNAL – TO – NOISE RATIO (dB)
$\Delta\nu T = 0$
$\Delta\nu T = 0.04$
$\Delta\nu T = 0.16$
$\Delta\nu T = 0.27$
$\Delta\nu T = 0.50$
$2\Delta f_d = 4.5R_b$

Figure 11

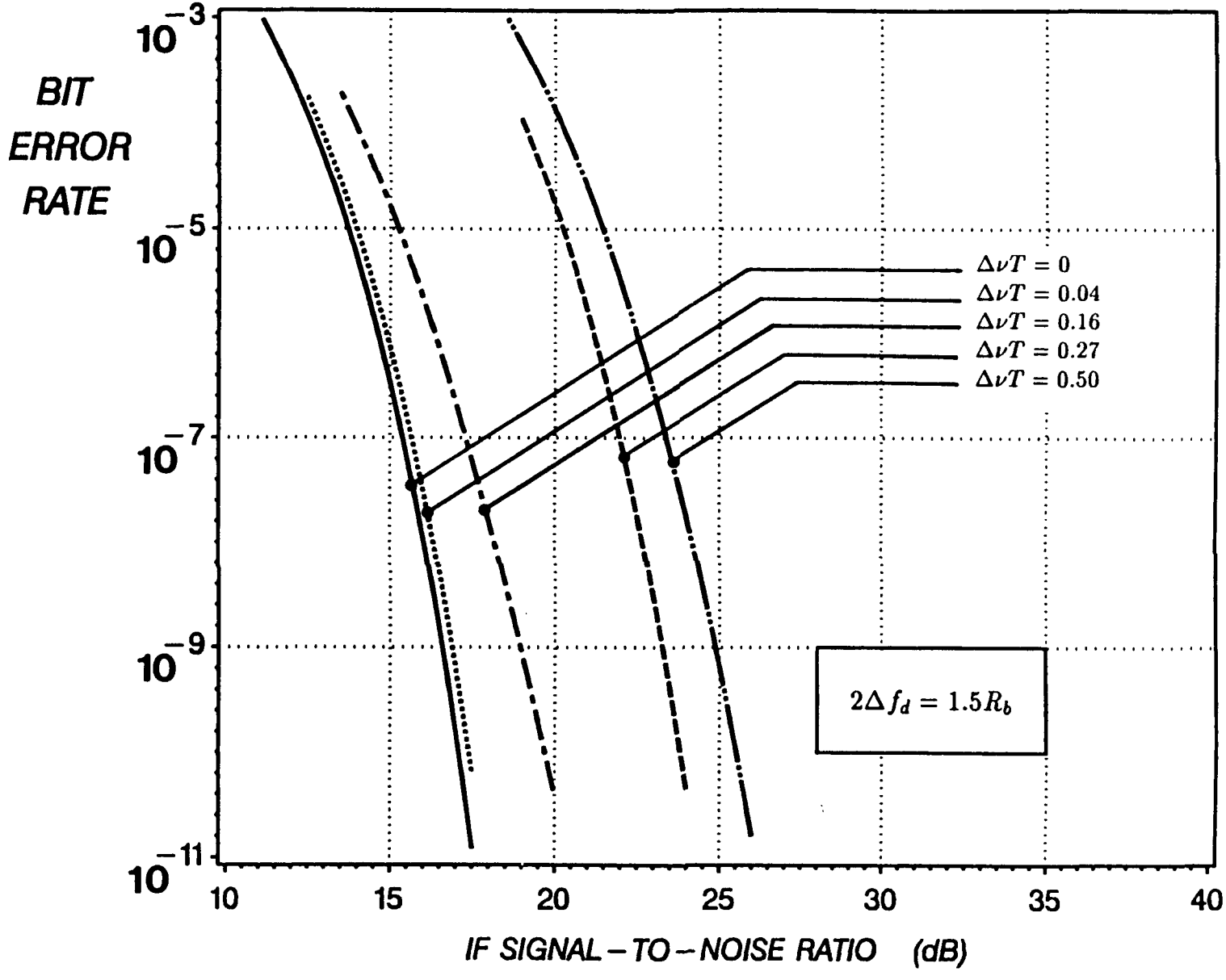
BIT ERROR RATE
10^{-3}
10^{-5}
10^{-7}
10^{-9}
10^{-11}
10
15
20
25
30
35
40
IF SIGNAL – TO – NOISE RATIO (dB)
$\Delta\nu T = 0$
$\Delta\nu T = 0.04$
$\Delta\nu T = 0.16$
$\Delta\nu T = 0.27$
$\Delta\nu T = 0.50$
$2\Delta f_d = 1.5R_b$

Figure 12

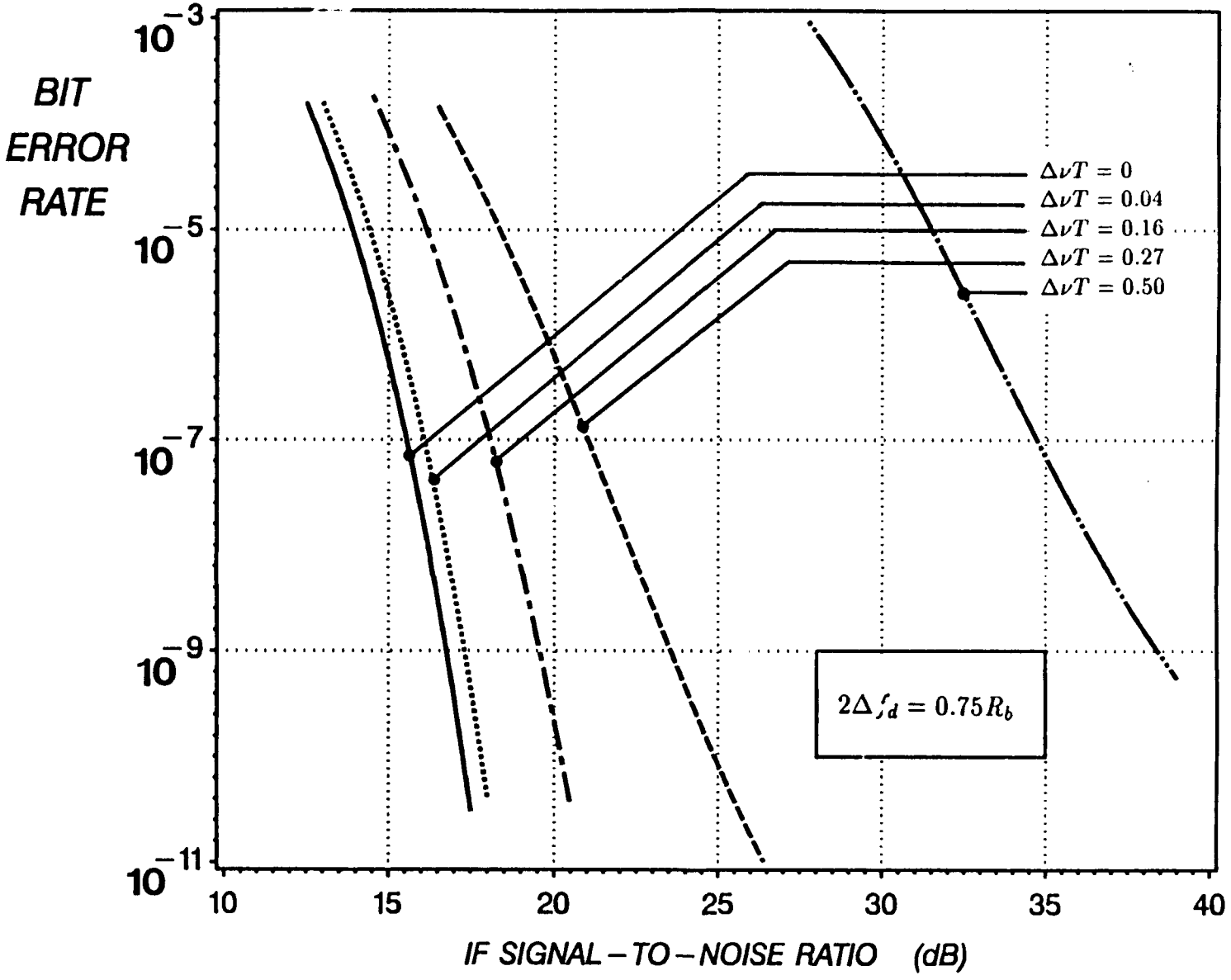
BIT ERROR RATE
10^{-3}
10^{-5}
10^{-7}
10^{-9}
10^{-11}
10
15
20
25
30
35
40
IF SIGNAL – TO – NOISE RATIO (dB)
$\Delta\nu T = 0$
$\Delta\nu T = 0.04$
$\Delta\nu T = 0.16$
$\Delta\nu T = 0.27$
$\Delta\nu T = 0.50$
$2\Delta f_d = 0.75 R_b$

Figure 13

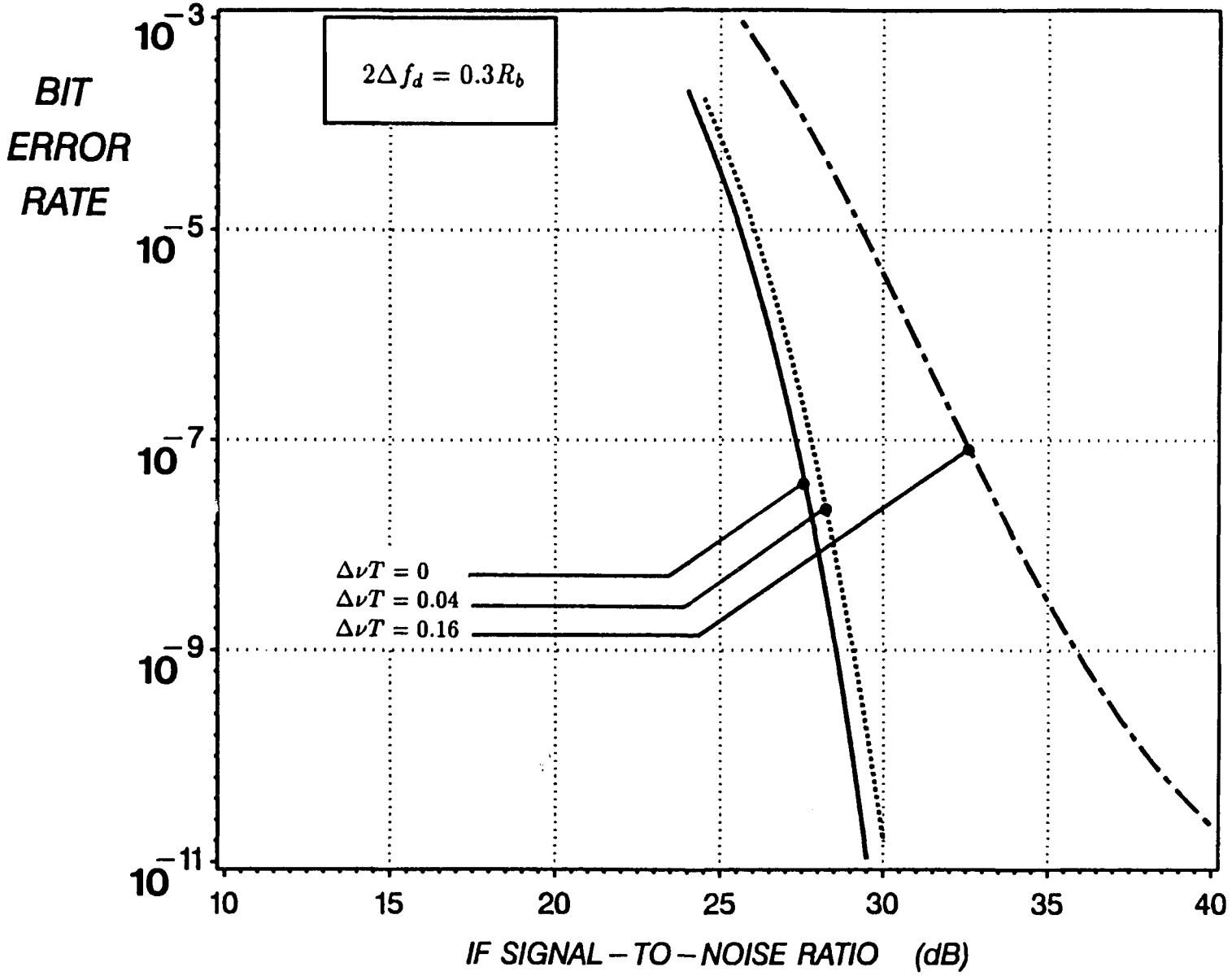
BIT ERROR RATE
10^{-3}
10^{-5}
10^{-7}
10^{-9}
10^{-11}
$2\Delta f_d = 0.3R_b$
$\Delta\nu T = 0$
$\Delta\nu T = 0.04$
$\Delta\nu T = 0.16$
10
15
20
25
30
35
40
IF SIGNAL – TO – NOISE RATIO (dB)

Figure 14

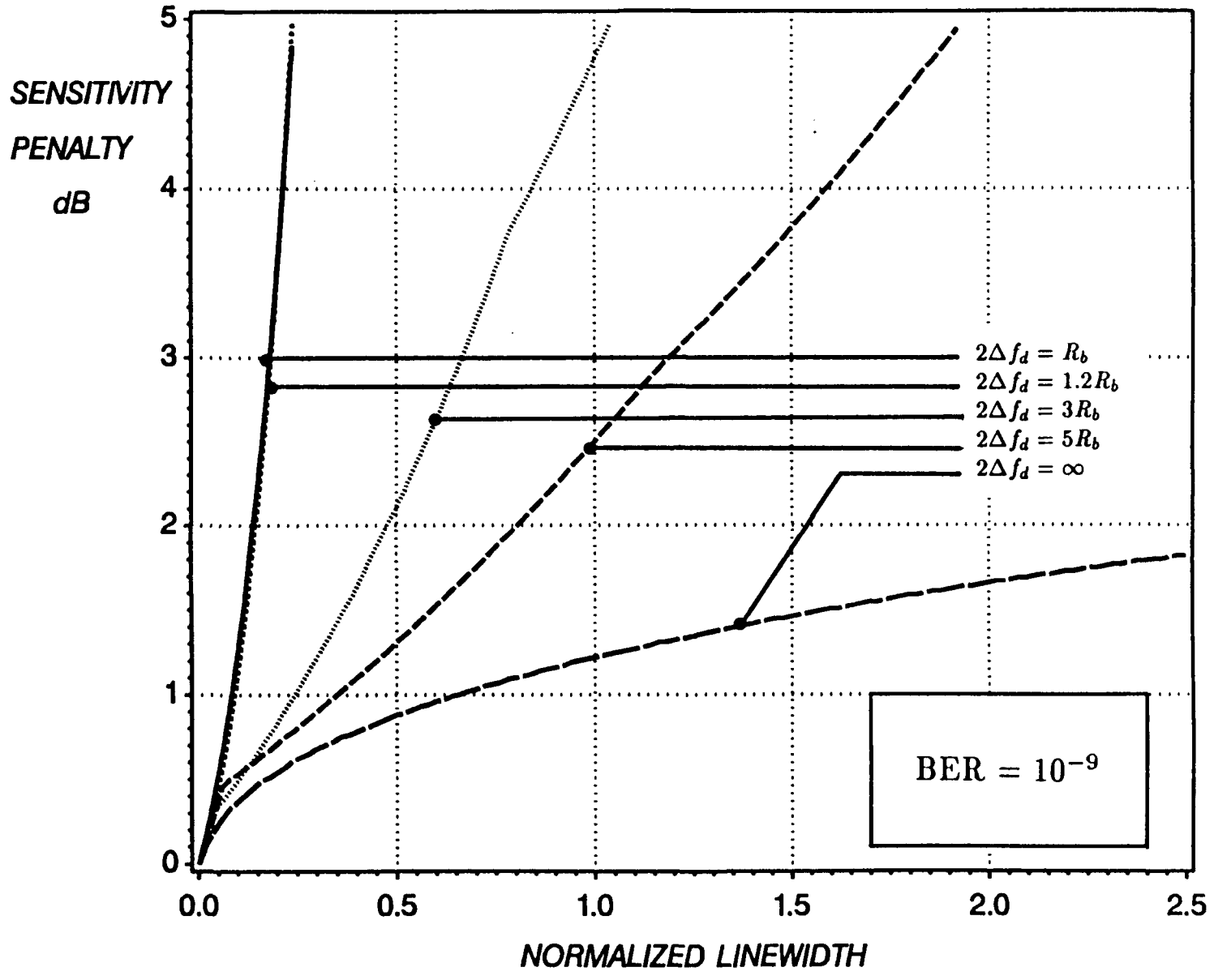
SENSITIVITY
PENALTY
dB
5
4
3
2
1
0
0.0
0.5
1.0
1.5
2.0
2.5
NORMALIZED LINEWIDTH
$2\Delta f_d = R_b$
$2\Delta f_d = 1.2R_b$
$2\Delta f_d = 3R_b$
$2\Delta f_d = 5R_b$
$2\Delta f_d = \infty$
BER = 10^{-9}

Figure 15

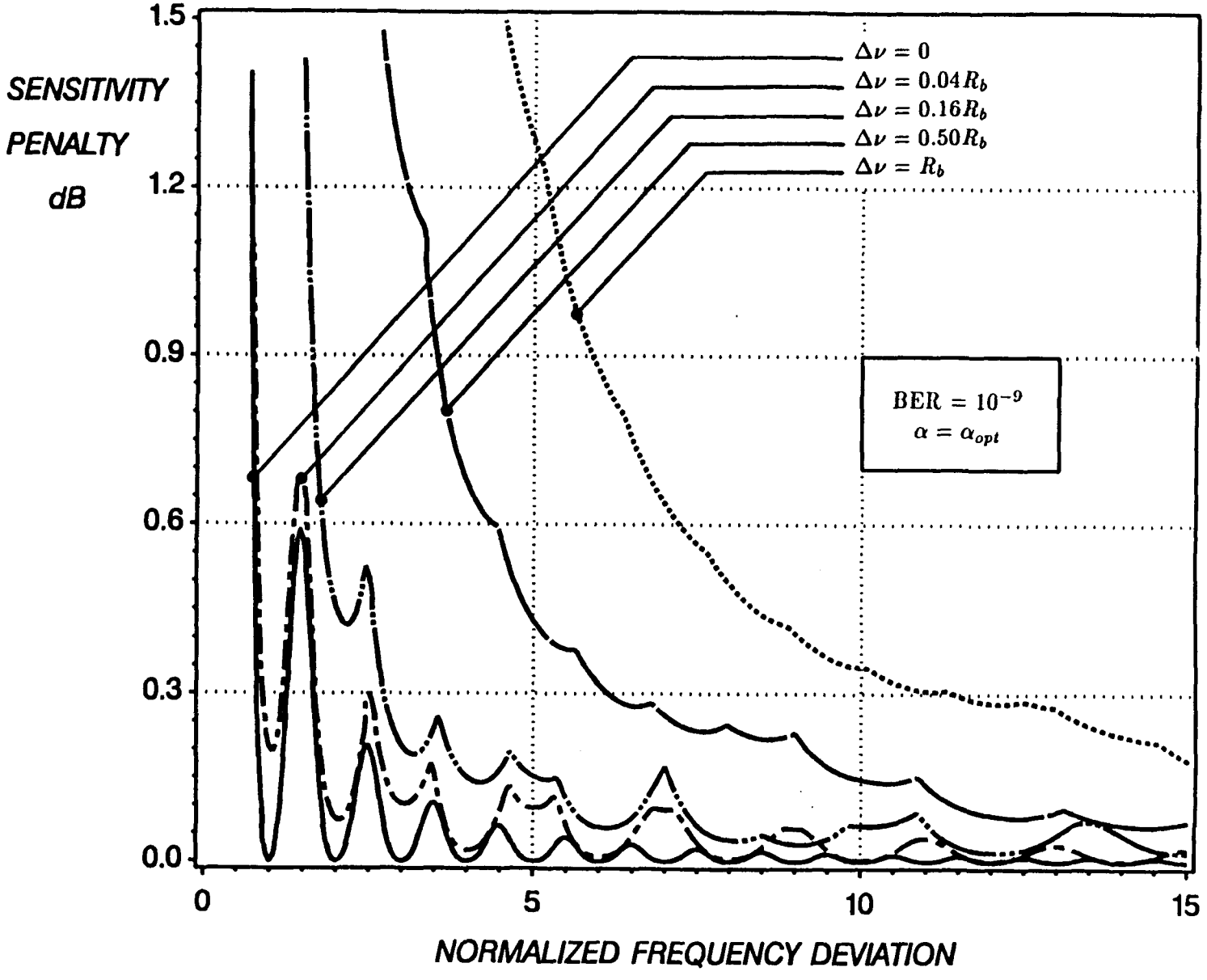
SENSITIVITY
PENALTY
dB
1.5
1.2
0.9
0.6
0.3
0.0
0
5
10
15
NORMALIZED FREQUENCY DEVIATION
$\Delta\nu = 0$
$\Delta\nu = 0.04R_b$
$\Delta\nu = 0.16R_b$
$\Delta\nu = 0.50R_b$
$\Delta\nu = R_b$
BER = 10^{-9}
$\alpha = \alpha_{opt}$

Figure 16

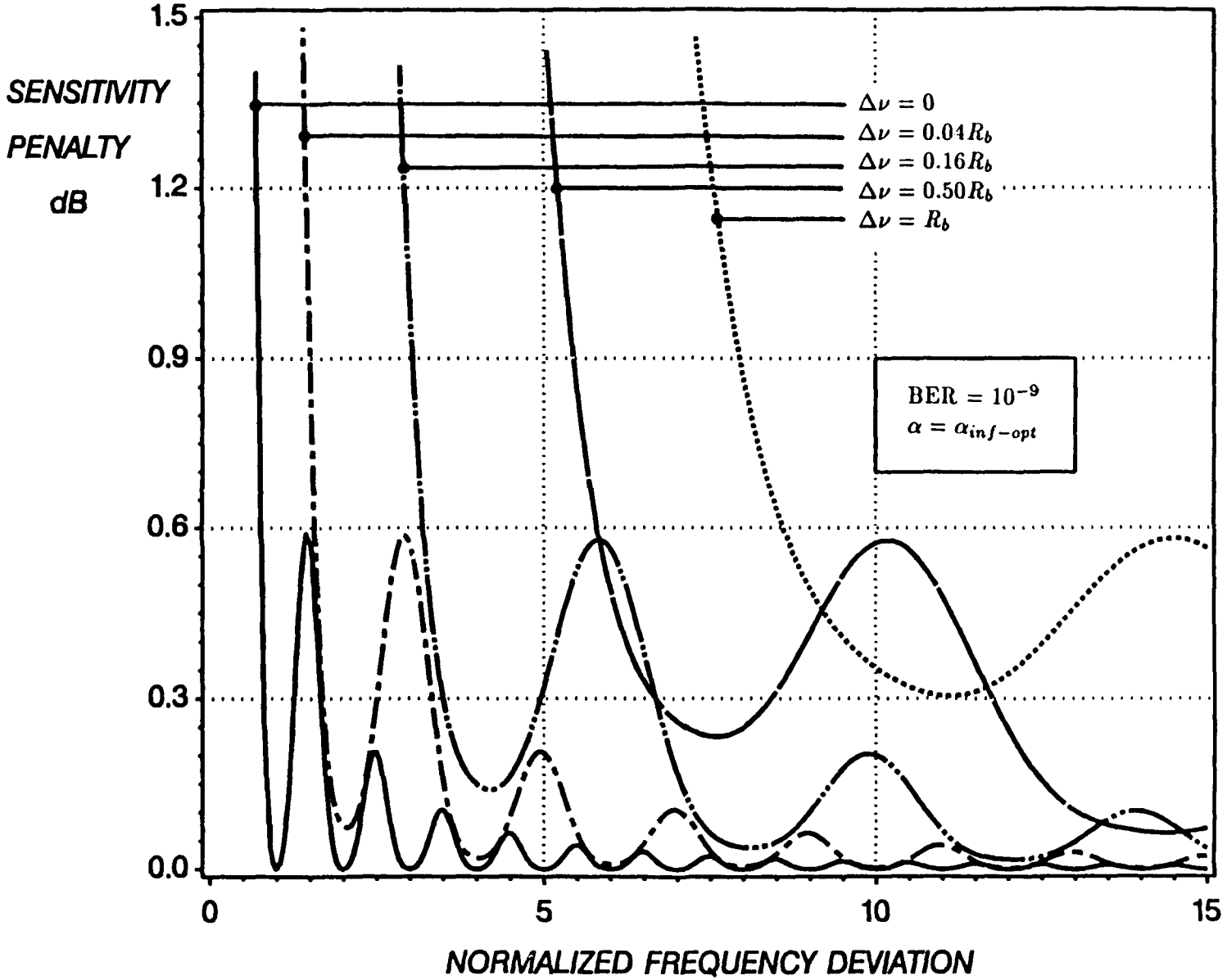
SENSITIVITY
PENALTY
dB
1.5
1.2
0.9
0.6
0.3
0.0
0
5
10
15
NORMALIZED FREQUENCY DEVIATION
$\Delta\nu = 0$
$\Delta\nu = 0.04R_b$
$\Delta\nu = 0.16R_b$
$\Delta\nu = 0.50R_b$
$\Delta\nu = R_b$
BER = 10^{-9}
$\alpha = \alpha_{inf-opt}$

Figure 17

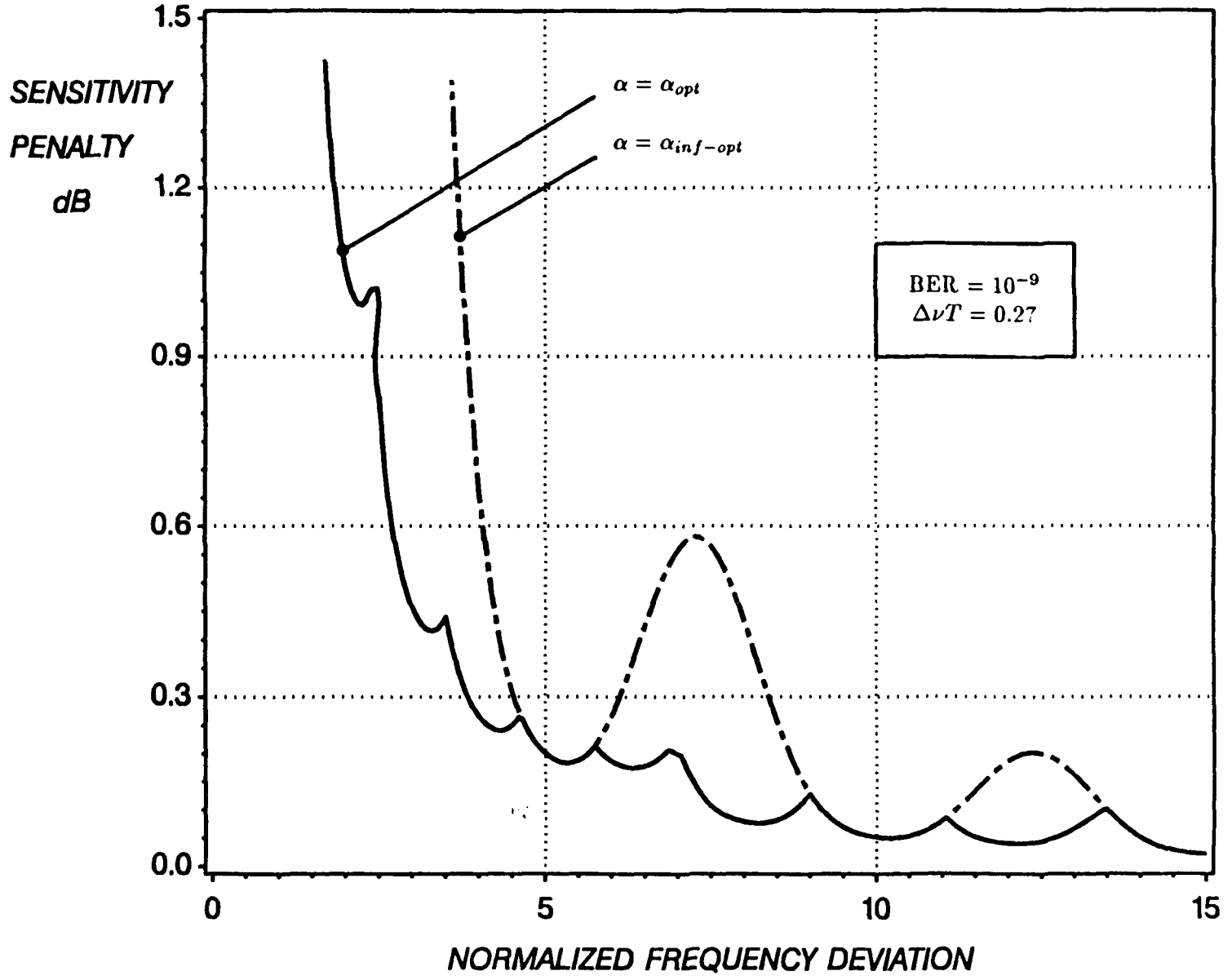
SENSITIVITY
PENALTY
dB
1.5
1.2
0.9
0.6
0.3
0.0
0
5
10
15
NORMALIZED FREQUENCY DEVIATION
$\alpha = \alpha_{opt}$
$\alpha = \alpha_{inf-opt}$
BER = 10^{-9}
$\Delta\nu T = 0.27$

Figure 18

LINEWIDTH-INSENSITIVE COHERENT OPTICAL ANALOG LINKS

Delfin Jay M. Sabido IX, Thomas K. Fong, Robert F. Kalman, and Leonid G. Kazovsky

Stanford University, Department of Electrical Engineering
202 Durand Bldg., Stanford, CA 94305-4055

ABSTRACT

Coherent optical analog links offer several important advantages over conventional direct detection links including the ability to separate wavelength-division multiplexed signals, frequency translation, and utilization of angle modulation formats. However, the wide linewidth of semiconductor lasers can cause substantial performance degradation of these links. This paper analyzes the signal-to-noise ratio and the dynamic range of amplitude modulated (AM) and frequency modulated (FM) coherent links, and compares them to direct detection links. It is concluded that a properly designed AM system is insensitive to laser linewidth. For optical powers less than 1mW, the performance of coherent AM links is better than that of direct detection links; for optical powers greater than 1mW, the performance of the two links is nearly the same. Coherent FM links have the potential to increase the SNR and the dynamic range by more than 10 dB as compared to direct detection and coherent AM links. However, FM links are potentially sensitive to laser linewidth, and require elaborate phase noise cancellation techniques when semiconductor lasers are used.

1. INTRODUCTION

There has been an increasing interest in the use of optical fiber for the transmission of high frequency, high dynamic range analog signals. Applications of analog optical links include antenna remoting, phased array radar, interconnection of microwave systems, and cable television systems [1, 2, 3]. Current approaches utilize direct detection and either Nd:YAG lasers [4, 5, 6] or semiconductor lasers [4, 7, 8]. In this paper, we investigate coherent links employing semiconductor lasers for both signal transmission and heterodyning in the receiver.

Coherent detection facilitates the separation of wavelength division multiplexed signals, can perform frequency translation, and allows the use of alternative modulation formats such as phase and frequency modulation. Semiconductor lasers are attractive due to their ruggedness, compactness, low power consumption, convenient frequency tunability and integratability with other optical and electrical devices. However, semiconductor lasers have the disadvantage of wide linewidths ranging from 1 MHz to 100 MHz. Since coherent systems can detect the phase of the optical signal, they are potentially susceptible to the effects of phase noise associated with wide laser linewidths. This phenomenon represents a major obstacle to the practical implementation of coherent analog optical links.

Several techniques for fighting laser phase noise have been proposed and demonstrated for *digital* systems. In contrast, the issue of obtaining linewidth-insensitive performance in coherent *analog* systems has received little -- if any -- attention. In this paper, we present optical signal transport systems which have the potential to be insensitive to laser linewidth. We perform a theoretical analysis of the signal-to-noise ratio (SNR) and the dynamic range of AM and FM heterodyne systems and compare the results to those of direct detection systems.

The rest of the paper is organized as follows: Section 2 contains the definition of the dynamic range. The performance of a conventional direct detection system is reviewed briefly in section 3 while AM and FM coherent systems are dealt with in sections 4 and 5, respectively. Comparison between coherent AM, coherent FM, and direct detection systems is conducted in section 6 and conclusions are contained in section 7.

2. DEFINITION OF DYNAMIC RANGE

The dynamic range is defined as the ratio of the maximum input RF power $P_{in,max}$ to the minimum input RF power $P_{in,min}$ that can be carried by the fiber optic link [9]:

$$DR = 10\log\left(\frac{P_{in,max}}{P_{in,min}}\right) \tag{1}$$

Since the square of the modulation index m is proportional to the input RF power, (1) can be rewritten as follows:

$$DR = 10\log\left(\frac{m_{max}^2}{m_{min}^2}\right) \tag{2}$$

where m_{min} and m_{max} are the minimum and maximum modulation indexes the system can handle, respectively. m_{min} is the modulation index of the input signal that results in equal signal and noise powers (SNR = 1). For systems with inherent nonlinearities in its components (in other words, for all practical systems), the maximum modulation index is limited by third order intermodulation distortions (IMD). To evaluate the relative magnitude of the IMDs, two equal amplitude signals at frequencies ω_1 and ω_2 are transmitted through the system and the amplitude of the third order terms at frequencies $2\omega_1$-ω_2 and $2\omega_2$ - ω_1 are measured. The third order IMDs increase as the cube of the input voltage while the useful signal grows linearly. This behavior is illustrated in Fig. 1a. m_{max} is the value of m that makes the IMD power equal to the noise power:

$$\left\langle i_{IMD}^2 \right\rangle\Big|_{m_{max}} = \left\langle i_{noise}^2 \right\rangle\Big|_{m_{max}} \tag{3}$$

where i_{IMD} and i_{noise} are the third order distortion and noise currents at the output of the receiver, respectively. When m_{max} is defined as per (3), the ratio defined by (2) is called the spurious-free dynamic range (SFDR):

$$SFDR = 10\log\left[\frac{m^2\big|_{IMD=noise}}{m^2\big|_{signal=noise}}\right] \tag{4}$$

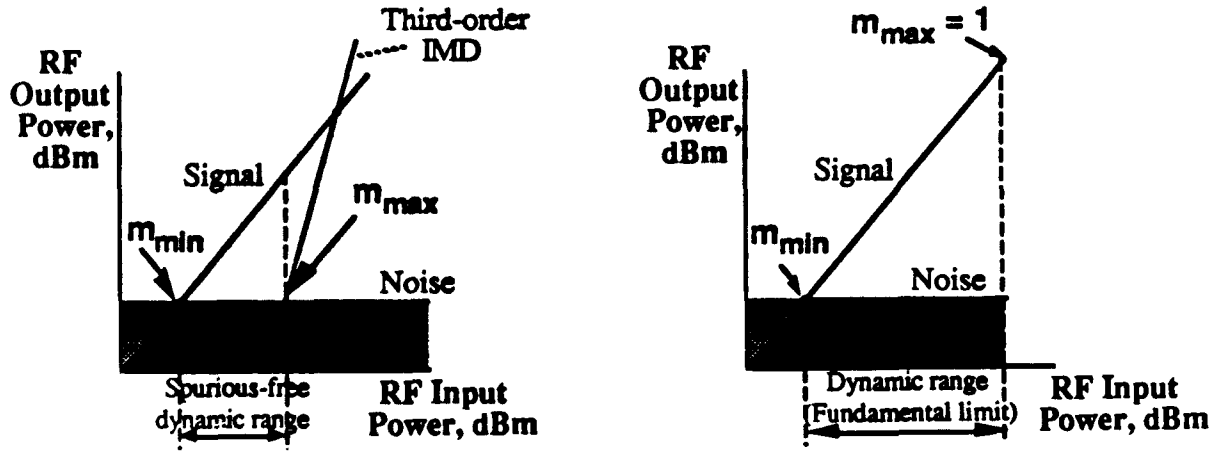

Fig. 1. Definitions of the dynamic range: (a) The spurious-free dynamic range (SFDR); (b) The fundamental limit of the dynamic range.

In the absence of any nonlinearities m_{max} equals one and (2) becomes:

$$DR_{fund} = 10\log\left(\frac{1}{m_{min}^2}\right) \tag{5}$$

where DR_{fund} is the fundamental limit of the dynamic range illustrated in Fig. 1b. Clearly, SFDR can never exceed DR_{fund}.

3. DIRECT DETECTION LINKS

In this section, we review direct detection links. The results of this section will serve as a basis for comparison with the coherent AM and FM systems presented in sections 4 and 5, respectively. The impact of laser relative intensity noise (RIN) is neglected in this section and in the initial analysis of the AM coherent system; it is dealt with in section 4.

The block diagram of an externally modulated direct detection system is shown in Fig. 2. The light from the transmitting laser is modulated by an external Mach-Zehnder modulator.

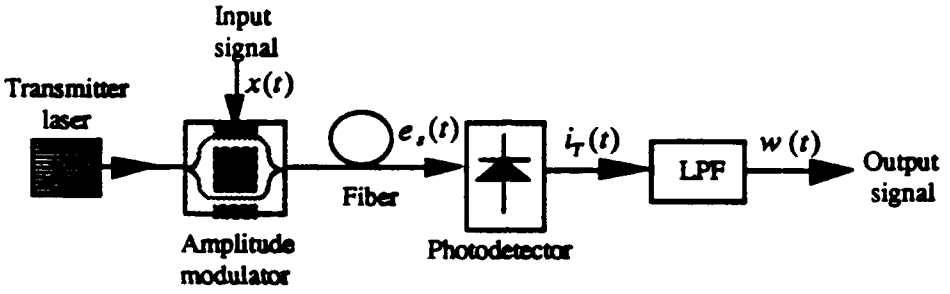

Fig. 2. Block diagram of a direct detection receiver.

It can be shown that the received optical field $e_S(t)$ is given by:

$$e_s(t) = \sqrt{\frac{P_s}{2}}\left\{\exp\left(j\left[\omega_s t + \phi_{ns}(t) + m\cdot x(t)\right]\right) + \exp\left(j\left[\omega_s t + \phi_{ns}(t) + \frac{\pi}{2}\right]\right)\right\} \tag{6}$$

where $x(t)$ is the input RF voltage (normalized to unity amplitude); P_S is the received optical power; ω_S and $\phi_{nS}(t)$ are the optical carrier frequency and phase noise of the laser transmitter, respectively; and m is the modulation index defined by the following expression:

$$m = \frac{\pi}{2}\frac{V_p}{V_\pi} \tag{7}$$

where Vp is the peak amplitude of the applied RF voltage and V_π is the half-wave voltage of the modulator. The output current of the photodetector is:

$$i_T(t) = R\left|e_s(t)\right|^2 + n(t) = RP_s\left[1+\sin\left(m\cdot x(t)\right)\right] + n(t) \tag{8}$$

where R is the photodetector responsivity and $n(t)$ is the additive white Gaussian noise at the output of the photodetector consisting of the shot and thermal noises. The single-sided PSD of $n(t)$ is given by:

$$S_n(f) = \eta = \eta_{sh} + \eta_{th} = 2eRP_s + \frac{4kT}{r}, \qquad \text{for } 0 < f < \infty \tag{9}$$

where η_{sh} and η_{th} are the PSD's of the shot noise and thermal noise, respectively, e is the electron charge, k is the Boltzmann's constant, T is the receiver noise temperature, and r is the input resistance of the amplifier.

To determine the fundamental limit of the performance of this system, we assume for a moment that the external modulator is replaced by an ideal modulator having no nonlinear distortions in the region of operation. Then $\sin m\,x(t) \approx m\,x(t)$ and (8) becomes:

Fundamental limit: $$i_T(t) = RP_s[1 + m \cdot x(t)] + n(t) \tag{10}$$

The SFDR is evaluated by assuming a nonlinear external modulator with the third order terms being the dominant IMDs. In this case,

$$\sin[m \cdot x(t)] \approx m \cdot x(t) - \frac{[m \cdot x(t)]^3}{3} \tag{11}$$

and (8) becomes

$$i_T(t) = RP_s\left\{1 + m \cdot x(t) - \frac{[m \cdot x(t)]^3}{3}\right\} + n(t) \tag{12}$$

Similar to [10] and [11], we assume the low pass filter to have an impulse response of

$$h_L(t) = \begin{cases} 2B, & \text{for } t \in \left[0, \frac{1}{2B}\right] \\ 0, & \text{for } t \notin \left[0, \frac{1}{2B}\right] \end{cases} \tag{13}$$

where B is the noise equivalent bandwidth. The output signal $w(t)$ is then expressed as:

$$w(t) = h_L(t) \bullet i_T(t) \tag{14}$$

Substituting (10) and (13) into (14) and evaluating the total received power, the SNR and DR_{fund} are found to be:

$$SNR = \frac{1/2 \cdot m^2 R^2 P_s^2 \cdot \mathrm{sinc}^2\left(\frac{\omega_m}{4\pi B}\right)}{\eta B} \tag{15}$$

$$DR_{fund} = 10\log\left[\frac{R^2 P_s^2 \cdot \mathrm{sinc}^2\left(\frac{\omega_m}{4\pi B}\right)}{2\eta B}\right] \tag{16}$$

where η is the PSD of the additive noise given by (9), and ω_m is the frequency (or center frequency of the two-tone signal) of the transmitted RF signal. Similarly, using (12) in (14) and evaluating the total output power, the SFDR is found to be:

$$SFDR = 10\log\left[4\left(\frac{R^2 P_s^2 \cdot \mathrm{sinc}^2\left(\frac{\omega_m}{4\pi B}\right)}{\eta B}\right)^{2/3}\right] \tag{17}$$

The numerators of (15), (16), and (17) represent the signal while their denominators represent the noise. In the following sections, we present AM and FM coherent systems and compare their performance with the direct detection results given by (15), (16), and (17).

4. AM-WIRNA HETERODYNE LINKS

Wideband filter-rectifier-narrow-band filter (WIRNA) processing has been shown to be effective in achieving linewidth insensitive performance in amplitude shift keying (ASK) and wide-deviation frequency shift keying (FSK) homodyne and heterodyne digital systems [11, 12, 13]. Since the phase information is discarded in the WIRNA receiver, it works effectively with amplitude modulation (AM). In this section, we analyze the SNR and dynamic range performance of the AM-WIRNA heterodyne receiver.

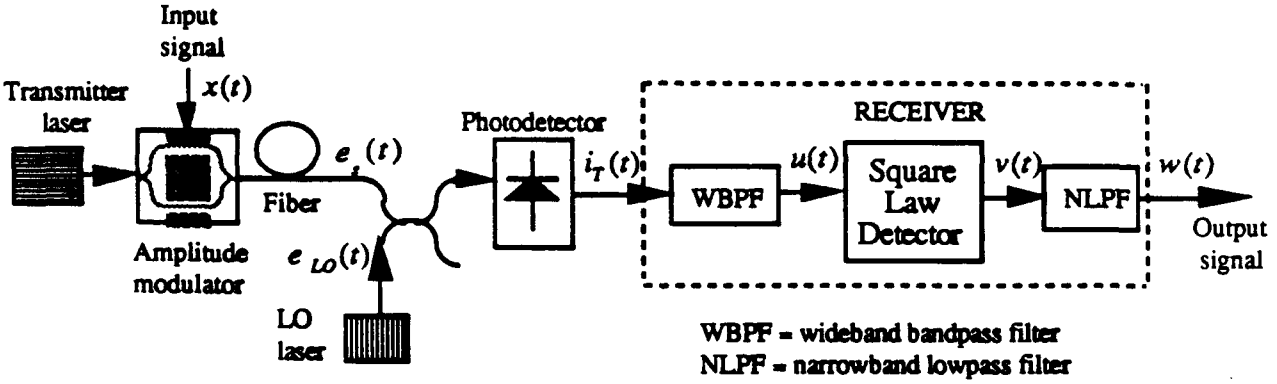

Fig. 3. Block diagram of the AM-WIRNA heterodyne link.

4.1 Analysis of the AM-WIRNA heterodyne link

The block diagram of the AM-WIRNA heterodyne system is shown in Fig. 3. Using the same modulator as in the direct detection system of section 3, the received optical signal $e_s(t)$ is given by (6). The local oscillator (LO) laser has an optical field $e_{LO}(t)$ given by:

$$e_{LO}(t) = \sqrt{P_{LO}} \cdot \exp\left\{j\left[\omega_{LO} t + \phi_{nLO}(t)\right]\right\} \tag{18}$$

where P_{LO}, ω_{LO} and $\phi_{nLO}(t)$ are the optical power, optical carrier frequency and phase noise of the local oscillator laser, respectively. The output current of the photodetector $i_T(t)$ is thus given by:

$$i_T(t) = R\left|e_s(t) + e_{LO}(t)\right|^2 + n(t)$$
$$= \frac{A_s}{\sqrt{2}}\left[\cos(m\cdot x(t))\cdot\cos(\omega t + \phi(t)) - (1+\sin(m\cdot x(t)))\cdot\sin(\omega t + \phi(t))\right] + n(t) \quad (19)$$

where A_S is the signal amplitude, ω is the intermediate frequency (IF) in radians per second, $\phi(t)$ is the total phase noise, and $n(t)$ is the total additive noise at the output of the photodetector with a PSD of:

$$S_n(f) = 2eR(P_{LO} + P_s) + \frac{4kT}{r}, \qquad \text{for } 0 < f < \infty \quad (20)$$

The quantities A_S, ω and $\phi(t)$ are given by the following expressions:

$$A_s(t) = 2R\sqrt{P_s P_{LO}} \qquad \text{amperes} \quad (21)$$

$$\omega = \omega_s - \omega_{LO} \qquad \text{radians per second} \quad (22)$$

$$\phi(t) = \phi_s(t) - \phi_{LO}(t) \qquad \text{radians} \quad (23)$$

The derivative of $\phi(t)$ has a zero mean Gaussian probability density with a power spectral density (PSD) of [14]:

$$S_{\dot\phi}(f) = 4\pi\Delta\nu, \qquad \text{for } 0 < f < \infty \quad (24)$$

where $\Delta\nu = \Delta\nu_s + \Delta\nu_{LO}$ is the full width-at-half-maximum (FWHM) linewidth at the IF, and $\Delta\nu_s$ and $\Delta\nu_{LO}$ are the linewidths of the transmitter and LO lasers, respectively.

To determine the fundamental limit of the dynamic range of this system, we assume that $\sin mx(t) \approx mx(t)$ and $\cos m\,x(t) \approx 1$; then (19) becomes:

Fundamental limit:
$$i_T(t) = \frac{A_s}{\sqrt{2}}\left[\cos(\omega t + \phi(t)) - (1 + m\cdot x(t))\cdot\sin(\omega t + \phi(t))\right] + n(t) \quad (25)$$

When nonlinearities are considered, the approximation in (11) is used for the sine term in (19) while $\cos m\,x(t) \equiv 1$ since the even-ordered terms are canceled by the receiver. Then (19) becomes:

$$i_T(t) = \frac{A_s}{\sqrt{2}}\left[\cos(\omega t + \phi(t)) - \left\{1 + m\cdot x(t) - \frac{(m\cdot x(t))^3}{3}\right\}\cdot\sin(\omega t + \phi(t))\right] + n(t) \quad (26)$$

The current $i_T(t)$ is processed by the bandpass filter (BPF) such that $u(t) = h_B(t)\cdot i_T(t)$, where $h_B(t)$ is the impulse response of the BPF. Similar to [10] and [11], we assume $h_B(t)$ to be:

$$h_B(t) = \begin{cases} 2B_1\cos\omega t, & \text{for } t \in \left[0, \dfrac{1}{B_1}\right] \\ 0, & \text{for } t \notin \left[0, \dfrac{1}{B_1}\right] \end{cases} \quad (27)$$

where B_1 is the noise equivalent bandwidth of the BPF. At the output of the square law detector (SLD):

$$v(t) = [u(t)]^2 \tag{28}$$

and finally, the output signal of the LPF and of the system $w(t)$ is expressed as:

$$w(t) = h_L(t) \cdot i_T(t) \tag{29}$$

where $h_L(t)$ is the impulse response of the LPF given by:

$$h_L(t) = \begin{cases} 2B_2, & \text{for } t \in \left[0, \dfrac{1}{2B_2}\right] \\ 0, & \text{for } t \notin \left[0, \dfrac{1}{2B_2}\right] \end{cases} \tag{30}$$

where B_2 is the noise equivalent bandwidth of the LPF. Since the laser phase noise causes the received signal spectrum to widen, the selection of B_1 and B_2 is critical to the system performance. If a narrow BPF (with respect to the signal bandwidth) is used, some of the signal power will be lost while a wider BPF will collect more additive noise. In this analysis, we select the BPF bandwidth B_1 to be wide enough to pass 95% of the signal power. From [15], the bandwidth required to accomplish this goal is related to the LPF noise equivalent bandwidth and the total laser linewidth as follows:

$$B_1 = \sqrt{(6B_2)^2 + (12.7 \cdot \Delta\nu)^2} \tag{31}$$

The autocorrelation function of $w(t)$ is evaluated as follows [16]:

$$R_w(\tau) = E\{w(t) \cdot w(t+\tau)\} \tag{32}$$

where $E\{\ \}$ denotes the expectation. Setting τ equal to zero in (32) gives the total output power, P_{out}. The evaluation of P_{out} is extremely complicated, and the resulting expression is very long (it consists of more than 30 convoluted terms). The total output power can be expressed as:

$$\begin{aligned} P_{out} = R_w(0) &= P_{sig} + P_n = P_{sig} + P_{sd} + P_{sn} + P_{nn} \\ &= \Gamma_1 m^2 A_s^4 + (\Gamma_2 m^2 + \Gamma_3) A_s^4 + (\Gamma_4 m^2 + \Gamma_5) A_s^2 \eta + \Gamma_6 \eta^2 \end{aligned} \tag{33}$$

where A_s is the signal amplitude defined in (21); η is the PSD of the additive noise given in (20); m is the modulation index; and all the Γ variables depend on B_1, B_2 and $\Delta\upsilon$ only (Γ_1 depends on B_1 and B_2 only). Table 1 shows values of the Γ variables. The first term in the right hand side of (33) is the desired signal power while the rest are noise contributions whose sum is denoted by P_n.

P_{sd} is the noise generated via the phase-to-intensity noise conversion in the BPF filter. The laser phase noise causes the received spectrum to widen. Therefore, part of the signal spectrum is cut off causing signal distortion and resulting in phase noise-to-amplitude noise conversion. This term is absent for a system with zero laser linewidth since the signal spectrum remains unchanged.

The other two noise terms P_{sn} and P_{nn} are due to the receiver additive noise, caused by shot and thermal noises, and stem from the squaring operation in the receiver. This results in the beat between the signal and the additive noise P_{sn} and the squared additive noise term P_{nn}. The signal distortion noise and signal-noise beat expressions have two terms each. This is caused by the received signal having a carrier and message term. In the

next subsections, the SNR and dynamic range of the AM system will be analyzed and compared with the direct detection receiver discussed in section 3.

Table 1: Values of the Γ variables.

Laser Linewidth	LPF bandwidth B_2	Γ_1	Γ_2	Γ_3	Γ_4	Γ_5	Γ_6
0 MHz	1 GHz	0.3849	0	0	7.58E+08	3.33E+09	8.67E+18
10 MHz	1 GHz	0.3849	4.68E-09	2.46E-09	3.95E+09	1.35E+09	7E+19

4.2 SNR performance of coherent AM links

The SNR of the AM-WIRNA coherent system can be evaluated by taking the ratio of the desired signal power P_{sig} to the total output noise P_n. Using (33), we obtain:

$$SNR = \frac{\Gamma_1 m^2 A_s^4}{\left(\Gamma_2 m^2 + \Gamma_3\right) A_s^4 + \left(\Gamma_4 m^2 + \Gamma_5\right) A_s^2 \eta + \Gamma_6 \eta^2} \tag{34}$$

It is clear from expression (34) that the system has three regions of operation corresponding to each noise term being dominant. For very small P_s, the squared additive noise term dominates and (34) becomes:

$$SNR \approx \frac{\Gamma_1 m^2 A_s^4}{\Gamma_6 \eta^2} = \frac{\Gamma_1 m^2 \cdot 16 R^4 P_{LO}^2 P_s^2}{\Gamma_6 \eta^2} \qquad \text{for very small } P_s \tag{35}$$

Expression (35) predicts a 20 dB/decade increase in the SNR with respect to P_s. For larger optical power, the signal-noise beat term is dominant; it gives a 10 dB/decade increase of SNR vs. P_s:

$$SNR \approx \frac{\Gamma_1 m^2 A_s^2}{\left(\Gamma_4 m^2 + \Gamma_5\right) \eta} = \frac{\Gamma_1 m^2 \cdot 4 R^2 P_{LO} P_s}{\left(\Gamma_4 m^2 + \Gamma_5\right) \eta} \qquad \text{for moderate values of } P_s \tag{36}$$

The signal distortion term due to imperfect phase noise cancellation dominates for large P_s:

$$SNR \approx \frac{\Gamma_1 m^2}{\left(\Gamma_2 m^2 + \Gamma_3\right)} \qquad \text{for large } P_s \tag{37}$$

Expression (37) predicts that the SNR is independent of P_s for large signal power. Thus, for AM coherent systems with a finite laser linewidth, there is a maximum SNR given by (37); increasing the optical power beyond this point will not improve the system performance. For the zero linewidth case, there is no signal distortion so that there are only two regions of operation given by (35) and (36).

The SNR performance of a direct detection receiver has two regions of operation. For small P_s, the dominant noise term is the thermal noise and (15) becomes:

$$SNR \approx \frac{1/2 \cdot m^2 R^2 P_s^2 \cdot \mathrm{sinc}^2\left(\frac{\omega_m}{4\pi B}\right)}{\eta_{th} B} \qquad \text{for small } P_s \qquad (38)$$

while for large P_s the system is shot noise-limited with the SNR given by:

$$SNR \approx \frac{1/2 \cdot m^2 R^2 P_s \cdot \mathrm{sinc}^2\left(\frac{\omega_m}{4\pi B}\right)}{2eRB} \qquad \text{for large } P_s \qquad (39)$$

Expressions (38) and (39) predict 20 dB/decade and 10 dB/decade SNR vs. P_s curves, respectively.

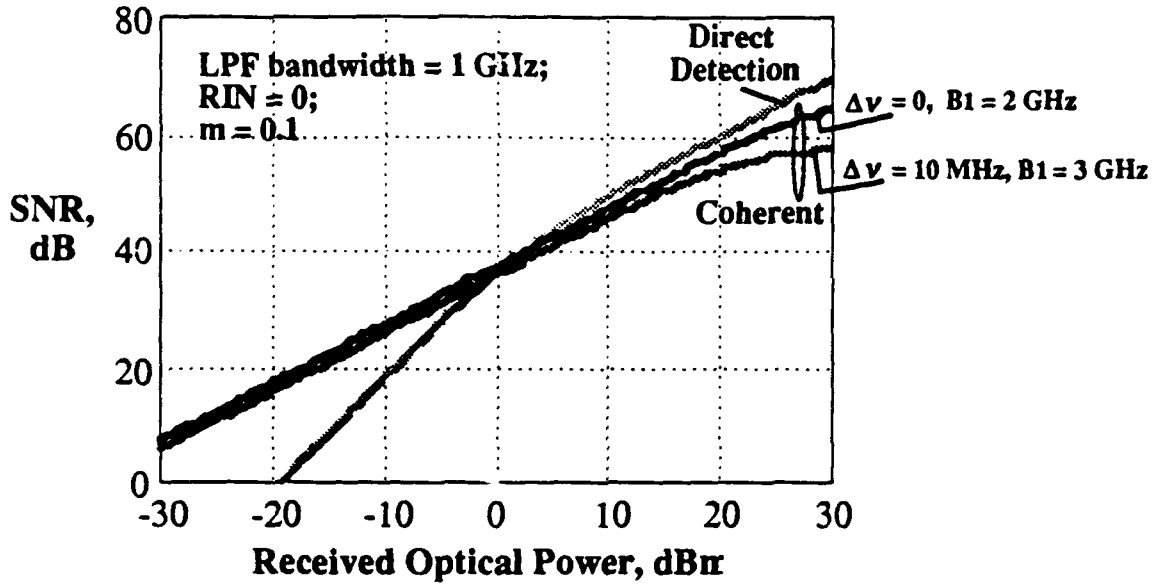

Fig. 4. The SNR versus the received optical power for the AM-WIRNA receiver; r = 50Ω, R = 0.8 A/W, T = 300K, and P_{LO} = 30 dBm.

Fig. 4 shows SNR versus the received optical power for the direct detection and for the AM-WIRNA heterodyne systems. This figure clearly shows the two regions of operation of the direct detection receiver. For small P_s (less than 0 dBm) the AM-WIRNA coherent system performs better than the direct detection system. This is because the thermal noise is dominant in the direct detection case whereas the coherent system is shot noise limited. As P_s is increased, the shot noise for the direct detection system increases until it becomes dominant. For large optical power, the direct detection system performs slightly better. Fig. 4 indicates that there is approximately a 3 dB difference between the direct detection and the zero linewidth AM coherent system for very large P_s.

It is also clear from Fig. 4 that in the coherent system, the signal-noise beat term dominates for the range of Ps considered. Since systems with larger linewidths have larger BPF bandwidths as per (31), more additive noise is collected resulting in a bigger signal-noise beat term and thus a lower SNR for the same P_s. The effect of signal distortion due to non zero linewidth begins to strongly affect the system only for P_s approximately equal to one watt. Thus, for reasonable values of received optical power, the impact of phase noise is small rendering the system linewidth-insensitive.

4.3 Dynamic range of the AM-WIRNA links

The fundamental limit and spurious-free dynamic ranges can be obtained using expressions (5) and (4), respectively, using the procedure discussed in section 2. Since the carrier power is much larger than the signal power and m is much less than one, (33) can be approximated by:

$$P_{out} \approx \Gamma_1 m^2 A_s^4 + \Gamma_3 A_s^4 + \Gamma_5 A_s^2 \eta + \Gamma_6 \eta^2 \tag{40}$$

Further, m_{min} is the modulation index producing $P_{sig} = P_n$. The resulting fundamental limit of the dynamic range is found to be:

$$DR_{fund} = 10 \log \left[\frac{\Gamma_1 A_s^4}{\Gamma_3 A_s^4 + \Gamma_5 A_s^2 \eta + \Gamma_6 \eta^2} \right] \tag{41}$$

For SFDR, m_{max} is the modulation index corresponding to the IMD power equal to P_n. Using the above results and (4), the spurious-free dynamic range for the AM-WIRNA system is:

$$SFDR = 10 \log \left[8 \cdot \left(\frac{\Gamma_1 A_s^4}{\Gamma_3 A_s^4 + \Gamma_5 A_s^2 \eta + \Gamma_6 \eta^2} \right)^{2/3} \right] \tag{42}$$

Fig. 5 shows the dynamic range versus optical power. The dynamic range curves for both the fundamental limit and the SFDR behave very similar to the SNR curves in Fig. 4: for small P_s (less than 0 dBm) the AM-WIRNA coherent system performs better than the direct detection system; for large received optical power, direct detection performs slightly better. There is a 5 to 20 dB difference between the fundamental limit and the SFDR.

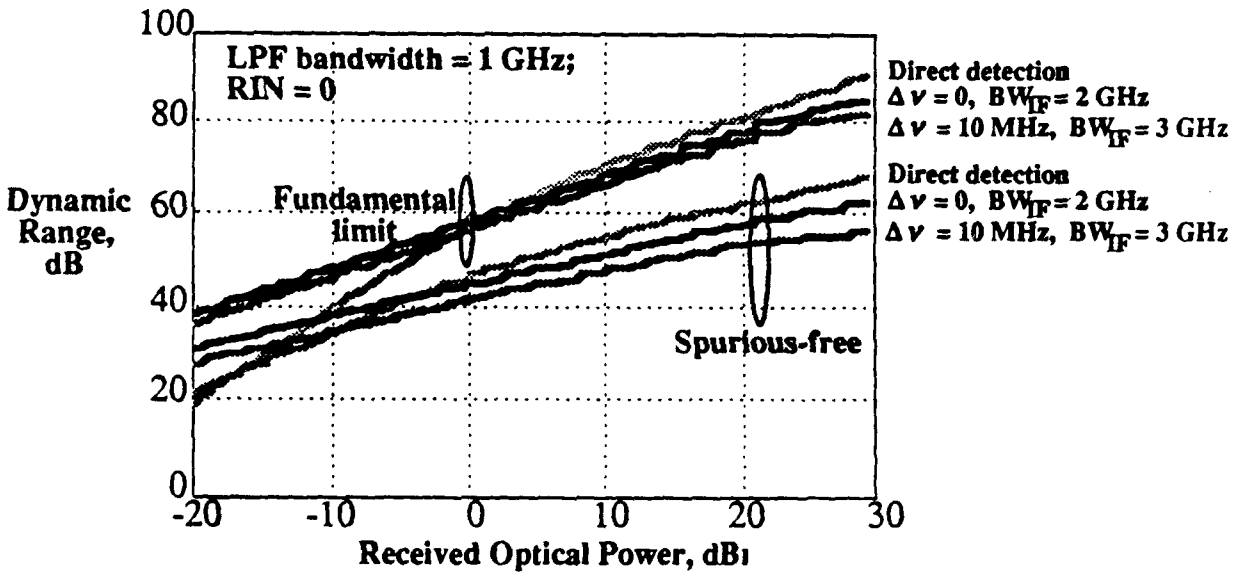

Fig. 5. The dynamic range versus the received optical power for the AM-WIRNA receiver.

4.4 Impact of the LPF bandwidth on the system performance

Fig. 6 shows the fundamental limit of the dynamic range and the spurious-free dynamic range versus the LPF bandwidth B_2 for both direct detection and coherent AM links. The BPF bandwidth B_1 was selected as per (31). Inspection of Fig. 6 shows that direct detection and coherent links have approximately the same performance. This is expected for P_s = 1mW. For large B_2, DR_{fund} is inversely proportional to B_2 while the SFDR is inversely proportional to $B_2^{2/3}$ corresponding to calculated values of 155 dB-Hz and 108 dB-Hz$^{2/3}$, respectively.

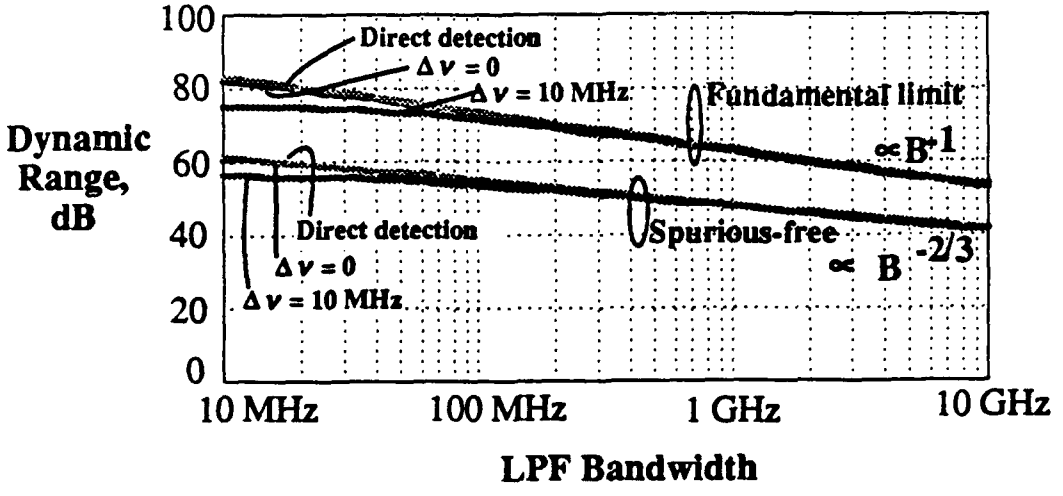

Fig. 6. The dynamic range versus the LPF bandwidth for direct detection and coherent AM-WIRNA links; Ps = 1mW, P_{LO} = 10mW and RIN = 0.

4.5 Impact of laser RIN on the system performance

The impact of laser relative intensity noise (RIN) is easily taken into account by making the following substitutions in the equations for the signal and LO fields:

$$P_s \rightarrow P_s\left[1 + n_{s,RIN}(t)\right] \tag{43}$$

$$P_{LO} \rightarrow P_{LO}\left[1 + n_{LO,RIN}(t)\right] \tag{44}$$

where $n_{s,RIN}(t)$ and $n_{LO,RIN}(t)$ are the RINs of the transmitter and LO lasers, respectively. The power spectral density (PSD) of the laser RIN η_{RIN} is assumed to be white in the region of operation and is given by:

$$\eta_{RIN} = 10^{\frac{RIN}{10}}, \qquad \text{for } 0 < f < \infty \tag{45}$$

where RIN is in dB/Hz. For the direct detection system, RIN manifests itself as an additive noise in the receiver and (9) thus becomes:

$$S_n(f) = \eta = \eta_{sh} + \eta_{th} + R^2 P_s^2 \eta_{RIN} = 2eRP_s + \frac{4kT}{r} + R^2 P_s^2 \cdot 10^{\frac{RIN}{10}}, \qquad \text{for } 0 < f < \infty \tag{46}$$

The expressions for the SNR, DR_{fund} and SFDR for the direct detection receiver still hold true, but with η given by (46).

Due to the presence of two lasers in a coherent system -- the transmitter and LO lasers -- the degradation due to RIN will be greater than that for a direct detection system. RIN affects a coherent system in two ways: first, as an additive noise at the output of the photodetector:

$$S_n(f) = \eta = 2eRP_s + \frac{4kT}{r} + R^2P_s^2 \cdot 10^{\frac{RIN}{10}} + R^2P_{LO}^2 \cdot 10^{\frac{RIN}{10}}, \qquad \text{for } 0 < f < \infty \tag{47}$$

and secondly, as an additional noise term at the receiver output such that (33) becomes:

$$\begin{aligned} P_{out} = {} & \Gamma_1 m^2 A_s^4 + \left(\Gamma_2 m^2 + \Gamma_3\right) A_s^4 + \left(\Gamma_4 m^2 + \Gamma_5\right) A_s^2 \eta + \Gamma_6 \eta^2 \\ & + \Gamma_1 A_s^4 \left(\eta_{s,RIN} B_2 + \eta_{LO,RIN} B_2\right) \end{aligned} \tag{48}$$

Two possible photodetector configurations for a coherent system are: the single photodiode receiver and a balanced receiver. The balanced receiver is more advantageous in that it eliminates the additive laser RIN term at the output of the photodetector (given in (47)). Fig. 7 illustrates the impact of laser RIN on the SFDR. A direct detection system clearly outperforms a coherent system. If good semiconductor lasers with RINs of -160 dB/Hz or better are used, then a coherent system using a balanced receiver is 3 dB worse than a direct detection system. For a coherent system, using a balanced receiver improves the SFDR by 1 to 3 dB.

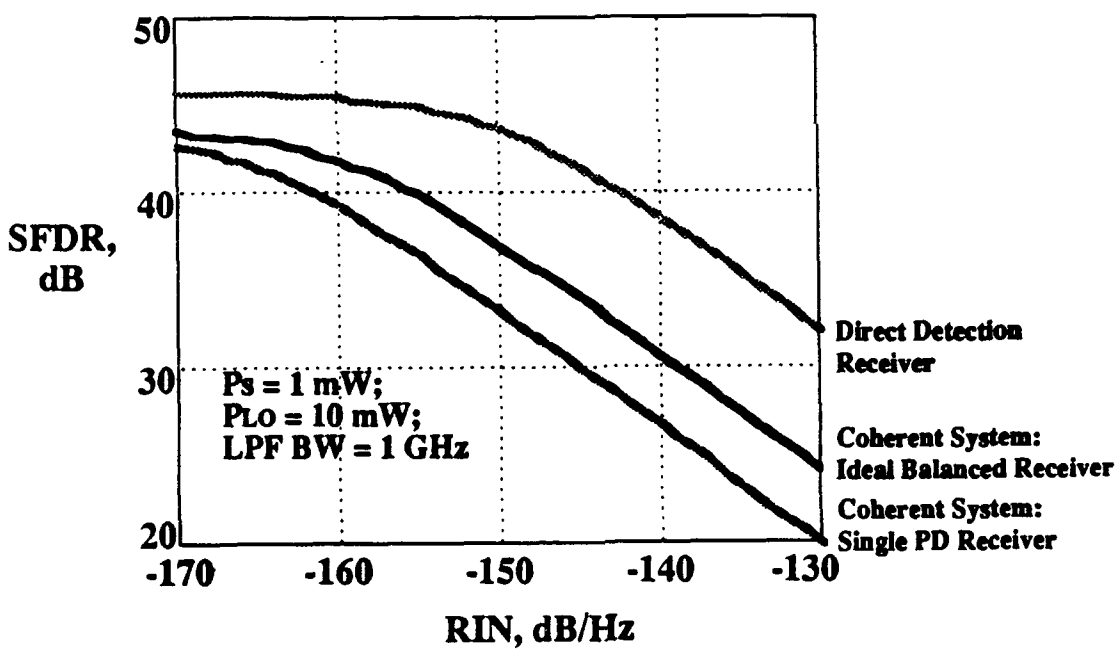

Fig. 7. Impact of laser RIN on the dynamic range of the AM-WIRNA and direct detection receivers.

5. COHERENT FM LINKS

Because the phase information is preserved in the course of coherent detection, angle modulation can be used. Of particular interest is frequency modulation (FM). FM is widely used in commercial radio broadcasting, and offers substantial potential improvements in signal-to-noise ratio (SNR) over AM systems. In this section, we

analyze the SNR of a basic coherent FM optical link. We then consider a modified receiver structure which can provide substantial suppression of phase noise effects.

5.1 Basic FM System Performance

A diagram of the basic system is shown in Fig. 8. The input signal directly frequency modulates a laser diode. The optical output of the laser diode propagates through a fiber to a directional coupler, where it is combined with the light from the LO laser. The combined optical signal is then detected. After detection, the signal encounters a limiter and a FM discriminator, which consists of a differentiator and an envelope detector. Finally, the signal is low pass filtered.

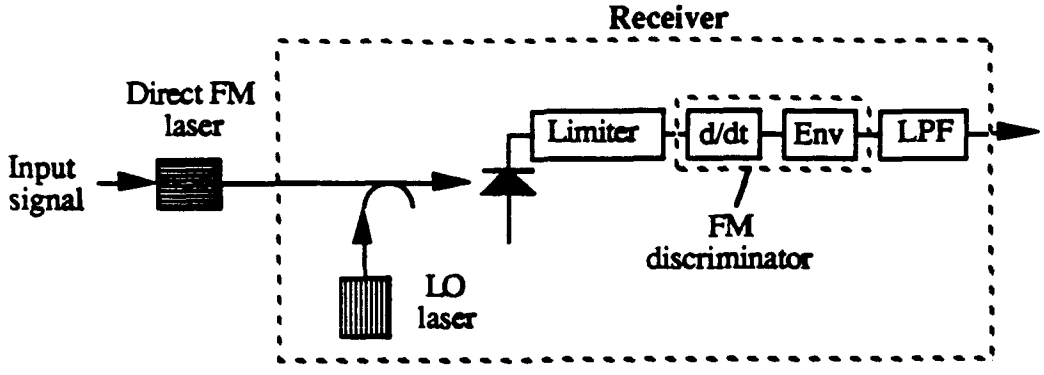

Fig. 8. Coherent FM optical link.

The output optical field from a frequency modulated laser diode is given by

$$e_s(t) = A_s(t)\exp j\left[\omega_s t + \omega_\Delta \int_0^t x(t')dt' + \phi_{ns}(t)\right] \tag{49}$$

where $x(t)$ is the input electrical signal (normalized to unity amplitude), ω_Δ is the angular frequency deviation, ω_S is the optical carrier frequency, $\phi_{nS}(t)$ is the phase noise on the signal laser, and $A_S(t)$ is the field amplitude. Variations in the field amplitude are caused by relative intensity noise (RIN) and by spurious amplitude modulation of the laser output power by the applied signal.

The field emitted by the LO laser is given by

$$e_{LO}(t) = A_{LO}(t)\exp j[\omega_{LO} t + \phi_{nLO}(t)] \tag{50}$$

where ω_{LO} is the optical carrier frequency, $\phi_{nLO}(t)$ is the phase noise on the signal laser, and $A_{LO}(t)$ is the LO field amplitude with variations arising from RIN. The field from the signal laser is heterodyned with the field from the LO laser on the detector, resulting in a detected current of

$$\begin{aligned} i_1(t) &= R\left|e_s(t) + e_{LO}(t)\right|^2 + n_1(t) \\ &= 2RA_s(t)A_{LO}(t)\exp j\left[\omega t + \omega_\Delta \int_0^t x(t')dt' + \phi_n(t)\right] + n_1(t) + \text{D.C. terms} \end{aligned} \tag{51}$$

where R is the detector responsivity, $A_{LO}(t)$ is the amplitude of the LO laser field incident on the detector (variations due to RIN), ω is the IF frequency, and $\phi_n(t) = \phi_{nS}(t) - \phi_{nLO}(t)$. The additive white Gaussian (AWG) noise $n_1(t)$ consists of contributions from both shot and thermal noise (see (20)). The IF bandwidth of the signal is given by Carson's rule as [17]

$$B_{IF} \cong 2(D+1)B \tag{52}$$

where D is the deviation ratio given by $D = \omega_\Delta/(2\pi B)$, and B is the signal bandwidth.

Because variations in the signal amplitude are undesirable in a FM link, a limiter is used in the receiver. It is assumed that this eliminates the effects of spurious amplitude modulation and RIN, allowing the amplitude of the signal and LO to be replaced by their average values. Assuming that the directional coupler couples half of the light from the signal and the LO laser to the detector, the average power levels on the detector are related to the field amplitudes by $P_S = A^2_S/2$ and $P_{LO} = A^2_{LO}/2$.

The frequency discriminator consists of a differentiator followed by an envelope detector. The current emerging from the differentiator is given by

$$i_2(t) = \tau_D\left\{R\sqrt{P_s P_{LO}}\left[\omega + \omega_\Delta x(t) + \frac{d\phi_n}{dt}\right]\exp j\left[\omega t + \omega_\Delta \int_0^t x(t')dt' + \phi_n(t)\right] + \frac{dn_1}{dt}(t)\right\} \tag{53}$$

where τ_D is the time constant of the differentiator. At the output of the low pass filter, the power of the AWG noise is [17]

$$N_{AWG} = \frac{\eta_{n_1}}{3}(2\pi B\tau_D)^2 \tag{54}$$

After envelope detection and lowpass filtering, the phase noise (24) contributes a noise power

$$N_{phase} = 4\pi\tau_D^2\rho^2 P_s P_{LO}\Delta\nu B \tag{55}$$

The baseband signal power emerging from the receiver is given by

$$S = \omega_\Delta^2\tau_D^2\rho^2 P_s P_{LO}|s(t)|^2 \tag{56}$$

From (54)-(56), we see that the SNR is given by

$$SNR = \frac{\omega_\Delta^2\rho^2 P_s P_{LO}|s(t)|^2}{B\left[\frac{\eta}{3}(2\pi B)^2 + 4\pi\rho^2 P_s P_{LO}\Delta\nu\right]} \tag{57}$$

In the absence of phase noise, this expression reduces to

$$SNR = 3D^2\frac{\rho^2 P_s P_{LO}|s(t)|^2}{\eta B} \tag{58}$$

This expression shows the expected $3D^2$ SNR advantage of FM over a coherent AM link for the same transmitted power.

Fig. 9 shows the post-detection SNR of an FM link for several values of linewidth for a frequency deviation of 10 GHz. The impact of phase noise is seen to be severe. At lower signal bandwidths and larger linewidths, the SNR is dominated by phase noise. For large bandwidths, corresponding to small frequency deviation ratios, the AWG noise is dominant. Fig. 10 shows the SNR as a function of frequency deviation. As seen from the plots, the SNR increases by 20 dB per decade of frequency deviation.

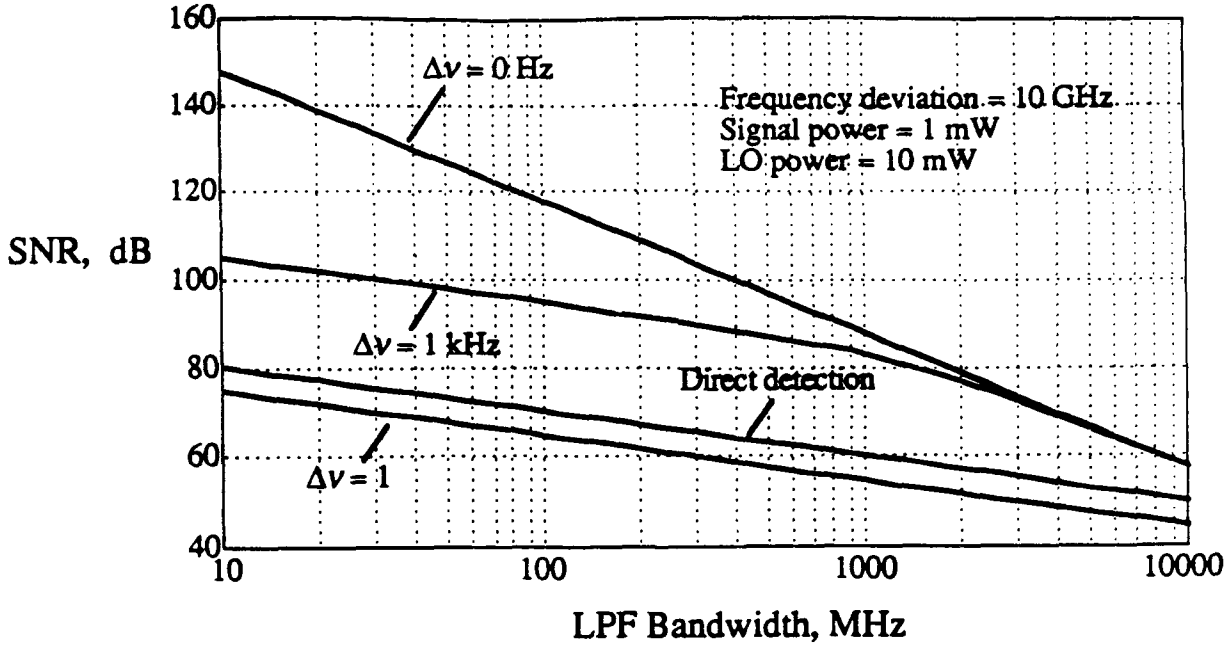

Fig. 9. SNR vs. LPF bandwidth for the FM link with 3 different linewidths. The performance of the direct detection link is shown for comparison.

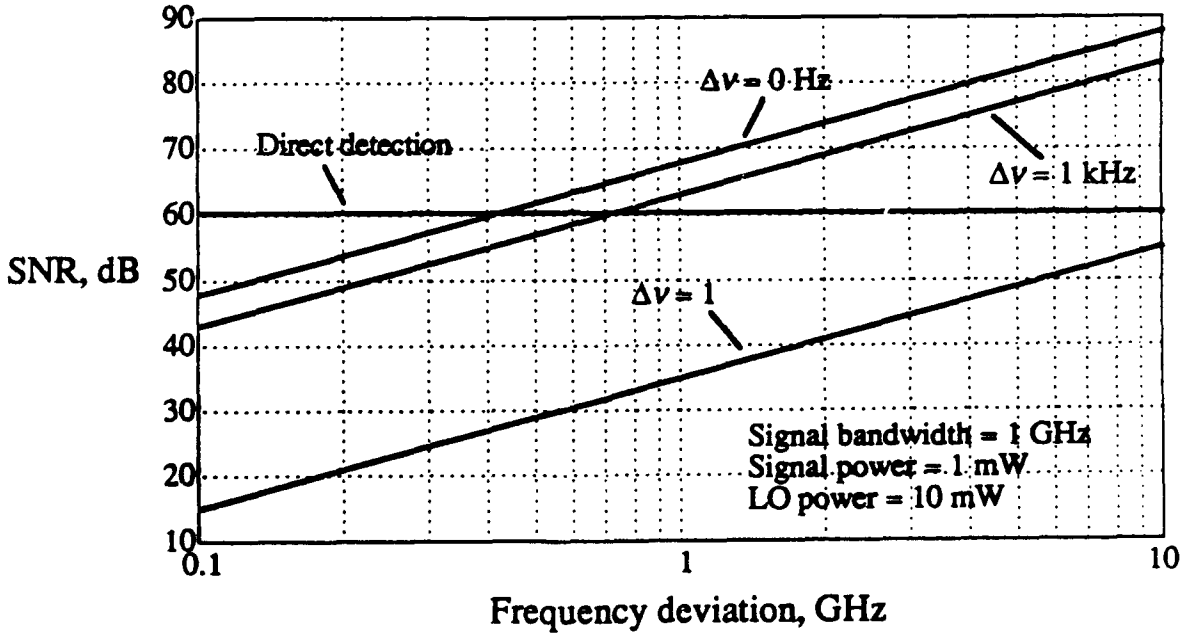

Fig. 10. SNR vs. frequency deviation for the FM link with 3 different linewidths. The performance of the direct detection link is shown for comparison.

5.2 Phase Noise Suppression

Given the significant impact of phase noise on FM coherent systems and the large linewidth (1 - 100 MHz) of current DBR and DFB lasers, it is necessary to suppress phase noise effects before a FM system becomes useful. A receiver structure proposed and demonstrated by Gross et al [18] achieves significant phase noise cancellation (PNC). The structure of this receiver is shown in Fig. 11. After detection, the (unmodulated) IF carrier term is filtered out from the signal spectrum. This filtered carrier is used as a "reference" and mixed with the signal spectrum. Because the carrier and signal terms both contain the same phase noise, the phase noise is canceled in the course of mixing.

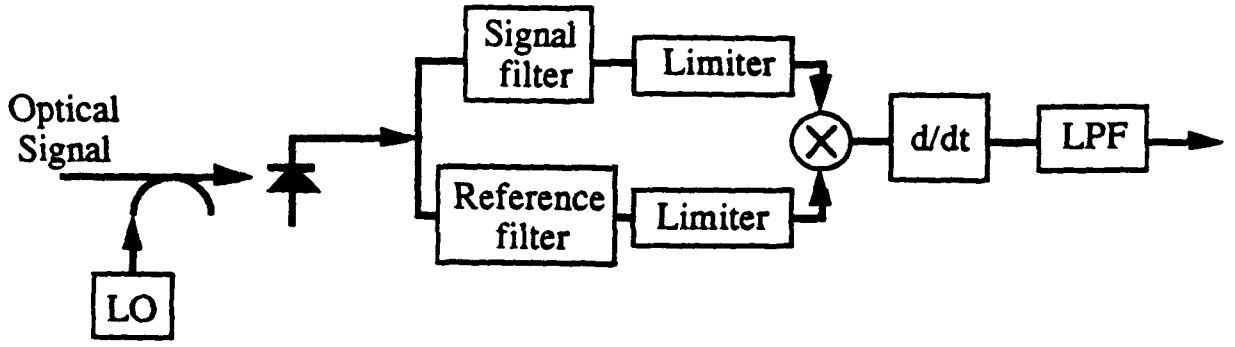

Fig. 11. Coherent FM receiver with the phase noise cancellation (PNC) circuit.

The cancellation of the phase noise is imperfect since the phase noise spectrum is of infinite extent, and is convolved with the signal and carrier spectra. When the carrier is separated from the signal by filtering, some of the phase noise spectrum is truncated, resulting in a loss of information. A reference filter with a cutoff frequency lying half way between the carrier frequency and the lowest signal frequency f_{min} truncates a fraction of the phase noise-broadened carrier spectrum a which is given by

$$a = 1 - \frac{1}{\pi}\tan^{-1}\left(\frac{f_{min}}{\Delta\nu}\right) \tag{59}$$

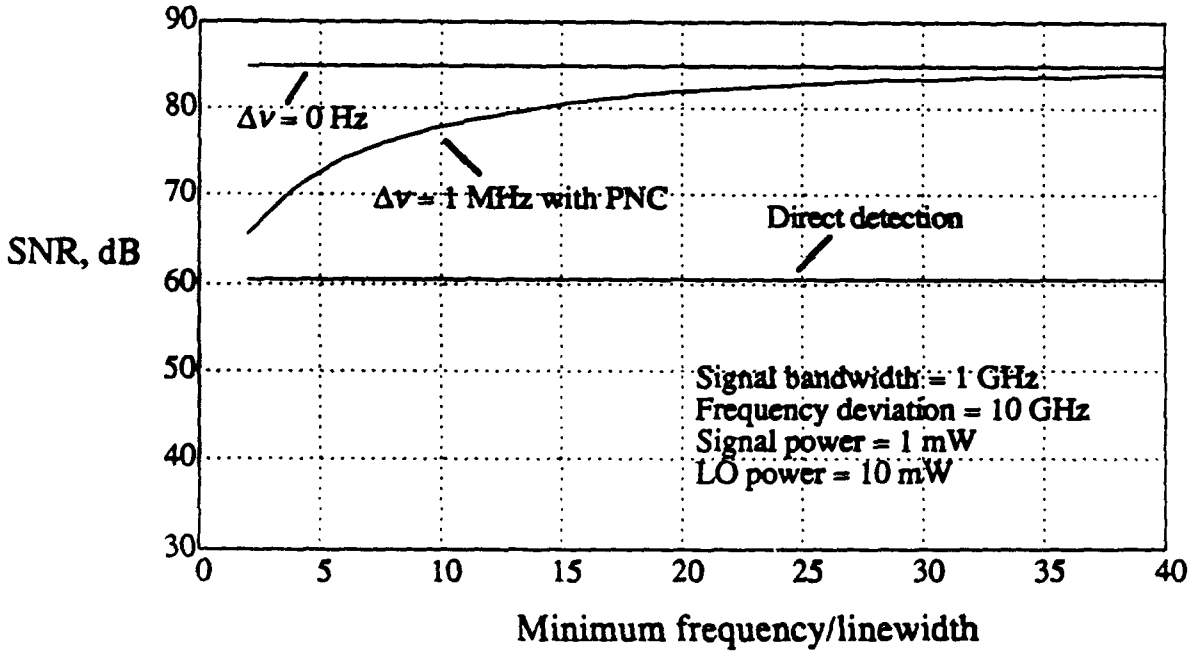

Fig. 12. SNR vs. lowest signal frequency with PNC.

If we assume that all of this truncated power results in noise which is captured by the output lowpass filter, then the phase noise cancellation circuit effectively reduces the linewidth by a factor of a^2,

$$\Delta\nu_{eff} = a^2\Delta\nu \tag{60}$$

The impact of this reduction can be seen in Fig. 12, where the performance of a receiver incorporating PNC is compared to that of a receiver with no PNC and the ideal case of zero laser linewidth. For the case shown, the PNC receiver offers a SNR improvement of 20 dB for $f_C/\Delta\nu = 20$. It is clear that a PNC receiver cannot handle low frequency signals (relative to the linewidth) and achieve large phase noise suppression simultaneously.

5.3 Dynamic Range of Directly Modulated FM Systems

An ideal laser for directly modulated FM links would exhibit a linear change in optical frequency as a function of applied current. In reality, there is a finite range over which the optical frequency vs. current is highly linear. Nonlinearity in this characteristic results in intermodulation distortion, and in this sense, frequency deviation in FM links is analogous to modulation index in AM links. Another potential source of nonlinearity stems from a non-ideal differentiator in the receiver.

At certain currents, laser structures suitable for direct FM (DBR or DFB lasers) exhibit discontinuous "hops" in the frequency as the laser shifts from one longitudinal mode to another. The wavelength tuning range between mode hops is typically on the order of 0.1 nm. These hops will limit the useful frequency deviation which can be obtained from a laser. Multi-section DBR and DFB lasers have, under special drive conditions, demonstrated continuous tuning ranges of 5 nm [19].

Even if it was possible to obtain a frequency deviation of more than 10 GHz, there are practical limitations due to the required IF bandwidth. Present photodetectors and IF electronics would be hard-pressed to accommodate an IF bandwidth in excess of 20 GHz. Thus, frequency deviations of more than 10 GHz may be of limited usefulness.

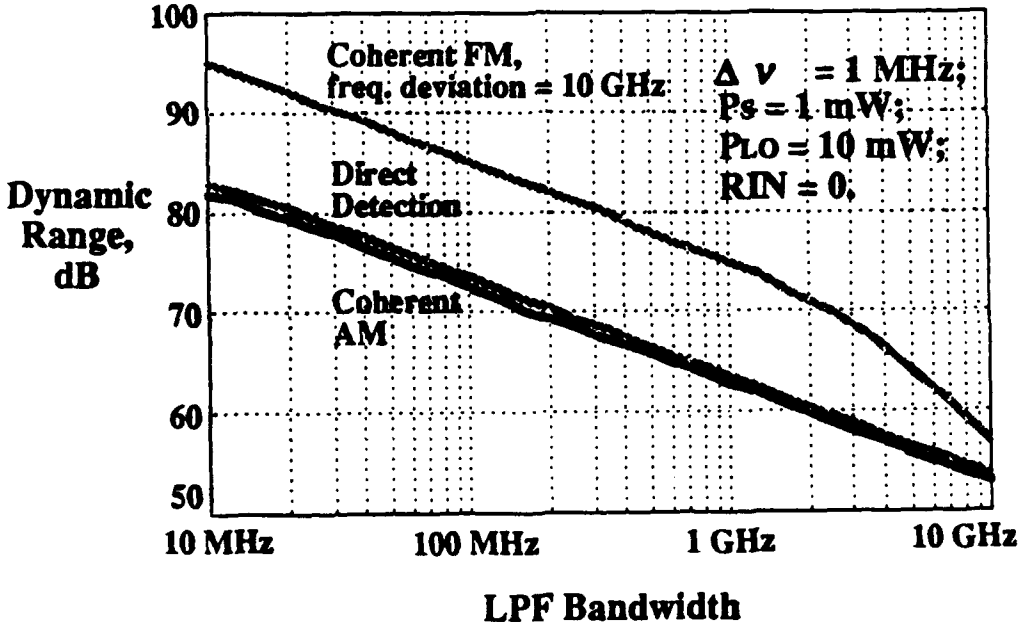

Fig. 13. Comparison between the coherent AM, coherent FM and direct detection systems.

6. COMPARISON BETWEEN COHERENT AM, COHERENT FM AND DIRECT DETECTION LINKS

Fig. 13 shows the fundamental limit of the dynamic range for coherent AM, coherent FM and direct detection links. The direct detection and coherent AM links perform very much the same. For moderate values of the LPF bandwidth, FM links show an improvement in the dynamic range by 10 to 15 dB with respect to direct detection links. This is due mainly to the FM improvement factor discussed in section 5. However, for larger bandwidths, more additive noise is collected by the FM system, degrading its performance as compared to a direct detection system. In Fig. 13, a linewidth of 1 MHz was used. The situation may change for larger linewidths since FM systems are sensitive to phase noise.

7. CONCLUSIONS

In this paper, we analyzed coherent optical analog links. These links have important advantages such as the capability of handling multiple signals through a single fiber and frequency translation. Two types of coherent receivers (AM and FM) were investigated and the impact of the phase noise on the SNR and the dynamic range of the links were analyzed.

The first structure studied was the AM-WIRNA heterodyne system. WIRNA, which stands for WIdeband filter-Rectifier-NArrowband filter, refers to the signal processing at the receiver. For applications where the received optical power is small (e.g., distribution systems like CATV and long distance transmission of analog signals), the AM-WIRNA system has a better SNR and dynamic range than the direct detection system. For medium power applications, like antenna remoting, the performance of this coherent system is very similar to that of the direct detection system. The AM-WIRNA system is essentially linewidth insensitive for reasonable semiconductor laser powers and signal bandwidths. The AM coherent system is susceptible to RIN, but with a balanced receiver structure a 3 dB improvement in the spurious-free dynamic range can be achieved over a conventional single photodiode receiver.

The second structure investigated was a FM coherent link. Through frequency modulation, substantial suppression of additive white Gaussian noise and RIN can be achieved. However, unless special measures are taken, phase noise has a substantial adverse impact on the performance of FM links. The 1 - 100 MHz linewidths typical of DBR and DFB lasers reduces the performance to below that of AM links, negating FM's potential performance advantage. Through the use of a phase noise cancellation (PNC) receiver structure, the impact of phase noise can be reduced substantially. For a 1 GHz bandwidth signal with a minimum frequency of 20 times the linewidth, the SNR can be improved by 20 dB for a frequency deviation of 10 GHz.

The improvement due to FM is due to using large frequency deviation ratio. Maximum useful frequency deviations on the order of 10 GHz may be achievable with current DBR and DFB lasers. Experimental measurements must be performed to investigate the linearity of the FM characteristics of semiconductor lasers.

8. ACKNOWLEDGMENTS

This work is supported by the Department of the Air Force through contract no. F30602-91-C-0141 and by the Office of Naval Research through contract no. N00014-91-J-1857. The authors would like to express their gratitude to Brian Hendrickson and Jim Hunter of the Dept. of the Air Force for their support and encouragement. The definition of the fundamental limit of the dynamic range was proposed by Brian Hendrickson.

9. REFERENCES

[1] R. Simons, Optical Control of Microwave Devices, chap. 1, Artech House, Boston, 1990.

[2] P. Johnson, B. Debney, A. Carter, "Components and applications for high-speed optical analog links", *High Frequency Analog Fiber Optic Systems*, SPIE Vol. 1371, 1990, pp. 87-97.

[3] H. Sobol, "The application of microwave techniques in lightwave systems", *J. Lightwave Technol.*, vol. LT-5, no. 3, March 1987.

[4] C.E. Cox, G.E. Betts, and L.M. Johnson, "An analytic and experimental comparison of direct and external modulation in analog fiber-optic links", *IEEE Trans. MTT*, vol. 38, no. 5, May 1990.

[5] G.E. Betts, L.M. Johnson, and C.H. Cox III, "High-dynamic-range, low-noise analog optical links using external modulators: analysis and demonstration", *High Frequency Analog Fiber Optic Systems*, SPIE Vol. 1371, 1990, pp. 252-257.

[6] R.B. Childs and V.A. O'Bryne, "High dynamic range fiber-optic link using external modulator diode pumped Nd:YAG lasers", *High Frequency Analog Fiber Optic Systems*, SPIE Vol. 1371, 1990, pp. 223-232.

[7] E. Ackerman, D. Kasemset, S. Wanuga, D. Hogue, and J. Komiak, "A high-gain directly modulated L-band microwave optical link", *1990 IEEE MTT-S International Microwave Symposium Digest*, Dallas, 1990.

[8] S. Wanuga, E. Ackerman, D. Kasemset, D. Hogue, and S.R. Chinn, "A low loss L-band microwave fiber optic link for control of a T/R module", *Integrated optics and Optoelectronics II*, SPIE Vol. 1374, 1990.

[9] W.E. Stephens and T.R. Joseph, "System characteristics of direct modulated and externally modulated RF fiber-optic links", *J. Lightwave Technol.*, vol. LT-5, no. 3, March 1987.

[10] J.R. Barry, E. Lee, "Performance of coherent optical receivers", *Proceedings of the IEEE*, vol. 78, no. 8, August 1990.

[11] L.G. Kazovsky, P. Meissner, and E. Patzak, "ASK multiport optical homodyne receivers", *J. Lightwave Technol.*, vol LT-5, no.2, pp. 770-791, June 1987.

[12] L.G. Kazovsky, R. Welter, A.F. Elfefaie, and W. Sessa, "Wide-linewidth phase diversity homodyne receivers", *J. Lightwave Technol.*, vol. 6, no. 10, October 1988.

[13] L.G. Kazovsky, O.K. Tonguz, "ASK and FSK Coherent Lightwave Systems: A Simplified Approximate Analysis", *J. Lightwave Technol.*, vol. LT-8, no. 3, pp. 338-352, March 1990.

[14] K. Kikuchi, T. Okoshi, M. Nagamatsu, and N. Henmi, "Degradation of bit-error rate in coherent optical communications due to spectral spread of the transmitter and the local oscillator", *J. Lightwave Technol.*, vol. LT-2, no. 6, pp. 1024-1033, Dec. 1984.

[15] L.G. Kazovsky, "Impact of laser phase noise on optical heterodyne communication systems", *J. Opt. Commun.*, 7 (1986) 2, 66-78.

[16] D. Middleton, Introduction to Statistical Communication Theory, chap. 3, Peninsula Publishing, Los Altos, 1987.

[17] A. C. Carlson, Communication Systems, third ed., McGraw-Hill: New York, p. 331.

[18] R. Gross, R. Olshansky, M. Schmidt, "Coherent FM-SCM System Using DFB Lasers and a Phase Noise Cancellation Circuit", *IEEE Technol. Letters*, Vol. 2, No. 1, January 1990.

[19] L. A. Wang, Y. H. Lo, M. Z. Iqbal, A. S. Gozdz, P. S. D. Lin, R. Bhat, and H. Shirokmann, "Tunable four-wavelength DFB laser array with 10-Gbit/s speed and 5-nm continuous tuning range," *OFC '92*, pp. 277-278.

lated, causing enhanced noise below the resonance frequency and a more damped resonance peak. We have successfully modeled for the first time the translation of the low frequency noise of a semiconductor laser to the signal band in the presence of modulation and dispersion. Experimental results verified the theoretical predictions.

REFERENCES

[1] R. Olshansky and V. A. Lanzisera, "60 channel FM video subcarrier multiplexed optical communication system," *Electron Lett.*, vol. 22, p. 1196, 1987.

[2] P. A. Roscher, M. J. Ramsay, and F. V. C. Mendis, "Broadband video distribution over passive optical network using subcarrier multiplexing techniques," *Electron Lett.*, vol. 25, p. 115, 1989.

[3] G. J. Meslener, V. S. Shukla, M. Murphy, and R. F. Kearns, *OFC'91*, San Diego, CA, Feb. 1991, paper ThC4.

[4] C. B. Su, J. Schlafer, and R. B. Lauer, "Explanation of low-frequency relative intensity noise in semiconductor lasers," *Appl. Phys. Lett.*, vol. 57, p. 27, 1990.

[5] X. Lu, C. B. Su, and R. B. Lauer, "Increase in laser RIN due to asymmetric nonlinear gain and fiber dispersion," *OFC'92*, San Jose, CA 1992, paper TuM6.

[6] G. R. Gray and G. P. Agrawal, "Correlation between linewidth rebroading and low-frequency RIN enhancement in semiconductor lasers," *Electron Lett.*, vol. 27, p. 1150, 1991.

[7] K. Y. Lau and H. Blouvelt, "Effect of low-frequency intensity noise on high-frequency direct modulation of semiconductor injection lasers," *Appl. Phys. Lett.*, vol. 52, p. 694, 1988.

[8] G. J. Meslener, "Analysis of mode-partition noise for subcarrier modulated transmission systems," *OFC'92*, San Jose, CA, 1992.

[9] J. Manning, R. Olshansky, D. B. Fye, and W. Powazinik, "Strong influence of nonlinear gain on spectral and dynamic characteristics of InGaAsP lasers," *Electron Lett.*, vol. 21, p. 496, 1985.

[10] R. H. Wentworth, G. E. Bodeep, and T. E. Darcie, "Laser mode partition noise in lightwave systems using dispersive optical fiber," *J. Lightwave Technol.*, vol. 10, p. 84, 1992.

[11] J. Wang and K. Petermann, "Small signal analysis for dispersive optical fiber communication systems," *J. Lightwave Technol.*, vol. 10, p. 96, 1992.

[12] V. S. Shukla, R. F. Kearns, and L. W. Ulbricht, *ECOC'90*, Amsterdam, The Netherlands, 1990, paper WeB1.6.

Noise Analysis of Subcarrier-Multiplexed Coherent Optical Video Transmission Systems Using Direct Frequency Modulation of Semiconductor Lasers

J. C. Fan and L. G. Kazovsky

Abstract—**This letter presents a noise analysis of an analog subcarrier-multiplexing coherent optical system for video transmission using direct frequency modulation of semiconductor lasers. Receiver sensitivity using the FM subcarrier modulation format is analyzed for realistic values of receiver thermal noise (3.31×10^{-22} A^2/Hz), laser linewidth (up to 100 MHz), RIN (-130 *to* -170 dB/Hz), and optical bandwidth (20 GHz). Linewidth-induced performance degradation is negligible for up to 50 channels, and RIN-induced performance degradation becomes dominant as RIN increases above -140 dB/Hz. A sensitivity floor of about -40 dBm (for RIN = -160 dB/Hz) exists for small numbers of channels (up to 50) due to the FM threshold effect at the IF demodulator.**

Manuscript received January 7, 1992; revised March 6, 1992. This work was supported in part by ONR under Contract N00014-91-J-1857, by a gift from the GTE Corporation, and by the National Defense Science and Engineering Graduate (NDSEG) Fellowship Program.

The authors are with the Department of Electrical Engineering, Stanford University, Stanford, CA 94305-4055.

IEEE Log Number 9201129.

INTRODUCTION

THE simultaneous transmission of many video channels through subcarrier multiplexing (SCM) on a single optical carrier is feasible using the high available bandwidths of distributed-feedback (DFB) lasers and p-i-n photodiodes. The use of subcarrier multiplexing in coherent optical systems for analog and digital video distribution has been explored experimentally [1]–[3]; using phase modulation of the optical carrier, receiver sensitivities of -32 and -27 dBm have been achieved for 60 FM video channels and 20 frequency-shift-keyed (FSK) video channels, respectively [3]. Direct frequency modulation of the optical carrier is also an attractive modulation format due to the avoidance of external modulation and to the high output signal-to-noise ratio (SNR) attainable through FM enhancement [4]. This letter reports the results of a theoretical analysis of SCM coherent systems using direct

1041-1135/92$03.00

frequency modulation of the optical carrier and FM video subcarriers.

System Description

Fig. 1 shows a block diagram of the system analyzed. FM video signals on microwave subcarriers are combined, generating a signal which is used for direct frequency modulation of a laser. The transmitted optical signal travels over single-mode fiber to a coherent receiver, where it is combined with an optical local oscillator signal using a directional coupler. The resulting signal is heterodyne-detected by a p-i-n photodiode, amplified, and demodulated. After the first FM demodulator, the SCM channels are separated using a bandpass filter array, downconverted to a common frequency, and amplified. A set of FM demodulators and lowpass filters recovers the baseband video signals. Each FM demodulator consists of an ideal limiter followed by an ideal phase-shift discriminator.

Analysis

The goal of this analysis is to evaluate the limitations imposed by system noises on the optical receiver sensitivity, defined as the received optical power (P_s) required to achieve a 56 dB peak-to-peak SNR at the output video ports. Tables I and II contain definitions of variables and numerical values of parameters used in this analysis.

The normalized SCM signal $g(t)$ used to frequency modulate the optical carrier is given by

$$g(t) = \sum_{k=1}^{N} \beta_k \cos\left(2\pi f_k t + 2\pi f_d \int_{t_0}^{t} d_k(t')\,dt' + \varphi_k\right). \quad (1)$$

Modulation indices $\{\beta_k\}$ are chosen such that $|g(t)| \le 1$. For simplicity, $\{\beta_k\}$ are set equal to a common value $\beta = 1/\sqrt{N}$, which is approximately equal to the optimum modulation index for an SCM signal using intensity modulation of the transmitter [5]. This is a good estimate for N independent and uniform channels and becomes increasingly accurate for large N.

The signal and LO fields are mixed by the photodiode, giving a detected photocurrent

$$i(t) = R\left(P_s + P_{LO} + 2\sqrt{P_S P_{LO}} \cdot \cos\left(2\pi f_{IF} t + 2\pi f_\Delta \int_{t_0}^{t} g(t')\,dt' + \phi_p(t)\right)\right). \quad (2)$$

The dc currents RP_s and RP_{LO} will contribute to the photodetector shot noise and to the total relative-intensity noise (RIN). The third term in (2) is the useful signal. The phase noise process $\phi_p(t)$ is assumed to have a power spectral density [6]

$$S_\phi(f) = \frac{\Delta\nu}{\pi f^2} \qquad (f > 0). \quad (3)$$

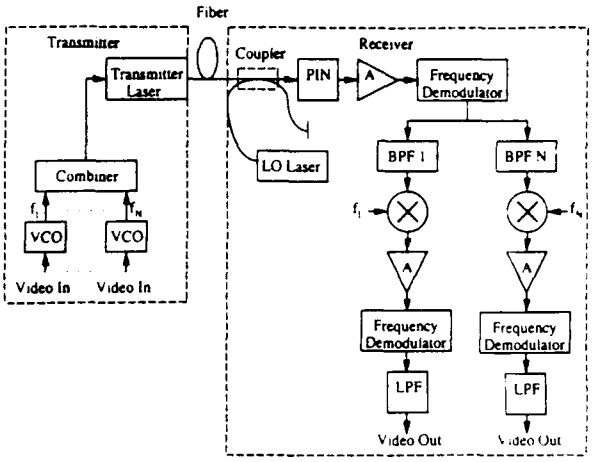

Fig. 1. Block diagram of a coherent SCM system using direct laser frequency modulation to transmit FM video channels. The N branches after the downconverters are identical.

TABLE I
Definitions of Variables

P_s	Optical signal power
f_s	Optical signal frequency
f_Δ	Single-sided maximum optical frequency deviation
N	Number of channels
β_k	Modulation index for channel k
f_k	Subcarrier frequency for channel k
f_d	Single-sided maximum subcarrier frequency deviation
$d_k(t)$	video signal for channel k (baseband)
φ_k	Phase of channel k (subcarrier)
P_{LO}	Optical local oscillator power
$f_{IF} = f_s - f_{LO}$	Receiver intermediate frequency
$\phi_p(t)$	Combined phase noise of received signal and optical local oscillator
B_{IF}	IF bandwidth = optical bandwidth
RIN	Relative-intensity noise (in dB/Hz)
f_h	Highest frequency in SCM signal
$D = f_\Delta/f_h$	Optical frequency deviation ratio
$\Delta\nu$	Sum of linewidths of optical transmitter and LO

TABLE II
Parameter Definitions and Values

$R = 0.7$ A/W	Photodiode responsivity
$q = 1.6 \times 10^{-19}$ C	Charge of electron
$k = 1.381 \times 10^{-23}$ J/°K	Boltzmann's constant
$T = 300$°K	Room temperature
$R_L = 50\ \Omega$	Amplifier load resistance
$\{v_a^2\} = 4 \times 10^{-20}$ A^2/Hz	Amplifier voltage noise
$B_T = 50$ MHz	SCM channel bandwidth
$f_d/f_v = 2.68$	Subcarrier frequency deviation ratio
1 mW	Optical LO power
60 MHz	Subcarrier separation
100 MHz	Lowest subcarrier frequency
20 GHz	Optical bandwidth

The transmitter dynamic linewidth, which becomes smaller with increasing drive current and with increasing transmitter instantaneous frequency, is assumed to correspond to the lowest drive current for the worst case analysis.

After amplification, the signal and noise enter the radio frequency (RF) demodulator. The carrier-to-noise ratio (CNR) at the input of the intermediate frequency (IF)

demodulator is given by

$$\mathrm{CNR} = \frac{2R^2P_SP_{LO}}{\left(2qR(P_S+P_{LO}) + \dfrac{4kT}{R_L} + \dfrac{4\{v_a^2\}}{3R_L^2}\right)B_{\mathrm{IF}} + R^2\left((P_S+P_{LO})^2 - P_SP_{LO}\right)10^{\frac{\mathrm{RIN}}{10}}B_{IF}} \tag{4}$$

where the first combined term in the denominator, hereafter denoted by σ_w^2, is the white noise power (consisting of shot, thermal, and amplifier noise powers). The second term in the denominator is the RIN power, denoted in the remainder of this letter by σ_{RIN}^2. B_{IF}, which is linearly dependent on the total number of channels, is given by Carson's rule:

$$B_{\mathrm{IF}} = \begin{cases} 2(D+1)f_h, & D > 10 \text{ and } D < 2 \\ 2(D+2)f_h, & 2 < D < 10 \end{cases} \tag{5}$$

D is the optical frequency deviation ratio. Note that the modulation index does not affect the CNR in (4).

We evaluated the SNR at the output of the IF demodulator by performing an analysis similar to that in [4, pp. 428–443]. The fundamental impact of the FM demodulation on the noise sources is 1) the conversion of additive white noise at the input to parabolic noise with a zero at dc at the output and 2) the conversion of the frequency noise at the input to white noise at the output. The noise enhancement which occurs as FM demodulator operation breaks down for CNR below the FM threshold (approximately 10 dB) is quantified using the threshold model of Rice [7].

Channel N, the channel with the highest subcarrier frequency, has the lowest CNR at the input to the subcarrier FM demodulator due to the parabolic noise spectrum, which has f^2 frequency dependence. Hence, system output SNR is limited by that for channel N. The impact of the noise on channel N is approximated by white noise with density equal to that of the parabolic noise at f_h, the highest frequency of the SCM signal. The SNR at the output of the FM demodulator for channel N is

$$\mathrm{SNR}_N \cong \frac{3f_\Delta^2 f_d^2 \beta^2}{(\sigma_w^2 + \sigma_{\mathrm{RIN}}^2)\dfrac{f_h^2 f_v^3}{2R^2P_SP_{LO}B_{\mathrm{IF}}} + (\sigma_P^2 + \sigma_T^2)\dfrac{f_v^3}{B_T}} \tag{6}$$

where $\sigma_P^2 = (\Delta v/\pi)B_T$ is the phase noise power at the input to the FM demodulator for channel N [8]. The threshold noise power at the demodulator input is

$$\sigma_T^2 = \left(\frac{4\pi^2 B_{\mathrm{IF}}\,\mathrm{erfc}\,(\sqrt{\mathrm{CNR}})}{\sqrt{3}} + 4\pi^2\sqrt{2}f_\Delta \exp(-\mathrm{CNR})\right)B_T. \tag{7}$$

Carson's rule for $2 < D < 10$ is used to find B_T in our numerical calculations. Assuming an emphasis improvement factor of 13.1 dB as per international (CCIR) standards for FM video transmission systems [9], an SNR_N of 42.9 dB is required for a destination SNR of 56 dB. The threshold noise due to the subcarrier FM demodulator is negligible because its input CNR must be on the order of 20 dB to achieve an output SNR of 56 dB.

The optical bandwidth required to maintain the desired frequency deviation ratio must increase with increasing modulation index to avoid distortion. The impact of clipping distortion is difficult to quantify and is the subject of a separate study currently in progress.

Results

Figs. 2 and 3 show samples of our results for the system parameters given in Table II. In both figures, the optical receiver sensitivity is plotted versus the number of channels; constant optical bandwidth is assumed. The values of sensitivity have been obtained using an iterative numerical technique to solve (6) for P_s. Inspection of Fig. 2 reveals that increasing linewidth places a limitation on the number of SCM channels which one can transmit with a reasonable sensitivity. However, receiver sensitivity is only weakly dependent on linewidth for lower channel counts, since the maximum optical frequency deviation increases linearly as the number of channels decreases (the phase noise power term in (6) remains constant). The limitation on receiver sensitivity due to system noises is approximately −40 dBm for up to 50 channels, even with 100 MHz linewidth. This is comparable to the fundamental limit on sensitivity for the assumed optical bandwidth (−45 dBm) and the fundamental limit for 50-channel coherent transmission of analog FM SCM video channels using intensity modulation of the transmitter (−35 dBm) [5]. There is also a potential floor in attainable receiver sensitivity for low channel counts due to the threshold effect of the IF demodulator, even though the available optical bandwidth remains at 20 GHz. The threshold noise power in (7) will increase exponentially with decreasing CNR.

Inspection of Fig. 3 shows that performance is degraded for high values of transmitter and local oscillator RIN. As RIN increases beyond −150 dB/Hz, local oscillator relative-intensity noise becomes increasingly dominant. For example, a sensitivity loss of nearly 10 dB for low channel counts occurs as RIN increases from −140 to −130 dB/Hz. RIN degradation can be softened using a balanced receiver [10].

Discussion

The foregoing analysis focuses exclusively on the impact of system noises. Other effects also have a significant impact on the performance of FM video systems. These effects include clipping distortion, degradation due to

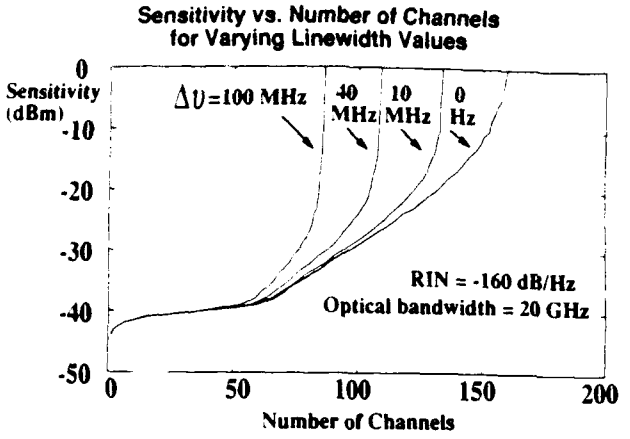

Fig. 2. Receiver sensitivity (for output SNR = 56 dB) versus the number of transmitted channels for several values of linewidth; RIN = −160 dB/Hz. The linewidths shown ($\Delta\upsilon$) correspond to the sum of the transmitter and *LO* laser linewidths. Numerical values of system parameters are shown in Table II.

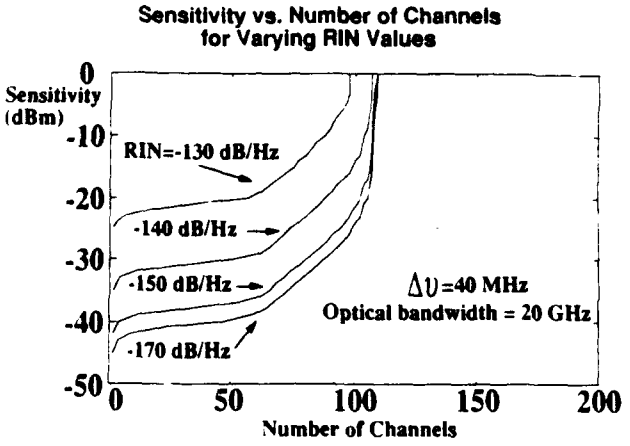

Fig. 3. Receiver sensitivity (for output SNR = 56 dB) versus the number of transmitted channels for several values of RIN. The sum of the linewidths of the transmitter and *LO* lasers is 40 MHz. Numerical values of system parameters are shown in Table II.

nonlinearities resulting from non-ideal frequency discrimination and from imperfect limiting, and residual AM resulting from direct modulation of the transmitter. Further work must be done to investigate the impact of these factors on system channel capacity.

Summary

Noise analysis of analog coherent systems for transmission of subcarrier-multiplexed FM video predicts that such systems will have good receiver sensitivity. For example, receiver sensitivity should be about −30 dBm for 80-channel systems with lasers having 100 MHz linewidth. For up to 50 channels, receiver sensitivity is essentially independent of laser linewidth up to 100 MHz. This effect results from phase noise suppression in a receiver employing double FM demodulation and is similar to that in digital ASK and FSK systems [11]. Relative-intensity noise effects are more severe than linewidth effects, particularly for low channel counts, where the local oscillator RIN is dominant. For example, a degradation in the sensitivity floor of about 15 dB occurs as RIN increases from −150 to −130 dB/Hz. A balanced receiver may be used to reduce RIN-induced degradation. Other system imperfections such as imperfect FM demodulation, clipping, and residual AM resulting from direct modulation must be analyzed to complete the evaluation of the potential of such systems.

Acknowledgment

The authors are grateful to Dr. R. Gross and Dr. R. Olshansky of GTE Labs for their support and helpful discussions.

References

[1] T. E. Darcie, "Subcarrier multiplexing for lightwave networks and video distribution systems," *IEEE J. Select. Areas Commun.*, vol. 8, pp. 1240–1248, 1990.

[2] W. I. Way, "Subcarrier multiplexed lightwave system design for subscriber loop applications," *J. Lightwave Technol.*, vol. LT-7, pp. 1806–1818, 1989.

[3] R. Gross and R. Olshansky, "Subcarrier multiplexed coherent lightwave systems for video distribution," *IEEE J. Select. Areas Commun.*, vol. 8, pp. 1268–1275, 1990.

[4] P. F. Panter, *Modulation, Noise, and Spectral Analysis*. New York: McGraw-Hill, 1965.

[5] A. A. M. Saleh, "Fundamental limit on number of channels in subcarrier-multiplexed lightwave CATV system," *Electron. Lett.*, vol. 25, pp. 776–777, 1989.

[6] L. G. Kazovsky, "Performance analysis and laser linewidth requirements for optical PSK heterodyne systems," *J. Lightwave Technol.*, vol. LT-4, pp. 415–425, 1986.

[7] H. Taub and D. Schilling, *Principles of Communications Systems*, 2nd ed. New York: McGraw-Hill, 1986.

[8] J. Wu *et al.*, "Performance analysis of coherent heterodyne analog FM optical receiver," to be published.

[9] D. Roddy, *Satellite Communications*. Englewood Cliffs, NJ: Prentice Hall, 1989.

[10] G. Abbas, V. W. S. Chan, and T. Lee, "A dual-detector optical heterodyne receiver for local oscillator noise suppression," *J. Lightwave Technol.*, vol. LT-3, pp. 1110–1122, 1985.

[11] L. G. Kazovsky and O. K. Tonguz, "ASK and FSK coherent lightwave systems: A simplified approximate analysis," *J. Lightwave Technol.*, vol. 8, pp. 338–352, 1990.

Space Division Switches Based on Semiconductor Optical Amplifiers

R. F. Kalman, L. G. Kazovsky, and J. W. Goodman

Optivision, Inc.
4009 Miranda Ave.
Palo Alto, CA 94304
Telephone: (415) 855-0200
Fax: (415) 855-0222

Department of Electrical Engineering
Stanford University, Stanford, CA 94305
Telephone: (415) 725-5890
Fax: (415) 723-9251
Email: robk@loki.stanford.edu

Abstract

Multiple space-division switches based on semiconductor optical amplifiers (SOAs) can be cascaded to obtain larger switching fabrics. We present a general analysis of optical switching fabrics using SOAs, considering noise and saturation effects associated with amplified spontaneous emission. We find that the SOA saturation output power limits the number of switches which can be cascaded. For example, a saturation output power of 100 mW limits the size of switching fabrics to 100 64x64 switches or 200 8x8 switches if distributed gain matrix-vector multiplier (MVM) switches or Benes switches are employed. The corresponding limit for lumped gain MVM fabrics is 10 64x64 or 100 8x8. The Benes switch may be more suitable for large switch sizes ($N > 16$) because it requires fewer SOAs.

1. Introduction

All-optical space-division switches can be constructed using optical splitters, combiners, and semiconductor optical amplifiers (SOAs) [1] which provide gain and binary on/off switching in 1 - 10 ns. Multiple switches can be interconnected to form larger switching fabrics.

Switches built from SOAs have been examined by a number of authors [1, 2], and at least one paper has considered the size limitations of a specific SOA-based switch [3]. The objective of this paper is to evaluate the limitations on the size of switch fabrics constructed using SOA-based switches. The results we derive are based on signal-to-noise ratio and saturation constraints. In Section 2, we analyze the behavior of systems based on SOAs. In Section 3, we evaluate the size limitations of three specific switch implementations. Discussion and conclusions are presented in Sections 4 and 5, respectively.

2. SOA and Switch Behavior

2.1 The Evolution of Spontaneous Emission

The output optical power from a SOA, P_{out}, is related to the input power, P_{in}, by

$$P_{out} = L_{in}L_{out}GP_{in} + L_{out}pn_{sp}(G-1)h\nu_c\Delta\nu, \qquad (1)$$

where G is the internal SOA gain, and L_{in} and L_{out} are the input and output coupling losses to the SOA, respectively, ν_c is the center frequency of the amplifier bandpass, and $\Delta\nu$ is the effective amplifier optical bandwidth. n_{sp} is the excess spontaneous emission factor [4] and p is a factor which ranges from 1 for a device which amplifies only one polarization to 2 for a polarization-insensitive device.

Consider a cascade of M identical stages, each stage consisting of a system loss, L_s, and a SOA with its associated coupling losses. Using Eq. (1), we find that the power output from the M^{th} stage, P_M, is given by

$$P_M = G_{sig}P_{in} + G_{sp}n_{sp}p_{eff}h\nu_c\Delta\nu_{eff} \qquad (2)$$

where $\Delta\nu_{eff}$ is the effective overall gain bandwidth due to the cascade of SOAs, and p_{eff} is the effective polarization-dependent factor which ranges from 1 to 2 in a manner similar to p. The net signal gain through the system, G_{sig} is given by

$$G_{sig} = \left(L_s L_{in} L_{out} G\right)^M \tag{3}$$

By analogy to the signal gain, we can define a spontaneous emission gain, G_{sp},

$$G_{sp} = \left(\frac{G_{sig}^{1/M}}{L_s L_{in}} - L_{out}\right)\frac{1-G_{sig}}{1-G_{sig}^{1/M}} \equiv M\left(\frac{G_{sig}^{1/M}}{L_s L_{in}} - L_{out}\right)\frac{G_{sig}-1}{\ln G_{sig}} \tag{4}$$

The second equality in Eq. (4) holds for large M.

2.2 Saturation and Signal-to-Noise Ratio Constraints

Due to the high spontaneous emission level emerging from a cascade of SOA-based stages, the post-detection noise in a receiver placed at the output of the last SOA is typically dominated by signal-spontaneous and spontaneous-spontaneous beat noise. This leads to a post-detection signal-to-noise ratio (SNR), γ, of approximately [5]

$$\gamma = \frac{\left(G_{sig}P_{in}\right)^2}{4G_{sp}n_{sp}h\nu_c B_e\left(G_{sig}P_{in} + G_{sp}n_{sp}h\nu_c B_o\right)} \tag{5}$$

where B_e is the electrical noise bandwidth of the receiver and B_o ($B_o \le \Delta\nu_{eff}$) is the bandwidth of an optical filter placed in front of the receiver. To achieve a 10^{-9} bit error ratio (BER), we require $\gamma > 144$.

SOAs exhibit nonlinear distortion characterized by a saturation output power, P_{sat}, at which the gain has dropped to $1/e$ of its unsaturated value [6]. Saturation leads to a number of undesirable effects: a decrease in gain, intersymbol interference (ISI) and, in frequency-division multiplexed systems, crosstalk. We consider the simple saturation constraint

$$\left(G_{sig}P_{in} + G_{sp}p_{eff}n_{sp}h\nu_c\Delta\nu_{eff}\right)\frac{1}{L_{out}} \le P_{sat} \tag{6}$$

Eq. 6 indicates that the total power emerging from the endface of the last SOA in a cascaded amplifier system (i.e. before its output coupling loss) must be less than P_{sat}.

2.3 Specific Switch Architectures

In this paper, we examine switches based on two versions of the matrix-vector multiplier (MVM) crossbar switch [7, 8] (Fig. 1) and the Benes switch [1] (Fig. 2). The structure of the three switches allows the direct application of the analysis of Section 2.1. For each of the switches, Table 1 gives the number of stages traversed by a signal, M_s, the system loss per stage, L_s, and the number of SOAs required to implement a switch with N inputs/outputs.

The MVM switches allow completely general nonblocking interconnections between the inputs and outputs [7]. The distributed gain MVM (DGMVM) switch differs from the lumped gain MVM (LGMVM) switch in that it incorporates additional SOAs after each 1x2 splitter and 2x1 combiner. The Benes switch provides a rearrangeably nonblocking interconnection [1]. From Table 1, note that the number of SOAs in the MVM switches grows as N^2 vs. only $N \log_2 N$ for the Benes switch.

Multiple switches can be interconnected to form larger switching fabrics. For practical reasons, these larger switch fabrics will be dilute and thus highly blocking. A signal traveling though a switch fabric containing M_c cascaded switches encounters a total of M_t stages where

$$M_t = M_s M_c \tag{7}$$

3. System Size Limitations

We consider system size limitations based on two phenomena: required signal-to-noise ratio (SNR) at the system output, and saturation of the SOAs. For a given value of the signal gain G_{sig}, we can solve Eqs. (5) and (6) simultaneously to find the maximum allowable spontaneous gain, $G_{sp\ max}$, and the optimum input signal level. Using G_{sig} and $G_{sp\ max}$, and solving Eq. (4) for the maximum permissible total number of stages, M_{max}, we find

$$M_{max} = G_{sp\,max}\left(\frac{G_{sig}^{1/M}}{L_s L_{in}} - L_{out}\right)^{-1} \frac{\ln G_{sig}}{G_{sig} - 1} \qquad (8)$$

Utilizing the relationships between M_s, L_s, and N for the three switch types (Table 1) and using Eqs. (7) and (8), we can find the maximum number of switches of a given size which can be cascaded. Fig. 3 shows the maximum number of 8x8 switches which can be cascaded for the three switch types as a function of P_{sat}. Similarly, Fig. 4 shows the maximum number of 64x64 switches which can be cascaded.

4. Discussion

From Figs. 3 and 4, the number of switches which can be cascaded can be seen to be proportional to the saturation output power of the SOAs. Current SOAs exhibit saturation power levels in the range of 1 - 100 mW (the latter being achieved in quantum well devices).

Because their system loss per stage is small, DGMVM and Benes switches typically utilize low gain SOAs which have relatively small on/off extinction ratios, leading to crosstalk. At the expense of increasing n_{sp}, the off-state absorption of a SOA can be made arbitrarily large by increasing its length. Figs. 3 and 4 assume a n_{sp} of 5, which corresponds to an extinction ratio of 50 dB for a device with an internal gain of 10. This high absorption prevents crosstalk from impacting system performance. Because they typically utilize high gain SOAs, LGMVM switches tend not to exhibit crosstalk problems.

Due to the large numbers of required SOAs, achieving practical switches requires integration of SOAs and optical waveguides. Electrical pin-out constraints of packages suggest that monolithic integration of drive electronics with the optical devices may also be necessary to achieve $N > 8$. As noted in Table 1, for large switch sizes (N>16) the Benes switch requires considerably fewer SOAs than the MVM structures and may thus be the preferred architecture for large switches.

5. Conclusions

The size of optical switching fabrics based on SOAs are ultimately limited by signal-to-noise ratio (SNR) and saturation considerations, both of which are associated with

spontaneous emission from the SOAs. The number of switches which can be cascaded is proportional to the saturation output power of the SOAs.

Three specific SD switch architectures were considered. Based on consideration of saturation and signal-to-noise ratio, it was found that, for the distributed gain matrix-vector multiplier (DGMVM) switch and the Benes switch, cascades of 100 64x64 switches or nearly 200 8x8 switches can be achieved for SOAs with saturation output powers of 100 mW. For lumped gain matrix-vector multiplier (LGMVM), approximately 10 64x64 switches or 100 8x8 switches can be cascaded for SOAs with saturation output powers of 100 mW. For large switch sizes, the DGMVM and Benes switches, both of which distribute gain throughout the switch, are notably better than the LGMVM switch, which lumps gain in two "planes." The Benes switch may be more suitable for large switch sizes ($N > 16$) because it requires fewer SOAs.

Acknowledgment

This work was supported by DARPA through NOSC contract #N66001-86-C-0382 and ONR contract #N00014-91-J-1857. We would also like to thank the reviewers for their helpful suggestions.

References

[1] J. D. Evankow and R. A. Thompson, "Photonic Switching Modules Designed with Laser Diode Amplifiers," *IEEE J. Select. Areas Commun.*, vol. 6, pp. 1087-1094, 1988.

[2] M. Ikeda, "Laser Diode Switch," *Electron. Lett.*, vol. 17, no. 22, pp. 899-900, 1981.

[3] M. Gustavson and L. Thylen, "Switch Matrix with Semiconductor Laser Amplifier Gate Switches: A Performance Analysis," *OSA Proc. on Photonic Switching*, vol. 3, pp. 77-79, 1989.

[4] C. H. Henry, "Theory of Spontaneous Emission Noise in Open Resonators and its Application to Lasers and Optical Amplifiers," *J. Lightwave Technol.*, vol. 4,.no. 3, pp. 288-297, 1986.

[5] N. A. Olsson, "Lightwave Systems with Optical Amplifiers," *J. Lightwave Technol.*, vol. 7, no. 7, pp. 1071-1082, 1989.

[6] A. A. M. Saleh and I. M. I. Habbab, "Effects of Semiconductor-Optical-Amplifier Nonlinearity on the Performance of High-Speed Intensity-Modulation Lightwave Systems," *IEEE Trans. Commun.*, vol. 38, no. 6, pp. 839-846, 1990.

[7] A. R. Dias, R. F. Kalman, J. W. Goodman and A. A. Sawchuk, "Fiber-optic crossbar switch with broadcast capability", *Opt. Engin.*, vol. 27, no. 11, 955-960, 1988.

[8] A. Himeno and M. Kobayashi, "4x4 Optical Gate Matrix Switch," *J. Lightwave Technol.*, vol. 3, no. 2, pp. 230-235, 1985.

Figure Captions

Table 1. Number of stages (M), system loss per stage (L_s), and number of SOAs, for LGMVM, DGMVM, and Benes switches of size N.

Figure 1. MVM crossbar switches: (a) lumped gain; (b) distributed gain. As an example, 4x4 switches are shown.

Figure 2. Benes switch. As an example, a 4x4 switch is shown.

Figure 3. Maximum number of cascaded 8x8 switches vs. P_{sat} for the three switch types.

Figure 4. Maximum number of cascaded 64x64 switches vs. P_{sat} for the three switch types.

Table 1

	LGMVM	DGMVM	Benes
Number of stages (M_s)	2	$2 \log_2 N$	$2 \log_2 N - 1$
System Loss per Stage (L_s)	$1/N$	0.5	0.5
Number of SOAs	$N(N+1)$	$3N(N-1)$	$2N(2\log_2 N - 1)$

Figure 1

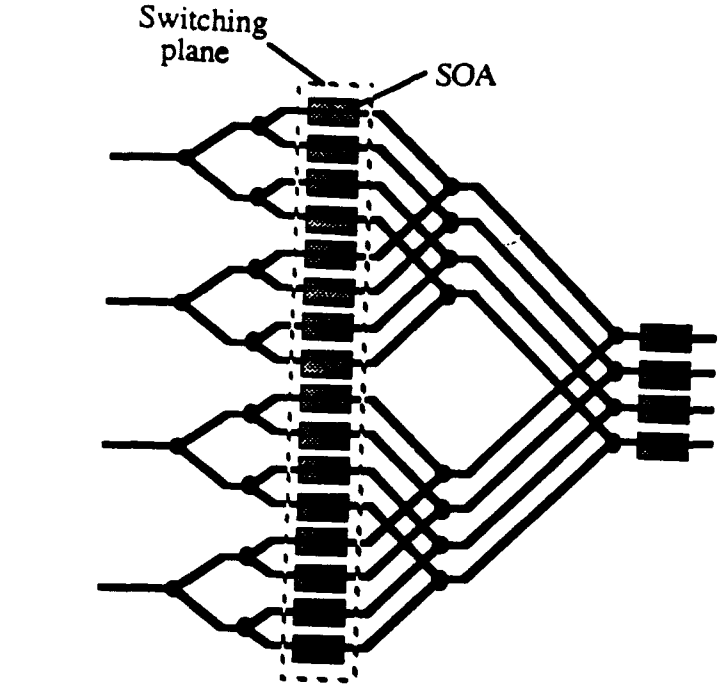

(a)

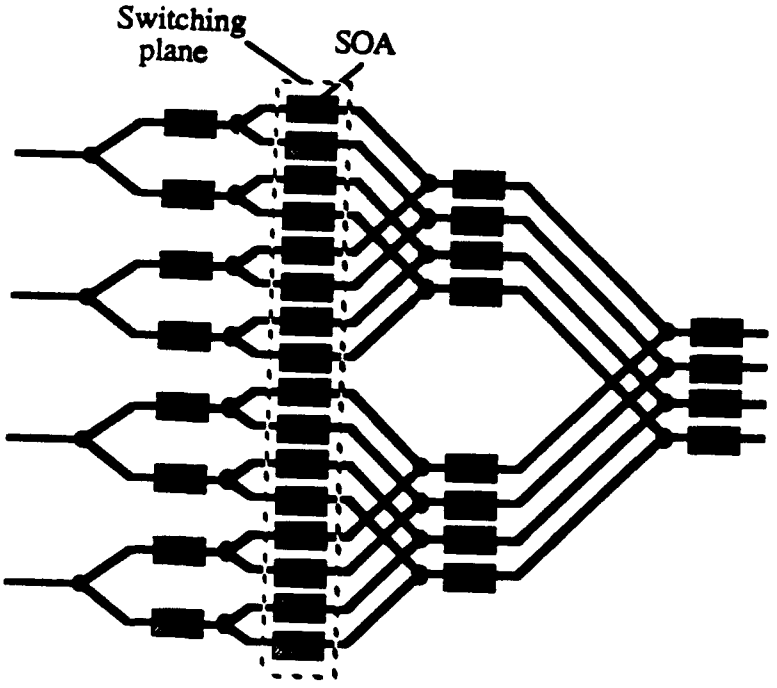

(b)

Figure 2

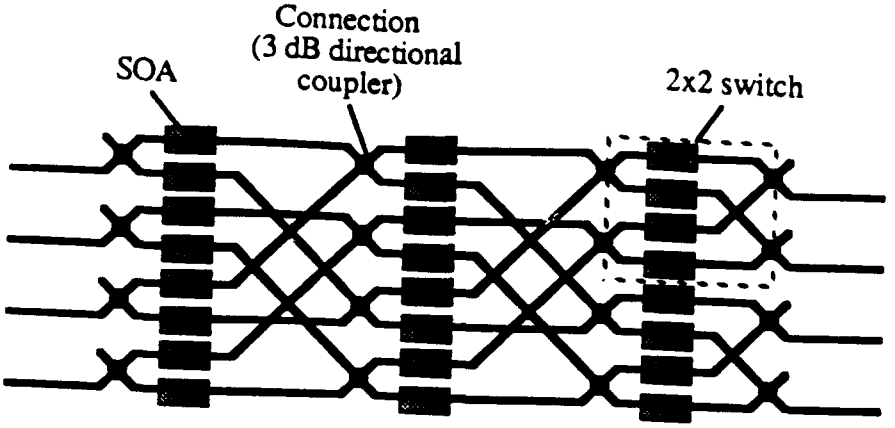

Figure 3

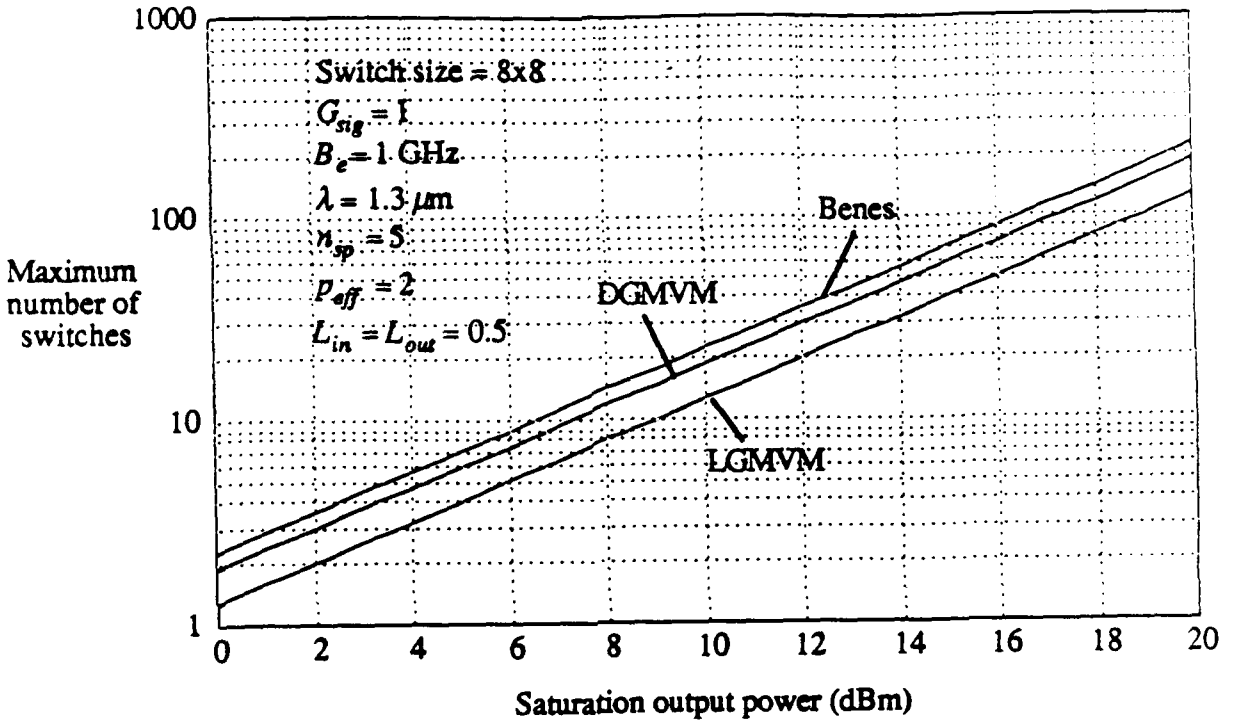
1000
100
10
1
Maximum number of switches
Switch size = 8x8
$G_{sig} = 1$
$B_e = 1$ GHz
$\lambda = 1.3\ \mu m$
$n_{sp} = 5$
$p_{eff} = 2$
$L_{in} = L_{out} = 0.5$
Benes
DGMVM
LGMVM
0
2
4
6
8
10
12
14
16
18
20
Saturation output power (dBm)

Figure 4

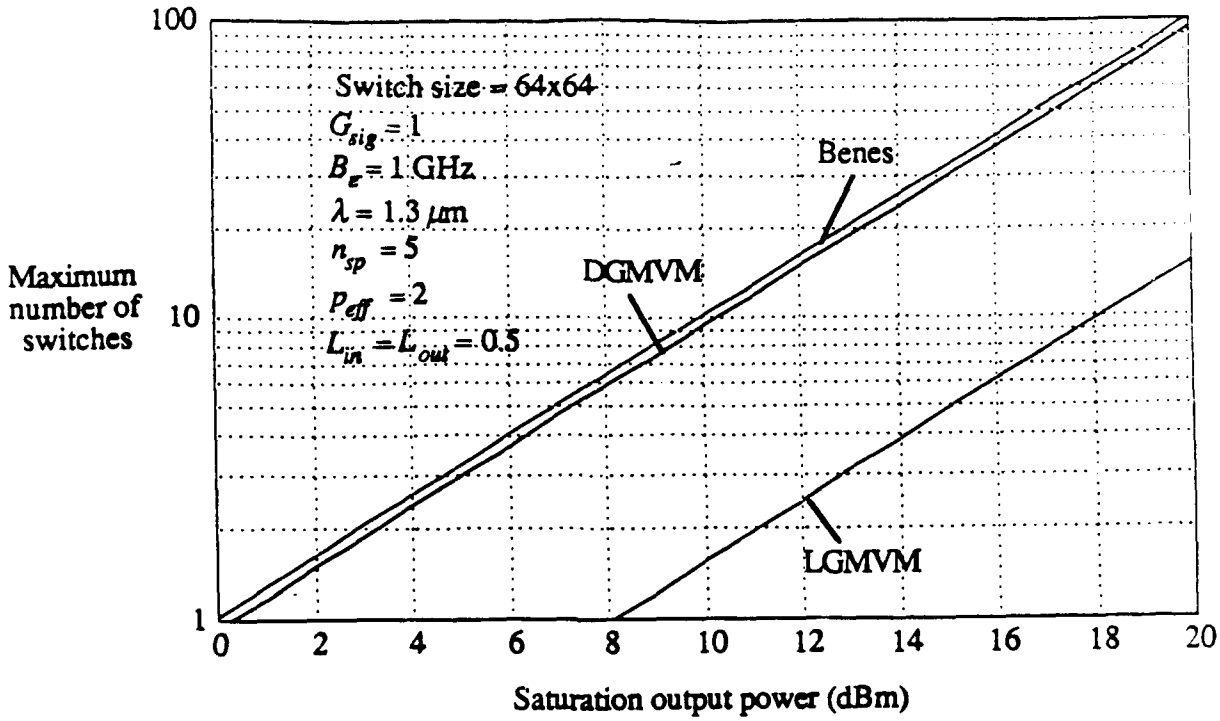
100
10
1
Maximum number of switches
Switch size = 64x64
$G_{sig} = 1$
$B_e = 1$ GHz
$\lambda = 1.3\ \mu$m
$n_{sp} = 5$
$P_{eff} = 2$
$L_{in} = L_{out} = 0.5$
Benes
DGMVM
LGMVM
0
2
4
6
8
10
12
14
16
18
20
Saturation output power (dBm)

[4] J. K. Butler, D. E. Ackley, and M. Ettenberg, "Coupled-mode analysis of gain and wavelength oscillation characteristics of diode laser phased arrays," *IEEE J. Quantum Electron.*, vol. QE-21, pp. 458-463, May 1985.
[5] I. Suemune, T. Terashige, and M. Yamanishi, "Phase-locked, index-guided multiple-stripe lasers with large refractive index differences," *Appl. Phys. Lett.*, vol. 45, no. 10, pp. 1011-1013, Nov. 1984.
[6] J. Dong, J. I. Shim, S. Arai, and K. Komori, "Theoretical analysis of in-phase lateral and single longitudinal mode InGaAsP/InP laser array," *Trans. IEICE*, to be published.
[7] D. Mehuys, W. Streifer, R. G. Waarts, and D. F. Welch, "Modal analysis of linear talbot-cavity semiconductor lasers," *Opt. Lett.*, vol. 16, no. 11, pp. 823-825, June 1991.
[8] J. Z. Wilcox, W. W. Simmons, D. Botez, M. Jansen, L. J. Mawst, G. Peterson, T. J. Wilcox, and J. J. Yang, "Design considerations for diffraction coupled arrays with monolithically integrated self-imaging cavities," *Appl. Phys. Lett.*, vol. 54, no. 19, pp. 1848-1850, May 1989.
[9] L. J. Mawst, D. Botez, T. J. Roth, W. W. Simmons, G. Peterson, M. Jansen, J. Z. Wilcox, and J. J. Yang, "Phase-locked array of antiguided lasers with monolithic spatial filter," *Electron. Lett.*, vol. 25, no. 5, pp. 365-366, Mar. 1989.
[10] D. Botez, L. J. Mawst, G. L. Peterson, and T. J. Roth "Phase-locked arrays of antiguides: modal content and discrimination," *IEEE J. Quantum Electron.*, vol. QE-26, pp. 482-495, Mar. 1990.
[11] E. Kapon, J. Katz, and A. Yariv, "Supermode analysis of phase-locked arrays of semiconductor lasers," *Opt. Lett.*, vol. 10, no. 4, pp. 125-127, Apr. 1984.
[12] J. K. Butler, D. E. Ackley, and D. Botez, "Coupled-mode analysis of phase-locked injection laser arrays," *Appl. Phys. Lett.*, vol. 44, no. 3, pp. 293-295, Feb. 1984.
[13] K. Komori, S. Arai, Y. Suematsu, I. Arima, and M. Aoki, "Single-mode properties of distributed-reflector lasers," *IEEE J. Quantum Electron.*, vol. QE-25, pp. 1235-1244, June 1989.
[14] I. Arima, J. I. Shim, S. Arai, I. Morita, R. Somchai, Y. Suematsu, and K. Komori, "1.5 μm GaInAsP/InP distributed reflector (DR) lasers with SCH structure," *IEEE Photon. Technol. Lett.*, vol. 2, pp. 385-387, June 1990.
[15] T. Asano and T. Okumura, "1.3 μm high-power BH laser on p-InP substrates," *IEEE J. Quantum Electron.*, vol. QE-21, pp. 619-622, June 1985.

Three-Wave Envelope Solitons: Can the Speed of Light in the Fiber be Controlled?

Y. N. Taranenko and L. G. Kazovsky

Abstract—**Theory predicts that three-wave envelope solitons (TWES) can be generated in dual-mode optical fibers by injecting two copropagating lightwaves or a lightwave and a flexural acoustic wave. The mechanism of the three-wave interaction is the recently observed intermodal stimulated forward Brillouin scattering. The velocity of the TWES can be controlled by changing the pump power. Using 200 mW pump power for a typical dual-mode fiber, the average speed of the light pulse in the fiber can be made as low as 3×10^4 m/s.**

I. Introduction

A recent growth of interest in dual-mode (DM) optical fibers for a variety of nonlinear switching and modulation schemes [1]-[3] stems from the long interaction lengths and from the two nondegenerate copropagating optical modes (at the same optical frequency) offered by these fibers.

This letter presents theoretical results suggesting that the speed of light in optical fibers can be controlled by using a nonlinear resonant interaction between two copropagating lightwaves and an acoustic wave in a DM optical fiber. The second-order nonlinearity involved in this process is the intermodal *forward stimulated Brillouin scattering* (FSBS) in DM optical fibers. FSBS has been observed recently for the first time [4]. In our quantitative examples we use the fiber and wave parameters from that experiment.

Manuscript received January 9, 1992. This work was supported by NSF Grant DPP89-18326, ONR Grant N00014-91-J-1357, and by the Department of Electrical Engineering, Stanford University.

The authors are with STAR Laboratory, Department of Electrical Engineering, Stanford University, Stanford, CA 94305.

IEEE Log Number 9108078.

II. Physics of Three-Wave Envelope Solitons

In an optical fiber, two waves having frequencies $\omega_{1,2}$ and wavevectors $k_{1,2}$ can parametrically generate the third wave with frequency Ω and wavevector K determined by

$$\Omega = \omega_1 - \omega_2, \qquad K = k_1 - k_2. \tag{1}$$

In a *single*-mode optical fiber, this kind of process is possible only for lightwaves propagating in opposite directions. In a *dual*-mode fiber, the LP_{01} and LP_{11} modes and a flexural acoustic wave satisfy the phase matching conditions (1), making possible the three-wave interaction of copropagating lightwaves [6]. For stimulated Brillouin scattering (SBS), only one lightwave (which is called the pump) is injected into the fiber and the other two waves are amplified from spontaneous levels.

In this letter we consider the case when two of the three waves are injected into the fiber as shown in Fig. 1. They can be two lightwaves with slightly different frequencies $\omega_1 > \omega_2$ or a light wave and an acoustic wave. A beating signal generates, via electrostriction (or the strain-optical effect), a flexural acoustic wave (or the second lightwave). After this wave is amplified, a coupled nonlinear field distribution

1041-1135/92$03.00

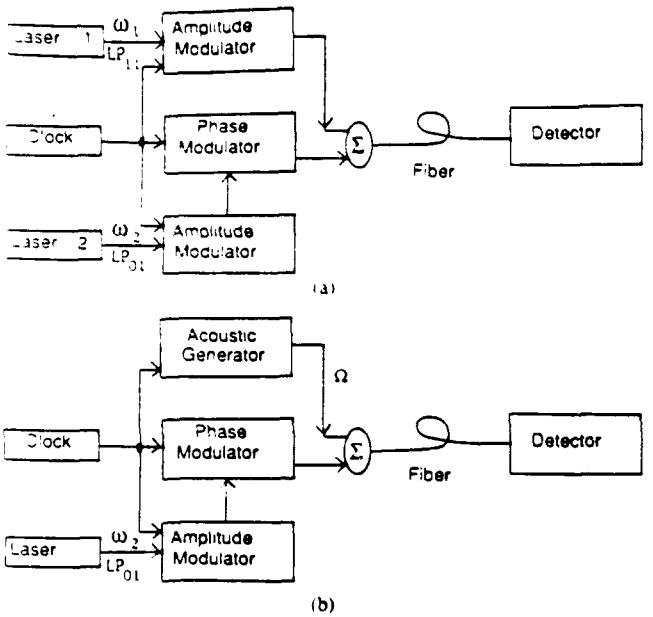

Fig. 1. (a) The block-diagram of the proposed experiment with injection of two light waves. (b) The block-diagram of the proposed experiment with injection of a light wave and an acoustic wave.

appears in the fiber. In general, this nonlinear complex can propagate with widely varying speeds having acoustic and lightwave velocities as two extremes for the cases when the power of the acoustic or lightwaves is dominant.

The detailed evolution of the waves in the fiber depends on the amplitude and phase modulation of the injected waves. This process is described by a time-dependent set of nonlinear equations:

$$\left(\frac{\partial}{\partial t} + V_l\frac{\partial}{\partial x}\right)A_{1,2} = \mp\alpha_l A_{2,1}U,$$

$$\left(\frac{\partial}{\partial t} + V_a\frac{\partial}{\partial x} + \Gamma\right)U = \alpha_a A_2 A_1 \qquad (2)$$

where x, t are space and time variables, V_l is the group velocity of the light waves, V_a is the group velocity of the acoustic wave, $A_{1,2}(t, x)$ are real slowly varying amplitudes of the light waves, $U(t, x)$ is a real slowly varying amplitude of the flexural wave, and Γ is an acoustic wave phenomenological absorption [6]. The relative phase of the waves $\psi = \varphi_1 - \varphi_2 - \varphi_3$ is assumed to be equal to $\pi/2$ or $3\pi/2$ throughout the interaction. The coupling coefficients α_l and α_a are given in [6]. We neglect the absorption of light waves since we use a short fiber ($\leq$ 1 km).

III. Generation of Three-Wave Envelope Solitons

Let us show that equations (2) have soliton solutions. To simplify the derivation, we neglect the absorption ($\Gamma = 0$). We are searching for the solitary impulse propagating with a constant velocity V [7]:

$$A_1 = A_0\cosh^{-1}\Phi,\quad A_2 = A_0\tanh\Phi,\quad U = U_0\cosh^{-1}\Phi,$$

$$\Phi = \frac{x - x_0 - Vt}{\Delta} \qquad (3)$$

where Δ determines the spatial width of the solution, U_0 is the maximum amplitude of the acoustic wave, A_0 is the maximum amplitude of the light waves, and x_0 specifies an initial position of the soliton. Solution (3) represents pulses of the lightwave with the higher frequency ω_1 and the acoustic wave. The second lightwave has a constant amplitude A_0 almost everywhere, except for the vicinity of the center of the soliton ($\Phi = 0$), where it has a local dip; thus, the relative phase ψ has a π-jump at the center of the soliton. More general TWES solutions have been discussed in references [8]–[10], [12]. We call the wave with the lower frequency $\omega_2 < \omega_1$ a pump wave since it has constant amplitude A_0 at the entrance to the fiber (assuming $x/\Delta \gg 1$ when $\Phi = 0$) and supplies energy into the fiber. This is different from SBS processes where the pump wave has higher frequency [5], [6].

Substitution of solitary-like solution (3) into the set of equations (2) gives unique values of Δ and $\delta \equiv \Delta/V$ as functions of the amplitudes A_0, U_0:

$$\Delta = \frac{V_l - V_a}{U_0\alpha_l(1 + R)},\quad \delta = \frac{\Delta}{V} = \frac{V_l - V_a}{U_0\alpha_l(V_l R + V_a)} \qquad (4)$$

where $R = \alpha_a A_0^2/\alpha_l U_0^2$ is the normalized ratio of the power densities of acoustic and light waves. The soliton velocity V is uniquely expressed as a function of the amplitudes

$$V = \frac{V_l R + V_a}{1 + R}. \qquad (5)$$

However, since $\Delta(A_0, U_0)$ behaves nonmonotonously as a function of A_0 and U_0, the plot of V versus δ has two branches (see Fig. 3). The two branches correspond to light ($V_l \geq V \geq 2V_a$) or acoustic ($2V_a \geq V \geq V_a$) dominated power:

$$V = \frac{V_l + V_a \pm \sqrt{(V_l - V_a)^2 - 4\tau_{NL}^{-2}\delta^2 V_l V_a}}{2 \times (1 + \tau_{NL}^{-2}\delta^2)} \qquad (6)$$

where $\tau_{NL}^2 = 1/A_0^2\alpha_l\alpha_a$ is a nonlinear time scale.

The TWES can be generated by injection of all three waves modulated at the entrance to the fiber ($x = 0$) in accordance to expressions (3). This type of boundary conditions for the TWES generation is the exact reproduction of the soliton fields at the entrance as it would propagate from the left-hand part of the fiber ($x < 0$). However, for a case when acoustic ($V \sim V_a$) or light ($V \gg V_a$) power is dominant, it is sufficient to inject only two of the three waves into the fiber to generate the TWES [9].

For example, soliton generation by two laser beams [10] is possible for the case of light dominated power ($V \gg V_a$) if we switch on the pump wave with the lower frequency ω_2 and then modulate this signal by a "dark" pulse with the π phase shift in the middle. Simultaneously the "bright" light pulse with the higher frequency $\omega_1 > \omega_2$ has to be launched into the fiber. These modulations are described by expressions (3) for $A_{1,2}(x = 0, t)$; the ratio δ to τ_{NL} has to give $V \gg V_a$ for a "+" sign in (6) [10]. The corresponding

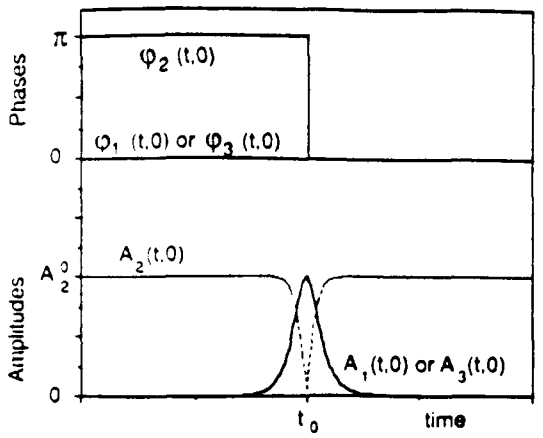

Fig. 2. Amplitudes and phases of the two waves injected into the fiber.

TABLE I
NUMERICAL VALUES OF PARAMETERS

Parameter	Notation	Value	Units
Acoustic Velocity	V_3	5.76×10^3	m/s
Light Power	W_l	200	mW
Acoustic Power	W_a	$-10^{-12} W_l/R$	mW
Laser Wave Length	λ	514.5	nm
Overlap Integrals	Q	0.15	Dimensionless
Refractive Index	n	1.5	Dimensionless
Refractive Index Difference	Δn	0.003	Dimensionless
Fiber Density	ρ	2.3	g/cm^3
Fiber Cladding Radius	a	62.5	μm
Acoustic Wave Frequency	$\Omega/2\pi$	16.6	MHz
Acoustic Wave Absorption	$1/\Gamma$	3.5	ms
Young's Modulus	E	73	GPa

amplitude and phase modulation of the input signals is shown in Fig. 2. This mechanism of soliton generation has been used for soliton experiments in stimulated Raman scattering in a para-H_2 medium [11]. Another way to generate the TWES (the case of acoustic dominated power $V \simeq V_a$) is to launch acoustic envelope $U(x, t)$ described by (3) with $V \sim V_a$ and $\Delta \simeq V_l/\alpha U_0$ and then inject the constant laser pump wave $A_2 = A_0$ in the fiber [9]. So, the two solutions with the different signs in expression (6) approximately correspond to the two mechanisms of soliton generation.

IV. Numerical Example

Consider parameters given in Table I—they are close to the parameters of the experiment [4] and are discussed in [6]. Fig. 3 shows the resulting soliton velocity V and width 6Δ versus the time duration δ. Inspection of Fig. 3 reveals that for 200 mW light wave power and pulse time duration of several μs to several ms, the average speed of the light pulse in the fiber can be as low as 3×10^4 m/s. This value is limited by the lifetime of the TWES which is approximately equal to the attenuation time of the acoustic wave (3.5 ms).

V. Summary

The results of this letter suggest that three-wave envelope solitons (TWES) can be generated by injecting two copropagating light waves or one lightwave and one acoustic wave into a dual mode optical fiber. This allows one to control the speed of light pulses in the fiber by adjusting the power of light wave. The mechanism of interaction is the recently observed intermodal stimulated forward Brillouin scattering. For 200 mW light wave power and pulse time duration of several μs to several ms, the average speed of the light pulse in the fiber can be as low as 3×10^4 m/s. This value is limited by the lifetime of the TWES which is approximately equal to the attenuation time of the acoustic wave (3.5 ms).

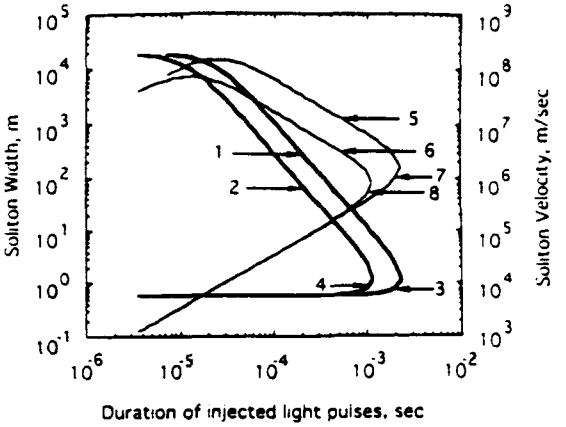

Fig. 3. The TWES velocity V (thick lines) and width 6Δ (thin lines) versus the temporal duration of the injected light signals. Curves 1 and 5 correspond to the soliton with light dominated power (the fast solution) for 200 mW of the pump and curves 2 and 6 for 50 mW of the pump. Curves 3 and 7 correspond to the soliton with acoustically dominated power (the slow solution) for 200 mW of the pump and curves 4 and 8 for 50 mW of the pump.

Acknowledgment

The authors are grateful to G.P. Agrawal, A.R. Chraplyvy, Y. Silberberg, and A.M. Weiner for their useful comments on the initial version of this letter.

References

[1] B. Y. Kim, J. N. Blake, and H. J. Shaw, "All-fiber acousto-optic frequency shifter," *Opt. Lett.*, vol. 11, pp. 389-391, 1986.
[2] S. R. Friberg, Y. Silberberg, M. K. Oliver, M. J. Andrejco, M. A. Saifi, and P. W. Smith, "Ultra-fast all-optical switching in dual-core fiber nonlinear coupler," *Appl. Phys. Lett.*, vol. 51, pp. 1135-1137, 1987.
[3] S. Trillo, S. Wabnitz, and G. I. Stegeman, "Nonlinear codirectional guided wave mode conversion in grating structures," *J. Lightwave Technol.*, vol. 6, pp. 971-976, 1988.
[4] P. St. J. Russell, D. Culverhouse, and F. Farahi, "Experimental observation of forward stimulated Brillouin scattering in dual-mode single-core fibre," *Electron. Lett.*, vol. 26, pp. 1195-1196, 1990.
[5] G. P. Agrawal, *Nonlinear Fiber Optics*. New York: Academic, 1989.
[6] P. St. J. Russell, D. Culverhouse, and F. Farahi, "Theory of forward stimulated Brillouin scattering in dual-mode single-core fibers," *IEEE J. Quantum Electron.*, vol. 27, pp. 836-842, 1991.
[7] K. Nozaky and T. Taniuty, "Propagation of solitary pulses in interactions of plasma waves," *J. Phys. Soc. Japan*, vol. 34, no. 3, pp. 796-800, 1973.
[8] G. N. Burlak, V. V. Grimal'skii, and Yu. N. Taranenko, "Feasibility of controlling the motion of acousto-electromagnetic solitons," *Sov. Phys. Tech. Phys.*, vol. 31, no. 2, pp. 259-260, 1986.
[9] G. N. Burlak, N. Ya. Kotsarenko, and Yu. N. Taranenko, "Envelope solitons in parametric wave interactions," in *Proc. Int. Conf. Plasma Physics*, vol. 2, pp. 35-38, Kiev, Naukova Dumka, 1987.
[10] ——, "Possibility of controlled slowing of light pulses in optical fibers," *Sov. Tech. Phys. Lett.*, vol. 14, no. 11, pp. 840-841, 1988.

[11] K. Druhl, R. G. Wenzel, and J. L. Carlsten, "Observation of solitons in stimulated Raman scattering," *Phys. Rev. Lett.*, vol. 51, no. 13, pp. 1171-1174, 1983.

[12] K. L. Druhl, J. L. Carlsten, and R. G. Wenzel, "Aspects of soliton propagation in stimulated Raman scattering," *J. Stat. Phys.*, vol. 39, pp. 615-620, 1985.

Analysis of Soliton Transmission in Optical Fibers with the Soliton Self-Frequency Shift Being Compensated by Distributed Frequency Dependent Gain

Ming Ding and Kazuro Kikuchi

Abstract—**Distributed optical fiber amplifiers with frequency dependent gain can be used to compensate the soliton self-frequency shift (SSFS) which is the major problem on subpicosecond soliton pulse transmission in fibers. In this letter, the characteristics of soliton evolution with SSFS being compensated by linearly frequency dependent gain are analyzed. An expression for estimating the effective distance of the compensation method, which is limited by the amplified dispersive waves at higher frequencies, are also obtained. As an example, we show that dispersion-shifted distributed Er^{3+}-doped fibers can provide almost distortion-free SSFS compensation for pulses of about 800 fs over several tens of kilometers.**

I. Introduction

In soliton-based optical fiber communication systems, subpicosecond pulses are required for bit-rates higher than several hundred gigabit/second. However, for subpicosecond pulses, stable soliton propagation in fibers becomes impossible because of the soliton self-frequency shift (SSFS) caused by the intrapulse stimulated Raman scattering (ISRS) [1] even though we neglect the effect of fiber loss. By using bandwidth limited parabolic gain spectrum in distributed optical fiber amplifiers, Blow *et al.* showed that the SSFS can be compensated by frequency dependent gain [2]. On the other hand, the recent development of Er^{3+}-doped fibers has made it possible to provide such frequency dependent gain in distributed optical amplifiers [3], [4]. The purpose of this paper is to investigate how the frequency dependent gain in Er^{3+}-doped fibers is effective for the SSFS compensation.

Manuscript received December 11, 1991. M. Ding was supported by a scholarship from the Japanese government (Monbusho).

The authors are with the Department of Electronic Engineering, Faculty of Engineering, University of Tokyo, Tokyo 113, Japan.

IEEE Log Number 9107499.

We show that the effective component of gain spectrum for SSFS compensation is the linearly frequency dependent gain (which will be abbreviated to LFDG, in the following, for simplicity). Analytic solutions for soliton transmission through fibers with SSFS being compensated by LFDG is derived for the first time in this letter. We find that the effective distance of the compensation method is limited by the amplified dispersive waves at higher frequencies, and an expression for this distance is derived. Numerical examples show that low loss dispersion-shifted (DS) distributed Er^{3+}-doped fibers can provide almost distortion-free SSFS compensation for pulses of about 800 fs over several tens of kilometers.

II. Analytic Solutions

For pulse widths larger than several picoseconds, the nonlinear optical pulse propagation in fibers at wavelengths of negative group velocity dispersion (GVD) can be described by the nonlinear Schrödinger equation (NLS):

$$i\frac{\partial u}{\partial \xi} + \frac{1}{2}\frac{\partial^2 u}{\partial \tau^2} + |u|^2 u = 0 \qquad (1)$$

where $\xi = |k''|\, z/t_0^2$, $\tau = (t - k'z)/t_0$, and u is the normalized complex pulse envelope. Symbols k' and k'' respectively denote the group delay and GVD at the central frequency ω_0 of input pulse, and t_0 represents the pulse width. The general single soliton solution of (1) is characterized by four independent constants $\{\eta, \Omega_c, \theta_0, \phi_0\}$ as

$$u(\xi, \tau) = \eta \operatorname{sech}\left[\eta(\tau + \Omega_c \xi - \theta_0)\right] \cdot \exp\left[-i\Omega_c \tau + i\frac{\xi}{2}(\eta^2 - \Omega_c^2) - i\phi_0\right]. \qquad (2)$$

When pulse widths become to few picoseconds or shorter,

1041-1135/92$03.00

WDM Local Area Networks

Wavelength-division multiplexing puts multiple channels on a single optical fiber and allows dynamic channel allocation.

Leonid G. Kazovsky, Charles Barry, Michael Hickey, Ciro A. Noronha Jr., and Pierluigi Poggiolini

The advent of new services, such as multimedia communications, high-volume file transfer, high-definition image transmission, and video/audio retrieval, has created a need for high-speed data networks. Future networks are expected to support, in an integrated fashion, services with highly diverse traffic requirements. Due to the high data rates involved, such networks will use optical fiber as the transmission medium.

It has been recognized that current network topologies, employing single shared channels to provide connectivity between the nodes, are inadequate to provide these new services, thus creating the need for multichannel networks. One way to realize multiple channels on the optical fiber is through the use of wavelength-division multiplexing (WDM). With WDM, there is an additional flexibility—by using tunable transceivers, one can dynamically allocate channels, as required by the traffic.

This paper focuses on WDM local area networks (LANs). Following a discussion of services and possible network topologies, we investigate the technological issues related to the implementation of such topologies and describe some experimental implementations reported in the literature.

Broadband Services

In addition to existing services (remote logins, file transfer, voice), high-speed LANs will be required to support broadband services. Broadband interactive services have been classified by CCITT Recommendation I.121 [1] into the following categories:

- Conversational services: real-time end-to-end information transfer (e.g., videotelephony, high-definition image transfer, high-speed data transfer)
- Messaging services: communication via store-and-forward (e.g., multimedia mail)
- Retrieval services: retrieval of information stored in databases (e.g., video on demand, or high-fidelity audio)

To provide the services described above, a network will have to handle both stream traffic (i.e., uncompressed video and audio) and bursty traffic (i.e., variable bit rate video, bursty data, etc.) at a range of data rates which spans several orders of magnitude. Some data rates required to provide broadband services are shown in Fig. 1.

Network Topologies

Current Topologies

Commercially available LANs usually are organized as buses or rings, with data rates ranging from 10 Mb/s (Ethernet) to 100 Mb/s (Fiber Distributed Data Interface [FDDI]). New standards, like the IEEE 802.6 metropolitan area network, will push data rates up to 150 Mb/s and above. A problem with these architectures is that connectivity between the nodes is provided by a small number (one, or two in the case of IEEE 802.6) of shared channels. Therefore, the electronics in each node must operate at the network aggregate speed. On the average, the maximum capacity available to each node is C/N, where C is the channel capacity and N is the number of nodes. In practice, this number is even lower due to the overheads associated with the medium access protocol. These topologies are inadequate to provide the broadband services described above. Multiple-channel topologies are needed, and due to the data rates involved, optical transport mechanisms are an excellent choice.

Future Networks

Due to high data rate requirements, single channel networks (like buses or rings) will not be able to provide the expected level of service because each node would have to operate at the network's aggregate speed. This is neither possible (due to the speeds required) nor desirable (due to the resulting low efficiency). The network, therefore, will have to provide multiple concurrent channels. One way to accomplish this in an optical network is by allocating a different wavelength for each channel (WDM).

One advantage of using WDM is that, with the use of tunable transmitters and/or receivers on

DR. LEONID G. KAZOVSKY is a professor of electrical engineering at Stanford University.

CHARLES BARRY is currently a Ph.D. student at Stanford University studying on a DEC fellowship.

MICHAEL HICKEY is a Ph.D. student in his third year at Stanford University.

CIRO A. NORONHA, JR. has been a Ph.D. student at Stanford University since 1989.

PIERLUIGI POGGIOLINI started a Ph.D. program at Politecnico di Torino in 1989. At present, he is on leave at Stanford University.

the nodes, the logical network topology becomes independent of the physical network topology, as long as all nodes have access to all wavelengths. This allows greater network flexibility as channels can be dynamically allocated according to the traffic requirements. This process is illustrated in Fig. 2, where a four-node network is shown. The nodes are connected to a star coupler, as indicated in Fig. 2a. The star coupler combines the light from all transmitters and makes it available to the receivers. By properly assigning wavelengths to receivers, different logical topologies can be created, as indicated in Figs. 2b and 2c.

In general, a node may have multiple transmitters and receivers. The number of transmitters and receivers present at each node, however, is typically much less than the number of nodes on the network. Therefore, connectivity can be provided in two ways: 1) by having a multihop network, i.e., if node A does not have a direct channel to node B, data from A to B will be sent via a number of intermediate nodes; 2) by coordinating in time the use of each wavelength; communication is always single-hop, at the expense of added delay. There are several methods to assign source-destination pairs to specific wavelengths; these methods range from classical multiple-access algorithms to fixed-assignment TDM [3–9]. A discussion of these methods is beyond the scope of this paper.

Technological Issues

Optical Transmitters and Receivers

Optical transmitters can modulate coherent light in amplitude (ASK), phase (PSK), or frequency (FSK). Optical receivers can be divided into two categories: direct detection and coherent (as shown in Fig. 3).

In direct detection receivers (Fig. 3a), the received light signal is applied directly to the photodiode. Since photodiodes essentially are broadband devices and respond only to the signal power, direct detection receivers can be used to demodulate ASK and, with filtering, wide-deviation FSK.

A coherent receiver (Fig. 3b) employs a local oscillator (LO) laser tuned to an optical frequency near that of the transmitted signal. Use of an LO frequency equal to that of the signal frequency is known as homodyne detection; use of an LO frequency which differs from the signal frequency is referred to as heterodyne detection.

The received signal and the local laser fields are added with a fiber combiner and coupled to a photodiode. Because the output current from a photodiode is proportional to the square of the incident electric field, the photodiode acts a mixer and produces an intermediate-frequency (IF) current at the difference frequency of the signal and the LO. Demodulation of the IF current recovers the transmitted data.

A problem that must be faced with coherent receivers is polarization control. The state of polarization (SOP) of the received signal must be aligned with the SOP of the light from the local oscillator laser to create the desired interaction between the two signals.

Realization of the full potential of a WDM network requires electronically tunable transmitters and/or receivers. Tunable transmitters can be

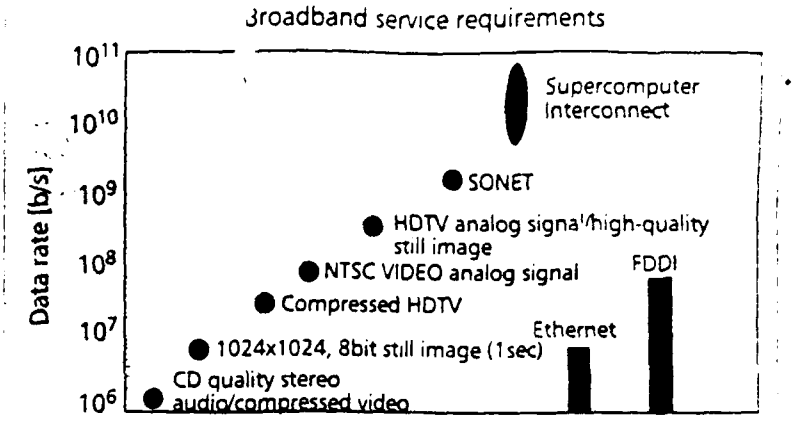

■ Figure 1. *Data rates required for broadband services. Note limitations of existing network standards such as Ethernet and FDDI*

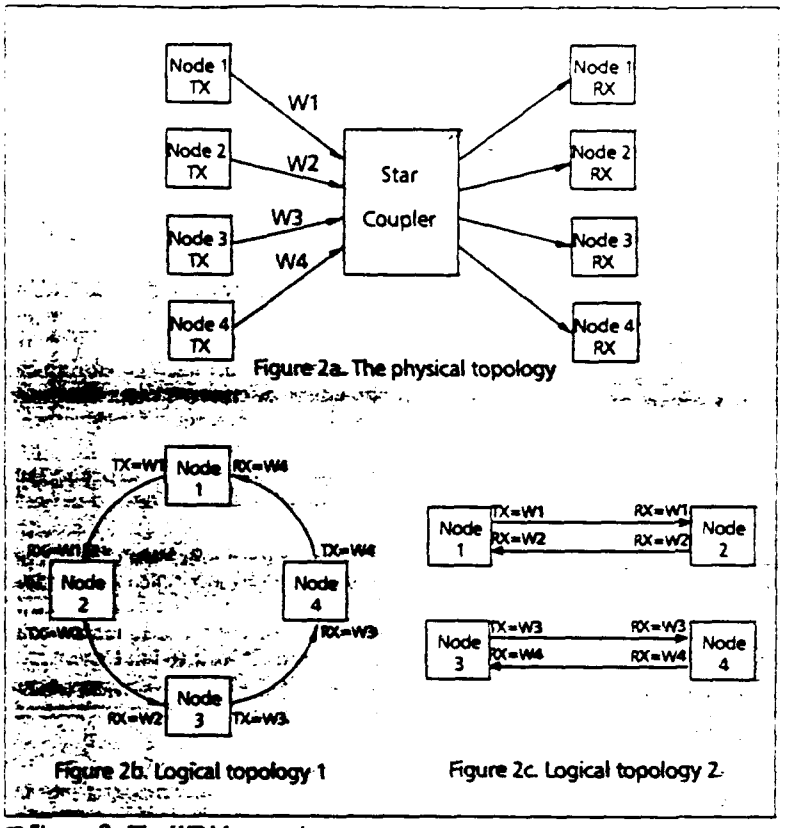

■ Figure 2. *The WDM network.*

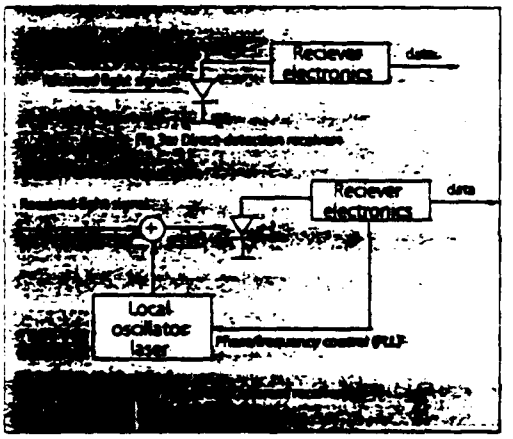

■ Figure 3. *Receiver structures.*

Technology	Acoust optics	Electro-optics	2-Section DFB	3-Section DFB	3-Section DFR	2-Section VCF
Tuning range	70nm	7nm	3.3nm	2nm	4.4nm	57nm
Kind of tuning	discrete	discrete	continuous	continuous	continuous	discrete
Laser linewidth	n.a.	60kHz	15 MHz	500 kHz	1.9 MHz	n.a.
Speed	3 μs	100 μs	n.a.	n.a.	10 μs	n.a.

■ Table I. *Tunable laser characteristics*

made using tunable lasers. A direct-detection tunable receiver can be realized by placing a tunable optical filter before the conventional direct-detection receiver shown in Fig. 3a. Tunable coherent receivers can be realized by using tunable lasers as local oscillators, because only the specific received wavelength matching that of the local oscillator will be demodulated.

In the following section, we discuss tunable lasers and tunable filters needed to build tunable transmitters and receivers. We also discuss the issues of polarization control in coherent receivers and frequency stabilization of WDM networks.

Tunable Lasers

Lasers can be tuned by providing a wavelength-tunable element inside the laser cavity. Generally speaking, there are two kinds of tunable lasers: external cavity and integrated lasers. The tuning method generally represents a tradeoff between tuning speed, linewidth, and tuning range. Moreover, depending on the method, the tuning can be either continuous or discrete over a certain range.

External cavity tuning methods [10,11] provide very low linewidth (due to the long cavity) and large tuning ranges, at low to moderate speeds. Tuning is frequently discrete (i.e., the device can generate only a discrete set of wavelengths inside the tuning range). Two classes of tuning methods have been demonstrated: acousto-optical and electro-optical. These configurations demand precise alignment between the laser and the external cavity and are difficult to implement

Integrated tunable lasers [12–16] can potentially be tuned at very high speeds (nanoseconds for some devices; although practical tuning speeds for those devices are still being investigated) at the expense of tuning range and linewidth. Some devices also are capable of continuous tuning over a range of frequencies.

There are two basic kinds of integrated tunable lasers: distributed feedback (DFB) and distributed Bragg reflector (DBR). A new kind of three-section laser has been recently reported, with discrete tuning over 57 nm, utilizing an integrated vertical coupler filter (VCF) [41]. Usually, there is a tradeoff between linewidth and tuning speed.

Table I presents a summary of the tunable laser characteristics. The table indicates that the main problem with tunable lasers is their limited range, which limits the number of channels they can resolve.

Tunable Filters

Wavelength filtering can be achieved by the following mechanisms [17]: wavelength dependence of interferometric phenomena (Fabry-Perot and Mach-Zehnder filters); wavelength dependence of coupling between modes, caused by external perturbations (electro-optic and acousto-optic filters); and resonant amplification in active semiconductor devices.

As shown by Table II [17], current tunable filter technology severely limits either the tuning speed or the tuning range that can be achieved by direct-detection tunable receivers.

Polarization Control

Coherent receivers require that the polarization of the local oscillator matches the polarization of the incident light. Otherwise, the useful signal generated at the photodiode can be attenuated or even fade completely. As light propagates through conventional single-mode optical fiber, its polarization is transformed to an arbitrary state by small perturbations in the fiber. Several approaches to match the signal and local oscillator polarizations follow.

Polarization-maintaining fiber and connectors [18] – By appropriately shaping or stressing the fiber core, it is possible to produce special fibers that do not change the polarization of the transmitted light, provided that the state of polarization of the light launched on the fiber is aligned with one of the fiber's main axes.

Technology	Fabry-Perot	Acousto-optics	Electro-optics	Active Semiconductor
Tuning range	50	100	10	40
Bandwidth (nm)	<0.01	1	1	0.05
Number	100	100	10	40
Loss (dB)	5	5	5	0
Cost	low	high	high	low

■ Table II. *Tunable filter characteristics*

Polarization-diversity receivers [19] – Before (or after) mixing the light from the local oscillator with the incoming light, polarization-diversity receivers divide the light into two orthogonal polarizations and detect them separately. After photodetection and demodulation, the resulting signals are combined. The combined signal is independent of the state of the received light's polarization.

Polarization switching [20] – During each bit, the polarization of the transmitted light is switched between horizontal and vertical (i.e., half of the time it remains in the vertical polarization, and the other half in horizontal). With this scheme, the receiver is simpler than a polarization-diversity receiver, but a 3 dB penalty on the receiver sensitivity is introduced.

Polarization tracking [21] – In the same way as a PLL tracks the frequency of its input signal, it is possible to have the local oscillator track the polarization of the incoming light, at a cost of greatly increased receiver complexity.

Frequency Stabilization

Absolute and relative optical frequency stabilization may be required in multichannel optical systems with tight channel spacing. Absolute frequency stabilization techniques involve frequency locking to a stable atomic or molecular absorption phenomenon. Absolute frequency references have been achieved in both the 1300 nm and 1500 nm windows [22, 23]. Relative frequency stabilization techniques include locking to the sidebands of an FM modulated master laser [24], and optical phase locking to the sidebands of a RF phase modulated master laser [25].

WDM Network Experiments

The last five years have witnessed a steady transition of WDM experiments from proof of concepts to experimental networks, with field trials planned in the near future. Several notable experiments illustrate the progression of this technology: demonstrations of single channel transmission with multi-gigabit data rates [26, 27], broadcast of 100 direct detection channels [28], 16-channel coherent broadcast experiment [29], computer-controlled tuning of an eight-channel coherent experiment [30], and demonstration of a fully engineered coherent broadcast experiment [31]. The following two sections are devoted to descriptions of recent experimental demonstrations of WDM optical metropolitan and local area networks, both direct detection and coherent.

Direct Detection WDM Optical Networks Several experiments are currently investigating direct detection WDM networks. These experimental networks use direct detection optical receivers and tunable optical filters for channel selection. Direct detection technology was chosen for its reduced cost and complexity. Description of two of these experiments follow.

TeraNet

TeraNet [32] is an experimental network being developed to study all seven layers of the OSI standard. The network provides either 1 Gb/s ATM packet-switched or 1 Gb/s circuit-switched access using a passive star topology, as shown in Fig. 4. A hybrid multiple access scheme combines wavelength-division-multiplexing and subcarrier frequency division multiplexing to divide the available optical bandwidth. This method of multiple access reduces the bandwidth requirements on the optical filters, but still allows the use of additional channels through electronic means.

The transmitters utilize DFB lasers. Each user is assigned a unique address consisting of a specific wavelength and a subcarrier multiplexed frequency. Wavelength channels are spaced by 1.5 nm, or 187 times the bit rate. Each wavelength supports four to six subcarrier channels. The subcarrier modulation format can be either BPSK or QPSK, while the subcarrier's amplitude modulates the optical signal.

The receivers use fiber-optic Fabry-Perot (FFP) tunable filters to select wavelengths. Subcarriers are selected by electronic filtering.

A packet-switched network, conforming to the ATM standard [33], is being implemented through a multihop architecture. The network can be configured to support up to 64 users. Interfaces also are being developed for SONET and HIPPI. A limited campus field trial is planned for 1992.

RAINBOW Network

The RAINBOW network [34] is a metropolitan area network designed to cover a diameter of 55 km. This network connects 32 IBM PS/2s through a 32 x 32 passive star coupler and allows the computers to communicate circuit-switched data at a rate of 200 Mb/s/node. The physical topology is the WDM star shown in Figure 2a. Each computer is equipped with its own fixed frequency optical transmitter and tunable optical receiver mounted on plug-in computer cards.

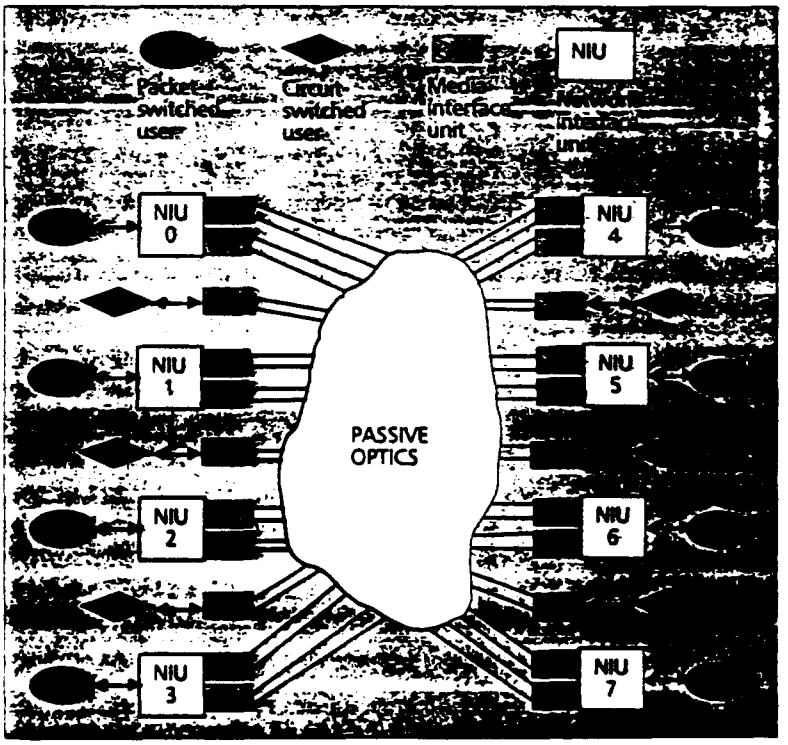

■ Figure 4. *TeraNet packet and circuit switching lightwave network (adapted from ref. [32]).*

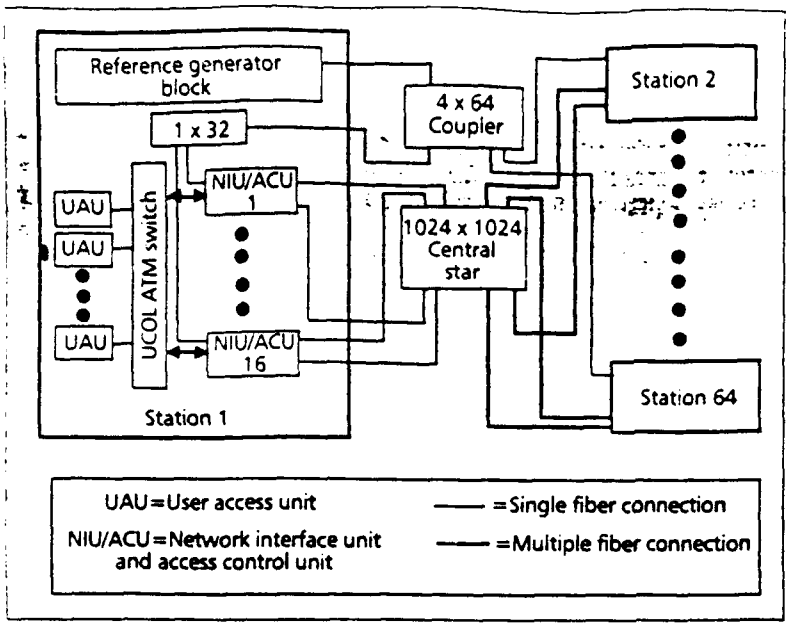

■ Figure 5. *UCOL system block diagram (adapted from ref. [35])*

The optical transmitters utilize directly modulated distributed feedback (DFB) laser diodes. The optical channel spacing is roughly 1.6 nm, or 1040 bit rates. This channel spacing is wide enough so that temperature control is adequate for frequency stabilization. The modulation format is on/off keying (OOK).

Wavelength selection is accomplished with a tunable fiber Fabry-Perot filter. The interferometer cavity spacing is varied piezoelectrically to achieve a tuning speed of 2 ms over the tuning range of 50 nm.

The signaling protocol for coordinating the retuning of the optical receivers is a simple in-band polling procedure. This method is simpler than a faster out-of-band protocol, which would require a separate signaling channel.

Experimental results reveal that a power budget of 8.5 dB with a 3 dB margin is typically achieved. This budget would allow a network diameter of 28 km.

Coherent WDM Computer Networks The direct-detection experiments described above demonstrate the potential of WDM computer networks and show that increasing network performance will require improved power budgets, tighter channel spacing, increased tuning speeds, or new network architectures. Coherent technology is one option for increasing the power budget and decreasing the channel spacing. Below we describe one WDM coherent experiment, and in the next section we will discuss STARNET, a coherent WDM network being implemented at Stanford University.

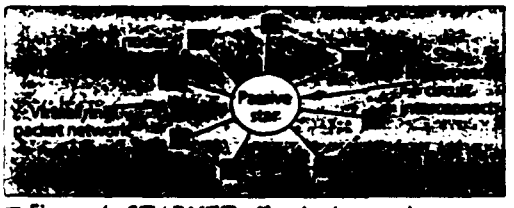

■ Figure 6. *STARNET offers both a moderate-speed packet switch network and a high-speed broadband circuit interconnect on a physical passive star topology*

UCOL – UCOL is being developed as an ultra-wideband coherent optical local area network [35]. This network has network interface units/access control units (NIU/ACUs) that communicate on 20 wavelength division multiplexed optical channels over a passive star topology, as indicated in Fig. 5. The user can access each channel through a time division multiplexing access mode (UCOL ATM SWITCH). This technique supports data rates from a fraction of a Mb/s up to 155 Mb/s. The frequency reference for all transmitters and receivers is provided over a separate star coupler by a reference generator block (RGB). The reference frequencies are generated by modelocking an external cavity semiconductor laser. Channel spacing is 3.6 GHz, or about 23 bit rates.

The transmitters are external cavity lasers, tunable over 1 nm in the 1.5 nm wavelength window. DPSK modulation is accomplished with an external $LiNbO_3$ modulator.

The receivers are polarization-diversity, delay-line DPSK demodulators. The transmit power is set for operation with a BER of 10^{-6}. Error-correcting codes are then used to decrease the BER to a value less than 10^{-10}.

STARNET

The foregoing network experiments have shown the feasibility of relatively dense WDM networks. These experiments, however, have not addressed the need to support all the heterogeneous data traffic types as outlined in this paper's introduction. STARNET [36] is a new coherent broadband optical local area network (BOLAN) architecture. The STARNET architecture offers all users both a high-speed packet-switched network and a multi-gigabit broadband circuit interconnect based on a WDM transport facility, as shown in Fig. 6. As a result, the STARNET architecture efficiently supports diverse types of traffic.

An experimental demonstration of STARNET is currently under development in the Optical Communications Research Laboratory at Stanford University. The initial STARNET experiment will interconnect four workstations through a 4 x 4 passive star coupler. The data rate for the broadband circuit switched network is 3 Gb/s/station. The packet-switched network data rate is 100 Mb/s.

STARNET Architecture

STARNET's physical topology is the passive star shown in Fig. 2a. However, each node transmitter transmits two independent data streams, stream C (circuit data) and stream P (packet data), as depicted in Fig. 7. Each node has a tunable receiver that can be tuned to any transmitter and decodes the C stream, thus enabling a broadband circuit interconnect among all the nodes. In addition, every node is equipped with a fixed receiver which decodes the P stream of the previous node in the frequency comb, as shown in Fig. 7. The first node of the chain is equipped with a receiver that decodes the P stream of the last node. In this manner, a unidirectional store-and-forward logical ring topology similar to that of FDDI is formed, as shown in Fig. 6

STARNET Physical Implementation

The experimental STARNET will connect four workstations through a passive star coupler. Each node consists of a transmitter, a 3 Gb/s broadband receiver for the circuit interconnect, and a 125 Mb/s receiver for the packet-switched network. The network operates at a center wavelength of 1319 nm over conventional single mode fiber with a network diameter of 4 km.

A STARNET transmitter is illustrated in Fig. 8. The laser source is a 25 mW, 1319 nm Nd:YAG laser. The light carrier passes through an isolator and is then coupled into a conventional single mode fiber. Subsequently, the light passes through a 50 percent splitter; half the power is sent to the external modulator, while the other half is used as the LO for the packet-switched network receiver. The external modulator is a $LiNbO_3$ dual phase/amplitude modulator. The 3 Gb/s circuit switch data is PSK modulated on the optical carrier. The 100 Mb/s packet data is 4B/5B encoded and then ASK modulated on the optical carrier at 125 Mb/s by modified FDDI hardware in the workstation. After modulation, the optical signal is sent to the star.

The PSK receiver (Fig. 9) uses a thermally tunable Nd:YAG laser as the LO. The polarization of the LO light is manually aligned with the polarization of the network signal and then both signals are combined with a 3 dB coupler. The mixed optical signal is applied to a PIN photodiode with a low-impedance front-end. The resulting electronic signal is centered around an IF of 8 GHz. The signal is then mixed with a 8 GHz RF local oscillator to bring it to baseband. A portion of the baseband signal is used to maintain phase lock of the receiver [27]. The remainder of the baseband signal is low-pass filtered to recover the 3 Gb/s data. The system is designed to ensure a BER of 10^{-9} with a 10 dB system margin.

The ASK receiver (Fig. 9) uses the transmitter laser as the LO. After polarization alignment and 3 dB coupling, the ASK heterodyne optical signal is sent to a PIN photodiode with a low-impedance front-end amplifier. The resulting IF signal is squared to remove the phase modulation and sent to a low-pass filter to recover the baseband 125 Mb/s data. The data is then decoded by the FDDI hardware in the workstation.

The following is a discussion of some of the design decisions that were made for the initial STARNET experiment.

Modulation format – Heterodyne PSK was chosen for the 3 Gb/s interconnect because of its superior receiver sensitivity and efficient bandwidth utilization.

Transmitter/modulator – Since heterodyne PSK detection is used, lasers with low-laser linewidths are required [37]. Nd:YAG lasers were selected for their ultra-narrow linewidth, excellent frequency stability, and large optical output power (25mW).

Network frequency allocation – Node transmitter frequencies are allocated in a bandwidth efficient manner [38], as shown in Fig. 10a. The signal spectrum at the IF stage of the packet network fixed receiver is shown in Fig. 10b. Note that the carriers corresponding to the previous and next node are both visible. The minimum optical channel spacing is 8 GHz, resulting in packet network IFs of 8 GHz or 16 GHz depending on the position of the receiver node. The IF for the 3 Gb/s broadband circuit is 8 GHz

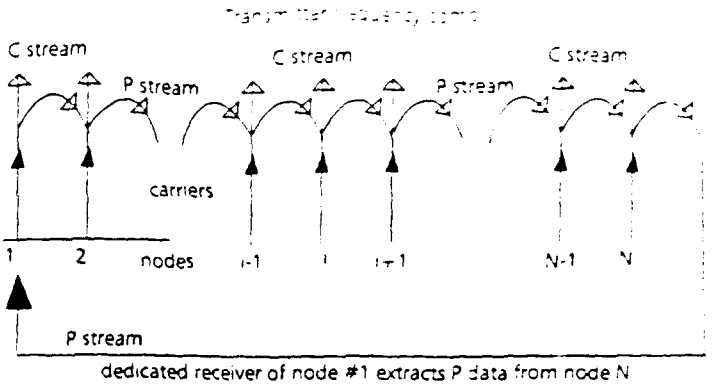

■ Figure 7. *Two independent data streams (C and P) are multiplexed onto each carrier. The first node of the chain extracts the P stream of the last node in the comb, and closes the ring.*

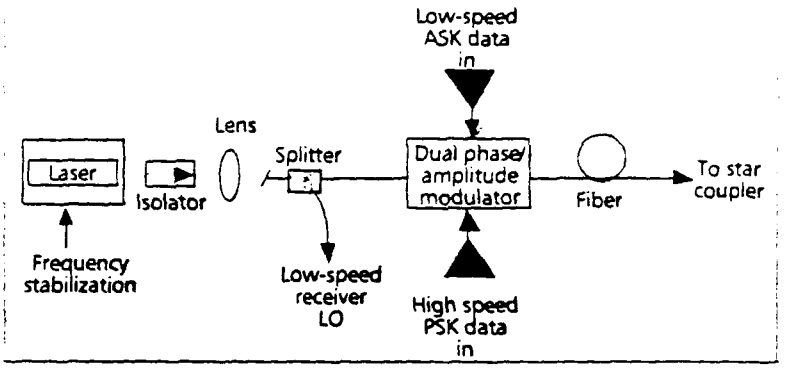

■ Figure 8. *STARNET node transmitter*

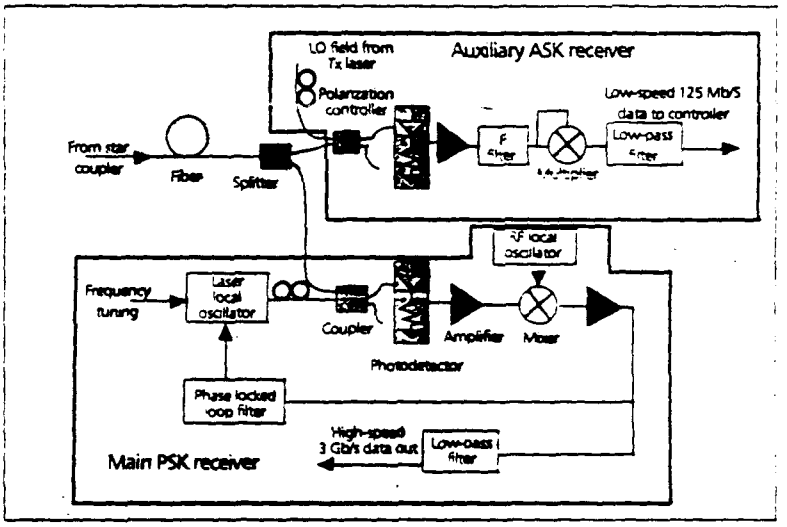

■ Figure 9. *STARNET node receiver.*

for all nodes and is set by the tunable receiver LO. For the four node experiment, the range of transmitter frequencies is 32 GHz. At 1319 nm center wavelength, this results in an extremely dense optical channel spacing of just 0.04 nm, or 2.67 bit rates. Although the channel spacing is very narrow, less than 2 dB of channel crosstalk power penalty is foreseen [39].

Tunable receiver—The tunable receiver LO is an ultra-low linewidth Nd:YAG laser. Unfortunately, the narrow linewidth is accompanied by slow thermal tuning (several seconds) and a small tun-

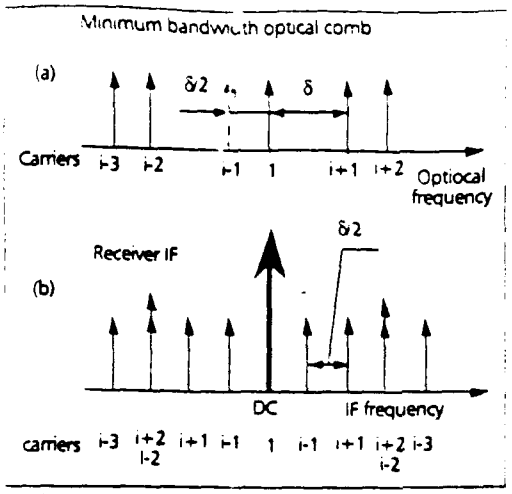

■ Figure 10. *Carrier visibility at IF in the fixed receiver of node i, employing the node carrier as LO and minimum optical bandwidth allocation of carriers. In this case, the privious node IF is at δ/2; the next node IF is δ. The value of δ is 16 GHz in STARNET.*

ing range (40 GHz). A PIN photodiode with a low-impedance front-end amplifier is used for photodetection of the heterodyne PSK signal. The greater sensitivity of a balanced receiver is sacrificed for the reduced cost and complexity of the single-ended receiver. The IF demodulator utilizes commercially available microwave components.

Frequency stabilization – STARNET uses a novel approach to achieve relative frequency stabilization of the network. The fixed receiver keeps its LO tuned to the previous node in the frequency comb. In STARNET, the LO of the fixed receiver is also the node transmitter laser. Therefore, the frequency control operated by the fixed receiver to keep its LO locked on the previous node carrier also establishes relative frequency stabilization between the two nodes. Since each node is locked to the previous node, overall network frequency stabilization is achieved.

Polarization control – Polarization control of the initial STARNET experiment is manual, which reduces receiver complexity. A mature implementation will require polarization diversity, polarization-switching or polarization-maintaining fibers.

Conclusions

The characteristics of the WDM network experiments discussed in this paper are summarized in Table III. As indicated by the table, coherent networks achieve denser channel spacing and higher data rates at the expense of added complexity.

Multi-Gb/s broadband networks are required for future high-speed applications such as broadband video and supercomputer interconnection. In addition, these future networks must also handle current low-speed applications such as electronic mail and file transfer. As indicated by Table III, direct detection and coherent technology both offer solutions to the networking of many high-speed channels using WDM.

Although experimental WDM systems take advantage of the huge bandwidth of the optical fiber, both optical filter and laser tuning speeds are not yet fast enough to support very high-speed packet-switched data. One solution to this problem is offered by STARNET. The STARNET architecture provides two logical networks, a multi-gigabit broadband circuit switched network simultaneously with a high-speed, packet-switched network.

An experimental STARNET is being constructed at Stanford University. It will interconnect four workstations with a data rate of 3 Gb/s/node for the circuit switch network and 100 Mb/s for the packet-switched network.

Many challenges are yet to be resolved before multi-Gb/s optical networks become practical. Among these challenges are the development of fast tunable and narrow linewidth lasers, tunable filters, automatic frequency selection, frequency

	TERANET	RAINBOW	UCOL	STARNET
Modulation format	ASK	ASK	DPSK	PSK
Data rate	1 Gb/s	200 Mb/s	155 Mb/s	3 Gb/s
Channels separation	187 Bit rates	1040 Bit rates	23 Bit rates	2.7 Bit rates
Kind of receiver	Direct detection	Direct detection	Coherent	Coherent
Tunable element	Fabry-Perot filter	Fabry-Perot filter	Laser	Laser
Frequency stabilization	Thermal	Thermal	External reference	Provided by the architecture
Polarization control	Not needed	Not needed	Polarization diversity	Manual
Receivers per node	2/tunable	1/tunable	1/tunable	1/tunable 1/fixed
Transmitters per node	2/fixed	1/fixed	1/tunable	1/fixed
Extra features	Multiple subcarrier channels		Wide range of data rates supported	Lower-speed packet network imbedded

■ Table III. *WDM network experiments*

stability of the network, design of network protocols efficient for high-speed bursty and continuous traffic, and selection of network topologies which optimize both throughput and latency.

Acknowledgments

Support for the STARNET experiment is provided by the National Science Foundation, through Grant No. ECS-9111766, and by the Office of Naval Research, through Grant No. N00014-91-J-1857. Michael Hickey is supported by an NSF graduate fellowship. Ciro Noronha is supported by an FAPESP fellowship. Charles Barry is supported by a DEC fellowship.

References

[1] CCITT Recommendation I.121, "Broadband Aspects of ISDN," *Blue Book*, fascicle III.7, pp. 34-61, Melbourne 1988.

[2] F. Tobagi, "High-Speed Networking and B-ISDN," INFOCOM 1991 Tutorial, Bal Harbour, Fla., April 9-11, 1991.

[3] J. Bannister, L. Fratta, and M. Gerla, "Topological Design of the Wavelength-Division Optical Network," IEEE INFOCOM 1990, San Francisco, June 3-7, 1990.

[4] J. Bannister, L. Fratta, and M. Gerla, "Routing in Large Metropolitan Area Networks Based on Wavelength-Division Multiplexing Technology," in *High-Capacity Local and Metropolitan Area Networks – Architecture and Performance Issues*, G. Pujolle (ed.) (Springer-Verlag, 1990).

[5] J.-F. Labourdette and A. Acampora, "Wavelength Agility in Multihop Lightwave Networks," IEEE INFOCOM 1990, San Francisco, June 3-7, 1990.

[6] J.-F. Labourdette and A. Acampora, "Partially Reconfigurable Multihop Lightwave Networks," IEEE GLOBECOM 1990, San Diego, Dec. 2-5, 1990.

[7] I. Habbab, M. Kavehrad, and C. Sundberg, "Protocols for Very High-Speed Optical Fiber Local Area Networks Using a Passive Star Topology," *IEEE J. of Lightwave Tech.*, Vol. LT-5, No. 12, pp. 1782-93, Dec. 1987.

[8] I. Chlamtac and A. Ganz, "Design Alternatives of Asynchronous WDM Star Networks," IEEE ICC 1989, Boston, June 11-14, 1989.

[9] A. Ganz and Z. Koren, "WDM Passive Star—Protocols and Performance Analysis," IEEE INFOCOM 1991, Bal Harbour, Fla., April 9-11, 1991.

[10] G. Coquin, K. W. Cheung, and M. M. Choy, "Single- and Multiple-Wavelength Operation of Acousto Optically Tuned Semiconductor Lasers at 1.3 Microns," *Proc. 11th IEEE Int. Semiconductor Laser Conf.*, Boston, Aug. 29-Sept. 1, 1988.

[11] F. Heismann et al., "Narrow-Linewidth, Electro-Optically Tunable InGaAsP-Ti:LiNbO3 Extended Cavity Laser," *App. Phys. Lett.*, Vol. 51, pp. 164-65, 1987.

[12] M. Okai, S. Sakano, and N. Chinone, "Wide-Range Continuous Tunable Double-Sectioned Distributed Feedback Lasers," 15th European Conf. Optic. Comm., Gothenburg, Sweden, 1989.

[13] H. Imai, "Tuning Results of 3-Sectioned DFB Lasers," Semiconductor Laser Workshop, CLEO'89, Baltimore, MD, 1989.

[14] T. L. Koch et al., "Continuously Tunable 1.5 mm Multiple-Quantum-Well GaInAs/GaInAsP Distributed-Bragg-Reflector Lasers," *Electron. Lett.*, Vol. 24, No. 23, Nov. 1988.

[15] K. Kobayashi and I. Mito, "Single Frequency and Tunable Laser Diodes," *J. Lightwave Tech.*, Vol. LT-6, No. 11, pp. 1623-33, Nov. 1988.

[16] T. P. Lee and C. E. Zah, "Wavelength-Tunable and Single-Frequency Semiconductor Lasers for Photonic Communications Networks," *IEEE Communications Mag.*, pp. 42-52, Oct. 1989.

[17] H. Kobrinski and K.-W. Cheung, "Wavelength-Tunable Optical Filters: Applications and Technologies," *IEEE Communications Mag.*, pp. 53-63, Oct. 1989.

[18] S. E. Miller and I. P. Kaminow, *Optical Fiber Telecommunications II*, pp. 79-90 (Academic Press, 1988).

[19] L. G. Kazovsky, "Phase- and Polarization-Diversity Coherent Optical Techniques," *J. Lightwave Tech.*, Vol. LT-7, No. 2, pp. 279-92, Feb. 1989.

[20] N. Caponio et al., "Polarisation Insensitive Coherent Transmission by Synchronous Intrabit Polarisation Spreading," *Electron. Lett.*, Vol. 27, No. 4, Feb. 14, 1991.

[21] F. Heismann et al., "Integrated-Optic Polarization Controller with Unlimited Transformation Range," *Appl. Phys. Lett.*, Vol. 57, No. 9, Aug. 1990.

[22] Y. C. Chung et al., "WDM Coherent Star Network with Absolute Frequency Reference," *IEEE Electron. Lett.*, Vol. 24, No. 21, pp. 1313-14, Oct. 13, 1988.

[23] S. Sudo, Y. Sakai, and T. Ikegami, "Frequency Stabilization Scheme for DFB Laser Diodes Using Acetylene Absorption Lines in 1.51-1.55 mm," OFC '91, San Diego, paper FB7, 1991.

[24] L. G. Kazovsky, "Novel Relative Frequency Stabilization Technique for Multichannel Optical Communication Systems," *IEEE PTL*, Vol. 1, No. 12, pp. 453-57, Dec. 1989.

[25] L. G. Kazovsky, "Experimental Relative Frequency Stabilization of a Set of Lasers Using Optical Phase-Locked Loops," *IEEE PTL*, Vol. 2, No. 7, pp. 516-18, July 1990.

[26] T. Saito et al., "High Receiver Sensitivity at 10 Gb/s Using an Er-Doped Fiber Preamplifier Pumped with a 0.98 mm Laser Diode," *IEEE PTL*, Vol. 3, No. 6, pp. 551-53, June 1991.

[27] L. G. Kazovsky and D. A. Atlas, "Optical Phase-Locked PSK Heterodyne Experiment at 4 Gb/s," *IEEE PTL*, Vol. 2, No. 8, Aug. 1990.

[28] H. Toba et al., "A 100-channel Optical FDM Transmission/distribution at 622 Mb/s Over 50 km," *J. Lightwave Tech.*, Vol. 8, No. 9, pp. 1396-1401, Sept. 1990.

[29] R. E. Wagner et al., "16-Channel Coherent Broadcast Network at 155 Mb/s," OFC '89, Houston, paper PD12, 1989.

[30] B. Glance and O. Scaramucci, "Computer-controlled Multichannel Heterodyne Optical Communication System," *IEEE PTL*, Vol. 3, No. 1, pp. 83-85, Jan. 1991.

[31] G. Heydt et al., "CMC Broadband Customer Access: CMC System Application Areas and Evolution Access," Fourth R1010 report, CMC 8-142-1, Sept. 1991.

[32] R. Gidron et al., "TeraNet: A Multi Gigabit Per Second Hybrid Circuit/packet Switched Lightwave Network," *Proc. SPIE Adv. Fiber Comm. Tech.*, pp. 40-48, Boston '91, Sept. 3-4, 1991.

[33] ANSI, "Broadband ISDN ATM Aspects-ATM Layer Functionality and Specification T1S1 5/90-058R2," Aug. 27, 1990.

[34] N. R. Dono et al., "A Wavelength Division Multiple Access Network for Computer Communication," *IEEE JSAC*, Vol. 8, No. 6, pp. 983-94, Aug. 1990.

[35] A. Fioretti et al., "An Evolutionary Configuration for an Optical Coherent Multichannel Network," GLOBECOM '90, pp. 779-83, San Diego, Dec. 2-5 1990.

[36] P. T. Poggiolini and L. G. Kazovsky, "STARNET: an Integrated Services Broadband Optical Network with Physical Star Topology," Adv. Fiber Comm. Tech., Leonid G. Kazovsky (ed.), *Proc. SPIE 1579*, pp. 14-29, 1991.

[37] L. G. Kazovsky, "Performance Analysis and Laser Linewidth Requirements for Optical PSK Heterodyne Communications Systems," *J. Lightwave Tech.*, Vol. LT-4, No. 4, April 1986.

[38] V. O'Byrne, "A Method for Reducing the Channel Spacing in a Coherent Optical Heterodyne System," *IEEE PTL*, Vol. 2, No. 7, July 1990.

[39] L. G. Kazovsky and J. L. Gimlett, "Sensitivity Penalty in Multichannel Coherent Optical Communications," *J. Lightwave Tech.*, Vol. 6, No. 9, Sept. 1988.

[40] W. B. Sessa, et al., "Multichannel Frequency Control for Multilocation Network Applications," *OFC '91, Proc.*, Paper WH5, p. 98, San Diego, Feb. 19-22, 1991.

[41] R. C. Alferness et al., "Widely Tunable InGaAsP/InP Laser Based on a Vertical Coupler Intracavity Filter," *OFC '92 Postdeadline Papers*, Paper PD2, pp. 321-24, San Jose, Feb. 2-7, 1992.

Biography

DR. LEONID G. KAZOVSKY (M-80, SM-83, F-90) received his M.Sc. and Ph.D. degrees in electrical engineering from the Leningrad Electrotechnical Institute of Communications, Leningrad, USSR, in 1969 and 1972, respectively. From 1974 to 1984 (with a one-year interruption for active military service), Dr. Kazovsky was teaching and doing research at Israeli and U.S. universities. From 1984 to 1990 he was with Bellcore, Red Bank, New Jersey. In 1990, Dr Kazovsky joined Stanford University as professor of electrical engineering.

CHARLES BARRY received his B.S. in physics from MIT in 1982 and his M.S.E.E. from Stanford University in 1988. Mr. Barry has been a principal design engineer with Digital Equipment Corporation since 1983 and is currently a Ph.D. student at Stanford University studying on a DEC fellowship. Mr. Barry is a licensed professional engineer (CA).

MICHAEL HICKEY (M-91) received his B.S.E.E. from Rice University, Houston, Texas, in 1988 and his M.S.E.E. from Stanford University, Stanford, California, in 1990. He is in his third year at Stanford University studying on a National Science Foundation graduate fellowship.

CIRO A. NORONHA, JR. received his B.S.E.E. and M.S.E.E. degrees from the Instituto Tecnológico de Aeronáutica, São José dos Campos, Brazil, in 1985 and 1988, respectively. Noronha was a design engineer with Elebra Telecom SA, São Paulo, Brazil, from 1986 to 1987. From 1987 to 1989 he was with the telecommunications department of the Instituto Tecnológico de Aeronáutica, São Jose dos Campos, Brazil. Since 1989 he has been a Ph.D. student at Stanford University.

PIERLUIGI POGGIOLINI was awarded the Laurea degree cum laude at Politecnico di Torino in 1988. He was with the Italian State Telephone Company Research Center CSELT (Turin) for nine months, as a grantholder. In 1989 he started a Ph.D. program at Politecnico di Torino. At present, he is on leave at Stanford University. Pierluigi Poggiolini is supported by the Italian Ministry of Education and the Italian State Telephone Company.

STARNET: a Multi-Gbit/s Optical LAN Utilizing a Passive WDM Star.

L. G. Kazovsky, P. T. Poggiolini

Department of Electrical Engineering, Stanford University*
Durand Building, room 202, Stanford, CA 94305-4055
FAX (415) 7239251, E-mail leonid@sierra.stanford.edu

Abstract

We propose a new broadband local area network, STARNET, based on a physical passive star topology. Over a single physical network, STARNET offers all users both a moderate-speed packet network and a high-speed WDM circuit interconnect. Based on these two data transport facilities, several topological and protocol solutions are available to the users. As a result, STARNET supports traffic of widely different speed and continuity characteristics. Each node of the network requires only two lasers and its structure facilitates the achievement of frequency stabilization for the whole network. An effort toward an experimental demonstration of a 4-node, 3 Gbit/s per node, FDDI-compatible (at the packet network level) STARNET is currently in progress at the Optical Communication Research Laboratory of Stanford University.

1 Introduction

Future LAN's are expected to provide the wide variety of services shown in Fig. 1. The low speed services of Fig. 1 could be handled by evolutionary versions of the presently available

*This work was partially supported by ONR under contract number N00014-91-J-1857 and by NSF under grant number ECS-9111766.

networks. The high speed ones require a new generation of local area networks. The target is therefore an *integrated services Broadband Optical Local Area Network* (BOLAN) that supports the whole spectrum of traffic shown in Fig. 1.

Packet switching and circuit switching have both been considered for operating a BOLAN. Currently, the prevailing approach is that of packet switching, because packet switching seems to be more effective in handling very different data rates and permits a more efficient processing of bursty data.

As far as physical implementations of BOLAN's are concerned, the WDM passive star solution seems to be one of the promising options, because it offers a theoretically huge bandwidth. However, this bandwidth comes in the form of a large number of optical WDM independent *channels* and realizing a packet mode of transmission in this intrinsically circuit switched environment represents a challenging task. To this end, different media access strategies and node configurations have been devised.

Some of these proposals rely on the use of very fast tunable receivers [1, 2, 3]; others impose strict requirements on the node ability to maintain synchronization with the other nodes and/or to operate in a time-slotted environment [4, 5, 6, 7]; still others are based on the use of multi-hop logical topologies [8, 9, 10, 11, 12], where each node performs some routing functions. Some of the above proposals require that each node have many transmitters and/or receivers [7, 5].

The complexity of these proposals, or the high performance required for some components, show that the WDM star solution, although attractive from the bandwidth point of view, causes difficult implementation problems for *packet* transmission.

In this paper we describe a new BOLAN approach, STARNET, based on a passive WDM star, which aims at fully exploiting the bandwidth potential of this architecture but does not require extreme hardware and protocol complexity or performance. This result is achieved by giving up the attempt of delivering all kinds of traffic through a single packet network. Instead, two logical networks, a packet one and a circuit interconnect, are put together on the same physical medium.

STARNET has been conceived with the objective of an experimental realization, which is currently in progress. Therefore, serious attention has been devoted to implementation details. Feasibility with currently available (research) technology was set as a primary goal.

The paper is organized as follows.

In Section 2 we discuss the characteristics of the different types of traffic, and envisage suitable network solutions. The goals of STARNET, and in particular the idea of implementing both a packet network and a broadband circuit interconnect on the same physical star, are established. The rest of the paper is devoted to the presentation of the implementation details and performance analysis of STARNET. In Section 3 the node structure is described and the basic network configuration is introduced. Section 4 describes several implementation alternatives of the node structure introduced in Section 3; the problem of frequency stabilization is also addressed. In Section 5, some solutions for multiplexing more than one data stream on the same optical carrier are analyzed. In Sections 6 and 7 the performance of STARNET is assessed. Sections 8 and 9 are devoted to some substantial upgrades to the basic STARNET configuration. In Section 8 improved versions of the packet network are presented. In Section 9 broadband multihop packet transport by means of the circuit interconnect is discussed. In Section 10 broadcasting and video-conferencing using the STARNET circuit interconnect are dealt with. Section 12 deals with the feasibility of STARNET and describes the experimental testbed which is presently being assembled.

2 STARNET Goals

The target of a BOLAN is that of handling different types of traffic having diverse speed and continuity characteristics. Traffic can be broadly grouped into three categories:

1) low speed, bursty or continuous, including telephony;

2) high speed, continuous;

3) high speed, bursty.

Category 1 includes all the services shown in Fig. 1 as low-speed. Categories 2 and 3 share all the rest.

Packet transmission is an adequate solution for category 1. If the network has sufficient capacity, telephony can be offered too, on a virtual circuit basis.

A circuit-switched network seems to be suitable to handle continuous streams of data, especially when the duration of the connection is relatively long (category 2). This is the case for instance of video-conferencing or transfer of big files (images, books, movies, magazines). These services are often referred to as 'call oriented'. For this kind of traffic, switching time does not need to be extremely small.

Category 3 is mainly related to supercomputer interconnections. One-to-one connections can be handled on a circuit-switched basis, but when many supercomputers need to communicate simultaneously, *broadband* (multi-Gbit/s) packet communication may be necessary. This last scenario is bound to a very specific application, most likely involving only a small subset of nodes in the LAN.

Taking into account the above observations, our proposal, STARNET, offers to all nodes *both* a packet network for low and moderate speed services (category 1) *and* a broadband circuit interconnect for call-oriented services (category 2). These two entities operate independently and simultaneously over the same physical network.

The merit of this approach is that one does not need to push the performance of the packet network because it is devoted to low speed traffic. At the same time, the circuit interconnect implementation is greatly simplified by the relaxed switching time requirements of call-oriented traffic. Also, all the signaling and protocol management for the circuit interconnect is easily handled through the packet network.

Finally, *arbitrary subsets* of STARNET nodes can be upgraded so that a broadband packet network can be built among them. The upgrade involves only the electronics, *not the optics*, of the nodes. The broadband packet network can be set up without interfering with the lower speed packet network or the circuit interconnections of the other nodes in the network. This feature enables STARNET to cover category 3 of traffic, thus making it capable of supercomputer interconnections too[1].

As a result STARNET meets the goal of dealing with the different kinds of traffic effectively, while avoiding extreme constraints on network parameters or hardware and protocol features.

[1]STARNET is not designed to meet the specifications of a backplane for ***shared memory*** multiprocessing, which is believed to require transfer rates on the order of 30-40 Gbit/s per node [12]. STARNET may instead be suitable for ***distributed*** or ***message passing*** multiprocessor systems, especially in *loosely coupled* processing environments, where processors share the results of lengthy calculations performed locally, instead of interacting at the single instruction level. The objectives and the intrinsic nature of a BOLAN like STARNET are completely different from those of a backplane for direct-processor shared-memory interconnections, which can be seen as an internal resource of a multiprocessor supercomputing machine.

3 The Basic Node Configurations

Each node of STARNET is optically connected to all the other nodes through a passive optical star, as shown in Fig. 2.

The basic node configuration is shown in Fig. 3. Each node is equipped with *one* transmitter. Its light source is tunable, but tunability is required for network flexibility and fault tolerance only, rather than wavelength switching. In normal operation the light source is kept fixed at a certain wavelength. Each node keeps its source tuned to a different wavelength, so that a *comb of light carriers* is formed.

Using a suitable multiplexing strategy (see Section 5), the node transmitter transmits *two independent data streams*, stream 'P' and stream 'C' as depicted in Fig. 4. Letters 'P' and 'C' are mnemonic for 'Packet' and 'Circuit', and this distinction will become clear shortly.

Every node has a *tunable* receiver that can be tuned to any transmitter and decodes the 'C' stream only. 'C' stream transmission and tunable receivers are used to implement a circuit interconnect among all the nodes.

In addition, each node is equipped with a *fixed* (as opposed to tunable) *receiver* which is permanently tuned to the *previous node* in the frequency comb and receives the 'P' data stream only.

Therefore each node receives 'P' data from the previous node and transmits 'P' data to the following one. Exploting this feature, STARNET builds a logical 'chain' along the frequency comb. Through this chain packet information flows as depicted in Fig. 5, provided that the data received by the previous node is relayed towards the next.

To close this unidirectional store-and-forward chain, the first node of the chain (the one whose transmitter is the first in the frequency comb) is equipped with a receiver that decodes the 'P' stream of the last node in the chain. Then, it relays this information down the chain, by retransmitting it through its 'P' data stream (see Fig. 6). This way, a logical unidirectional ring along the frequency comb is created as shown in Fig. 7. This logical topology is similar to the one used, for instance, by FDDI.

The fact that the transmitters are capable of multiplexing the 'P' and 'C' data streams onto the same carrier not only avoids the need for another optical transmitter, but also eliminates the need to form a second comb of carriers, which would waste optical bandwidth.

Throughout the paper, this node structure will be referred to as Basic Node Configuration 1 (BNC1).

An alternative to BNC1 is to equip each node with a transmitter capable of multiplexing *three* data streams, stream 'C' and streams 'P1' and 'P2'. Similarly to BNC1, a tunable receiver can tune to any of the transmitters, and decode stream 'C'. The fixed receiver decodes stream 'P1' of the previous node in the frequency comb, and stream 'P2' of the *next* node in the frequency comb. We shall see in Section 4 that we can still use just *one* fixed receiver to accomplish this task.

This second arrangement will be called Basic Node Configuration 2 (BNC2). It permits to implement a bidirectional logical 'bus' (Fig. 8), similar to the one used by IEEE 802.6 DQDB.

Alternatively, this bidirectional chain can be terminated like in Fig. 6, but at both ends. In this case we get two independent counter-rotating rings (see Fig. 9).

All these topologies are suitable for the implementation of a packet network. Some of them conform to those used for popular network standards, like FDDI or DQDB. The configuration chosen for the experimental STARNET testbed is BNC1 with a unidirectional ring topology (Section 12).

Substantial enhancements to these topologies will be described in Section 8.

4 Node Implementation

In this section we discuss the implementation of the basic node configurations BNC1 and BNC2, starting with BNC1.

BNC1, as outlined in the previous section, has three different subsystems: a transmitter, a tunable receiver and a 'P' stream receiver permanently tuned to the previous node in the frequency comb. We analyze these subsystems one by one. Fig. 10 shows the overall node structure, to serve as a reference throughout this section.

For STARNET, we propose coherent heterodyne detection, with external optical modulation. The rationale behind these choices will be discussed in Section 11.

4.1 The Transmitter

The transmitter has to multiplex two independent data streams, the 'C' stream and the 'P' stream. For now, we consider the TDM multiplexing solution: the transmitter devotes

part of the time to 'C' data and part of the time to 'P' data. Other multiplexing solutions and their performance will be addressed in Section 5.

The transmission laser is kept at a fixed frequency in normal operation.

4.2 The Tunable 'C' Stream Receiver

The tunable 'C' stream receiver is a standard heterodyne receiver with a tunable Local Oscillator (LO). In the 'C' stream TDM frame only two 'slots' are present, the 'C' slot and the 'P' slot. Synchronization to the desired slot, 'C' in this case, can be achieved by putting a unique identifier[2] at the start of the slot. The length of both the 'P' and 'C' slots is fixed and the slots are interleaved. Since the identifier can be as short as a few bits, and the frame length can be several thousand bits, the overhead is negligible.

The receiver laser is tunable over the entire frequency comb. Since we are dealing with the 'C' links, which are used to support circuit-switched broadband traffic, acceptable tuning speeds could be on the order of milliseconds or even tens of milliseconds. This makes it easier to use tunable semiconductor lasers, in spite of thermal transients and mode hops. A successful experiment on millisecond laser tuning in a dense WDM environment is described in [13]. The relaxed constraints imposed by this network arrangement could make it possible to use direct thermal tuning of DFB sources as well.

Regarding polarization problems, any means of achieving polarization insensitivity (i. e. polarization diversity, polarization scrambling etc.) is compatible with our network (for a comprehensive review of these methods see [14]).

4.3 The Fixed Receiver

The fixed receiver is permanently tuned to the transmitter of the previous node in the frequency comb.

This task could be carried out by another independent tunable receiver, which would remain permanently locked on the previous node carrier. However, it is possible to build the additional receiver so that it does *not* require another tunable laser and at the same time eases frequency stabilization of the whole comb of carriers, as follows.

Part of the transmitter laser light is tapped out before it enters the optical modulator (Fig. 10) and is used as LO signal for the fixed receiver. If the frequency comb of channels

[2]For instance, FDDI makes use of a very short unique identifier to mark the beginning of a packet.

is equispaced, the IF spectrum in the fixed receiver looks as shown in Fig. 11. Both the previous and the following channel in the comb are present, but they overlap due to the heterodyning process and information cannot be recovered.

To solve this problem, we resort to a new carrier allocation strategy [15] shown in Fig. 12b. For comparison, the conventional equispaced frequency allocation is reported in Fig. 12a. The channel spacing in the new allocation strategy is determined as follows. First, the minimum *electrical* spacing at the heterodyne receiver IF for *equispaced* channels, $\frac{\delta}{2}$, is determined. This corresponds to an *optical* spacing equal to δ. Then, carriers are grouped in *pairs* along the optical comb. The optical separation between the channels belonging to the same pair is reduced to $\delta/2$, while the separation between different pairs is kept at the value δ. This carrier allocation still permits heterodyne reception of any of the channels without interference [15], and therefore does not adversely affect the 'C' stream interconnections established through the tunable receivers.

This new concept was originally conceived to save bandwidth: the theoretical bandwidth wasting due to heterodyne detection, with respect to homodyne detection, is decreased by at least 50% as compared to the equispaced channel arrangement.

In STARNET, an additional effect occurs: at IF, in the fixed receiver, the spectra of the previous and the next carrier in the comb are now separated, although the IF at which they are located can be either one of two values. In Fig. 13 we show the new signal spectrum at the output of the IF stage of the fixed receiver.

With the simpler node structure BNC1, only one of the two channels is demodulated. With BNC2, both the previous node signal and the next node signal are demodulated. With both BNC1 and BNC2, the receiver controller has to find out 'which is which' between the two channels, due to the IF location ambiguity shown in Fig. 13. This identification is needed at the network set-up time only.

Through IF filters, the desired channel is isolated and sent to the demodulator, where the 'P' TDM frame is extracted. 'P' stream TDM frame synchronization acquisition is done at the network set-up time. Then, maintaining frame synchronization consists of just counting a number of bit intervals. As a result TDM frame synchronization is easily maintained as long as regular bit clock synchronization is not lost.

If direct modulation of the transmitter laser were used, it would not be possible to utilize part of the light of this laser for heterodyning at the fixed receiver. Therefore the fixed receiver would need a separate LO laser. Also, in STARNET direct modulation of the

transmitter laser would make it difficult to take advantage of the frequency stabilization method described below.

4.4 Frequency Stabilization

Like any coherent receiver, the fixed receiver must keep its LO tuned so that reception of the desired channel takes place. Since the LO of the fixed receiver is also the node transmitter laser, the frequency control operated by the fixed receiver to keep its LO locked on the previous node carrier also provides relative frequency stabilization between the two nodes. Since this is done by all the nodes in the comb, each node is frequency locked to the previous node and overall network frequency stabilization is achieved.

The above idea needs experimental confirmation, since it is not clear what the effects of propagation of random frequency fluctuations along the comb would be.

However, a recent experiment [16] has shown that semiconductor lasers exhibit a surprisingly good frequency stability once their temperature is tightly stabilized. This conclusion suggests that in STARNET, once the network has been set up, tightly temperature-controlled lasers might need only a very slow control, or even just occasional adjustments, to keep them at their nominal frequencies. If this is the case, propagation of random frequency fluctuations along the chain could be reduced or even avoided. Tuning adjustments could be triggered or controlled by the network protocol, and information on the overall stability of the comb could be exchanged through the packet network.

Finally, the first node in the comb has to be locked to an absolute reference. This reference needs to be ***one stable spectral line only***, which would establish the 'origin' of the frequency comb.

If direct modulation of the transmitter laser were used, then the fixed receiver would have to use a separate LO laser. The above frequency stabilization method could still be used indirectly by keeping the node transmitter laser locked onto the fixed receiver LO, but at the cost of a much greater complexity.

4.5 Implementation of BNC2

The BNC2 transmitter is identical to the BNC1 one, except for the fact that there are three TDM data streams instead of two: 'C', 'P1' and 'P2'. The 'C' stream receiver is identical. The fixed receiver extracts the 'P1' stream from the left adjacent node and the

'P2' stream from the right adjacent node in the optical frequency comb. Both are visible at IF in the fixed receiver (Fig. 13). Frequency stabilization is again done with respect to the previous carrier in the frequency comb.

BNC2 is therefore only slightly more complex than BNC1. As shown in Section 3, BNC2 permits a greater variety of packet network logical topologies and therefore a wider compatibility (above the physical layer) with existing standards, which makes it an interesting alternative to BNC1.

5 Data Stream Multiplexing

In the previous section we assumed that TDM was used to multiplex the 'C' and 'P' data streams on the same carrier. In this section we explore and compare the following alternative solutions:

- TDM;
- combined modulation formats;
- subcarrier multiplexing;
- multilevel modulation.

We define the 'power penalty due to multiplexing' (Δ) as the ratio between the power needed to transmit both 'C' and 'P' streams, and the power needed to transmit the 'C' stream only, at the same fixed error probability.

5.1 Time Division Multiplexing

When TDM is used, transmission speed has to be increased with respect to transmission of the 'C' stream alone in order to accomodate the 'P' stream. As a result, the bit duration is decreased and so is the energy per bit. To restore the level of energy per bit that was available with the 'C' stream alone, and therefore obtain the same error probability, extra power is needed, and the multiplexing power penalty is (see Appendix A.2):

$$\Delta = 10 \log_{10} \left(1 + \frac{[\text{bit rate of 'P' stream}]}{[\text{bit rate of 'C' stream}]} \right) \tag{1}$$

A plot of the power penalty Δ versus the bit rate ratio:

$$\rho = \frac{\text{speed of 'C' stream}}{\text{speed of 'P' stream}} \tag{2}$$

is shown in Fig. 14. The performance of TDM is the best among all the solutions considered here. However, a negative aspect of TDM is that both the transmitter and the receivers must work at the aggregate speed of the two multiplexed data streams.

5.2 Combined Modulation

Some modulation formats can be utilized simultaneously on the same carrier and detected independently. For instance, low-modulation-index ASK can be used simultaneously with any modulation format which does not rely on transmission power variations (PSK, DPSK, FSK, POLSK, etc.).

We computed the performance of the combined modulation approach for ASK with heterodyne PSK and DPSK. In both cases the ASK stream is extracted by squaring the IF signal to get rid of the phase modulation. IF filtering has to be very loose to ensure complete cancellation of the phase modulation in the squarer. Instead, post-detection filtering is tight. The ASK modulation depth is adjusted so that the error probability of ASK and the companion (D)PSK stream are equal. In Fig. 14 the power penalty Δ with respect to transmission of (D)PSK alone is plotted versus the speed ratio:

$$\rho = [\text{bit rate (D)PSK}]/[\text{bit rate ASK}] \tag{3}$$

The derivation is given in Appendix A.1. Assuming then that the 'P' stream is ASK encoded and the 'C' stream is PSK encoded, both Δ and ρ are consistent with those defined in (1) and (2) for TDM, so that the curves shown in Fig. 14 are directly comparable.

The penalty of combined modulation is considerably higher than that of TDM. For $\rho < 5$ it is about 6 dB. This solution is therefore more attractive if the speeds of the 'P' and 'C' links are substantially different: for $\rho > 20$ the penalty is less than 3dB.

The advantage of combined modulation with respect to TDM is that combined modulation does not need 'P' and 'C' stream buffering and synchronization at the transmitter, and time-demultiplexing at the receivers. Also, 'C' and 'P' stream transmission speeds do not add up.

Both phase and amplitude modulation can be performed by means of commercially available multiport *single* $LiNb0_3$ modulators. Therefore no additional light power loss due to the use of two cascaded modulators occurs.

Combined modulation is well suited for BNC1, since only one 'P' stream is to be supported. With BNC2, two 'P' streams are present and an additional multiplexing

strategy must be used to accomodate both.

5.3 Subcarrier Multiplexing

This technique has been extensively studied for television distribution networks. It has also been proposed for some BOLAN solutions [11]. Its feasibility has been proved in several experiments [21].

With subcarrier multiplexing, the multiplexed streams share the channel *amplitude* rather than the channel power[3], which lea to higher penalties than with TDM. The multiplexing power penalty Δ due to subcar r multiplexing of the 'P' and 'C' stream is shown in Fig. 14 as a function of the bit rat ratio ρ defined by (2). The derivations are shown in Appendix A.3.

Subcarrier multiplexing performs better than combined modulation but it has the unwelcome effect of greatly increasing the optical channel bandwidth. This effect is detrimental because the IF bandwidth of the receivers has to be increased as well. This is particularly harmful for the fixed receiver that always has to 'see' both adjacent nodes in its IF. As a result, the values of the two channels IF frequencies are likely to become extremely high.

Also, the spectrum of the transmitted SCM node signal becomes complicated because the spectrum of at least one of the two multiplexed streams is duplicated, i.e. at the receiver it appears to the left and to the right of the IF frequency of the channel. This is likely to make channel tuning and frequency stabilization more difficult. Thus, both TDM and combined modulation seem to be a better choice.

However, subcarrier multiplexing could be useful in conjunction with combined modulation to multiplex two 'P' streams for the BNC2 configuration. The two 'P' streams can be first AM electrically subcarrier multiplexed. Then the resulting signal is fed into the AM port of the $LiNbO_3$ modulator, while the 'C' (D)PSK stream goes into the phase modulation port.

[3]If the number of streams is very high, one can rely on the fact that not all of them are 'high' or 'low' at the same time and it can be thought that the needed *power* (not the amplitude) grows linearly with the number of streams. This is not the case, however, when the number of streams is only two or three.

5.4 Multilevel Transmission

In a multilevel transmission system, each transmitted symbol carries more than one information bit. If each symbol carries n bits, $n-k$ of these bits can be devoted to the 'C' link, and k of them to the 'P' link. This way, neither TDM multiplexing-demultiplexing circuitry, nor special combined-format modulators are needed. Also, multilevel transmission can be beneficial in a WDM network environment where bandwidth is the limiting factor for the maximum number of nodes (see next section).

On the other hand, coherent multilevel optical transmission, although theoretically feasible (using FSK, PSK, QAM or POLSK [22]), is complicated and needs experimental investigation.

6 Performance of the Circuit Interconnect

Fig. 15 shows the maximum number of nodes as a function of the 'C' link bit rate. The calculations are reported in Appendix B. The following assumptions were made in the analysis:

- The passive star consists of two-by-two couplers with an excess loss of 0.5 dB per coupler. The number of stages that each signal traverses is $\log(N)$ where N is the total number of nodes. The power splitting factor for each signal is $1/N$.
- The transmission format is DPSK with the ideal sensitivity of 21 photons per bit.
- The presence of two receivers in the node causes a 3 dB splitting loss. No penalty due to the multiplexing of the 'P' stream is accounted for, since different solutions lead to substantially different performances. The reader can easily scale the power budget results shown here on the basis of the penalties shown in Fig. 14.
- A system margin of 13 dB is imposed.
- The electrical channel spacing is set at three times the bit rate. The non-equispaced channel allocation is assumed (Fig. 12b) resulting in an optical channel spacing of 4.5 times the bit rate.
- The maximum available bandwidth is considered to be the width of the 1550 nm window, approximately 20 Thz.
- A value of 10 nm is used for the maximum tunability range of the lasers[4].

[4]A breakthrough result of 57 nm has just been announced [25]. However, since very little is known so far on the characteristics and reproducibility of the new component, we choose the safer assumption of

• Power loss in the fiber is considered to be part of the 'system margin'.

Fig. 15 shows that the 1550 nm window bandwidth limit is above the power budget limit. However, if a 7 dB system margin, instead of 13 dB, were chosen, the power budget curve would lie completely above the bandwidth limit. The limit due to the laser tunability range is stricter than both the power budget and the 1550 nm window bandwidth limit: at 1Gbit/s per node, the maximum number of nodes that it allows is 275.

An interesting result is that in this environment optical bandwidth cannot be considered an unlimited resource and there is a definite advantage in using bandwidth-efficient transmission schemes.

7 Packet Network

Fig. 16 shows the total mean packet transmission delay as a function of the offered traffic, including both propagation and queueing delays, for the single-ring logical topology with 100 and 1000 nodes. The following assumptions were made:

• The network is a token ring, working according to the exhaustive service discipline.

• Queues have unlimited length.

• Transmission speed is 100 Mbit/s.

• The packet length distribution is exponential, with a mean value of 2000 bits. The token packet has length 200 bits.

• The node geographical distribution is uniform over an area of 6 km in diameter, having the star at its center.

• Traffic is symmetric (each station generates the same traffic).

The curve was calculated using the analytical results of [26].

Fig. 16 shows that the total maximum throughput (i.e. the capacity) coincides with the line rate (100 Mbit/s), although for loads nearing the line rate the expected delay increases substantially. When the network is lightly loaded, the total mean delay is propagation-dominated. It amounts to about 2 ms for a hundred nodes and about 20 ms for a thousand nodes. For a load of 80% of the maximum throughput, these figures grow by a factor of five and become queueing-delay dominated. These numbers show that with this topology it is possible to achieve throughputs fairly close to the maximum with total delays on the order of 4-5 times the propagation delays.

---

10 nm tunability range.

With a thousand nodes, the maximum theoretical per-node capacity is 100 Kbit/s, while it is 1 Mbit/s for 100 nodes.

This topology, as reflected by the results of Fig. 16, offers a per-node capacity which is inversely proportional to the number of nodes and shows a linear growth of propagation delay with the number of nodes. By increasing transmission speed, it is possible to linearly push the capacity limit further away. However, this does not help to fight the packet delay floor due to propagation delays. Propagation delays may be of concern in STARNET, since due to its physical architecture the physical path between any two nodes has to go through the center star, irrespectively of how close the nodes are located. This may induce higher propagation delays as compared to networks where both the logical *and* the physical topology is a ring, and each node is linked to the following through the shortest possible path[5].

If the dual bus configuration is chosen (see Section 3) instead of the single ring, the performance is slightly different but the above general behavior of capacity and the presence of the propagation delay floor are unchanged.

Therefore, as a whole, the packet network of STARNET has a potential similar to today's commercial state-of-the-art optical networks, like FDDI, DQDB and CRMA. This can be already regarded as a satisfactory result, since the main data transport facility of STARNET consists of the circuit interconnect. However, as mentioned, the performance of the packet network degrades very fast with the number of nodes and could worsen to the point of becoming unacceptable even for the exchange of relatively low-speed data. In STARNET a poor performance could also impair the circuit-interconnect signaling and network-management functions that are supported by the packet network and that are vital for its operation.

In the next section we discuss some alternative logical topologies for the packet network that substantially improve its performance with little added complexity.

[5]However, in most cases people do not connect nodes through the shortest path, even when this would be permitted by the network physical topology. In most FDDI installations all the cables converge to a concentrator in a star-like fashion. Therefore the above drawback of STARNET physical topology may be more theoretical than actual.

8 Enhanced topologies

In Section 3 we introduced the basic packet network topologies. Here we explore some enhanced solutions, still based on the basic node configurations BNC1 and BNC2.

8.1 Description

On the same physical star we allocate M independent packet networks so that they are contiguous in the optical frequency domain (Fig. 17). Their logical topology can be any of the ones presented in Section 3. We call them *subnetworks*. Any node can still connect to any other by means of the high speed links, even if they belong to different subnetworks, since the circuit interconnect is not affected by the packet network segmentation.

One node per subnetwork serves as a *bridging node*. The bridging node is connected to its subnetwork by means of its 'P' stream and its fixed receiver. To make the different packet subnetworks talk to each other, the bridging nodes also establish connections among themselves by means of their tunable receiver and of the 'C' link.

An example of the logical topology that can be implemented this way is shown in Fig. 18. The packet subnetworks are rings and the backbone is a ring too. The bridging nodes are shown as B_j, with j ranging from 1 to M.

The nodes of a subnetwork send to the bridging node all the packets whose destination is *outside* the subnetwork. The bridging node reads these packets and queues them onto the backbone ring. The bridging node of the destination subnetwork takes care of reading the packets and queueing them into its subnetwork 'P' stream.

A remarkable point is that the backbone network could be implemented at a speed different from that of the subnetworks, being based on the use of part or all of the capacity of the 'C' link. In particular, it could be faster than the subnetworks, enabling heavy inter-subnetwork traffic to be exchanged without saturating the backbone.

8.2 Performance

We define three quantities:

- N: total number of nodes in the network;
- M: number of subnetworks into which the packet network is split (each subnetwork contains N/M nodes);

• α: fraction of traffic generated by a subnetwork whose destination is *outside* the subnetwork: $\alpha = 0.1$ means that 10% of the subnetwork traffic is sent to nodes that belong to other subnetworks.

Assuming first that the *backbone* network has unlimited capacity, the total maximum throughput[6] of the packet network is given by:

$$T_{tot} = \frac{1}{1+\bar{\alpha}} C_{sn} M \tag{4}$$

where C_{sn} is the capacity (assumed equal) of each subnetwork and $\bar{\alpha}$ is an effective parameter related to the individual α's of the subnetworks as described in Appendix C.1. If all subnetworks have the same α, then $\bar{\alpha} = \alpha$.

According to (4), the total throughput is bound by two values. When $\alpha = 0$ for all subnetworks, each subnetwork produces only traffic that stays within that subnetwork. Therefore, the whole network behaves like a set of disconnected entities and the total throughput is the sum of the throughputs of the individual subnetworks: $T_{tot} = C_{sn} M$. This is the maximum achievable value. At the other extreme, when $\alpha = 1$ for all subnetworks, i.e. all the traffic of each subnetwork has to be sent elsewhere, the total throughput is $\frac{1}{2}$ of the above, which corresponds to the minimum value.

These results show that total throughput can be ideally increased at will by segmenting the network more and more. The potential increase is at least proportional to $\frac{1}{2}M$.

However, the actual backbone capacity C_{back} is not unlimited, and (4) holds true only *as long as the backbone is not saturated.* The traffic that has to be processed by the backbone is:

$$T_{back} = \frac{\bar{\alpha}}{1+\bar{\alpha}} C_{sn} M \tag{5}$$

which shows that when $\bar{\alpha} = 1$ the capacity that the backbone has to have is $C_{back} \geq T_{back} = \frac{1}{2} C_{sn} M$, which is also equal to the total network throughput in that condition and hence possibly very high. However (5) also shows that the required C_{back} considerably decreases as $\bar{\alpha}$ decreases. Hence, having a low $\bar{\alpha}$ permits to obtain the total throughput promised by (4) with a much lower than worst-case C_{back}.

The chance that $\bar{\alpha}$ is substantially low relies on the circumstance that the network can be segmented into islands of heavy traffic which talk relatively little to one another.

[6] In the following we will refer to the 'total maximum throughput' T_{tot} dropping the 'maximum' qualifier, so that it will be 'total throughput'. This is because we are going to discuss the *maximum value* and the *maximization* of T_{tot} with respect to various parameters: the denomination 'maximum of the total maximum throughput' might sound confusing.

These islands can consist for instance of a mainframe and all its terminals, or a cluster of workstations with its servers. This concept is similar to that of *bridging* and is extensively used for example in Ethernet networks. In STARNET, groups of heavily interconnected users can be placed in the same subnetwork simply by assigning suitable frequencies to their transmitters. Subnetworks do not need to have the same size.

8.3 Total Throughput Maximization

To maximize the total throughput, it appears from expression (4) that the network ought to be segmented as much as possible, to increase M. Further and further network segmentation, however, would finally cause a sharp increase in $\bar{\alpha}$, which occurs when the size of the subnetworks becomes so small that they are not capable of containing a full traffic island anymore. For instance, if a mainframe has sixty terminals and the subnetwork size shrinks to thirty nodes, then thirty terminals will be in a different subnetwork from the mainframe and substantial inter-subnetwork traffic would have to be supported.

Even so, expression (4) indicates that increasing M could overcome the penalty due to the increase in $\bar{\alpha}$. However, expression (5) tells us that if we do not keep $\bar{\alpha}$ low, the backbone throughput would soar to very high values and could possibly exceed the backbone capacity

The problem of finding the best values of M, $\bar{\alpha}$, and C_{back} is difficult to solve analitically because it depends on parameters like the cost of increasing C_{back} or the dependence of $\bar{\alpha}$ on M which are difficult to characterize. However, if the subnetwork and backbone capacities are fixed *a priori*, then an optimization rule can be found, based only on the reasonable assumption that $\bar{\alpha}$ is a monotonically increasing function of the network segmentation[7] M.

In Fig. 19 we show a plot of network total throughput for a backbone capacity of 500 Mbit/s and a subnetwork capacity of 100 Mbit/s, versus $\bar{\alpha}$ and M. For low values of $\bar{\alpha}$ the curve shows a linear increase of the total throughput with respect to M, which corresponds to the behaviour predicted by (4). For higher values of $\bar{\alpha}$ the offered traffic for the backbone network increases according to expression (5) and it may eventually saturate the backbone. Backbone saturation causes the apparent levelling in the plot of Fig. 19, i.e. a flat region where the total throughput cannot increase with M because the

[7]More precisely, it is also necessary to assume that $\bar{\alpha}$ does not grow 'too rapidly' when M is increased. This constraint is discussed in Appendix C.2 and appears to be easily satisfied in a realistic environment.

backbone network is saturated. A clearly visible slope discontinuity on the plotted surface coincides with the boundary of the backbone saturation region.

It can be shown (Appendix C.2) that the highest possible total throughput is achieved precisely along that slope discontinuity. The corresponding optimal relationship between M and $\bar{\alpha}$ is:

$$M = \left(1 + \frac{1}{\bar{\alpha}}\right) C_{back}/C_{sn} \tag{6}$$

A plot of the best M versus $\bar{\alpha}$ for the example of Fig. 19 is shown in Fig. 20.

The relationship (6) can be regarded as a target for the optimization of an actual network: the network segmentation M should be increased as long as this brings $\bar{\alpha}$ closer to the optimal value given by (6).

To give a feeling of the performance improvement made possible by the segmented topology, we consider a 1000 node packet network having the characteristics specified in Section 7 for the single-ring network. We segment it into a ring-of-subring network like the one shown in Fig. 18. We assume that the throughput maximization process described above yields $M = 30$ (thirty subrings) and $\bar{\alpha}$ equal to 0.2. Assuming a backbone capacity of 500 Mbit/s and subring capacity of 100 Mbit/s, the total throughput is 2.8 Gbit/s, as opposed to the 100 Mbit/s of the unsegmented network. Delays show a remarkable improvement too. We computed the mean total delay of the segmented solution and compared it to the single-ring solution (Fig. 21). The calculations were carried out based on the analytical results reported in [27]. The plot shows that mean total delay is greatly reduced with respect to the single-ring solution.

8.4 Alternative solutions for the backbone network

The bridging nodes are essentially network-dedicated nodes. Instead of disseminating them throughout the geographical extension of the LAN, they could be gathered and sheltered at the same location, in order to improve their safety and simplify their maintenance.

Once the bridging nodes are put together, it becomes superfluous to connect them through the star. A more cost-effective solution may be that of hooking them up to one another with point-to-point links. But possibly the best way to exploit the co-location of the bridging nodes is that of connecting them through an ATM switch. ATM switches with total throughputs on the order of several Gbit/s are currently being built in research

labs and are expected to be commercially available soon.

Using subnetworks with 600 Mb/s capacity (like for instance the DQDB top standard), assuming a backbone based on an ATM switch with 4.5 Gbit/s throughput (30 inputs at 150 Mbit/s each), and otherwise using the parameters of the previous examples, the total throughput of the segmented packet network grows to 15 Gbit/s (with a backbone load of 3.6 Gbit/s), which would make it an extremely powerful data transport facility.

Concentrating the bridging nodes would not harm reliability. On the contrary, failure of one or more of the bridging nodes would result in just the merging of the subnetworks of the failed nodes with other subnetworks. If *all* the bridging nodes failed together, the STARNET packet network would always have the capability to survive in a single-ring configuration, or set-up a ring of subrings using the standard nodes present in the network.

9 High speed packet traffic

The solutions described so far are suitable for traffic which is either packetizable at low-to-medium speed, or conveyable at very high speed through circuit connections with relatively slow set-up time.

This scenario leaves out ***broadband packet traffic*** which requires that several nodes be able to exchange packets at sustained rates of several hundred Mbit/s *per node*[8]. This speed is too high for the lower-speed packet network. As for the circuit interconnect, its interconnection speed is inadequate to support the set-up and tearing-down of a high-speed link each time a packet has to be transmitted.

In the following we show that STARNET has the potential to accomodate broadband packet traffic too, by exploiting the high speed links in a different fashion.

9.1 High speed packet rings

An arbitrary subset of STARNET nodes can form a logical ring through the node 'C' links and the tunable receivers. A packet network can then be established on it, up to the full speed of the 'C' link.

This simple solution is very attractive for broadband packet exchange only if the number of nodes involved is small, since the per-node bandwidth is inversely proportional

[8]The HIPPI interface, for instance, is designed to handle fully packetized traffic at 800 Mbit/s.

to the number of nodes on the ring. Delays would be very low too, if the number of nodes to be traversed is low. More than one of these rings could exist in STARNET at the same time, since they would not interfere with each other or with the low-speed packet network.

However, if the number of nodes on the ring exceeds 6-8, then it is likely that per-node capacity becomes too low, and more sophisticated solutions are necessary.

9.2 Multihop subnetworks

Many recent proposals advocate the use of multihop logical topologies for optical networks (for instance perfect shuffles [18, 19], the Manhattan Street Topology [16, 17] or general multihop adaptive topologies [9]). These networks are thought to cover effectively the very high speed packet traffic segment for a high number of nodes.

Multihop topologies require that each node have m outgoing and m incoming high-speed data links, where m is called the 'order' of the multihop topology. In the following we will show that in STARNET it is possible to implement multihop packet networks of order two *without altering* the basic node configurations (BNC1 or BNC2).

The picture of the logical connectivity that we want to attain for a STARNET multihop node is shown in Fig. 22. Transmission of the two independent outgoing high speed data streams is obtained by just labelling the outgoing packets differently, according to which one of the two target nodes they are meant for. Then, all the packets are queued together on the (single) 'C' stream of the node. The two target nodes are tuned simultaneously to this 'C' stream and upon reception of a packet they accept it or drop it according to its label.

Each node has to support two incoming streams, but owns just *one* tunable receiver. The *fixed* receiver can be used to make up for the lack of a second tunable receiver. The only requirement is that the nodes hooked up in the multihop network are put contiguously in the optical frequency domain. Then, fixed receivers, besides extracting low-speed packet information, also extract the broadband packet information from one of the two adjacent nodes.

The fact that the fixed receiver can only receive the adjacent nodes in the frequency comb poses no limitations on the topology of the multihop network. *Any* fully-connected multihop topology contains a path, called Hamiltonian path, that connects *all* the nodes and in which every node appears only once. In other words, these topologies contain a

ring that links all the nodes of the multihop network. Since the Hamiltonian path is a ring, it can be implemented with the fixed receivers, in a fashion similar to the low speed packet network of Fig. 7.

The remaining links, necessary to complete the multihop topology, may follow more complicated patterns. However, since they utilize the *tunable* receivers, any connection pattern can be arranged. As a result, any order-two fully-connected multihop topology, like for example bi-dimensional Manhattan Street networks or order-two ShuffleNets, can be set up in STARNET.

To illustrate the concept, in Fig. 23 we show the case of a 16-node Manhattan Street network, which breaks down into four rings. The four rings are shown separated in Fig. 24. A similar topological decomposition of ShuffleNets is discussed in [20].

One node, and only one in the whole multihop network, needs to have two tunable receivers in order to close the Hamiltonian ring. This can be easily arranged but, as an alternative, a user can be given two standard nodes that, being at the same location, can be connected directly without going through the star.

For all but this one node, no additional optics is required with respect to BNC1 or BNC2 (that need just two lasers), making this solution very appealing. Also, topologies are easily reconfigurable and optimizable by re-tuning the tunable receivers or by changing the node order along the frequency comb. More than one independent multihop network can coexist in STARNET, without interfering with one another.

A higher order generic multihop network can be implemented among STARNET users if they own *two* (or more) elementary nodes. Each user would then have two (or more) high speed transmitters and two (or more) high speed tunable and fixed receivers.

9.2.1 Comparison with other multihop arrangements

The difference between implementing a broadband packet network and implementing a broadband packet network *in STARNET* is that in STARNET multihop users still have access to the low-speed packet network and therefore keep in touch with all the other (non-multihop) STARNET nodes. Thus, besides data, also control and management information can be exchanged among *all* the nodes.

STARNET multi-logical-network solution is attractive because, most likely, not all the nodes in the network need to have broadband packet transmission capabilities. Only the ones that really need it have to be equipped with upgraded electronics, thus increasing

cost-effectiveness.

10 Broadcasting and video-conferencing

The easy exchange of control information through the low-speed packet network effectively enhances the potential of the circuit interconnect.

High speed broadcast transmission is set-up by sending a (broadcast) packet announcing it through the packet network. Any node can tune independently to the broadcasting node.

Video-conferencing is seen as one of the most attractive facilities for a future network to provide. Several manufacturers are already testing video-conferencing products[9].

Video conferencing can be handled through the packet network and the use of broadcasting for a low-speed compressed video format ($\approx$ 2Mb/s per video signal). In this picture one node is *the broadcast node*. At the meeting set up, all the other participants are requested to tune to the broadcast node high speed link. A series of virtual circuits is also arranged on the packet network, linking each participant's terminal to the broadcast node. This node picks up all the data of these virtual circuits and TDM-multiplexes it onto its 'C' data stream, which is broadcast. Each node receives this flow of information that contains all the video signals in a TDM-multiplexed fashion, and displays them to the meeting attendee.

The above solution may turn out to be inadequate if either the packet network is not capable of supporting enough users, or if low-compressed or HDTV video quality is desired. In this case, another arrangement is possible, which completely relies on the high-speed links (except for control information).

The nodes involved in the meeting form a logical ring using their high speed links. Each node is assigned a TDM slot and retransmits what it receives. It takes out its own old data and puts new one in its time slot. Synchronization is established by the flow of the different TDM frames.

As a result, at each node the complete visibility of all the video signals is achieved and no overhead is borne by the packet network. The connection limit is set by the capacity of the high speed link.

[9]For instance DEC already has multimedia software that runs on X-window/X-media which fully implements video-conferencing for up to eight simultaneous participants.

Compressed HDTV has recently been proved feasible at 20 Mbit/s. With reasonable transmission speeds (1 Gbit/s) as many as 50 attendees per video-conference can be multiplexed. For standard (non-HDTV) compressed video the number grows to over 200.

These figures apply to the number of *active* attendees. The number of *spectators* is unlimited since every node in the network can tune to an active node and pick up the conference signal. Also, there is no limit to the number of simultaneous video-conferences, since they do not interfere with one another.

11 Why Coherent Detection?

STARNET is based on coherent transmission. In this section we comment on this choice.

Most of the novel solutions employed in STARNET rely on coherent detection: the use of the transm. ter laser as LO of the fixed receiver; the consequent visibility of the neighboring channels in the frequency comb, which allows the implementation of the packet network; the frequency stabilization method and data multiplexing through combined modulation. All of these could not be obtained with direct detection.

Nevertheless, none of the above implementation solutions is absolutely essential to the realization of a WDM network. The same *functions* could be implemented differently, without coherent technology. In general, it would be possible to design a direct detection WDM network *functionally* similar to STARNET. However, the final performance and/or cost of the direct-detection solution could be remarkably different from that of STARNET.

Incoherent technology proves simpler and cheaper as long as the required network performance is modest. Two examples are given by the successful experimental testbeds RAINBOW and LAMBDANET. RAINBOW [23] implements a pure circuit interconnect (no packet network embedded) with channel capacity of 200 Mbit/s and a maximum number of nodes of 32. The node optics and electronics was assembled on a standard IBM-PC board. LAMBDANET[10] [34] achieved transmission of 16 channels at 2 Gbit/s/channel.

However, if a star network with the capability of serving *hundreds* of nodes is desired, then direct detection has to resort to optical amplifiers and extremely tight optical filtering. The resulting complexity is similar to that of coherent technology but the obtained performance is not as good, at least at the present state of research: direct detection

[10]LAMBDANET is primarily meant to be a distribution network, but the experimental testbed gives an indication on the potential of direct detection WDM independently of the final application.

systems are limited by the 35 (or less) nm bandwidth of EDFA (Erbium Doped Fiber Amplifiers); optical filtering does not have the selectivity of electronic filtering[11].

In the long-term the key point that will most probably determine the success of either coherent or direct detection is *integration*. Both EDFA and optical filters are *not* integratable, while entire heterodyne receivers, including tunable lasers, have been monolithically integrated on the same substrate [24]. The process is claimed to be compatible with the integration of a new 57-nm tunable laser [25]. Several laboratories are working on the integration of a full polarization-diversity receiver.

Finally, coherent technology has the so far unexploited potential of reducing by a factor of up to 4-5 the channel bandwidth, through multilevel transmission.

The picture just presented could change dramatically in favour of either approach as a result of technological breakthroughs. Therefore the matter is far from being settled and it is not possible to rule out either technology on the basis of the present knowledge.

12 STARNET feasibility

Overall, STARNET relies on some long-studied (but still challenging) techniques, like WDM. It also contains several new concepts and solutions:

- the achievement of transversal connectivity along the frequency comb of nodes;
- the use of the transmitter laser of the node as LO for a fixed receiver;
- the achievement of relative frequency stabilization between adjacent nodes in the frequency comb, which in turn is used to ensure overall frequency stabilization in the network;
- multiple data stream multiplexing over the node carrier by means of innovative techniques, like combined modulation;
- the bridged medium-speed packet network and the flexible use of the high speed links to create virtual generic multihop topologies for broadband packet transport.

An experimental 4-node STARNET prototype is currently being built at the Optical Communication Research Laboratory of Stanford University. The testbed is meant to verify the feasibility and effectiveness of *all* aspects listed above. For some of them this

[11] Multiple-stage Fabry-Perot filters attaining a bandwidth of 0.01 nm ($\approx$ 6 Ghz) have been reported. However, these filters suffer from many problems that, presently, are thought to hinder their practical use [35]. Similar considerations can be made for multi-stage Mach-Zehnder filters.

will entail full realization of all networking features, up to the application layer, for others it will involve showing the feasibility and performance of the physical layer only.

The 'C' links are implemented through heterodyne PSK, at a speed of up to 3Gbit/s. The 'P' stream is multiplexed by combined PSK-ASK modulation (see Section 5.2). The packet network is organized on a single ring and makes use of standard FDDI electronics, while FDDI optics is replaced by STARNET optics. The high speed links carry data according to the SONET OC-48 2.4 GBit/s transmission standard. Each node will be controlled by a RISC workstation, where multimedia (DEC X-MEDIA) applications, like video-conferencing, will run and exchange information through STARNET.

13 Conclusions

We propose a new broadband local area network, STARNET, based on a physical passive star topology. STARNET offers all users two data trasport facilities: a moderate-speed packet network and a high speed WDM circuit interconnect, both running on the same physical network.

The moderate-speed packet network is used for control, reliability, rearrangeability, optimization, maintenance and exchange of low and medium speed data. Enhanced topological solutions can push the capacity of this packet network into the Gbit/s range.

The WDM circuit interconnect provides the users with high speed links that can be used for high speed node-to-node connections, broadcasting, or to build virtual broadband packet multihop networks among arbitrary subsets of nodes.

As a result, STARNET can effectively support many different kinds of traffic.

STARNET appears to be feasible with presently available research technologies. An effort toward an experimental demonstration of a 4-node, 3 Gbit/s per node, FDDI and SONET OC-48 compatible (with the packet network and the circuit interconnect, respectively) STARNET, that will be used to run X-MEDIA ™ multimedia and video-conferencing applications, is currently in progress at the Optical Communication Research Laboratory of Stanford University.

14 Acknowledgements

The authors thank Charles Barry, Michael Hickey and Ciro Noronha of the Optical Communications Research Laboratory (Stanford University) for the helpful discussions and useful suggestions that greatly contributed to improving this paper.

Appendices

A Data Stream Multiplexing Penalties

We define the 'power penalty due to multiplexing' (Δ) as the ratio between the power needed to transmit both 'C' and 'P' streams, and the power needed to transmit the 'C' stream only, at the same fixed error probability. In this appendix we report the calculations concerning the power penalty results presented in Section 5 for Combined Modulation, TDM and Subcarrier Multiplexing.

A.1 Combined Modulation

The penalty for Combined Modulation is calculated as follows. The IF signal in the receiver carries both the PSK and the ASK modulation and can be written in the *complex envelope form* as:

$$s(t) = \sum_{k=0}^{\infty}(1 - \beta_k\delta)\, u_T(t - kT)\sqrt{\frac{2E_{ASK}}{T}}\, e^{j\omega_{IF}t}e^{j\alpha(t)} + [n_c(t) + jn_s(t)]\, e^{j\omega_{IF}t} \qquad (7)$$

where:

$$u_T(t) = \begin{cases} 0 & \text{if } t < 0 \text{ or } t > T \\ 1 & \text{otherwise} \end{cases} \qquad (8)$$

The factor $e^{j\alpha(t)}$ represents PSK modulation, while $\beta_n \in \{0, 1\}$ represents binary ASK data. The factor δ determines the depth of the ASK modulation. The quantity E_{ASK} is the energy of the signal within a bit period T of the ASK stream (which can be different from that of the PSK stream). The processes $n_c(t)$ and $n_s(t)$ are white Gaussian and independent. Their two-sided noise spectral density is N_0 while $N_0/2$ is the power spectral density of the *real* (non complex-envelope) white noise originating them.

We first analyze the performance of the ASK stream reception.

We assume that the IF bandwidth of the receiver is large enough not to distort the IF signal substantially, and in particular not to cause conversion of the PSK modulation into amplitude modulation. Then, after squaring, the resulting baseband signal is:

$$b(t) = \frac{1}{2}\left\{\sum_{k=0}^{\infty} u_T(t-kT)\left[(1-\beta_k\delta)\sqrt{\frac{2E_{ASK}}{T}} + n_{F_c}(t)\right]^2 + n_{F_s}^2(t)\right\} \tag{9}$$

where $n_{F_c}(t)$ and $n_{F_s}(t)$ are independent Gaussian processes of variance $\sigma^2 = N_0 B_{IF}$. They originate from the IF filtering of the processes $n_c(t)$ and $n_s(t)$. The quantity B_{IF} is the equivalent noise bandwidth of the IF filter.

The baseband signal can be affected by a large amount of excess noise since we need very loose IF filtering. It is therefore necessary to use post-detection filtering. To deal with the statistics of noise in this case, we follow the procedure outlined in [28, 30]. First, we assume that the post-detection filter is an integrate-and-dump filter integrating over a time T. Then, we observe that:

$$\frac{1}{T}\int_{(k-1)T}^{kT} b(t)\,dt \approx \frac{1}{M}\sum_{m=1}^{M} b\left([k-1]T + \frac{m}{M}T\right) \tag{10}$$

i.e. the integrate-and-dump post-detection filter can be approximated as a discrete average. The number of discrete samples M is equal to the ratio between the IF filter bandwidth and the low-pass filter bandwidth $\gamma = \frac{B_{IF}}{B_{LP}}$. This condition also ensures that the M samples of $b(t)$ are *statistically independent.* The *decision variable* for the k-th symbol of the ASK stream is then:

$$d_k = \frac{1}{M}\sum_{m=1}^{M} b\left([k-1]T + \frac{m}{M}T\right) = \frac{1}{M}\sum_{m=1}^{M}\left[(1-\beta_k\delta)\sqrt{\frac{2\mathcal{E}_s}{T}} + n_{c_m}\right]^2 + n_{s_m}^2(t) \tag{11}$$

where for convenience we have defined:

$$n_{c_m} = n_{F_c}\left([k-1]T + \frac{m}{M}T\right); \qquad n_{s_m} = n_{F_s}\left([k-1]T + \frac{m}{M}T\right)$$

The probability density function (pdf) of the decision variable d_k is a Non-Central Chi-Square with $2M$ degrees of freedom [31]:

$$p_{d_k}(x) = \frac{1}{2\sigma^2}\left(\frac{x}{D_k}\right)^{\frac{M-1}{2}} e^{-\frac{D_k+x}{2\sigma^2}} \mathrm{I}_{M-1}\left(\frac{\sqrt{xD_k}}{\sigma^2}\right) \quad x > 0$$

where D_k is the value of d_k in the absence of noise, and $\mathrm{I}_{M-1}(\cdot)$ is a Bessel Function of order $M-1$.

From this pdf of d_k, an analytical *error probability* expression can be derived:

$$P(e)_{ASK} = \frac{1}{2}\left\{1 - Q_M\left(\sqrt{\frac{D_1}{\sigma^2}}, \sqrt{\frac{\theta}{\sigma^2}}\right) + Q_M\left(\sqrt{\frac{D_0}{\sigma^2}}, \sqrt{\frac{\theta}{\sigma^2}}\right)\right\}$$

where D_0 and D_1 are the values of D_k when β_k is equal to 0 and 1 respectively, Q_M is a Marcum function of order M [31] and θ is the threshold. The optimum value of θ depends on the signal-to noise ratio.

For the PSK stream, we find an upper-bound of the error probability by assuming that β_k is always 1. With synchronous demodulation, the error probability is:

$$P(e)_{PSK} = \frac{1}{2}\text{erfc}\left([1-\delta]\sqrt{\frac{E_{PSK}}{N_0}}\right) \tag{12}$$

while for non-synchronous (DPSK) demodulation it is:

$$P(e)_{DPSK} = \frac{1}{2}e^{-\left([1-\delta]^2\frac{E_{DPSK}}{N_0}\right)} \tag{13}$$

If no ASK modulation is applied, then $\delta = 0$ and expressions (12), (13) degenerate into the well-known error-probability expressions for PSK and DPSK. The symbol energy $E_{(D)PSK}$ is different from the quantity E_{ASK} defined for the ASK stream, since the rates of the two streams are, in general, different. We have:

$$\frac{E_{(D)PSK}}{E_{ASK}} = \frac{\text{(D)PSK bit rate}}{\text{ASK bit rate}} = \rho$$

The curves of Fig. 14 were calculated as follows. Given a value of ρ, a value of ASK modulation depth δ satisfying:

$$P(e)_{ASK} = P(e)_{(D)PSK} = 10^{-9}$$

was numerically found. Then, the penalty on the (D)PSK stream due to the concurrent transmission of the ASK stream is, from (12) and (13):

$$\Delta = 20\log_{10}(1-\delta)$$

A.2 Time Division Multiplexing

The energy per bit, when only one stream is transmitted, is given by:

$$E_s = P \cdot T = \frac{P}{B_{R1}}$$

where P is the available power, T is the bit duration and B_{R1} is the bit rate. When we squeeze in another stream, the bit rate must be increased and the bit duration decreased. The new bit duration is:

$$T' = \frac{1}{B_{R1} + B_{R2}}$$

where B_{R2} is the bit rates of the second data stream. If we keep the optical power constant, the energy per bit shrinks since now the energy per bit is:

$$E_s' = P \cdot T' = \frac{P}{B_{R_1} + B_{R_2}} < E_s$$

To restore the original amount of energy per bit (and therefore the original error probability) we need to increase power to a new value P':

$$P' = \frac{P}{B_{R_1}}(B_{R_1} + B_{R_2})$$

Defining ρ as the ratio of the bit rates of the two multiplexed data streams:

$$\rho = \frac{B_{R_1}}{B_{R_2}}$$

the multiplexing power penalty Δ, i.e. the ratio between the optical powers needed to ensure a bit energy equal to E_s *before and after* the multiplexing of the second data stream, can be written as follows:

$$\Delta = 10\log_{10}\left(\frac{P'}{P}\right) = 10\log_{10}\left(1 + \frac{1}{\rho}\right)$$

In Fig. 14 we assumed 'stream 1' to be the 'C' stream and 'stream 2' to be the 'P' stream.

A.3 Subcarrier Multiplexing

The penalty for subcarrier multiplexing was found as follows. Both streams were assumed to use the same modulation format. Therefore, the amount of energy per bit E_s that they need in order to show the same $P(e)$ is the same. Given the maximum electric field *amplitude*, the two streams share this amplitude. Putting together the constraints of having a constant E_s for each stream, independently of the bit rate, and that the sum of the amplitudes of the two streams is a constant (say, A), we get:

$$A = \sqrt{\frac{E_s}{T_1}} + \sqrt{\frac{E_s}{T_2}}$$

where T_1 and T_2 are the bit durations of the two streams. Taking as a reference the amplitude needed for the transmission of stream 1 alone (A_{ch1}), the ratio between A and A_{ch1} is:

$$\frac{A}{A_{ch1}} = \frac{\sqrt{\frac{E_s}{T_1}} + \sqrt{\frac{E_s}{T_2}}}{\sqrt{\frac{E_s}{T_1}}} = 1 + \sqrt{\frac{T_1}{T_2}} = 1 + \sqrt{\frac{1}{\rho}}$$

where ρ is the ratio of the bit rates of the two multiplexed data streams:

$$\rho = \frac{(\text{bit rate stream 1})}{(\text{bit rate stream 2})}$$

The resulting power penalty is:

$$\Delta = 20 \log_{10} \left(1 + \sqrt{\frac{1}{\rho}} \right)$$

In Fig. 14 we assumed 'stream 1' to be the 'C' stream and 'stream 2' to be the 'P' stream.

B Circuit Interconnect Performance

According to the assumptions listed in Section 6, a minimum electrical channel spacing of 3 times the bit rate was chosen. This spacing yields a penalty lower than 1dB with most coherent transmission formats [33]. Adopting the non-equispaced channel allocation (Fig. 12b), the resulting average *optical* channel spacing is 4.5 times the bit rate.

The 'laser tunability' and 'bandwidth' curves of Fig. 15 were found by dividing the relevant available optical bandwidth by the average optical channel spacing. For 10 nm laser tunability range, the corresponding available optical bandwidth is 1.25 Thz. The bandwidth of the 1550 nm window is about 20 Thz.

The power budget limit was computed as follows. The available number of *photons per second* at the receiver is:

$$P = P_l \, \frac{m}{2N} \, 10^{-\frac{A}{10} \log_2(N)}$$

where P_l is the launched number of photons per second, the factor $\frac{1}{2}$ accounts for the fact that at each node there are two receivers, N represents the power splitting at the star coupler and m is the system margin. The number of successive splitting stages through

which the signal has to pass at the star coupler is $\log_2(N)$. If s is the excess loss of each stage in dB, the factor $10^{-\frac{s}{10}\log_2(N)}$ represents the excess loss of the whole star.

According to the assumptions listed in Section 6, $m = 0.05$ (-13 dB), $P_l = 7.8 \cdot 10^{15}$ [ph/s] (0 dBm at 1550 nm) and $s = 0.5$ dB. Finally, dividing the number of available photons per second by the needed number of photons per bit (21 for DPSK) we find the maximum sustainable bit rate:

$$B_R = P/21$$

C Enhanced Packet Network Performance

C.1 Total Throughput Expressions

In Fig. 19 we show a three-dimensional plot of the total throughput of the enhanced packet network of Section 8 as a function of the parameters M (number of subnetworks) and α (fraction of out-of-subnetwork traffic) defined in Section 8.2. In this appendix we describe how this plot was obtained.

We first make the assumption that each subnetwork generates the same amount of traffic. For the time being we also assume that all subnetworks have the same α and that the outgoing traffic generated by each subnetwork is equally split among the other subnetworks. Later we will show how to compute an *effective* fraction of out-of-subnetwork traffic $\bar{\alpha}$ that permits to relax the assumption that all subnetworks have the same α.

When the backbone is not saturated, every subnetwork can operate at its maximum capacity C_{sn}. This capacity is used to process three types of traffic.

There is in-subnetwork traffic (traffic generated within the subnetwork whose destination is within the same subnetwork) which is equal to:

$$I_{sn} = (1 - \alpha)T_{sn}$$

where T_{sn} is the total amount of traffic generated within the subnetwork.

There is out-of-subnetwork traffic (traffic generated within the subnetwork whose destination is in other subnetworks). By definition of α, it amounts to:

$$O_{sn} = \alpha T_{sn}$$

Finally, there is out-of-subnetwork traffic which was generated in *other* subnetworks, whose destination is within the subnetwork under consideration. This traffic enters the

subnetwork and must be delivered to one of the nodes belonging to the subnetwork. Since we assumed uniform destination distribution of the out-of-subnetwork traffic generated by each subnetworks, this implies that the incoming out-of-subnetwork traffic must equal the outgoing out-of-subnetwork traffic and therefore it amounts to $\alpha T_{sn} = O_{sn}$ as well.

The final constraint is that the sum of these three contributions should equal the subnetwork capacity:

$$C_{sn} = I_{sn} + 2O_{sn} = (1+\alpha)T_{sn}$$

The total throughput T_{tot} of the whole network is M times T_{sn} and therefore:

$$T_{tot} = MT_{sn} = \frac{M}{1+\alpha}C_{sn} \tag{14}$$

which corresponds to expression (4) of Section 8.2.

When the backbone is saturated, the network total throughput is found as follows. The amount of out-of-subnetwork traffic that is exchanged in the network in this condition is exactly C_{back}. By definition of α, we can write:

$$C_{back} = \alpha M \cdot T_{sn}$$

On the average, every subnetwork generates and processes an amount of in-subnetwork traffic equal to $(1-\alpha)\,T_{sn}$, so that the total amount of *in-subnetwork* traffic of the overall network is:

$$I = (1-\alpha)\,M \cdot T_{sn} = \frac{C_{back}}{\alpha} - C_{back}$$

The network total throughput, when the backbone is saturated, including both in-subnetwork and out-of-subnetwork traffic, is then the sum of the above:

$$T_{tot} = C_{back} + I = \frac{1}{\alpha}C_{back} \tag{15}$$

The *actual* network total throughput for given values of C_{sn}, C_{back}, M and α is the minimum between expression (14) and (15):

$$T_{tot} = \min\left\{\frac{1}{1+\alpha}C_{sn}\,;\,\frac{1}{\alpha}C_{back}\right\} \tag{16}$$

In Fig. 19 C_{back} and C_{sn} are fixed and T_{tot} is plotted versus M and α.

If α is not equal for all subnetworks, in general (14) and (15) are not valid. However, if the amount of out-of-subnetwork traffic that enters a subnetwork is equal to the amount

of out-of-subnetwork traffic that exits that subnetwork, then the above expressions are still valid replacing α with an *effective* α ($\bar{\alpha}$) defined as follows:

$$\bar{\alpha} = \frac{1 - \sum_{i=1}^{M} \frac{1}{1+\alpha_i}}{\sum_{i=1}^{M} \frac{1}{1+\alpha_i}} \tag{17}$$

where α_i is the out-of-subnetwork traffic fraction generated by the i-th subnetwork.

C.2 Total Throughput Maximization

In Section 8.3 we claim that, given C_{back} and C_{sn}, the values of M and $\bar{\alpha}$ that maximize the network total throughput are given by (6), under the constraint that $\bar{\alpha}(M)$ is a monotonically increasing function, i.e.:

$$\frac{\partial \bar{\alpha}}{\partial M} \geq 0 \tag{18}$$

In words, the above condition means that further segmentation of the network causes a heavier exchange of out-of-subnetwork traffic.

In order to obtain (6), we first compute the gradient of the total throughput (16) with respect to $\bar{\alpha}$ and M:

$$\nabla \cdot T_{tot} = \begin{cases} \frac{C_{sn}}{1+\bar{\alpha}} \vec{M} - \frac{C_{sn} M}{(1+\bar{\alpha})^2} \vec{\bar{\alpha}} & \text{if backbone is } \textit{not} \text{ saturated} \\ -\frac{C_{back}}{\bar{\alpha}^2} \vec{\bar{\alpha}} & \text{if backbone is saturated} \end{cases} \tag{19}$$

Starting from a non-segmented network ($M = 1$), and as long as the backbone is not saturated, the above expression of the gradient shows that any increase in M causes an increase in total throughput, ***unless***:

$$\frac{\partial \bar{\alpha}}{\partial M} > \frac{1 + \bar{\alpha}}{M} \tag{20}$$

This condition is found by computing the direction of no growth of the total throughput, which is orthogonal to the gradient of T_{tot}.

If (20) is true, even only for some $(\bar{\alpha}, M)$, then no general rule can be found on the maximization of the total throughput. The problem must be solved on a case-by-case basis

However, condition (20) is extremely unlikely to occur, as a straightforward numerical substitution can show. Therefore, we assume that in a realistic environment the total

throughput *does* increase when M is increased, as long as the backbone is not saturated. As a result, increasing M brings us closer to the maximum of the network total throughput.

But M cannot be increased indefinitely. Eventually, the backbone saturation limit is reached. This is unavoidable, given the above assumptions. At the saturation point, the expression of the gradient (19) tells us that the only way to further increase T_{tot} is to decrease $\bar{\alpha}$. However, in order to decrease $\bar{\alpha}$, given (18), it is necessary to reduce M. This would cause moving back into the operating regime where the backbone is not saturated and where a reduction in M causes a reduction of the total throughput. Therefore, when the backbone saturation limit is reached, both increasing M *and* decreasing it will deteriorate the total throughput. Hence the maximum total throughput is achieved at the onset of backbone saturation.

Backbone saturation occurs when (14) and (15) become equal:

$$\frac{1}{1+\alpha} C_{sn} = \frac{1}{\alpha} C_{back}$$

which immediately yields equation (6).

References

[1] Habbab, I., M., I., et al.: "Protocols for very high speed optical fiber local area networks using a passive star topology"; IEEE JLT, vol. 5, no. 12, pp. 1782-1793, December 1987.

[2] Mehravari, N.: "Improved multiple access schemes for very high speed optical fiber local area networks using a passive star topology"; GLOBECOM '89, paper 8.2.1.

[3] Chlamtac, I., Ganz, A.: "Design alternatives of asynchronous WDM star networks"; ICC '89.

[4] Mon-Song Chen, et al.: "A media access protocol for packet-switched wavelength division multiaccess metropolitan area networks"; IEEE J-SAC, vol. 8, no. 6, pp. 1048-1057, August 1990.

[5] Ganz, A., Koren, : "WDM passive stars - Protocols and performance analysis": INFOCOM '91.

[6] Leung, Takawira, : "FDM packet multiple access network using coherent fiber optic communication"; ICC '90.

[7] Ofek, Y., Sidi, M.: "Design and analysis of a hybrid access control to an optical star using WDM"; INFOCOM '91, paper 2A.3.1.

[8] Labourdette, J., F., Acampora, A., S.: "Wavelength agility in multihop lightwave networks"; INFOCOM '90, pp. 1022-1029.

[9] Labourdette, J., F., Acampora, A., S.: "Partially reconfigurable multihop lightwave networks"; GLOBECOM '90, paper 300.6.1.

[10] Bannister, J., A., et al.: "Topological design of wavelength-division optical networks"; INFOCOM '90, pp. 1005-1013.

[11] Gidron, R., et al.: "TeraNet: a multi gigabit per second hybrid circuit/packet switched lightwave network"; SPIE Meeting, Conference 1579 'Advanced Fiber Communications Technologies', Proceedings vol. 1579, pp. 40-48, Boston, September 3-6 1991.

[12] Sauer, J., R.: "Multi-Gb/s optical computer interconnect"; SPIE Meeting, Conference 1579 'Advanced Fiber Communications Technologies', Proceedings vol. 1579, pp. 49-61, Boston, September 3-6 1991.

[13] Glance, B., S., Scaramucci, O.: "High-performance dense FDM coherent optical network"; IEEE JSAC, vol. 8, no. 6, pp. 1043-1047, August 1990.

[14] Noe', R., et al.:"Comparison of polarization handling methods in coherent optical systems"; IEEE Journal of Lightwave Technology, vol. 9, n. 10, pp. 1353-1366, October 1991.

[15] O'Byrne, V.: "A method for reducing the channel spacing in a coherent optical heterodyne system"; IEEE Photonics Technology Letters, vol. 2, no. 7, July 1990.

[16] Sessa, W., B., et al.: "Frequency stability of DFB lasers used in FDM multi-location networks"; OFC '92, paper ThC3, San José (CA), February 2-7, 1992.

[17] Maxemchuck, N., F.: "The Manhattan Street network"; IEEE Globecom 1985, New Orleans, December 1985.

[18] Maxemchuck, N., F.: "Routing in the Manhattan Street network"; IEEE Transactions on Communications, May 1987.

[19] Acampora, A., S.: "A multichannel multihop local lightwave network"; Proc. Globecom 1987, pp. 1500-1510.

[20] Hluchyj, M., G., Karol, M., J.: "ShuffleNet: an application of generalized perfect shuffles to multihop lightwave networks"; Proc. Infocom 1988.

[21] Karol, M., J., Gitlin, R., D.: 'High-performance Optical Local and Metropolitan Area Networks: Enhancements of FDDI and IEEE 802.6 DQDB'; IEEE JSAC, vol. 8, no. 8, pp. 1439-1448, October 1990.

[22] Olshansky, R., et al.: "Subcarrier multiplexed coherent lightwave systems for video distribution"; IEEE JSAC, vol. 8, no. 7, pp. 1268-1275, September 1990.

[23] Benedetto, S., Poggiolini, P.: "Performance evaluation of multilevel polarisation shift keying modulation"; IEE Electronics Letters, vol. 26, no. 4, pp. 244-246, February 25th, 1990.

[24] Dono, N., R., et al.: "A wavelength division multiple access network for computer communication"; IEEE JSAC, vol. 8, no. 6, pp. 983-994, August 1990.

[25] Koch, T., L., Koren, U.: "Photonic integrated circuits"; OFC '92, Tutorial TuP, Proceedings Tutorial Sessions, pp. 153-198, , San José (CA), February 2-7, 1992.

[26] Alferness, R., C., et al.: " Widely tunable InGaAsP/InP laser based on a vertical coupler intracavity filter"; OFC '92, paper PD2 (postdeadline), San José (CA), February 2-7, 1992.

[27] Hideaki Takagi:'Mean message waiting times in symmetric multi-queue systems with cyclic service'; ICC '85, Chicago, June 23-26,1985.

[28] Hideaki Takagi:'Queueing analysis of polling models: an update'; ACM computing surveys, vol. 20, no. 1, pp. 5-28, March 1988.

[29] Kazovsky, L., G., Meissner, P., Patzak, E.: "ASK multiport optical homodyne receivers"; IEEE JLT, vol. 5, no. 2, pp. 770-791, June 1987.

[30] Kazovsky, L., G., et al.: "Impact of laser intensity noise on ASK two-port optical homodyne receivers"; IEE Electronic Letters, vol. 23, no. 17, pp. 871-873, August 13th 1987.

[31] Foschini, G., J., Vannucci, G.: "Noncoherent detection of coherent lightwave signals corrupted by phase noise";
IEEE Transactions on Communications, vol. 36, no. 3, pag. 306-314, March 1988.

[32] J. G. Proakis: "Digital Communications". M^{c} Graw-Hill International Book Company, 1983, pp. 26-31.

[33] Kazovsky, L., G., Gimlett, J., L.: "Sensitivity penalty in multichannel coherent optical communications"; IEEE JLT, vol. 6, no. 9, pp. 1353-1365, September 1988.

[34] Goodman, M., S., et al: 'The LAMBDANET multiwavelength network: architecture, applications and demonstrations'; IEEE JSAC, vol. 8, no. 6, pp. 995-1004, August 1990.

[35] Kobrinski, H., Cheung, K.: 'Wavelength tunable optical filters: applications and technologies'; IEEE Communications Magazine, pp. 53-63, October 1989.

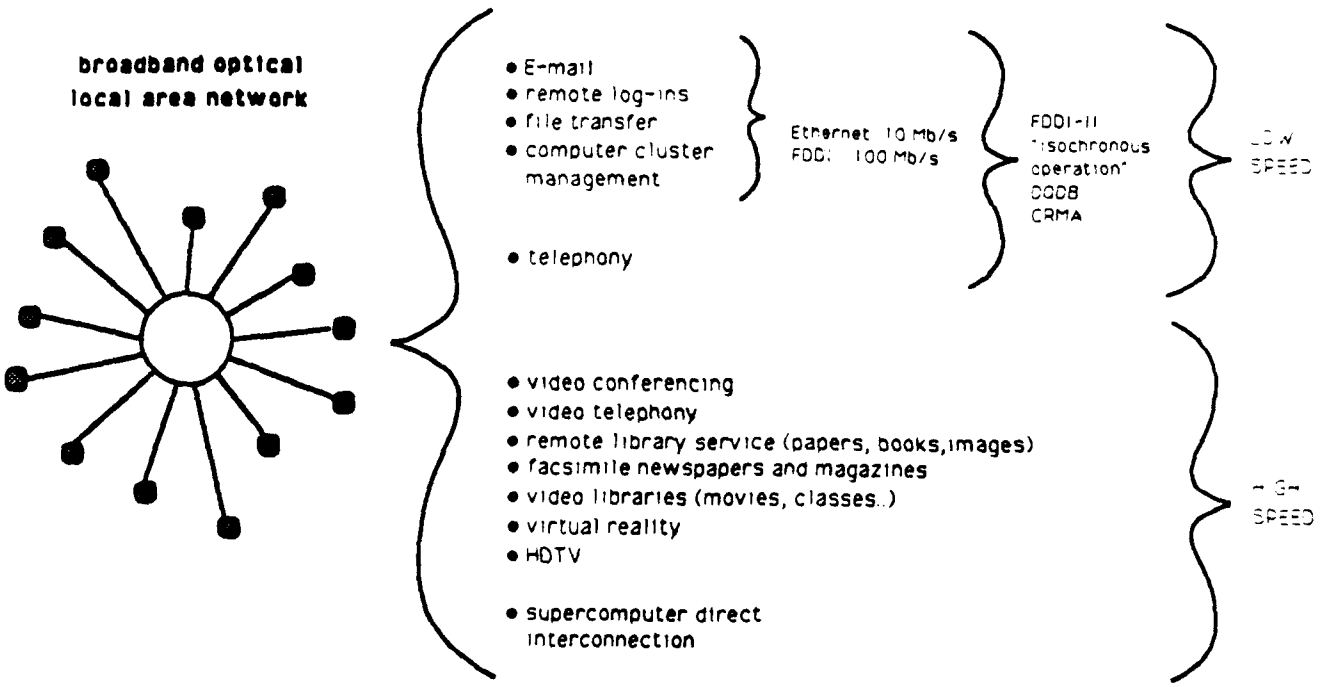

Figure 1: Some of today's and tomorrow's network services.

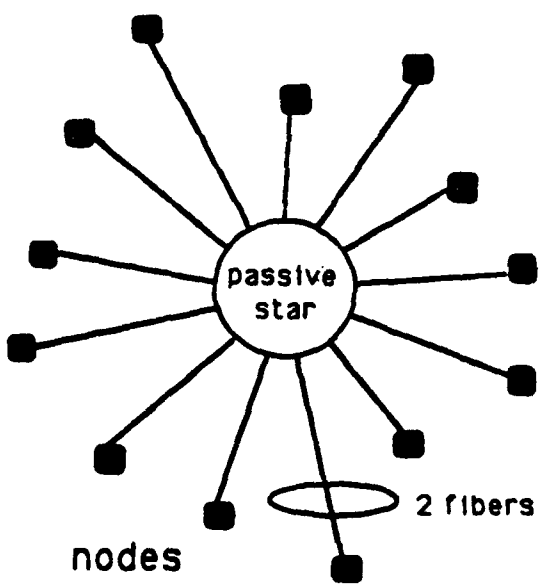

Figure 2: Each STARNET node has a two-fiber connection with the star: one carries the node signal to the star and the other brings from the star the signals of all the nodes.

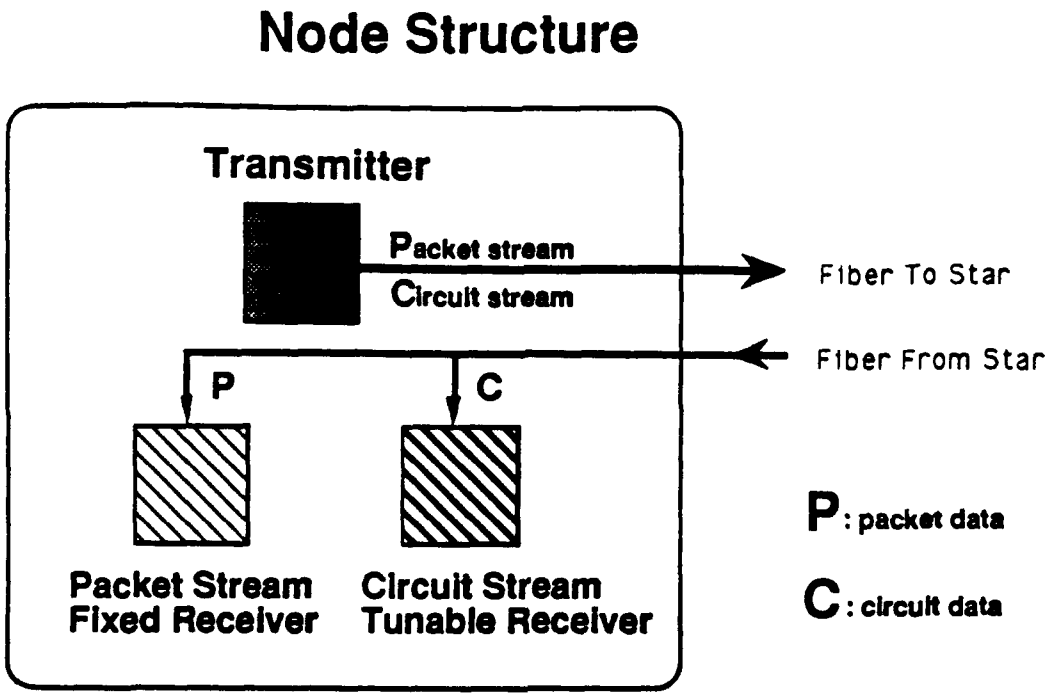

Figure 3: Block diagram of the basic node configuration.

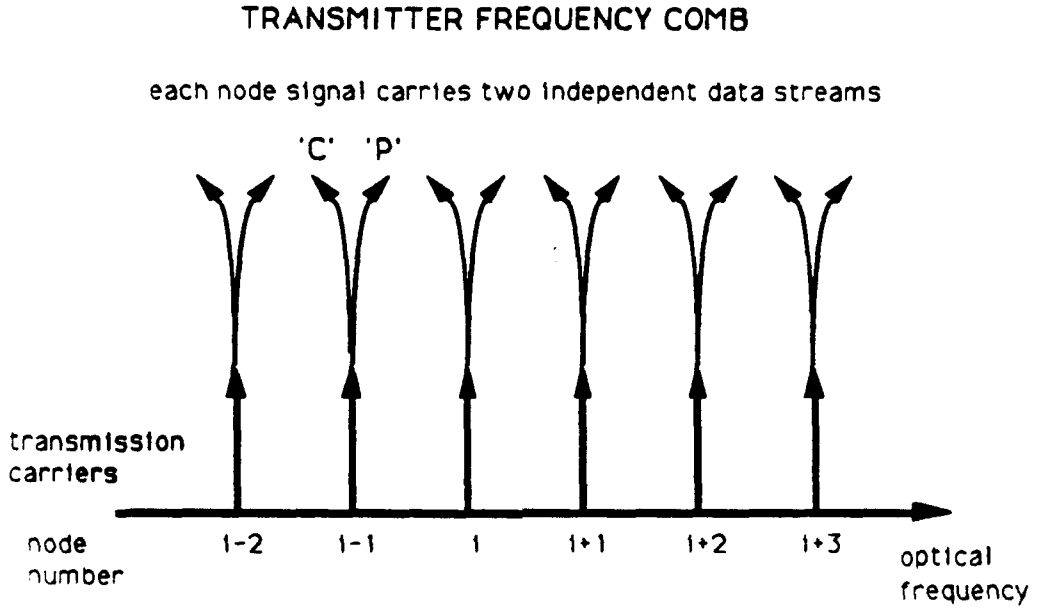

Figure 4: The node transmitter multiplexes two independent data streams onto the same lightwave carrier.

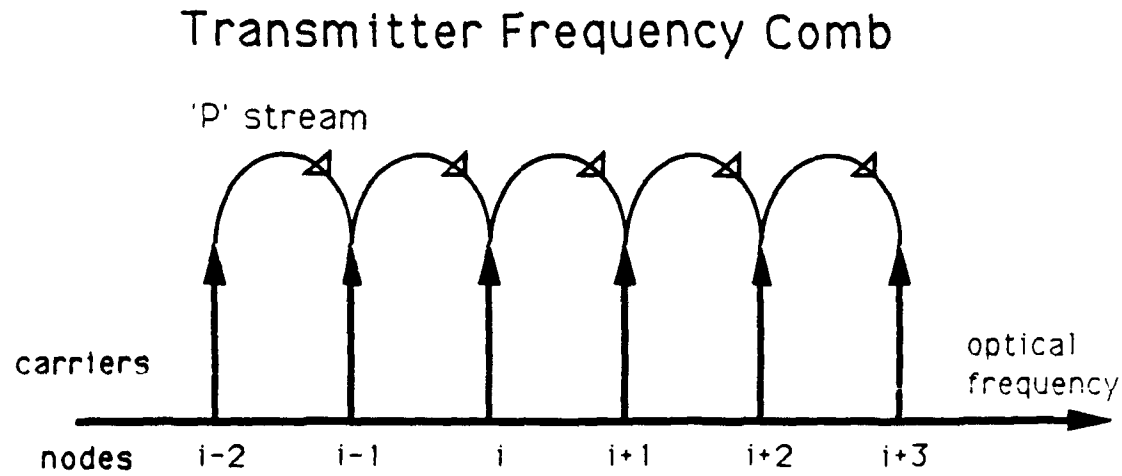

Figure 5: Each node 'sees' the 'P' stream of the previous node at all times. A logical chain connection is thus achieved.

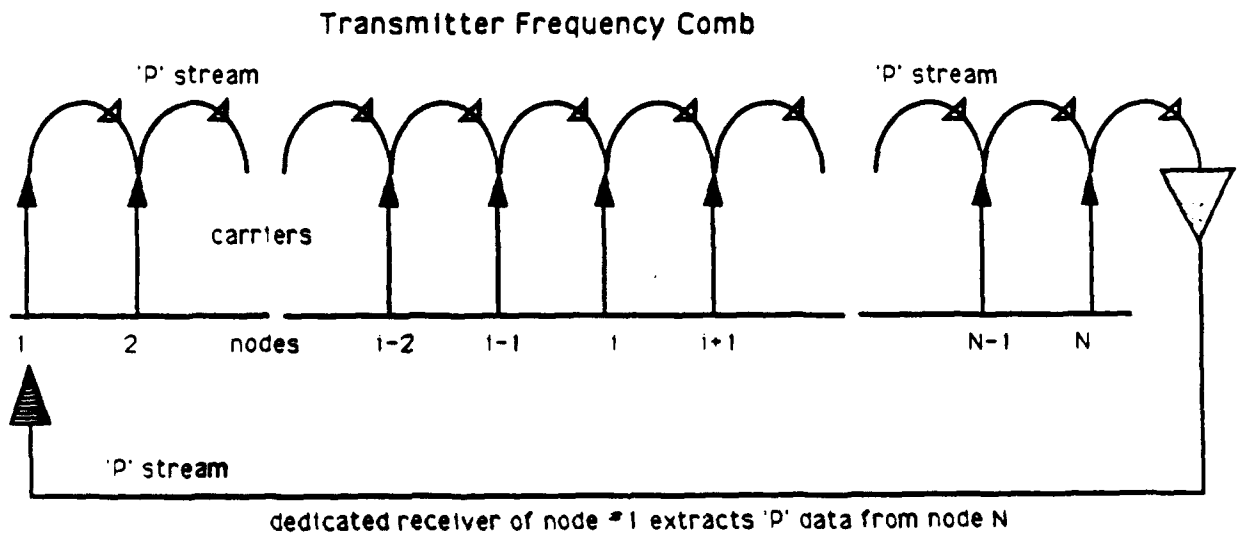

Figure 6: The first node (node 1) of the chain is equipped with a receiver which extracts the 'P' stream out of the last node in the comb.

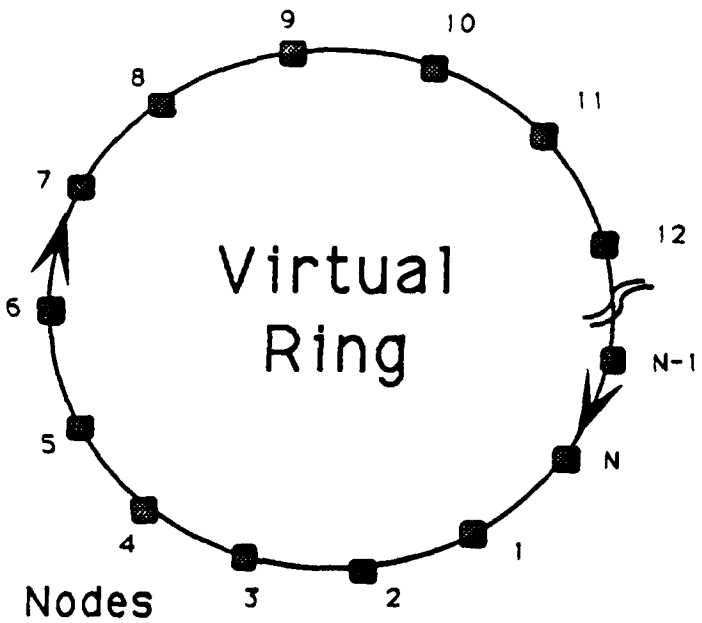

Figure 7: A logical unidirectional ring topology is arranged on the underlying physical star network.

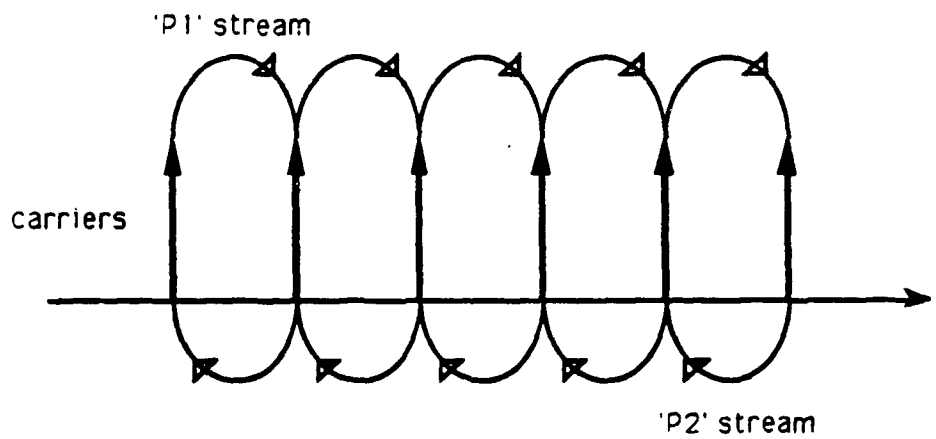

Figure 8: A virtual bidirectional store-and-forward chain is obtained using the logical connectivity of BNC2.

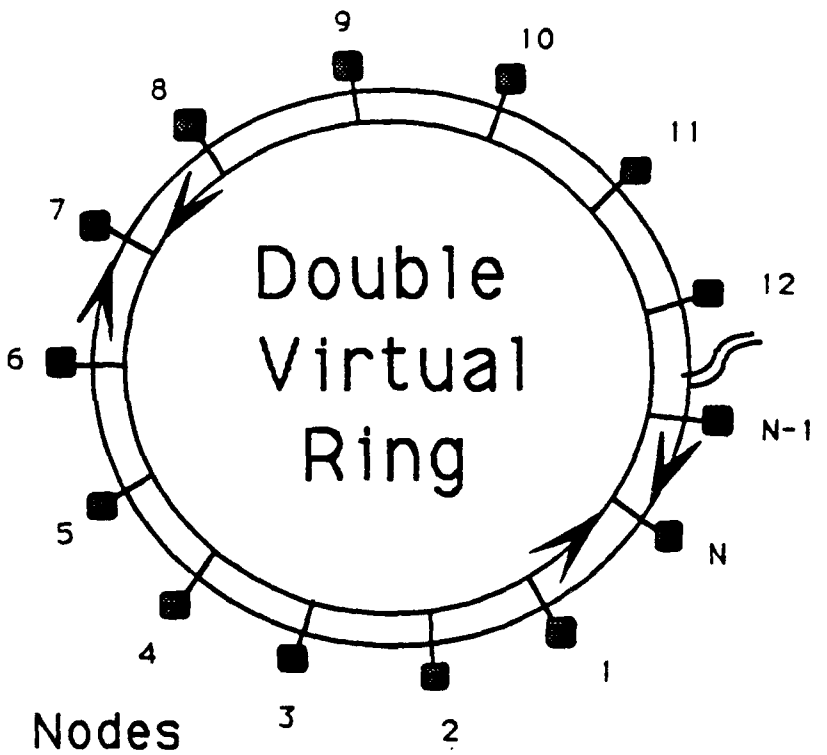

Figure 9: With BNC2, a virtual double counter-rotating ring topology can be arranged.

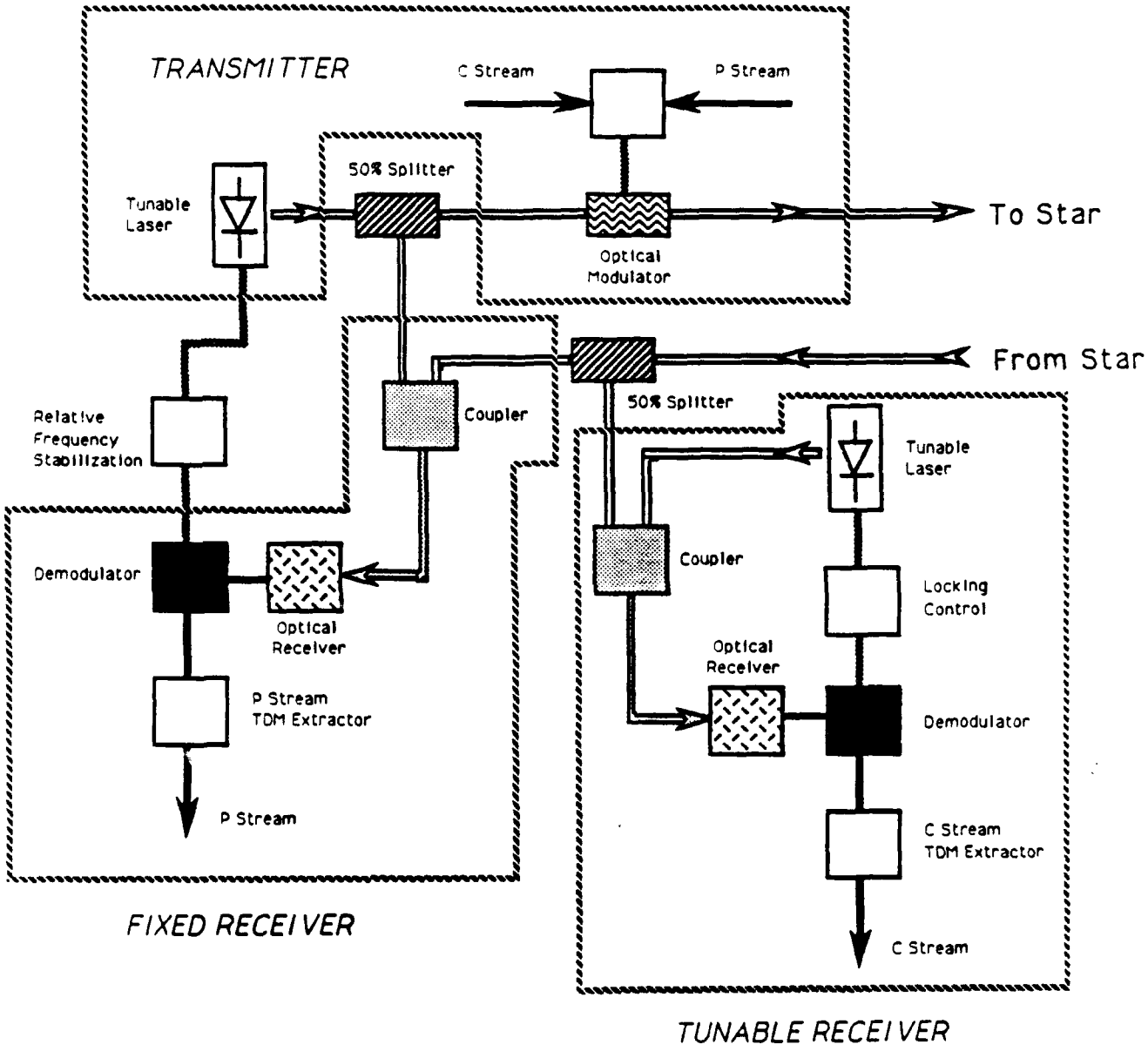

Figure 10: Schematic of a STARNET node.

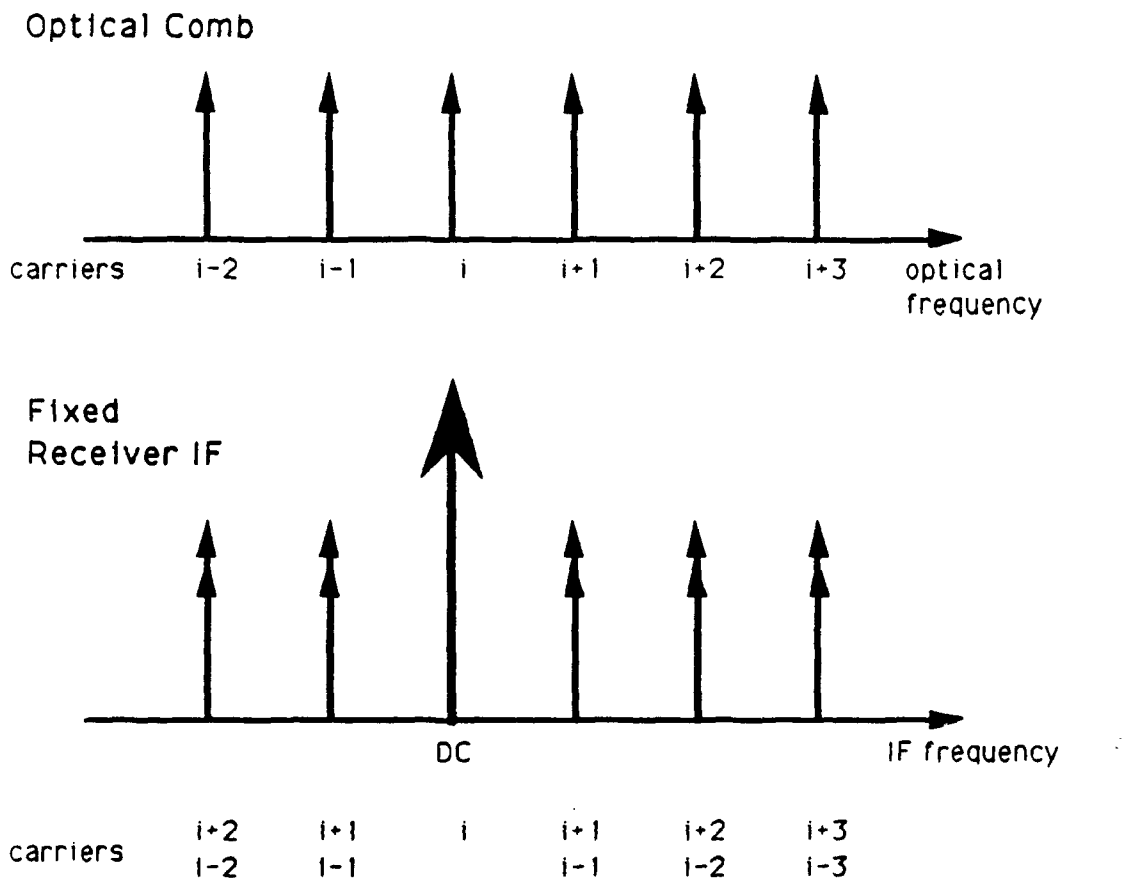

Figure 11: **Carrier visibility at IF in the fixed receiver of node i, employing the node transmitter laser as the local oscillator.**

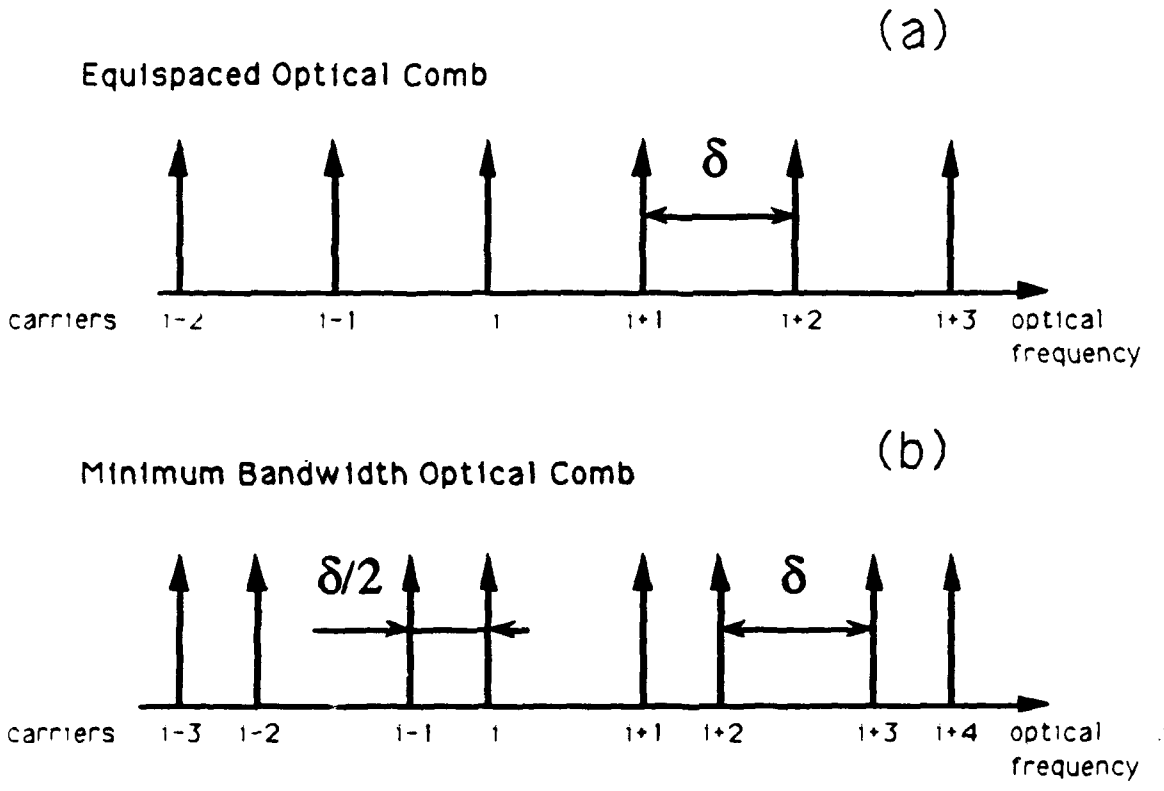

Figure 12: Equispaced and minimum optical bandwidth occupancy (for heterodyne detection [13]) frequency allocation. The quantity $\delta/2$ is the minimum acceptable electrical-domain channel spacing at the receiver IF.

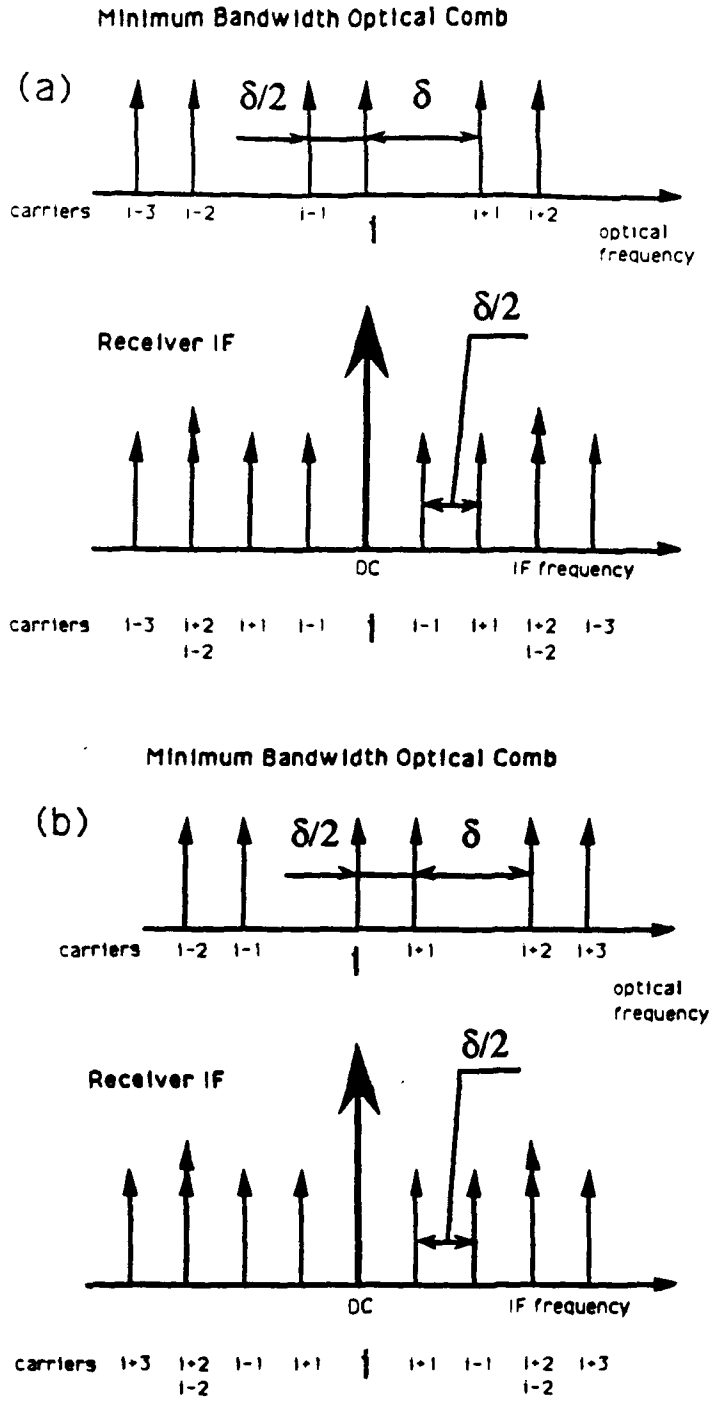

Figure 13: Carrier visibility at IF in the fixed receiver of node i, employing the node transmitter laser as LO and the non-equispaced allocation of carriers. In (a) and (b) the two possible IF spectra are shown, depending on the i-th node position in the comb.

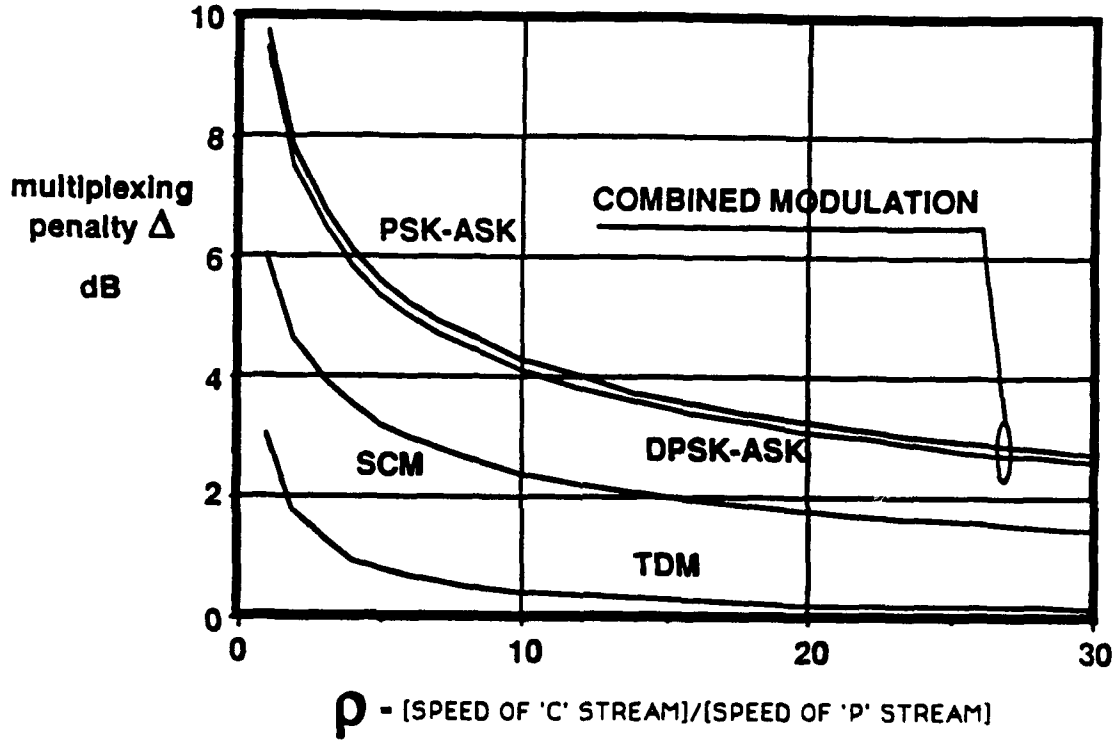

Figure 14: Plot of the multiplexing penalty Δ, defined as the ratio between the power needed to transmit both 'C' and 'P' streams and the power needed to transmit the 'C' stream only at a fixed error probability $P(e)=10^{-9}$, versus the speed ratio ρ = [speed 'C' stream]/[speed 'P' stream]. The curve TDM refers to Time Division Multiplexing whereas SCM stands for Subcarrier Multiplexing.

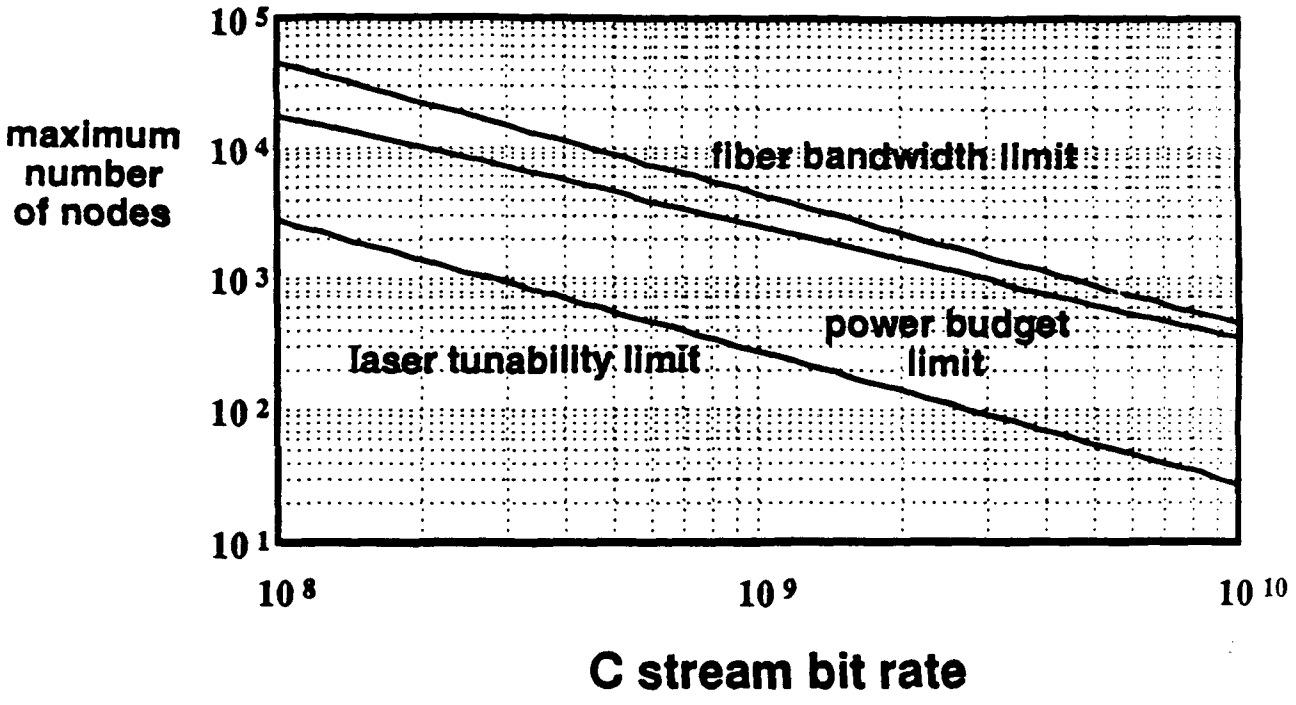

Figure 15: Maximum number of nodes versus the transmission rate of the circuit interconnect ('C') stream.

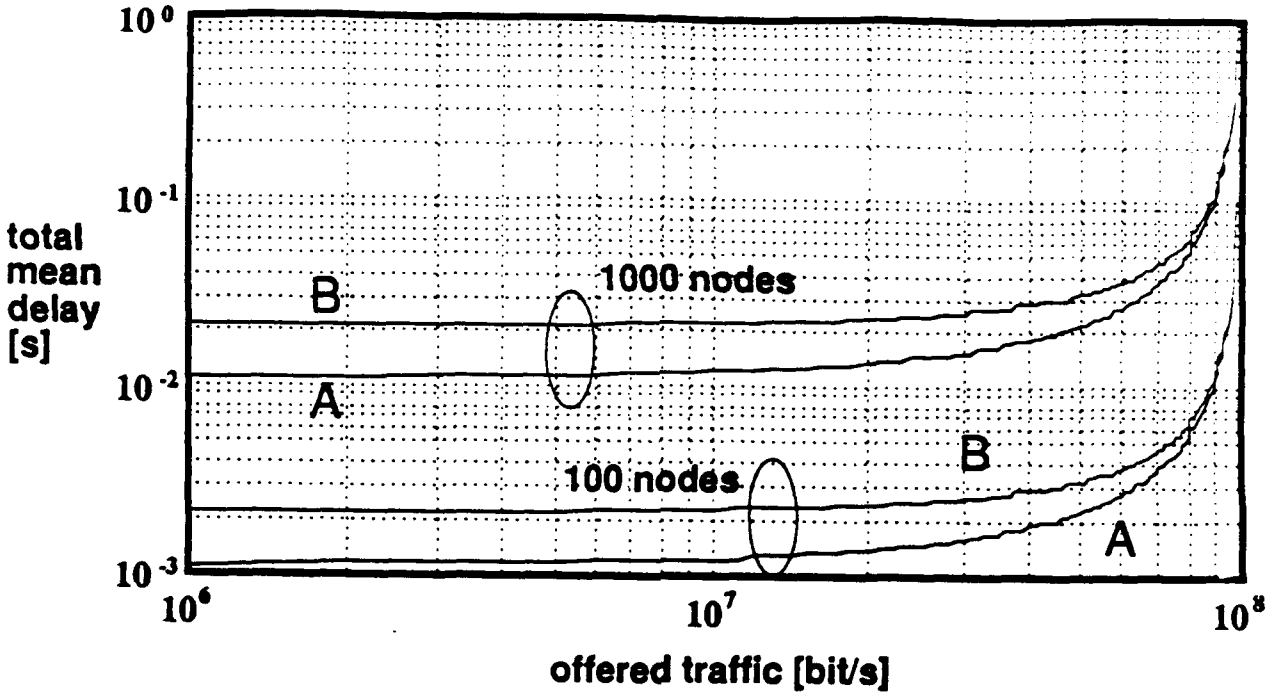

Figure 16: Mean packet delay for a hundred and a thousand nodes in a single-ring topology. Curves 'A' are queueing delay only, curves 'B' are total delay (queueing and propagation).

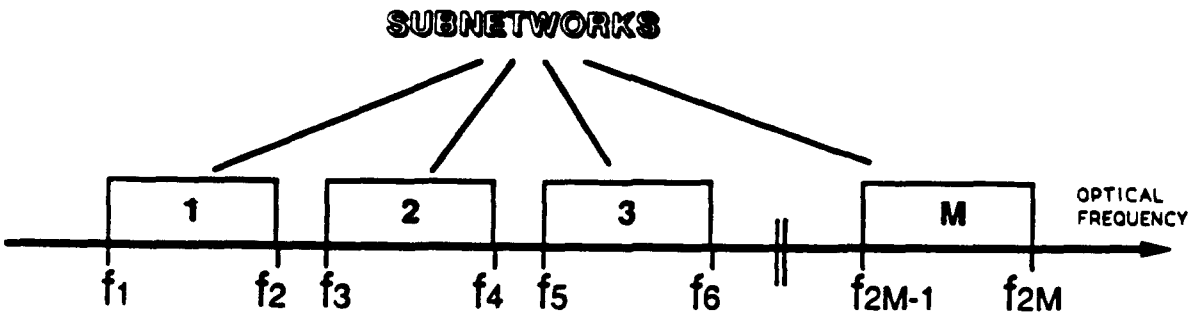

Figure 17: M basic packet networks are arranged on the same physical star so that they are contiguous in the optical frequency domain.

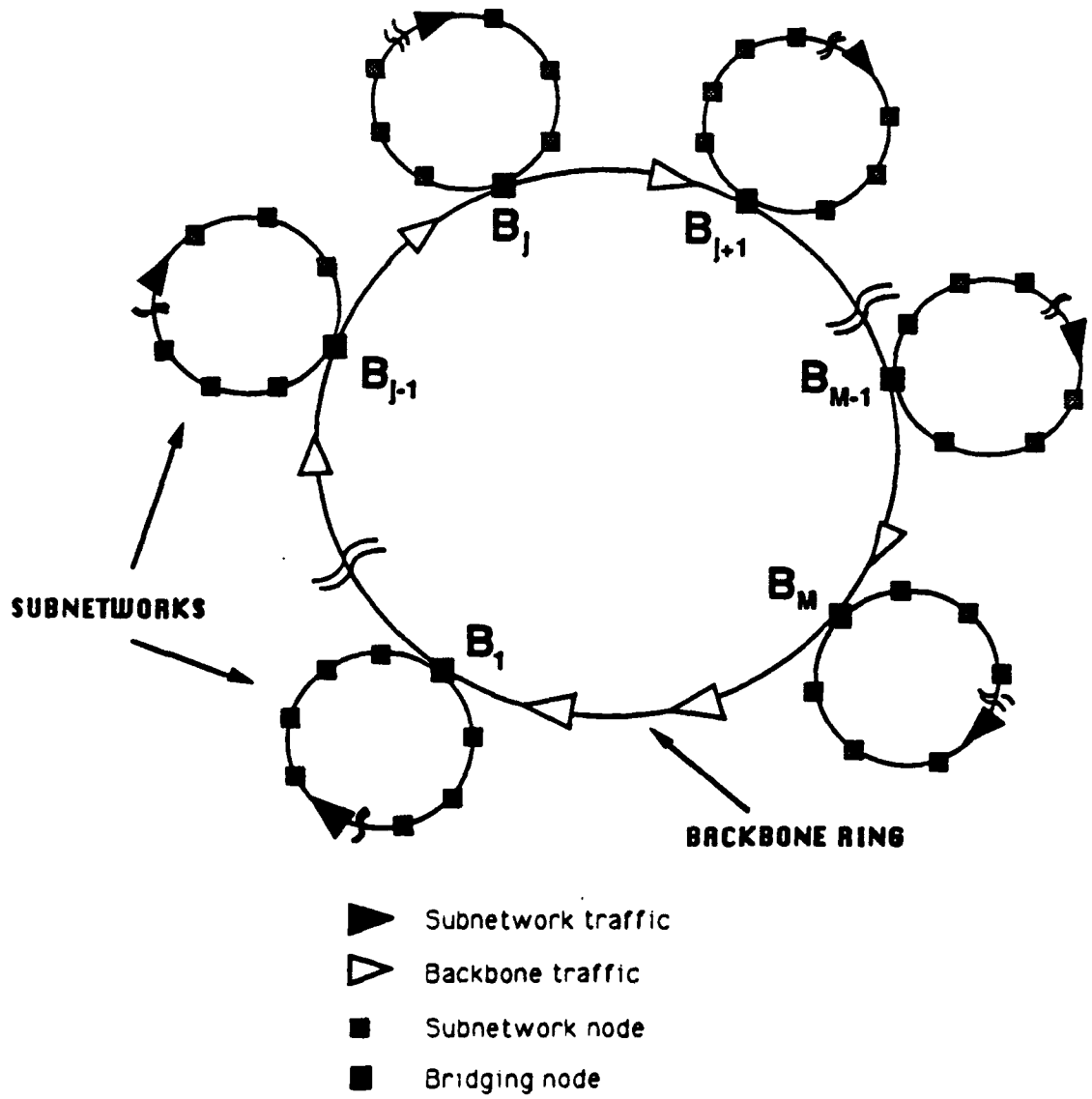

Figure 18: Data flow and virtual topology of a ring-of-subrings enhanced packet network. The B_j's are the bridging nodes.

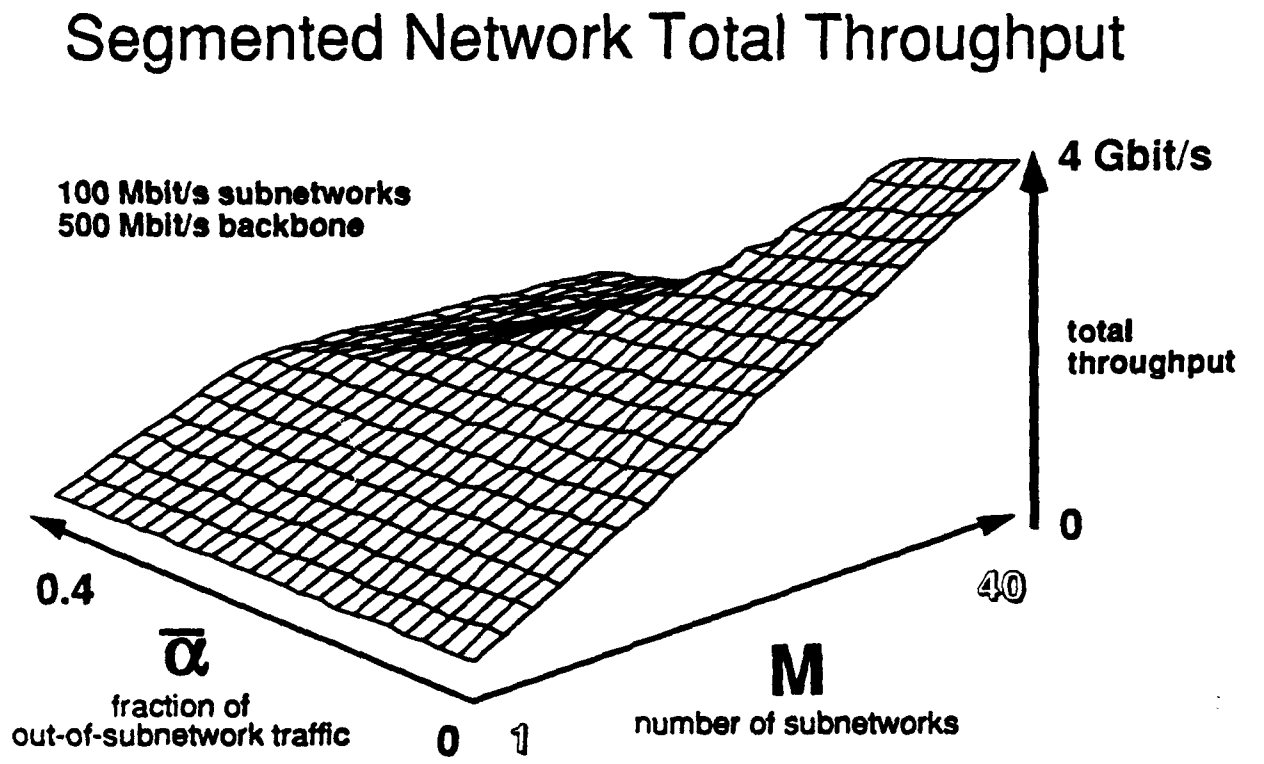

Figure 19: Total throughput of a segmented packet netowrk versus number of subnetworks M and out-of-subnetwork traffic fraction $\bar{\alpha}$. The subnetworks have a capacity of 100 Mbit/s, the backbone of 500 Mbit/s.

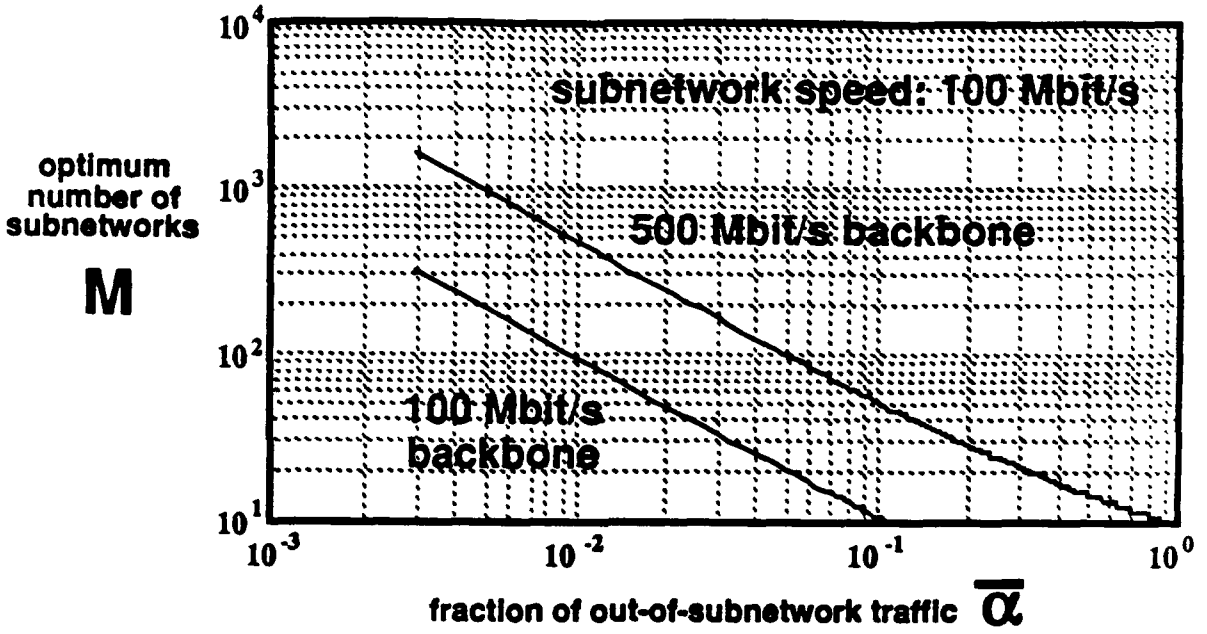

Figure 20: Optimum number of subnetworks M versus out-of-subnetwork traffic fraction $\bar{\alpha}$, for a backbone capacity of 100 and 500 Mbit/s.

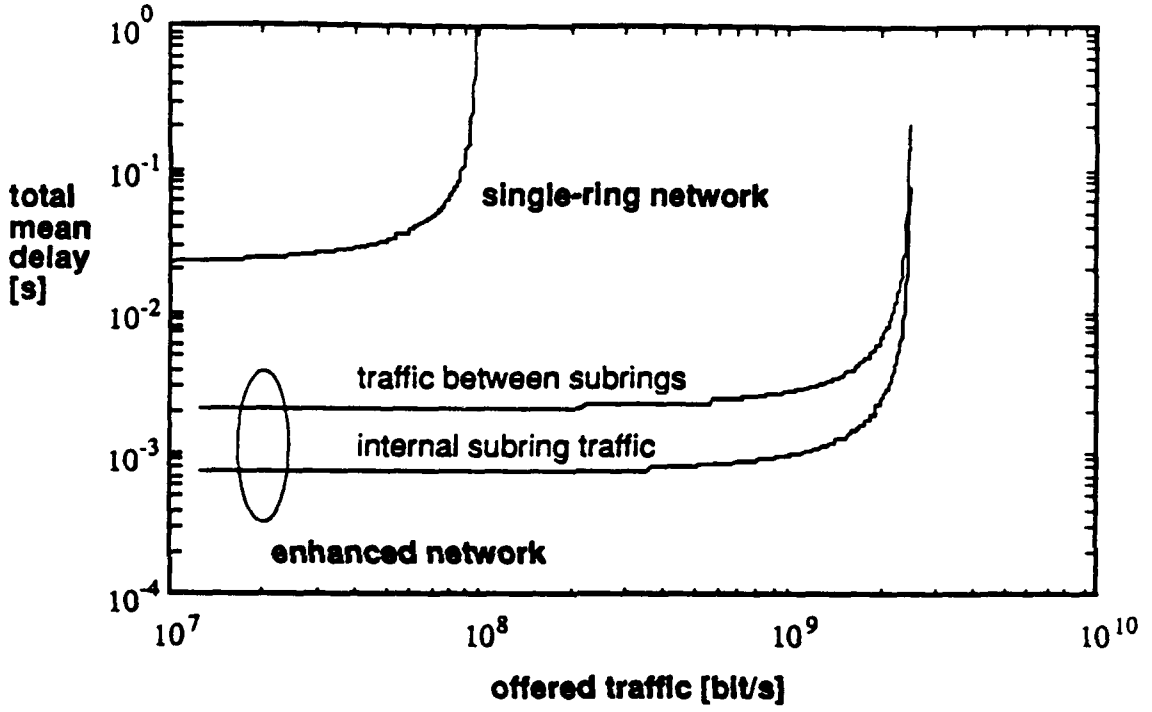

Figure 21: Total mean delay for the single-ring and ring-of-subrings packet networks. Parameter values are: 1000 nodes, subnetwork and single-ring capacity 100 Mbit/s, 30 subnetworks, backbone capacity 500 Mbit/s, $\bar{\alpha} = 0.2$. Other assumptions are listed in Section 7. Separate curves are shown for packets whose source and destination are in the same subnetwork or in different subnetworks.

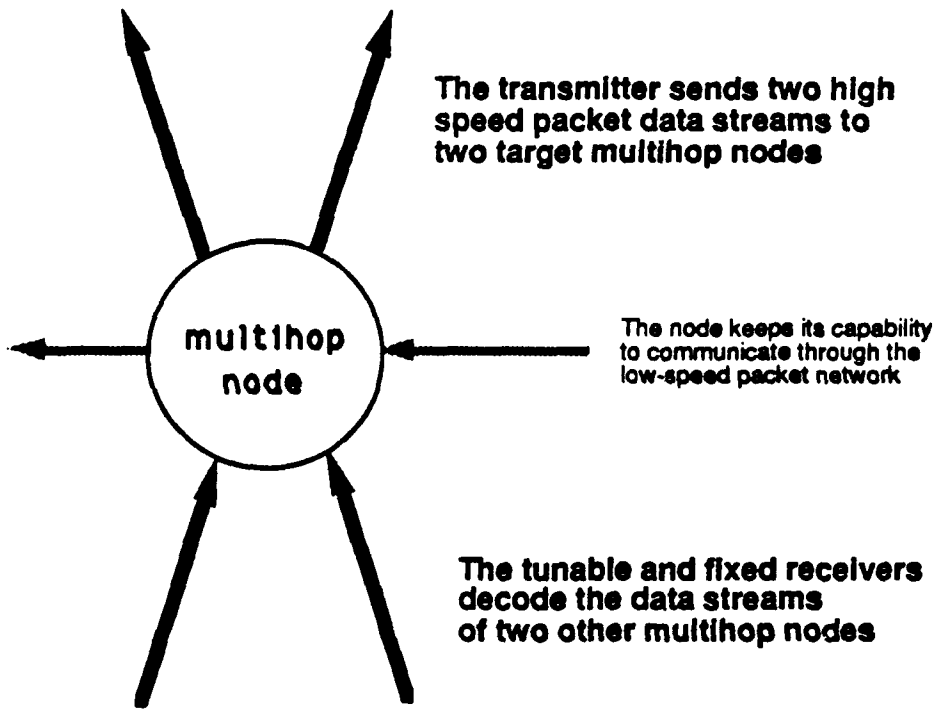

Figure 22: A multihop node has two outgoing and two incoming high speed logical links (black arrows).

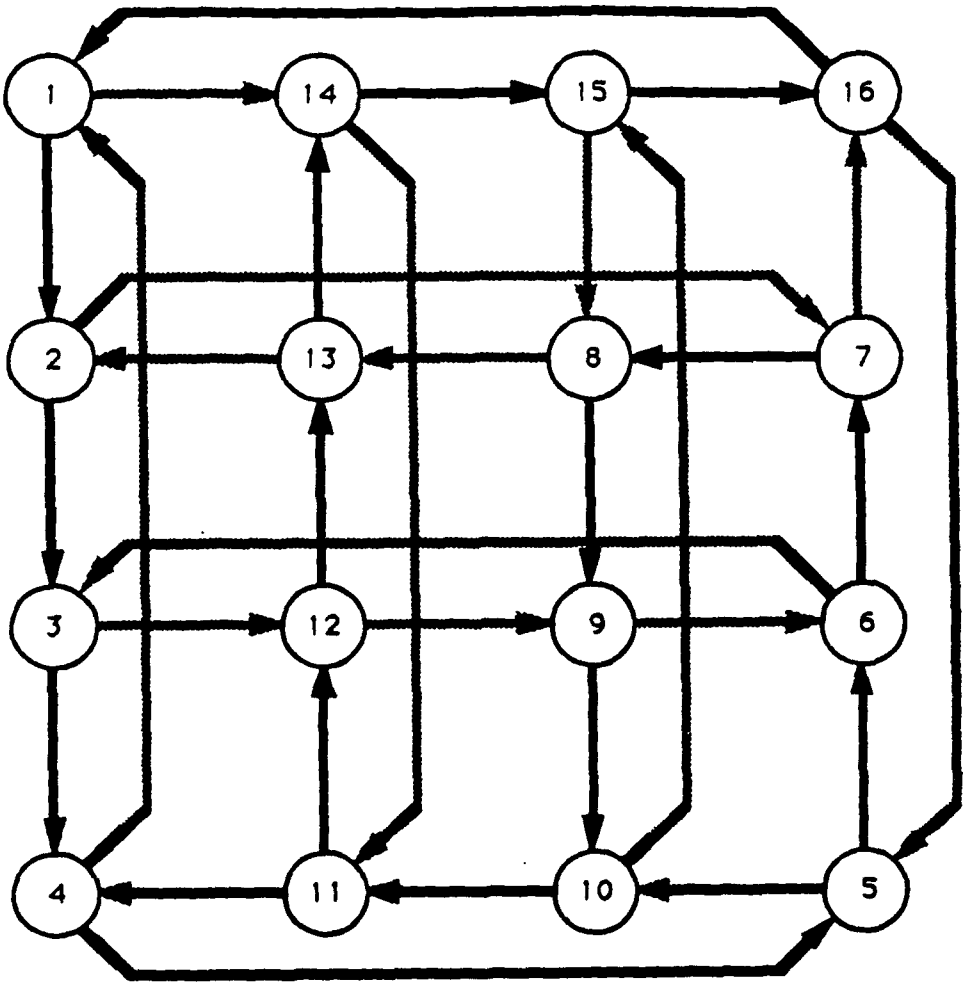

Figure 23: 16-node Manhattan Street Topology. The Hamiltonian path is shown in black. The remaining links (gray) form three smaller rings (see Fig. 24).

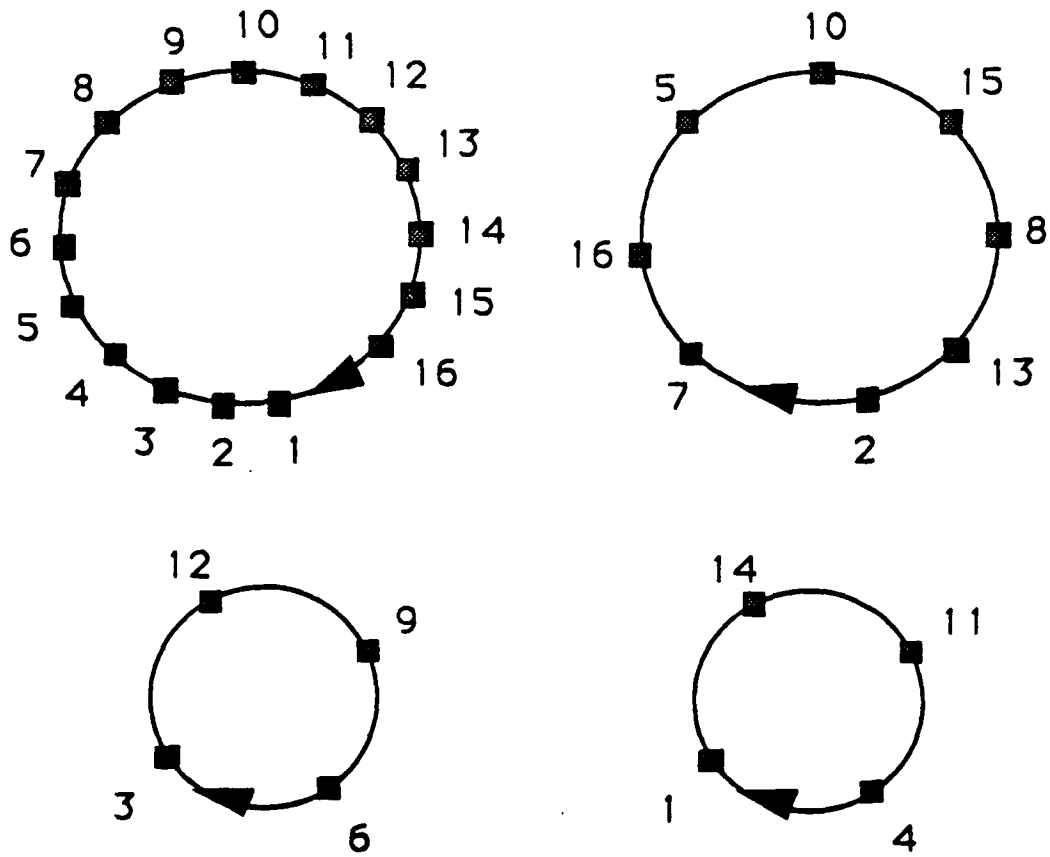

Figure 24: The node ordering in the optical frequency domain must follow the numbering shown in figure. The Hamiltonian ring (upper left) is then obtained using the fixed receivers, the other rings are set up by means of the tunable receivers.

Impact of Four Wave Mixing on Manchester Coded Optical WDM Communication Systems

Hojoon Lee and Leonid G. Kazovsky

Department of Electrical Engineering
Stanford University
Durand Building 202
Stanford, CA 94305-4055
Tel.(415) 725-3818, Fax.(415) 723-9251
E-mail leonid@sierra.stanford.edu

Abstract- The performance of Manchester-coded optical wavelength division multiplexing (WDM) systems is evaluated taking into account the shot noise and the four wave mixing (FWM) caused by fiber nonlinearities. The result is compared to conventional non-return-to-zero (NRZ) systems for ASK and DPSK modulation formats. Further, the dynamic range, defined as the ratio of the maximum input power (limited by the FWM), to the minimum input power (limited by receiver sensitivity), is evaluated. For 1.55 μm 16 channel WDM systems, the dynamic range of ASK Manchester coded systems shows a 2.0 dB improvement with respect to the NRZ; the corresponding number for DPSK is 2.1 dB. This result holds true for both dispersion-shifted fiber and conventional fiber; it has been obtained for 10 GHz channel spacing, 1 Gbps/channel bit rate and 100 Km transmission length.

I. INTRODUCTION

Future multichannel optical transmission systems will utilize the large bandwidth of single mode fibers using wavelength division multiplexing (WDM). The performance of optical WDM systems may be degraded by the nonlinearities of optical fibers [1,2]. One important fiber nonlinearity is four wave mixing (FWM). This effect occurs when two or more optical waves at different wavelengths mix to produce new optical waves at other wavelengths. The new optical waves may lead to crosstalk [3,4].

Several studies of four wave mixing in WDM communication systems have been published [5,6]. These studies showed that the FWM crosstalk limits the number of channels, the maximum allowed input power per channel and the channel frequency separation. The allowed power per channel, for a given number of channels and a given frequency separation, depends on the fiber dispersion and attenuation. Previous studies took into account FWM only, and neglected other noise sources, such as shot noise. In addition, the bit error rate in previous studies was calculated under the assumption that the entire power of the interference due to FWM falls into the signal bandwidth.

In this paper, the performance of optical Manchester coded WDM systems is evaluated. Our analysis takes into account the shot noise originating from the light detection process and FWM noise resulting from the optical fiber nonlinearity. These two effects limit the transmission distance as follows: the nonlinearity of the optical fiber limits the maximum transmission power, and the shot noise originating from the detection process limits the minimum receiver power. The ratio of the maximum transmitter power launched into the fiber to the minimum receiver power limits the acceptable attenuation and, therefore, the maximum transmission length. We show that Manchester coding reduces the impact of FWM on WDM systems. Our analysis does

take into account the spectral distribution of FWM, and so is believed to be more accurate than previous studies.

The rest of this paper is organized as follows. The system block diagram and the FWM are described in Section II. Receiver output signal and noises are described in Section III. Section IV deals with autocorrelation functions for the NRZ and Manchester codes and the signal-to-noise ratio. Bit error rate is evaluated in Section V. Numerical results and discussion are contained in Section VI. Finally, Section VII contains the conclusions of this paper.

II. WAVELENGTH DIVISION MULTIPLEXING SYSTEM AND FOUR WAVE MIXING

The block diagram of an optical WDM system employing Manchester coding is shown in Fig. 1. Encoders are used to convert NRZ data to Manchester-coded data. The matched filter is used as a decoder in the receiver. We assume that all transmitters use the same modulation format.

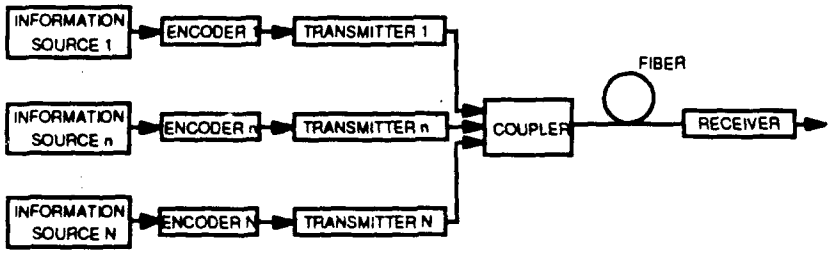

Fig. 1. Block diagram of an optical wavelength division multiplexing system.

To investigate the impact of FWM on the N-channel optical WDM system, we use the first order nonlinear differential equation that governs the optical wave propagation in a nonlinear medium. For the case of light with a finite spectral width, this equation looks as follows [1]:

$$\frac{d}{dz}E_\rho(\omega,z) = -\frac{1}{2}\alpha E_\rho(\omega,z) + \sum_{\mu,\nu} j\frac{2\pi\omega_c}{nc}(D\chi_{1111})\exp(j\Delta kz)$$

$$\cdot\exp(-\frac{3}{2}\alpha z)\int_{-\infty}^{\infty}d\omega'\int_{-\infty}^{\infty}d\omega'' E^*_{\mu+\nu-\rho}(\omega'+\omega''-\omega)\cdot E_\mu(\omega')\cdot E_\nu(\omega'') \quad (1)$$

where it is assumed that the light propagates along the z axis, E is electric field in the optical fiber, ω is angular light frequency, n is fiber core refractive index, c is the velocity of light in vacuum, α is the fiber power attenuation constant, χ_{1111} is third order nonlinear susceptibility, D is the degeneracy factor, μ,ν and $\rho = 1,2\cdots$ N and Δk is the phase mismatch given by [2]

$$\Delta k = 2\pi\lambda^2 C(f_\mu - f_{\mu+\nu-\rho})(f_\nu - f_{\mu+\nu-\rho})/c \quad (2)$$

where C is the group velocity dispersion (G.V.D.). In the derivation of (1), it is assumed that the field depletion due to FWM is small, so that the field amplitude is reduced solely by fiber attenuation. This assumption is valid when the field amplitude of the incident light at the fiber input is much larger than that of the converted wave at the fiber end. Nonlinear term due to four wave mixing is represented by the double convolution of the electric fields of three channels. Expression (1) is a first order nonhomogeneous differential equation. We can obtain the solution at z=L:

$$E_\rho(\omega,L) = u[E_\rho(\omega,0) + \sum_{\mu,\nu} j\frac{2\pi\omega_c}{nc}D\chi_{1111}L_e$$

$$\cdot\int_{-\infty}^{\infty}d\omega'\int_{-\infty}^{\infty}d\omega'' E^*_{\mu+\nu-\rho}(\omega'+\omega''-\omega)\cdot E_\mu(\omega')\cdot E_\nu(\omega'') \quad (3)$$

where the fiber attenuation u and the effective length in the presence of dispersion L_e are given by

$$u = \exp(-\alpha \cdot L/2) \tag{4}$$

$$L_e = \frac{1-u^2\exp(j\Delta kL)}{\alpha - j\Delta k} \tag{5}$$

Taking the inverse Fourier transform of (3), we obtain the complex amplitude of the electric field in the time domain:

$$E_\rho(t,L) = u'\left\{\sqrt{P_\rho(t)}\exp[j\phi_\rho(t)] + \sum_{\mu,\nu}\sqrt{P_n(t)}\exp[j\phi_n(t)]\right\} \tag{6}$$

where u' is defined by

$$u' = u/d \tag{7}$$

where d, the conversion factor between power and electric field, is defined by [1]

$$d^2 = \frac{nc}{8\pi}A_{eff} \tag{8}$$

where A_{eff} is the effective core area of the optical fiber. In equation (6), $P_\rho(t)$ and $\phi_\rho(t)$ are the signal power and phase at the fiber input, and $P_n(t)$ and $\phi_n(t)$ are the power and phase of the optical noise process due to FWM given by

$$P_n(t) = \kappa^2 D^2 \eta P_{\mu+\nu-\rho}(t) P_\mu(t) P_\nu(t) \tag{9}$$

$$\phi_n(t) = \phi_\mu(t) + \phi_\nu(t) - \phi_{\mu+\nu-\rho}(t) + Arg(L_e) - \frac{\pi}{2} \tag{10}$$

where the phase mismatch factor η denotes the ratio of the power of the generated waves without phase matching to their power with phase matching. The parameters κ and η are given by

$$\kappa = \frac{32\pi^3}{n^2 c\lambda} \frac{L_{eff}}{A_{eff}} \chi_{1111} \tag{11}$$

$$\eta = \frac{\alpha^2}{\alpha^2 + \Delta k^2} \left[1 + \frac{4\exp(-\alpha L)\sin^2(\Delta k L/2)}{\{1-\exp(-\alpha L)\}^2} \right] \tag{12}$$

where L_{eff} is the fiber effective length.

III. RECEIVER DESCRIPTION

We consider ASK and DPSK modulation formats in this paper. The block diagrams of ASK and DPSK receivers are shown in Fig. 2. We assume the lowpass filter just removes the second harmonic components resulting from the delay-and-multiply demodulator without changing the baseband components in the DPSK receiver of Fig. 2 b. Figures 3 and 4 show the impulse response of the matched filter and the time-domain signals for both receivers.

In a multichannel system, complex amplitudes of the received optical signal and local oscillator field are given by [7]

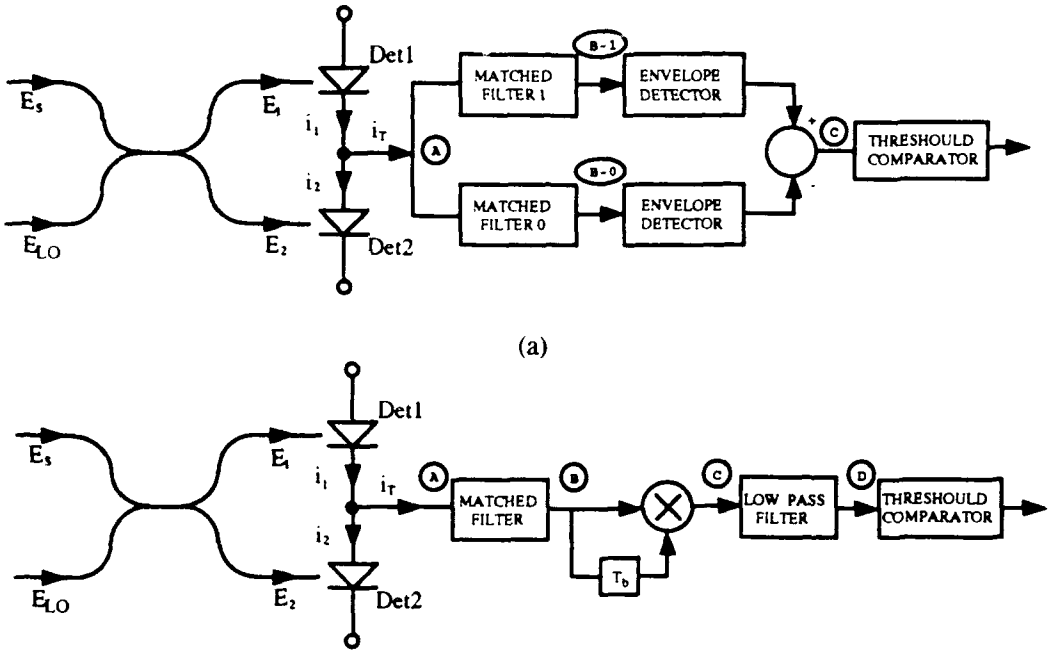

Fig. 2. (a) A Heterodyne ASK Receiver, (b) A Heterodyne DPSK Receiver.

$$E_S = \sum_{\rho=1}^{N} E_\rho(t,L) \qquad \rho = 1,2\cdots\cdots N \tag{13}$$

$$E_{LO} = \sqrt{P_{LO}}\,/\,d \tag{14}$$

where $F_\rho(t,L)$ is the complex amplitude of channel ρ, N is the total number of optical channels, P_{LO} is the local oscillator power, d was defined in expression (8) and E_{LO} is the electric field of the local oscillator. We assume that the channel separation is large enough to neglect the inter-channel crosstalk [7]. The directional coupler output amplitudes are then:

$$E_1(t) = \frac{1}{\sqrt{2}}[E_\rho(t,L) + E_{LO}] \tag{15}$$

$$E_2(t) = \frac{1}{\sqrt{2}}[E_\rho(t,L) - E_{LO}] \tag{16}$$

The resulting photocurrents are

$$i_1(t)=\frac{R}{2}\{u^2P_\rho(t)+u^2\sum_{\mu,\nu}P_n(t)+P_{LO}+2u^2\sum_{\mu,\nu}\sqrt{P_\rho(t)P_n(t)}\cos[\phi_\rho(t)-\phi_n(t)]$$

$$+2u^2\sum_{\mu',\nu'}\sum_{\mu\neq\mu',\nu\neq\nu'}\sqrt{P_n'(t)P_n(t)}\cos[\phi_n'(t)-\phi_n(t)]$$

$$+2u\sqrt{P_{LO}}\left\{\left[\sqrt{P_\rho(t)}+n_c(t)\right]\cos[\omega_{IF}t+\phi_\rho(t)]+n_s(t)\sin[\omega_{IF}t+\phi_\rho(t)]\right\}\}$$

$$+n_1(t) \qquad (17)$$

$$i_2(t)=\frac{R}{2}\{u^2P_\rho(t)+u^2\sum_{\mu,\nu}P_n(t)+P_{LO}+2u^2\sum_{\mu,\nu}\sqrt{P_\rho(t)P_n(t)}\cos[\phi_\rho(t)-\phi_n(t)]$$

$$+2u^2\sum_{\mu',\nu'}\sum_{\mu\neq\mu',\nu\neq\nu'}\sqrt{P_n'(t)P_n(t)}\cos[\phi_n'(t)-\phi_n(t)]$$

$$-2u\sqrt{P_{LO}}\left\{\left[\sqrt{P_\rho(t)}+n_c(t)\right]\cos[\omega_{IF}t+\phi_\rho(t)]+n_s(t)\sin[\omega_{IF}t+\phi_\rho(t)]\right\}\}$$

$$+n_2(t) \qquad (18)$$

where $P_n(t)$ and $P_n'(t)$ are the noise powers of ρ-th channel corresponding to μ,ν and μ',ν', respectively, R is the photodetector responsivity, $n_1(t)$ and $n_2(t)$ are shot noises originating from the detection process, and the in-phase and the quadrature components of noise are given by

$$n_c(t)=\sum_{\mu,\nu}\sqrt{P_n(t)}\sin\phi_{\mu\nu\rho}(t) \qquad (19)$$

$$n_s(t)=\sum_{\mu,\nu}\sqrt{P_n(t)}\cos\phi_{\mu\nu\rho}(t) \qquad (20)$$

The phase change due to FWM is given by

$$\phi_{\mu\nu\rho}(t) = \phi_{\mu}(t) + \phi_{\nu}(t) - \phi_{\rho}(t) - \phi_{\mu\nu\rho}(t) + Arg(L_e) \tag{21}$$

The phases $\phi_{\mu\nu\rho}(t)$ are regarded as independent random variables to simplify the analysis. The resulting output voltage is

$$V_T(t) = A\left\{\left[\sqrt{P_\rho(t)} + n_c(t)\right]\cos[\omega_{IF}t + \phi_\rho(t)] + n_s(t)\sin[\omega_{IF}t + \phi_\rho(t)]\right\} + n(t) \tag{22}$$

where the amplitude A and the shot noise n(t) are given by

$$A = 2Ru\sqrt{P_{LO}} \tag{23}$$

$$n(t) = n_1(t) - n_2(t) \tag{24}$$

IV. CODING METHODS AND SIGNAL-TO-NOISE RATIO

A. Power Spectral Density of Coded Signals

The signal-to-noise ratio for conventional NRZ coded signals and Manchester coded signals are given in this section. In the case of unipolar NRZ, the binary 1 is represented by a higher level (+A) and the binary 0 is represented by a zero level (0). In the Manchester code, the binary 1 is represented by a positive pulse occupying 50% of a bit slot followed by a negative pulse of the same duration. Similarly, a binary 0 is represented by a negative pulse followed by a positive pulse.

The baseband power spectral density (PSD) of a polar NRZ signal is given by [8]

$$G_{NRZ}(f) = T_b \sin c^2(fT_b) \tag{25}$$

where T_b is bit period, and the bit rate is $R_b=1/T_b$; the total signal power is normalized to unity. The autocorrelation function of the baseband NRZ signal is

$$R_{NRZ}(\tau)\begin{cases}1-\dfrac{|\tau|}{T_b} & |\tau|<T_b\\ 0 & |\tau|>T_b\end{cases} \tag{26}$$

The baseband power spectral density of the Manchester-coded baseband signal is given by [8]

$$G_{MAN}(f)=T_b\sin c^2(fT_b/2)\cdot\sin^2(\pi fT_b/2) \tag{27}$$

The bandwidth of the Manchester-coded signal measured to the first null is twice that of the NRZ bandwidth. The Manchester-coded signal has a zero dc level on the bit by bit basis. Moreover, long strings of zeros do not cause a loss of the clocking signal. The Manchester-coded signal is generated by multiplying frequency-doubled bit clock with the NRZ-coded signal. The autocorrelation function of the Manchester-coded baseband signal is given by

$$R_{MAN}(\tau)=\begin{cases}1-3\dfrac{|\tau|}{T_b} & |\tau|<\dfrac{T_b}{2}\\ \dfrac{|\tau|}{T_b}-1 & \dfrac{T_b}{2}<|\tau|<T_b\\ 0 & |\tau|>T_b\end{cases} \tag{28}$$

B. Signal-to-Noise Ratio

The matched filter output voltage at the terminal B of Fig. 2 is given by

$$V_O(T_b) = \int_0^{T_b} V_T(t) \cdot h(T_b - t)dt$$
$$= \int_0^{T_b} S(t) \cdot h(T_b - t)dt + \int_0^{T_b} n(t) \cdot h(T_b - t)dt \quad (29)$$

where h(t) is impulse response of the matched filter. The first term gives the signal, and the second term is a zero-mean Gaussian random variable; its variance is given by

$$\sigma^2 = \int_0^{T_b}\int_0^{T_b} R_n(t_1 - t_2)h(T_b - t_1)h(T_b - t_2)dt_1dt_2 \quad (30)$$

where $R_n(t_1\text{-}t_2)=E[n(t_1)n(t_2)]$ is the autocorrelation function of the noise.

Assume that all channels use the same modulation scheme and have the same power. Then, from expressions (19) and (20), the autocorrelation function of the noise due to FWM is given by

$$R_{n,FWM}(\tau) = \frac{A^2}{2}\kappa^2 P_\rho^3 R'(\tau)\sum_{\mu,\nu} D^2\eta \quad (31)$$

where $R'(\tau)$ is given by

$$R'(\tau) = R^3(\tau)\cos\omega_{IF}\tau \quad (32)$$

where $R(\tau)$ is the autocorrelation function of each signal. An explicit expression for $R(\tau)$ will be given in Section V for each modulation and coding format investigated in this paper. Substituting (31) into (30), we obtain the variance of FWM noise:

$$\sigma_{FWM}^2 = \frac{A^2}{2}\kappa^2 P_\rho^3 V^2 S^2 T_b^2 \tag{33}$$

where V^2 and S^2 are defined by

$$V^2 = \frac{1}{T_b^2}\int_0^{T_b}\int_0^{T_b} R(t_1 - t_2)h(T_b - t_1)h(T_b - t_2)dt_1 dt_2 \tag{34}$$

$$S^2 = \sum_{\mu,\nu} D^2\eta \tag{35}$$

The autocorrelation function of the shot noise is given by

$$R_{n,SN}(\tau) = qRP_{LO}\delta(\tau) \tag{36}$$

Substituting (36) into (30) we obtain the variance of the shot noise;

$$\sigma_{SN}^2 = qRP_{LO}T_b W \tag{37}$$

where W is given by

$$W = \frac{1}{T_b}\int_0^{T_b} h^2(T_b - t)dt \tag{38}$$

Therefore the total signal-to-noise ratio γ defined as the ratio of the signal power to the noise power, is given by

$$\gamma = \frac{A^2 T_b^2 P_\rho}{4k(\sigma_{FWM}^2 + \sigma_{SN}^2)} = \frac{1}{k[2\kappa^2 P_\rho^2 V^2 S^2 + qW / RT_b u^2 P_\rho]} \tag{39}$$

where k=4 for the Manchester-coded ASK system and k=1 for the three other modulation and coding formats considered in this paper. This equation shows that as the input signal power P_ρ increases, the signal-to-noise ratio γ first increases due to the relative suppression of the shot noise, and then decreases due to the FWM. Thus, at some value of P_ρ, a peak value of γ is reached corresponding to the optimum system performance.

V. ASK AND DPSK SYSTEM PERFORMANCE EVALUATION

A. Heterodyne ASK System

Bit Error Rate

We consider first the ASK receiver shown in Fig. 2 a. We assume that a matched filter is used in the receiver. The impulse responses of the matched filters for the NRZ and Manchester coded ASK signals are given by

$$h1_{ASK,NRZ}(t) = \begin{cases} \cos\omega_{IF} t & for \quad t \in [0, T_b] \\ 0 & for \quad t \notin [0, T_b] \end{cases} \tag{40}$$

$$h0_{ASK,NRZ}(t) = \{ \quad 0 \quad for \quad all \quad t \tag{41}$$

$$h1_{ASK\_MAN}(t) = \begin{cases} \cos\omega_{IF}t & for \quad t \in [T_b/2, T_b] \\ 0 & for \quad t \notin [T_b/2, T_b] \end{cases} \tag{42}$$

$$h0_{ASK\_MAN}(t) = \begin{cases} \cos\omega_{IF}t & for \quad t \in [0, T_b/2] \\ 0 & for \quad t \notin [0, T_b/2] \end{cases} \tag{43}$$

The impulse responses (40) to (43) are shown in the top of the Fig. 3.

To find the noise variance due to four-wave-mixing, we need the autocorrelation function R(τ) of each ASK signal:

$$R_{ASK\_NRZ}(\tau) = \frac{1}{4}[1 + R_{NRZ}(\tau)] \tag{44}$$

$$R_{ASK\_MAN}(\tau) = \frac{1}{4}[1 + R_{MAN}(\tau)] \tag{45}$$

where the baseband autocorrelation functions $R_{NRZ}(\tau)$ and $R_{MAN}(\tau)$ are given by expressions (26) and (28) respectively. Substituting (44) and (45) into (32), we obtain the autocorrelation function R'(τ). The power spectral density of the crosstalk due to four wave mixing is given in the Appendix. Next, we substitute (32) and (40) into (34) to obtain

$$V^2_{ASK\_NRZ} = 0.01916 \tag{46}$$

Similarly, substituting (32) and (42) into (34), we obtain

$$V^2_{ASK\_MAN} = 0.00385 \tag{47}$$

Substituting (40) and (42) into (38), we obtain $W_{ASK,NRZ} = 0.5$ and $W_{ASK,MAN} = 0.25$.

The bit error ratio of the heterodyne ASK system is given by [9]

$$BER_{ASK,NRZ} = \frac{1}{2}\exp\left[-\frac{\gamma}{8}\right] \tag{48}$$

$$BER_{ASK,MAN} = \frac{1}{2}\exp\left[-\frac{\gamma}{4}\right] \tag{49}$$

Using expressions (48), (49), (46), (47), (39) and (35), we obtain the numerical value of BER of the ASK multichannel system impaired by the shot noise and the four wave mixing.

Fig. 5 shows BER for the 8 th channel* of a 16 channel WDM system using a dispersion shifted (DS) fiber versus the optical fiber input power for several values of the fiber length; the assumed system parameters are given in Table I. Inspection of Fig. 5 shows that an increase of the input power results in a decrease of the BER for small powers and in an increase of the BER for large input powers. The increase of BER at high powers is due to the FWM that is proportional to the cube of the signal power.

Dynamic Range

The system dynamic range is defined as the ratio of the maximum input power to minimum input power to maintain BER below 10^{-9}; a more detailed description is contained in Section VI-B. Fig. 5 shows that the dynamic range of a Manchester-coded system is about 2.0 dB larger than that of an NRZ system. The maximum allowable power for the Manchester-coded system is 2.0 dB larger than that for the NRZ coded system, and receiver sensitivity for the Manchester coded system is same as that for the

* Other channels have better BER.

NRZ system. The maximum transmission distance of a system using the Manchester code is 220 Km, and is about 10 Km longer than that of the NRZ system.

B. DPSK Heterodyne System

Bit Error Rate

Fig. 2 b shows a block diagram of a DPSK receiver. The impulse responses of the matched filters for NRZ and Manchester coded DPSK signals are given by

$$h_{DPSK,NRZ}(t)=\begin{cases}\cos\omega_{IF}t & for \quad t\in[0,T_b]\\ 0 & for \quad t\notin[0,T_b]\end{cases} \tag{50}$$

$$h_{DPSK,MAN}(t)=\begin{cases}-\cos\omega_{IF}t & for \quad t\in[0,T_b/2]\\ \cos\omega_{IF}t & for \quad t\in[T_b/2,T_b]\\ 0 & for \quad t\notin[0,T_b]\end{cases} \tag{51}$$

Table I. System parameters

System Parameters		
Refractive Index,n		1.47
Wavelength, λ		1.55 μm
Attenuation Coefficient, α		0.2 dB / Km
Channel Spacing		10 GHz
Bit Rate		1 Gbps
Effective Fiber Core Area,A_{eff}	NDS Fiber	32 $\pi\mu m^2$
	DS Fiber	16 $\pi\mu m^2$
Group Velocity Dispersion,C	NDS Fiber	15 ps/Km nm
	DS Fiber	1 ps/Km nm

These impulse responses are shown in the top of Fig. 4.

To find the noise variance due to four wave mixing we need the autocorrelation function $R(\tau)$ of each DPSK signal:

$$R_{DPSK,NRZ}(\tau) = R_{NRZ}(\tau) \tag{52}$$

$$R_{DPSK,MAN}(\tau) = R_{MAN}(\tau) \tag{53}$$

where $R_{NRZ}(\tau)$ and $R_{MAN}(\tau)$ are the autocorrelation functions of the baseband NRZ signal and the baseband Manchester coded signal given by expressions (26) and (28), respectively. Substituting (53) and (54) into (32), we obtain the autocorrelation function $R'(\tau)$. The power spectral density of the crosstalk due to four wave mixing is given in the Appendix. Next, we substitute (32) and (50) into (34) to obtain

$$V^2_{DPSK,NRZ} = 0.10040 \tag{54}$$

Similarly, substituting (32) and (51) into (34), we obtain

$$V^2_{DPSK,MAN} = 0.03889 \tag{55}$$

Substituting expressions (50) and (51) into (38), we obtain $W_{DPSK,NRZ} = 0.5$ and $W_{DPSK,MAN} = 0.5$. The bit error ratio of the heterodyne DPSK system can now be found as [9]

$$BER_{DPSK} = \frac{1}{2}\exp\left[-\frac{\gamma}{2}\right] \tag{56}$$

Using expressions (56), (54), (55), (39) and (35), we obtain the numerical value of BER of the DPSK optical multichannel system impaired by the shot noise and the four wave mixing.

Fig. 6 shows the BER for the 8 th channel* of a 16 channel versus the optical fiber input power for several values of the fiber length; the system parameters are shown in Table I.

Dynamic Range

The Manchester code gives a 2.1 dB larger dynamic range than the NRZ. The minimum power due to shot noise is the same for NRZ and Manchester-coded systems. According to Fig. 6, the maximum transmission distance of Manchester coded systems is 247 Km, 10 Km more than that of NRZ coded system. Table II compares the maximum transmission length of DPSK and ASK systems utilizing NRZ and Manchester coding. The largest transmission distance is achieved using Manchester-coded DPSK system.

Table II. Maximum transmission length for a 16 channel WDM system (in Km)

Fiber Type \ Modulation Format / Coding		ASK	DPSK
DS	MAN	220	247
	NRZ	210	237
NDS	MAN	271	299
	NRZ	261	288

* Other channels have better BER.

VI. NUMERICAL RESULTS AND DISCUSSION

A. Maximum Transmission Length

The maximum transmission length of optical WDM systems is limited by the shot noise and the four wave mixing. The optical fiber input power corresponding to the minimum BER is obtained by differentiating expressions (48), (49) and (56) with respect to P_ρ and setting the derivative equal to zero. The maximum transmission distance is obtained by substituting that value into expressions (48), (49) and (56) for ASK and DPSK systems, respectively. Fig. 7 shows the maximum transmission length versus the number of channels for various modulation schemes and coding methods; all calculation are for the worst-case channel (i.e. channel N/2). The four-wave-mixing crosstalk is maximum for that channel. The upper four curves are for the non-dispersion shifted (NDS) fiber, while the lower four curves are for the dispersion-shifted (DS) fiber; fiber parameters are shown in Table I. All curves show that the maximum transmission length decreases with the number of channels.

Manchester coded systems have the maximum transmission distance larger than that of NRZ coded system by 10 Km for both DPSK and ASK modulation formats; this conclusion is valid for both kinds of fiber. It is interesting that for a large number of channels the NDS fiber outperforms the DS fiber. The reason is that the relatively small core area and improved phase matching due to small group velocity dispersion increase the four-wave mixing crosstalk in the DS fiber as compared to the NDS fiber (the transmission length is limited by the FWM rather than by chromatic dispersion in the particular case considered).

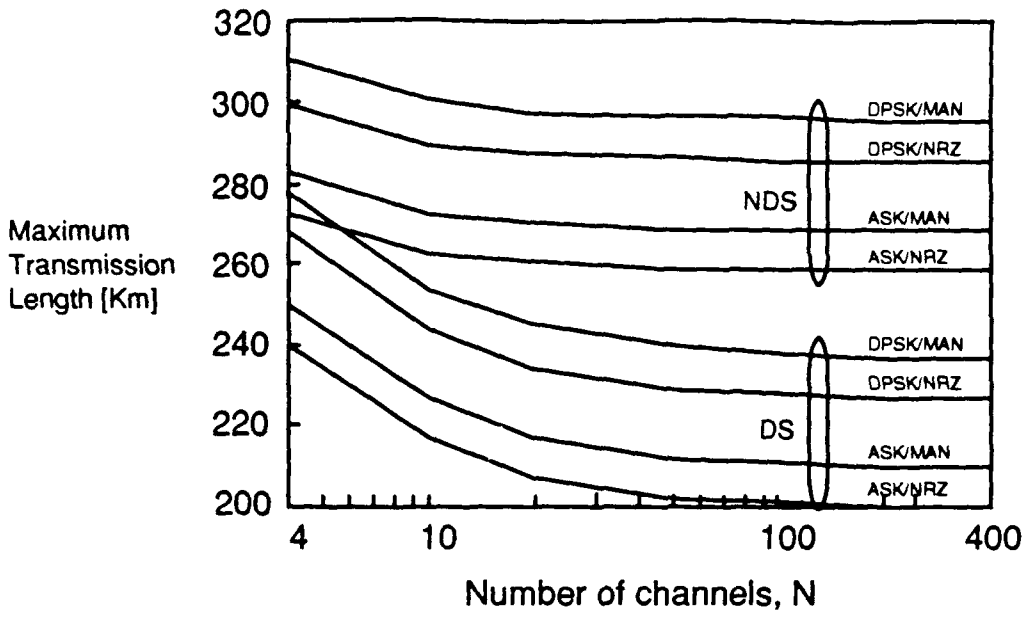

Fig. 7. Maximum transmission length versus number of channels for various modulation schemes and coding methods.

B. Dynamic Range and Power Budget

Dynamic Range

The fiber input power must be kept between the minimum value P_{min} and the maximum value P_{max} to maintain BER below 10^{-9}. The maximum input power P_{max} is determined by the four wave mixing, and the minimum value P_{min} is determined by the shot noise. The maximum and minimum input powers for 8 th channel of a 16 channels WDM system needed to maintain BER below 10^{-9} are shown in Fig. 8. The upper four curves are the maximum input power for various coding formats and optical fiber types and the lower two curves are the minimum input power for the same coding methods and fiber types. The ratio of the maximum power to the minimum power is defined as the dynamic range, and is an important factor in system design. For example, the dynamic range of a Manchester-coded ASK system with 1 Gbps bit rate and 100 Km non-dispersion sifted fiber is 38 dB, as shown in Fig. 8 a.

Fig. 9 shows the dynamic range of a 16-channel WDM system versus the length of optical fiber for two fiber types and various modulation and coding formats. The fiber parameters are the same as in Table I. The curves show that short-distance systems have a large dynamic range of some 70 dB but as the transmission distance increases, the dynamic range decreases, and falls to some 30 dB at 100 Km. Manchester-coded ASK and DPSK 100 Km systems have some 2.0 dB larger dynamic ranges than corresponding NRZ systems.

Power Budget

The power budget is defined as the ratio of the maximum input power to the minimum receiver power needed to keep BER below 10^{-9}. For example, the power budget of Manchester coded ASK system for the 8 th channel of a 16 channels WDM system with 1 Gbps and non-dispersion shifted fiber is about 58 dB and shown in Fig. 8 a. The drop of the power budget at long lengths is due to the drop of the maximum allowable input power caused by the four wave mixing. For very long fibers, the maximum power level remains almost the same, and therefore, the power budget remains almost the same. The power budgets of ASK and DPSK systems with various

Table III. Power budget of 100 Km, 16 channel WDM systems (in dB)

Fiber \ Modulation Format / Coding		ASK	DPSK
DS	MAN	48.1	53.6
	NRZ	46.1	51.5
NDS	MAN	58.4	63.9
	NRZ	56.4	61.8

modulation formats and fiber types are given in Table III. The power budget of DPSK is some 5.5 dB larger than that of ASK system. Manchester coded systems show about 2.0 - 2.1 dB improvement with respect to NRZ systems. And power budget of systems using NDS fiber is 10.3 dB larger than that of systems using DS fiber.

C. Polarization, Chromatic Dispersion and Interchannel Interference

The state of polarization of the received wave is random in the optical fiber system without polarization control. As a result, FWM crosstalk is decreased to 5/6 of the value expected for a fixed state of polarization [10]. In this paper, the case of random polarization is considered, so that all our results apply to systems NOT employing polarization-preserving fiber.

The chromatic dispersion can produce distortion in the demodulated waveform resulting in intersymbol interference in the received signal and reduction of transmission system performance. The chromatic dispersion limitations for coherent system were studied by many authors [11,12]. The receiver sensitivity degradation due to chromatic dispersion has been observed in an FSK transmission experiment at more than 4 Gbits/s [11]. However, transmission experiments from 1 to 2 Gbits/s have shown that the influence of chromatic dispersion on FSK systems is less than that on intensity-modulated system [12]. Receiver sensitivity degradation due to chromatic dispersion depends on the modulation and demodulation schemes used. The transmission distance limit due to chromatic dispersion is some 2,000 Km for 1.55 μm non-dispersion shifted ASK and DPSK systems [13]. Since the transmission distance constraints studied in this paper are less than 2,000 Km, the impact of chromatic dispersion can be (and is) neglected.

The bandwidth of the Manchester coded signal measured to the first null is twice that of the NRZ bandwidth. If several FDM channels are being transmitted, then a coherent system may suffer a performance degradation stemming from crosstalk generated by intermodulation interference. Prior work showed that balanced receivers are superior to single detector receivers in multichannel environment, and for small penalty (below 1 dB) both time and frequency analysis techniques yield essentially the same results [7]. Based on the results of [7], the electrical domain channel spacing of ASK and DPSK systems can be set as shown in Table IV. The maximum required electrical channel spacing for the four systems is 5.6. The optical domain channel spacing normalized to bit rate is [7]

$$D_{opt} = D_{nel} + 2 \cdot f_{IF} \cdot T_b \tag{57}$$

where D_{nel} is normalized electrical channel spacing. When the IF frequency for the Manchester-coded system is selected to be $2/T_b$, D_{opt} is less than 10. Thus, for all systems considered in this paper, the optical channel spacing of 10 bit rates is adequate. Thus, we select the optical channel spacing to be 10 GHz for all four 1 Gbits/s systems investigated in this paper.

Table IV. Electrical channel spacing normalized to bit rate of ASK and DPSK systems with 1 dB penalty

Coding \ Modulation Format	ASK	DPSK
Manchester	5.6	4.6
NRZ	3.7	3.0

VII. CONCLUSIONS

Wavelength division multiplexing systems are fundamentally limited by the receiver shot noise and by the fiber four wave mixing. In this paper, we analyzed the impact of these limitations on NRZ and Manchester coded systems. The minimum receiver power is determined by the shot noise, and maximum transmitter power is determined by the four wave mixing.

For 1.55 μm dispersion shifted 16 channel ASK systems, having 10 GHz channel spacing and 1 Gbps per channel bit rate, the maximum transmission length is about 210 Km for NRZ and 220 Km for Manchester codes, respectively. The corresponding numbers for DPSK systems are 237 Km and 247 Km, respectively. The maximum transmission length of the ASK system using non-dispersion shifted fiber is 261 Km for NRZ and 271 Km for Manchester codes, respectively. The corresponding numbers for DPSK systems are 288 Km and 299 Km, respectively. The physical reason is that the transmission length is limited by the FWM rather than by dispersion in this particular case.

To maintain system BER below 10^{-9}, the fiber input power must be kept between the maximum value determined by the fiber four wave mixing and the minimum value determined by the receiver shot noise. The ratio of the maximum input power to the minimum input power is defined as the dynamic range. The dynamic range of 100 Km Manchester coded systems is some 2 dB better than that of NRZ systems for both ASK and DPSK modulation formats.

ACKNOWLEDGMENT

This work has partially supported by ONR under contract number 4148130-01 and by the Korea Science and Engineering Foundation.

APPENDIX

The single-sided power spectral density of the noise due to FWM is obtained by the Fourier transform of the autocorrelation function (32). The result is given by [6]

$$G_{ASK,NRZ}(f) = \frac{1}{4^3}[\delta(f') + 3T_b \sin c^2(f'T_b) + \frac{3T_b}{2(\pi f'T_b)^2}\{3 - 2\sin c(2f'T_b) - \sin c^2(f'T_b)\}] \quad (f>0) \quad (A1)$$

$$G_{DPSK,NRZ}(f) = \frac{3T_b}{2(\pi f'T_b)^2}\{1 - \sin c^2(f'T_b)\} \quad (f>0) \quad (A2)$$

for the NRZ coded system, where f '= f - f_{IF}. Similarly, the single sided power spectral density of the noise due to FWM is given by

$$G_{ASK,MAN}(f) = \frac{1}{4^3}[\delta(f') + 3T_b\left\{\frac{6}{(\pi f'T_b)^2} + \frac{1}{4}\sin c^2(\frac{f'T_b}{2}) - \sin c^2(f'T_b)\right\} - \frac{3T_b}{(\pi f'T_b)^2}\{2\sin c(f'T_b) + \sin c(2f'T_b) - \frac{1}{2}\sin c^2(f'T_b) + \frac{7}{2}\sin c^2(\frac{f'T_b}{2})\}] \quad (f>0) \quad (A3)$$

$$G_{DPSK,MAN}(f) = \frac{3T_b}{4}\sin c^2(\frac{f'T_b}{2}) + \frac{3T_b}{(\pi f'T_b)^2}\{1 + 2\sin c(f'T_b) + \frac{1}{2}\sin c^2(f'T_b) - \frac{7}{2}\sin c^2(\frac{f'T_b}{2})\} \quad (f>0) \quad (A4)$$

for the Manchester coded system.

REFERENCES

[1]. K. O. Hill, D. C. Johnson, B. S. Kawasaki, R. I. MacDonald,"CW three wave mixing in single-mode optical fiber", J. of Appl. Phys., vol. 49, no. 10, pp. 5098-5106, 1978.

[2]. N. Shibata, R. P. Braun, R. G. Waarts,"Phase-mismatch dependence of efficiency of wave generation through four-wave mixing in a single-mode optical fiber," J. of Quantum Elec., vol. QE-23, no. 7, pp. 1205-1210, 1987.

[3]. A. R. Chraplyvy,"Limitations on lightwave communication imposed by optical-fiber nonlinearities," J. of lightwave Tech., vol. , no. 10, pp. 1548-1557, 1990.

[4]. R. G. Waarts, A. A. Friesem, E. Lichtman, H. H. Yaffe, R. P. Braun, "Nonlinear effects in coherent multichannel transmission through optical fibers," Proc. IEEE, vol. 78, no. 8, pp. 1344-1368, 1990.

[5]. K. Inoue, N. Shibata,"Theoretical evaluation of intermodulation distortion due to four-wave mixing in optical fibers for coherent phase-shift-keying-frequency-division-multiplexing transmission," Optics Lett., vol. 14, no. 11, pp. 584-586, 1989.

[6]. E. Lichtman,"Performance degradation due to four-wave mixing in multichannel coherent optical communication systems," J. of Optical Comm.,vol. 12, no. 2, pp. 53-58, 1991.

[7]. L.G. Kazovsky, "Sensitivity penalty in multichannel coherent optical communications," J. of Lightwave Tech. vol. 6, no. 9, pp. 1353-1365, 1988.

[8]. L. Couch, "Digital and analog communication systems," 3rd ed., New York, Macmillan, 1990.

[9]. T. Okoshi, "Ultimate performance of heterodyne / coherent optical fiber communications," J. of Lightwave Tech., vol. LT-4, no. 10, pp. 1556-1562, 1986.

[10]. J. Botineau, R. H. Stolen,"Effects of polarization on spectral broadening in optical fibers", J. Opt. Soc. Am. vol. 72, pp. 1592-1596, 1982

[11]. K. Iwashita and N. Takachio, "Compensation of 202 Km single-mode fibre chromatic dispersion in 4 Gb/s optical CPFSK transmission experiment," Electron. Lett., vol. 24, pp. 759-760, 1988

[12] A. Gnauck, R. Linke, B. Kasper, K. pollock, K. Reichmann, R. Valenzuela, and R. Alferness,"Coherent lightwave transmission at 2 Gb/s over 170 Km of optical fiber using phase modulation," Electron. Lett., vol. 23, pp. 286-287, 1987

[13] A. Elrefaie, R. Wagner, D. Atlas, and D. Daut,"Chromatic dispersion limitations in coherent lightwave transmission systems," J. of Lightwave Tech. vol. LT-6, no. 5, pp. 704-709, 1988

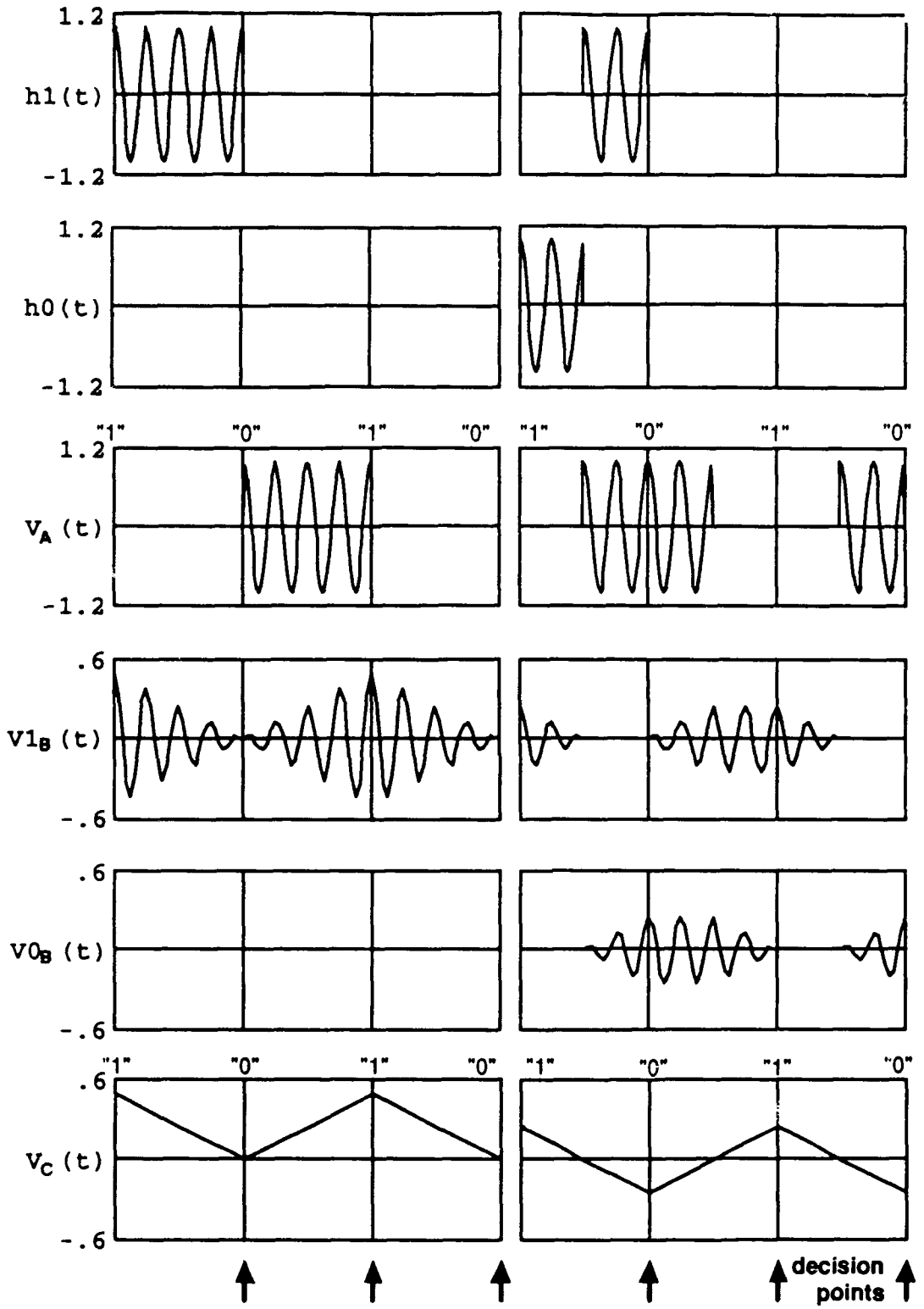

Fig. 3. Matched filter impulse response and time domain signals for ASK. (a) NRZ coded system, (b) Manchester coded system.

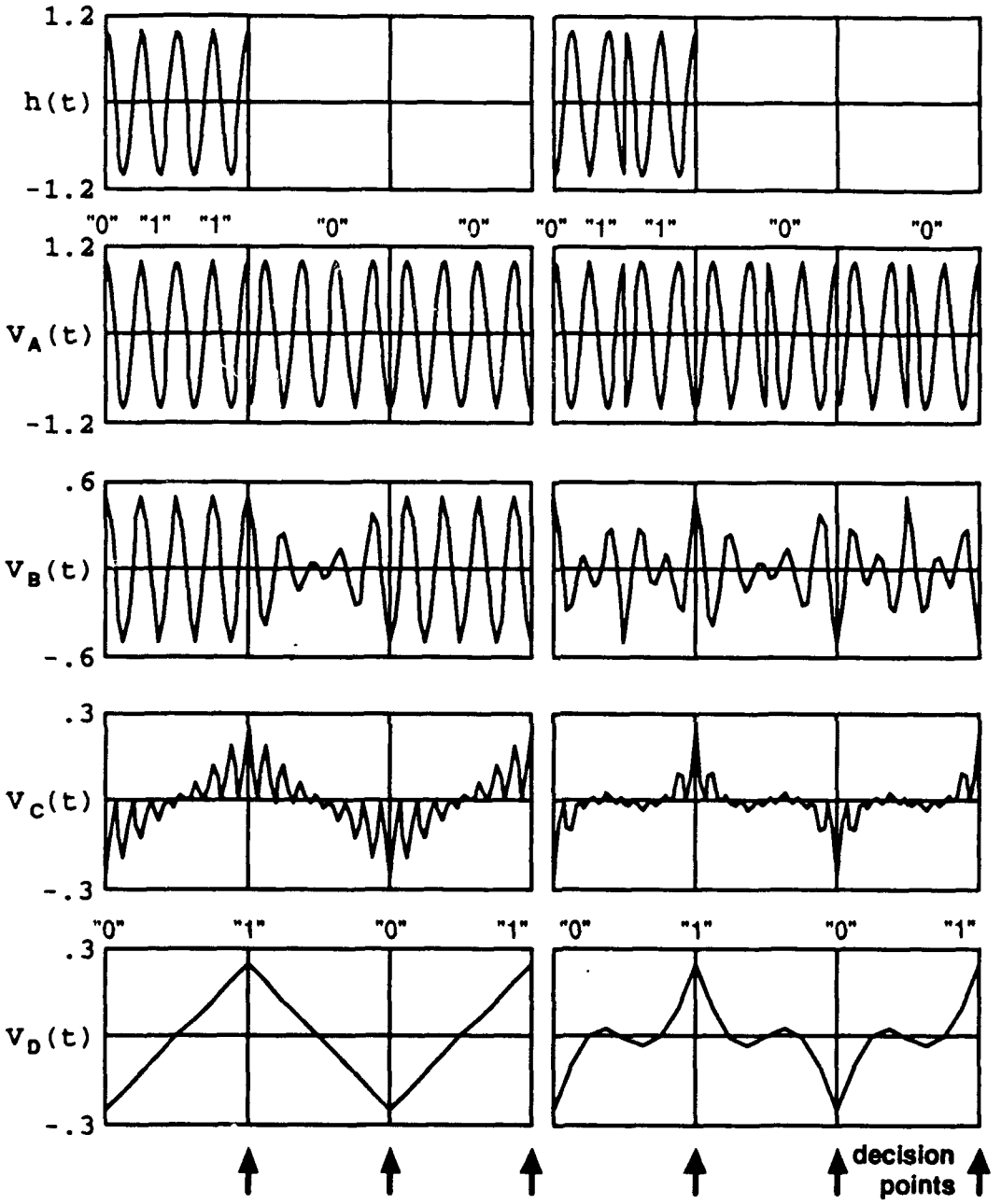

Fig. 4. Matched filter impulse response h(t) and time domain signals for DPSK. (a) NRZ coded system, (b) Manchester coded system.

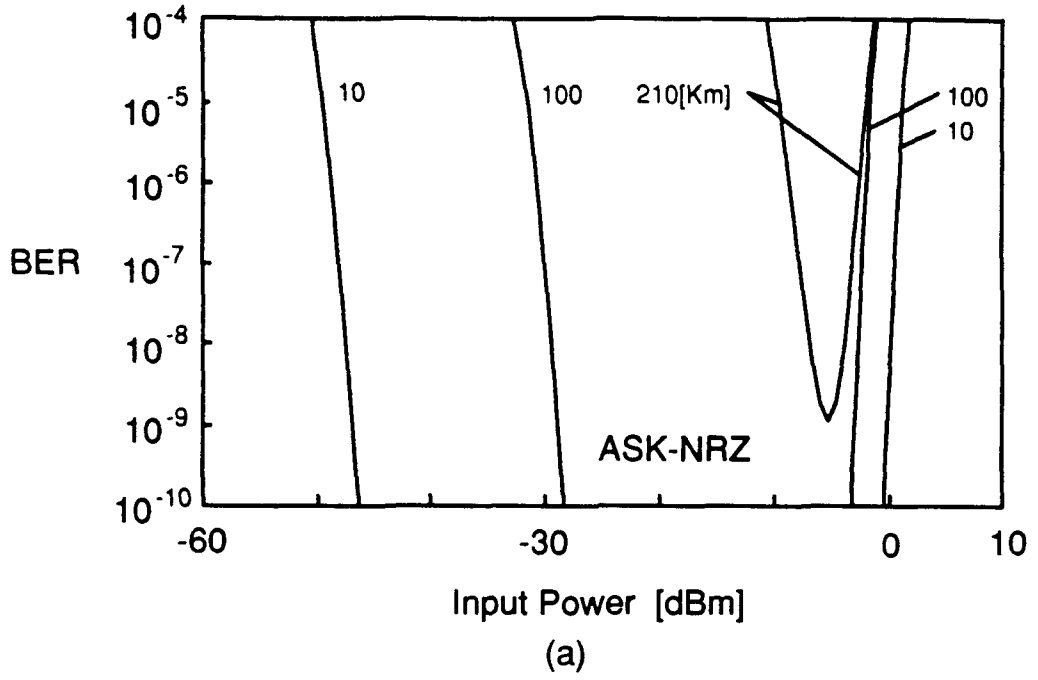

(a)

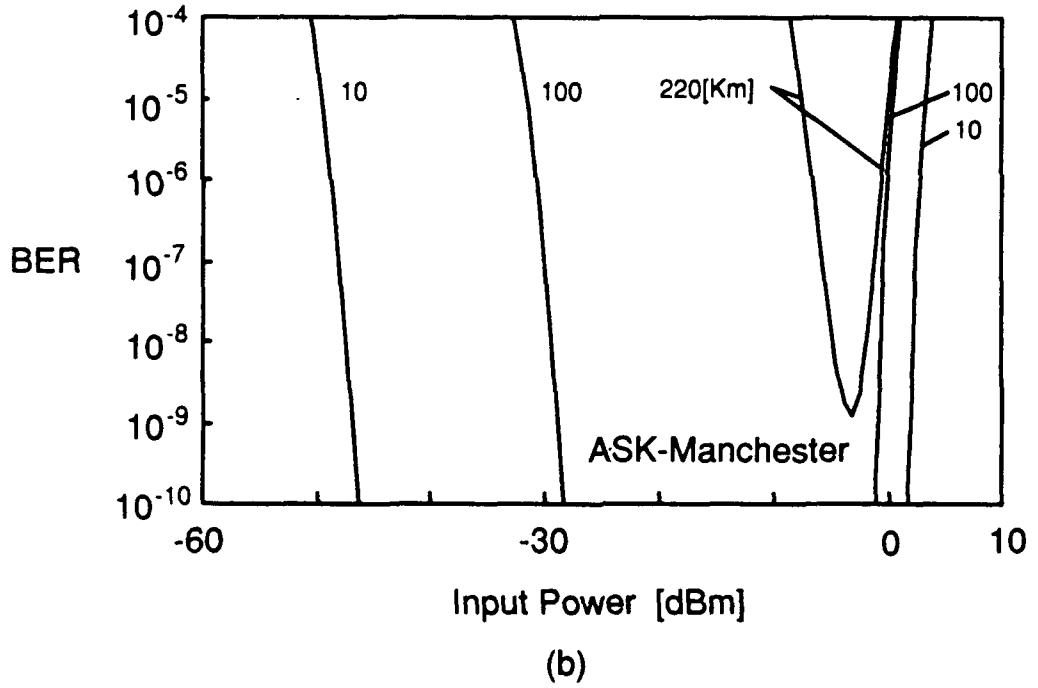

(b)

Fig. 5. The bit error rate of a 16 channel ASK coherent WDM system using the DS fiber versus the optical fiber input power; the parameter is the transmission distance.(a)NRZ-coded system,(b)Manchester-coded system.

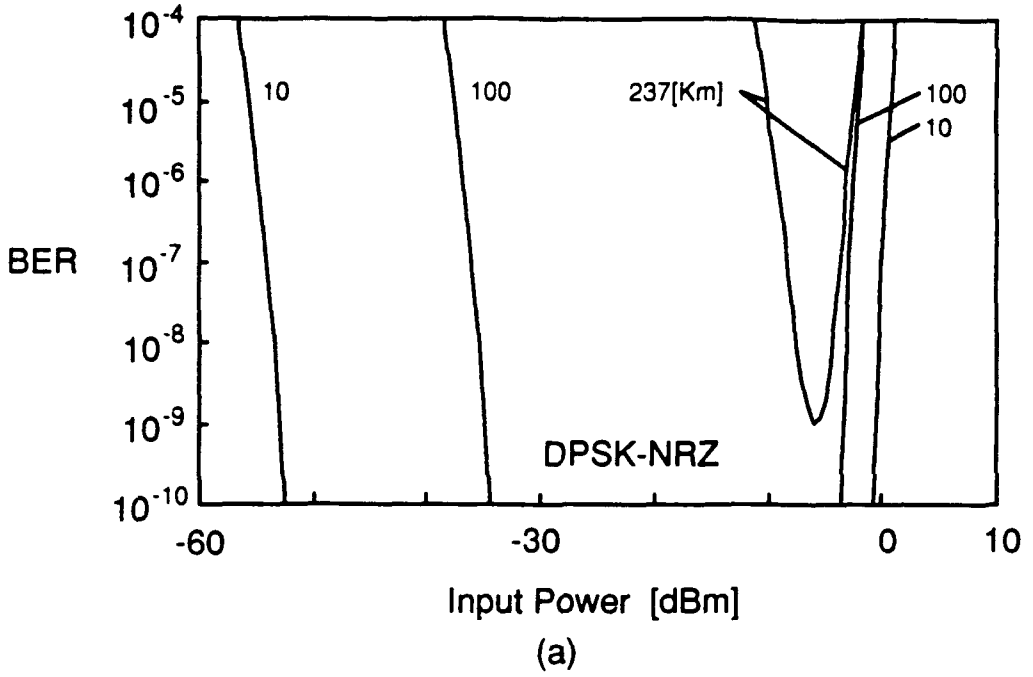

(a)

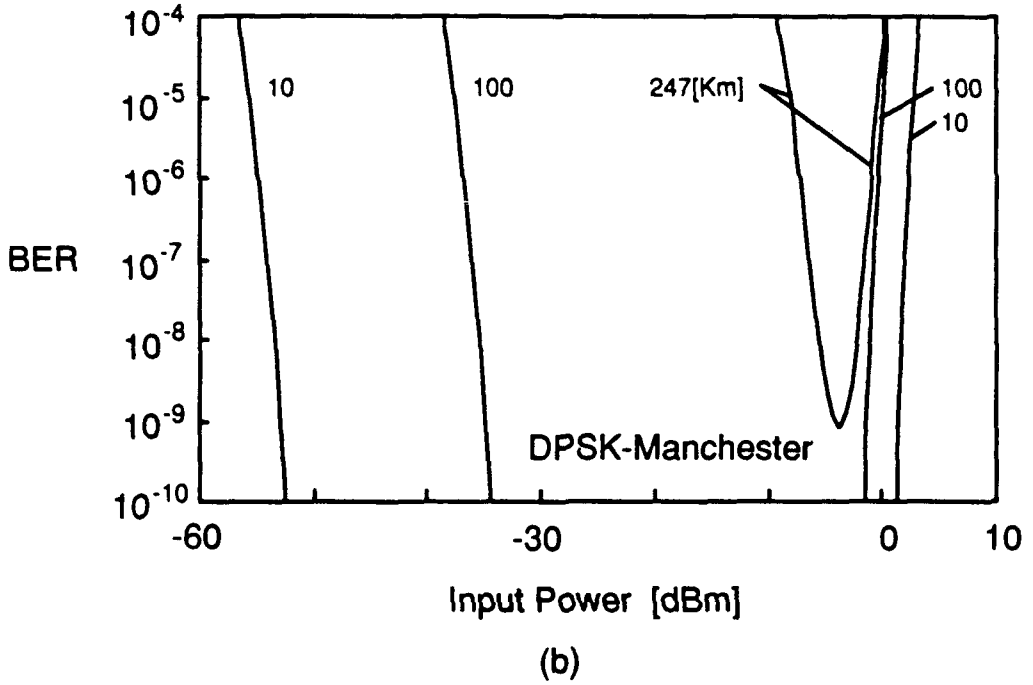

(b)

Fig. 6. The bit error rate of a 16 channel DPSK coherent system using dispersion shifted fiber versus optical fiber input power; the parameter is the transmission distance.(a)NRZ-coded system,(b)Manchester-coded system.

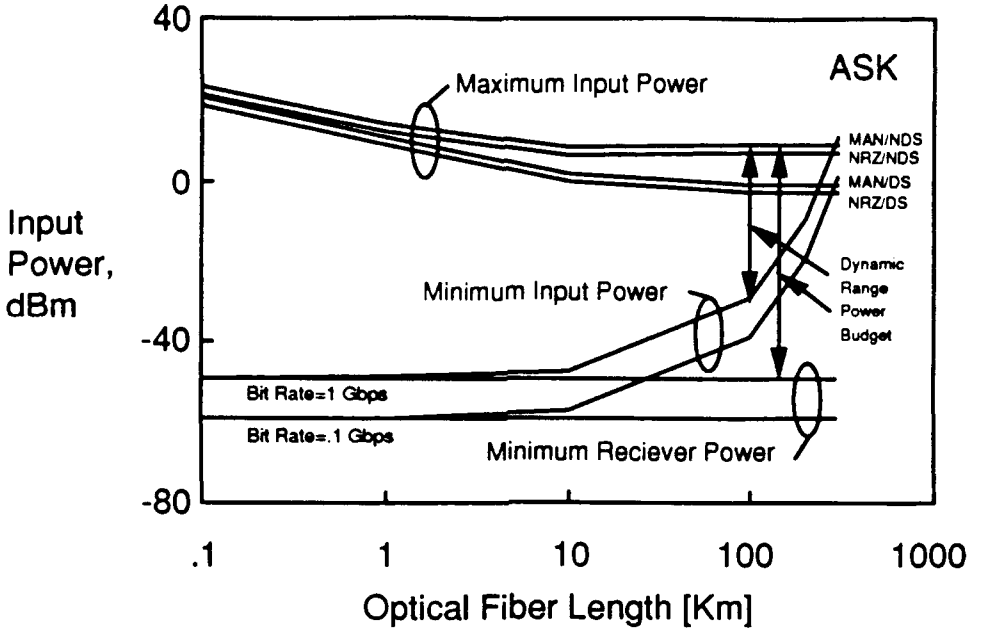

(a)

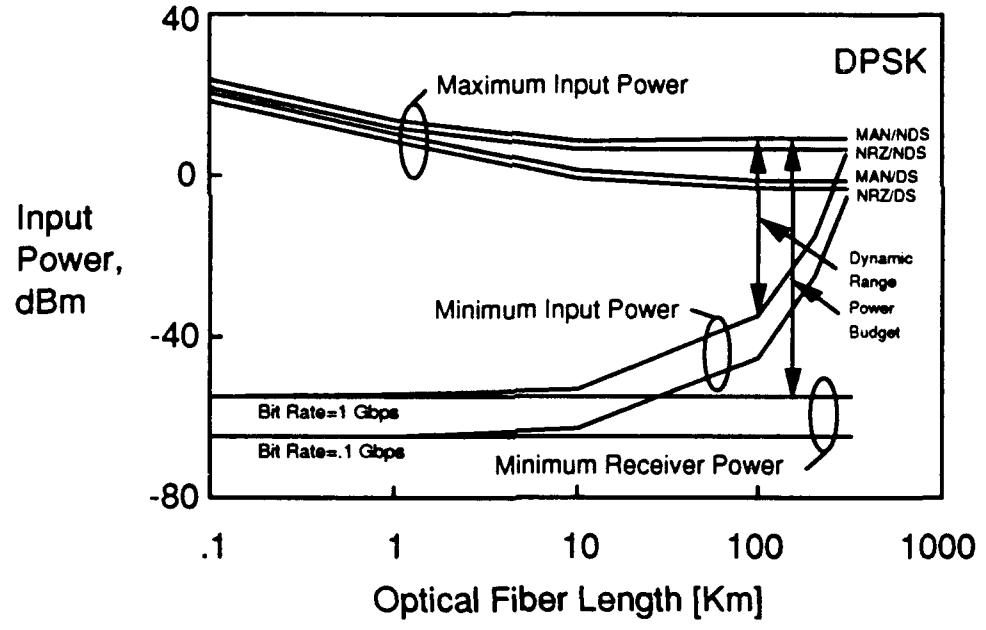

(b)

Fig. 8. Maximum input power, minimum input power and system dynamic range and system power budget versus optical fiber length for various fibers and modulation formats. (a)ASK, (b)DPSK.

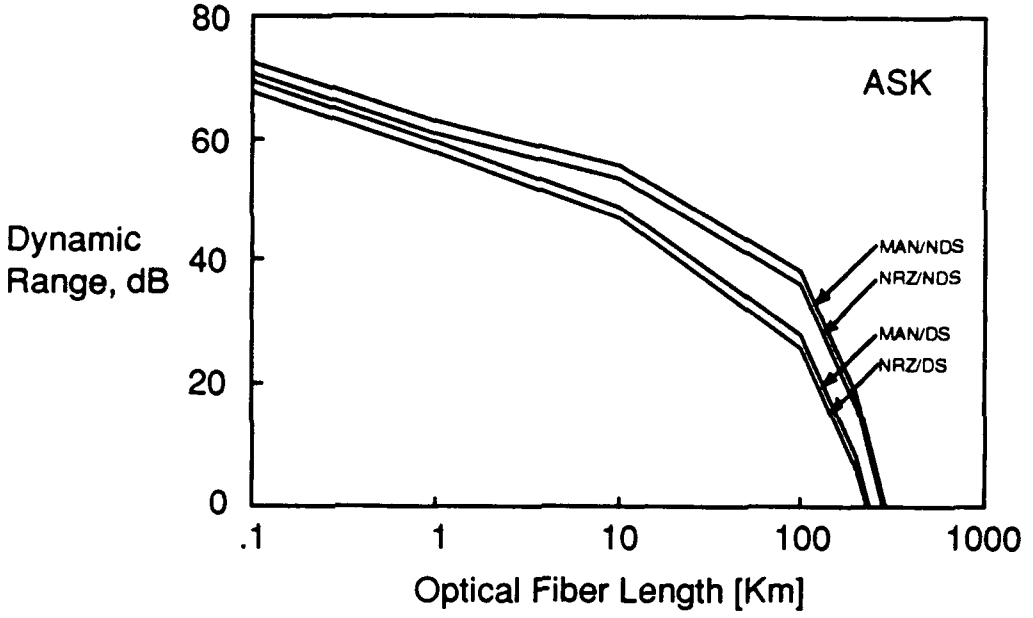

(a)

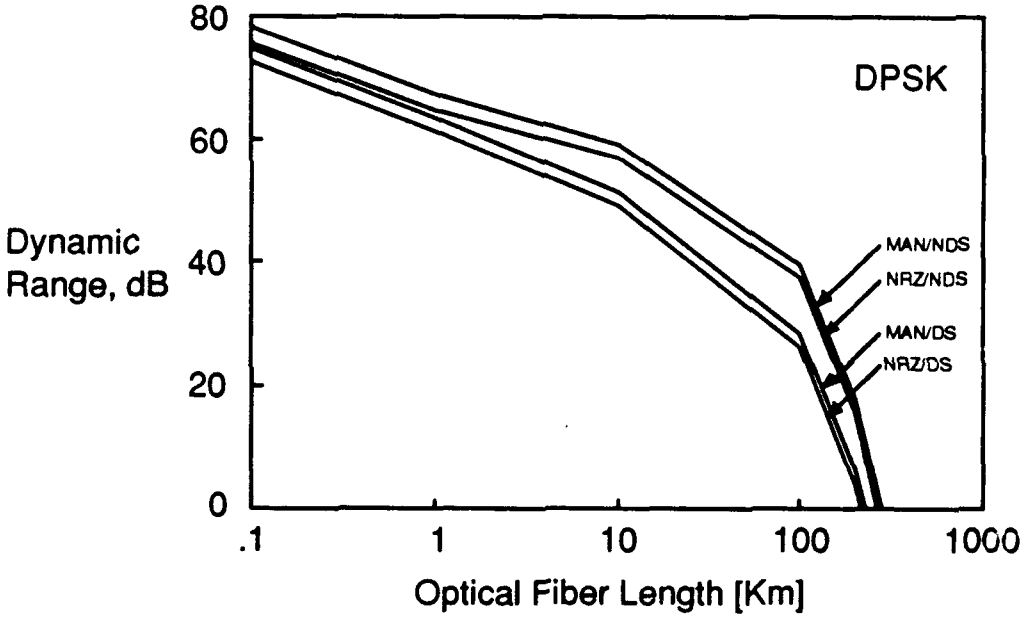

(b)

Fig. 9. Dynamic range of a 16 channel WDM system versus optical fiber length for (a)ASK, (b)DPSK systems.

Four Wave Mixing in ASK Optical WDM Communication Systems

Hojoon Lee and Leonid G. Kazovsky

Department of Electrical Engineering
Stanford University
Durand Building 202
Stanford, CA 94305-4055
Tel.(415) 725-3818, Fax.(415) 723-9251
E-mail leonid@sierra.stanford.edu

Abstract- The performance of Manchester-coded optical wavelength division multiplexing (WDM) systems is evaluated taking into account the shot noise and the four wave mixing (FWM) caused by fiber nonlinearities. The result is compared to conventional ASK non-return-to-zero (NRZ) systems. For 1.55 μm 16 channel WDM systems, the dynamic range of Manchester coded systems shows a 2.0 dB improvement with respect to NRZ. This result holds true for both dispersion-shifted fiber and conventional fiber; it has been obtained for 10 GHz channel spacing, 1 Gbps/channel bit rate.

INTRODUCTION

The performance of optical WDM systems may be degraded by the four wave mixing (FWM) due to nonlinearities of optical fibers [1,2]. When two or more optical waves having different wavelengths travel through an optical fiber, FWM may produce new optical waves at other wavelengths. The new optical waves may lead to crosstalk [3]. Previous studies investigated FWM in non-return-to zero (NRZ) systems only, and neglected other noise sources, such as shot noise [4]. In addition, the bit error rate was calculated in previous studies under the assumption that the entire power of the interference due to FWM falls into the signal bandwidth.

In this paper, the performance of optical WDM systems using the Manchester coded ASK modulation format is evaluated. Our analysis takes into account the shot noise originating from the light detection process and FWM noise resulting from the optical fiber nonlinearity. Our analysis does take into account the spectral distribution of FWM, and so is believed to be more accurate than previous studies.

WAVELENGTH DIVISION MULTIPLEXING SYSTEM AND FOUR WAVE MIXING

The block diagram of an optical WDM system employing Manchester coding is shown in Fig. 1 a. Encoders are used to convert NRZ data to Manchester-coded data. To investigate the impact of FWM on an N-channel optical WDM system, we use the first order nonlinear differential equation that governs optical wave propagation in a nonlinear medium. For the case of light with a finite spectral width, this equation looks as follows [1]:

$$\frac{d}{dz}E_\rho(\omega,z) = -\frac{1}{2}\alpha E_\rho(\omega,z) + \sum_{\mu,\nu} j\frac{2\pi\omega_c}{nc}(D\chi_{1111})\exp(j\Delta kz)$$

$$\cdot\exp(-\frac{3}{2}\alpha z)\int_{-\infty}^{\infty}d\omega'\int_{-\infty}^{\infty}d\omega'' E^*_{\mu+\nu-\rho}(\omega'+\omega''-\omega)\cdot E_\mu(\omega')\cdot E_\nu(\omega'') \quad (1)$$

where it is assumed that the light propagates along the z axis; E is electric field in the optical fiber; ω is angular light frequency; n is fiber core refractive index; c is velocity of light in vacuum; α is fiber power attenuation coefficient, χ_{1111} is third order nonlinear susceptibility; D is degeneracy factor; μ,ν and $\rho = 1,2\cdots N$; and Δk is phase mismatch.

The nonlinear term due to four wave mixing is represented by the double convolution of the electric fields of three channels.

The block diagram of an ASK receiver is shown in Fig. 1 b. Solving expression (1), the output voltage of balanced receiver is obtained [5]:

$$V_T(t) = 2R\sqrt{P_{LO}} \cdot \exp(-\alpha \cdot L/2)\{\sqrt{P_\rho(t)}\cos[\omega_{IF}t + \phi_\rho(t)] + n(t)\sin[\omega_{IF}t + \phi_n(t)]\} + n(t) \tag{2}$$

where $P_\rho(t)$ and $\phi_\rho(t)$ are the signal power and phase at the fiber input and the noise n(t) includes the shot noise originating from the detection process and the noise due to FWM given by

$$n(t) = \sqrt{\kappa^2 \sum_{\mu\nu} D^2 \eta P_{\mu+w-\rho}(t) P_\mu(t) P_\nu(t)} \tag{3}$$

where the phase mismatch factor η denotes the ratio of the power of the generated waves without phase matching to their power with phase matching. The phases $\phi_n(t)$ generated by FWM are regarded as independent random variables to simplify the analysis. The parameter κ is given by

$$\kappa = \frac{32\pi^3}{n^2 c\lambda} \frac{L_{eff}}{A_{eff}} \chi_{1111} \tag{4}$$

where L_{eff} is the fiber effective length and A_{eff} is the effective fiber core area.

The signal-to-noise ratio γ defined as the ratio of the signal power to the noise power at point B of Fig. 1 b given by

$$\gamma = \frac{1}{k[2\kappa^2 P_\rho^2 V^2 + qW / RT_b u^2 P_\rho]} \tag{5}$$

where k=1 for the NRZ-coded ASK system and k=4 for the Manchester-coded ASK system. The parameters V^2 and W are defined by

$$V^2 = \frac{1}{T_b^2}\int_0^{T_b}\int_0^{T_b} R^3(t_1 - t_2)\cos\{\omega_{IF}(t_1 - t_2)\}h(T_b - t_1)h(T_b - t_2)dt_1 dt_2 \cdot \sum_{\mu,\nu} D^2\eta \tag{6}$$

$$W = \frac{1}{T_b}\int_0^{T_b} h^2(T_b - t)dt \tag{7}$$

where $R(\tau)$ is the autocorrelation function of the optical signal in each WDM channel. Equation (5) shows that at some value of P_ρ, a peak value of γ is reached corresponding to the optimum system performance.

We assume that a matched filter is used in the receiver. The bit error ratio of the heterodyne ASK system is given by

$$BER_{ASK,NRZ} = \frac{1}{2}\exp\left[-\frac{\gamma}{8}\right] \tag{8}$$

$$BER_{ASK,MAN} = \frac{1}{2}\exp\left[-\frac{\gamma}{4}\right] \tag{9}$$

Using expressions (5), (8) and (9), we obtain the numerical value of BER of the ASK multichannel system impaired by the shot noise and the four wave mixing.

NUMERICAL RESULTS AND DISCUSSION

Bit Error Rate

Fig. 2 shows BER for the 8th channel* of a 16 channel WDM system using a dispersion shifted (DS) fiber versus the optical fiber input power for several values of the fiber length. Inspection of Fig. 2 shows that the maximum transmission distance of a Manchester coded system using the dispersion shifted fiber is 220 Km, and is about 10 Km longer than that of the NRZ system. The assumed system parameters are as follows: fiber refractive index 1.47, wavelength 1.55 μm, attenuation coefficient 0.2 dB/Km, channel spacing 10 GHz, bit rate 1 Gbit/s, effective core area $32\cdot\pi$ μm^2 for non-dispersion shifted fiber (NDS) and $16\cdot\pi$ μm^2 for DS fiber, and group velocity dispersion 15 ps/Km·nm for NDS and 1 ps/Km·nm for DS.

Dynamic Range

The maximum and minimum input power for 8th channel of a 16 channel WDM system needed to maintain BER below 10^{-9} are shown in Fig. 3. The ratio of the maximum power to the minimum power is defined as the dynamic range. Manchester-coded ASK system have some 2 dB larger dynamic range than the corresponding NRZ systems.

Power Budget

The power budget is defined as the ratio of the maximum input power to the minimum receiver power needed to keep BER below 10^{-9}. The drop of the power budget at long fiber lengths (see Fig. 3) is due to the drop of the maximum allowable input power caused by the four wave mixing. Manchester coded systems show about 2 dB

* Other channels have better BER.

improvement with respect to NRZ systems; the power budget of systems using NDS fiber is 10.3 dB larger than that of systems using DS fiber.

SUMMARY

Wavelength division multiplexing systems are fundamentally limited by the receiver shot noise and by the fiber four wave mixing. In this paper, we analyzed the impact of these limitations on NRZ and Manchester coded systems. For 1.55 μm dispersion-shifted 16 channel ASK systems, having 10 GHz channel spacing and 1 Gbps per channel bit rate, the maximum transmission length is about 210 Km for NRZ and 220 Km for Manchester codes, respectively. The maximum transmission length for non-dispersion shifted fiber is 51 Km more than the corresponding modulation and coding format. The dynamic range of 100 Km Manchester coded systems is some 2 dB better than that of NRZ systems.

ACKNOWLEDGMENT

This work has partially supported by ONR under contract number 4148130-01 and Korea Science and Engineering Foundation.

REFERENCES

[1]. K. O. Hill, D. C. Johnson, B. S. Kawasaki, R. I. MacDonald,"CW three wave mixing in single-mode optical fiber", J. of Appl. Phys., vol. 49, no. 10, pp. 5098-5106, 1978.

[2]. N. Shibata, R. P. Braun, R. G. Waarts,"Phase-mismatch dependence of efficiency of wave generation through four-wave mixing in a single-mode optical fiber," J. of Quantum Elec., vol. QE-23, nc. 7, pp. 1205-1210, 1987.

[3]. R. G. Waarts, A. A. Friesem, E. Lichtman, H.H. Yaffe, R.P. Braun, "Nonlinear effects in coherent multichannel transmission through optical fibers," Proc. IEEE, vol. 78, no. 8, pp. 1344-1368, 1990.

[4]. E. Lichtman,"Performance degradation due to four-wave mixing in multichannel coherent optical communication systems," J. of Optical Comm., vol. 12, no. 2, pp. 53-58, 1991.

[5]. L. G. Kazovsky, "Sensitivity penalty in multichannel coherent optical communications," J. of Lightwave Tech. vol. 6, no. 9, pp. 1353-1365, 1988.

FIGURE CAPTIONS

Fig. 1. (a) Block diagram of an optical wavelength division multiplexing system.
(b) A Heterodyne ASK Receiver.

Fig. 2. The bit error rate of a 16 channel ASK coherent WDM system
using DS fiber versus the optical fiber input power;
the parameter is the transmission distance. (a) NRZ code ,(b) Manchester code.

Fig. 3. Maximum input power, minimum input power and system dynamic range
and system power budget versus optical fiber length
for various fibers and coding formats.

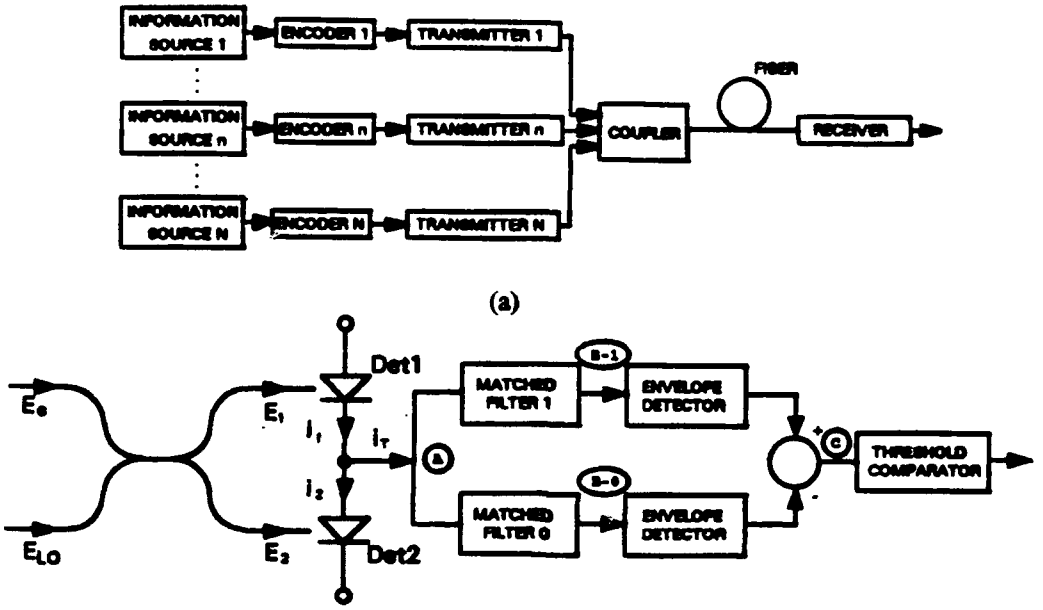

Fig. 1. (a) Block diagram of an optical wavelength division multiplexing system.

(b) A heterodyne ASK Receiver.

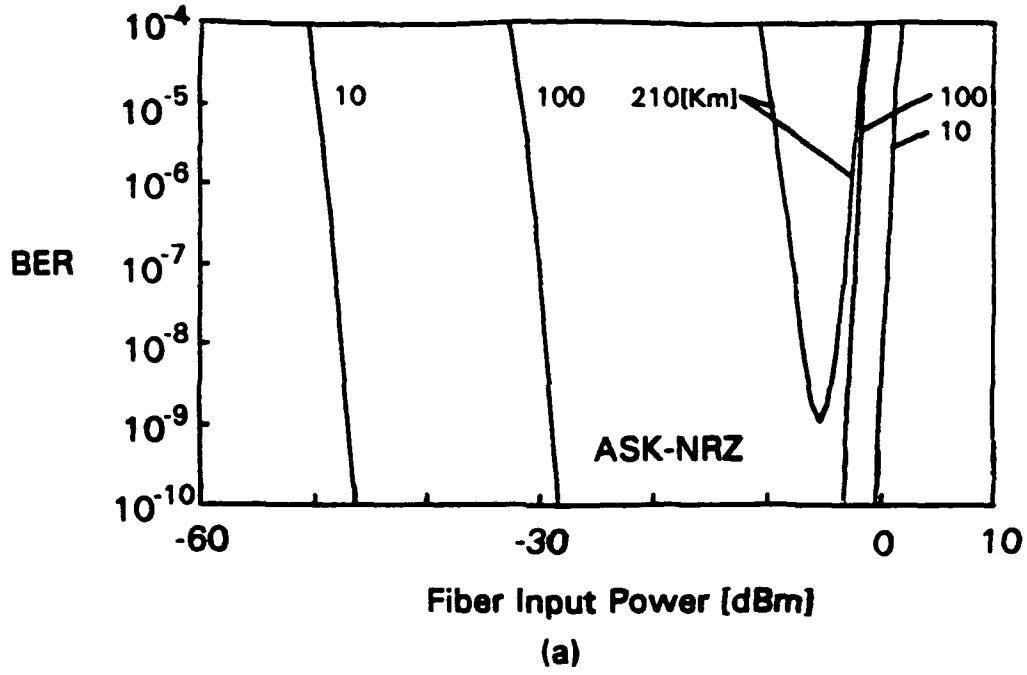

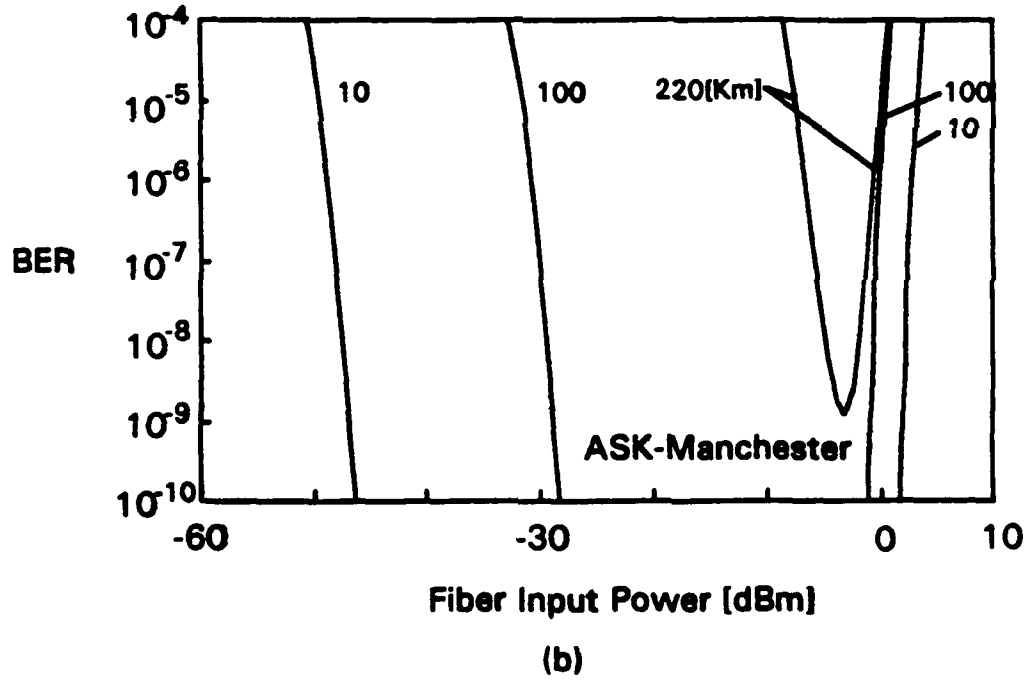

Fig. 2. The bit error rate of a 16 channel ASK coherent WDM system

using DS fiber versus the optical fiber input power;

the parameter is the transmission distance. (a) NRZ code ,(b) Manchester code.

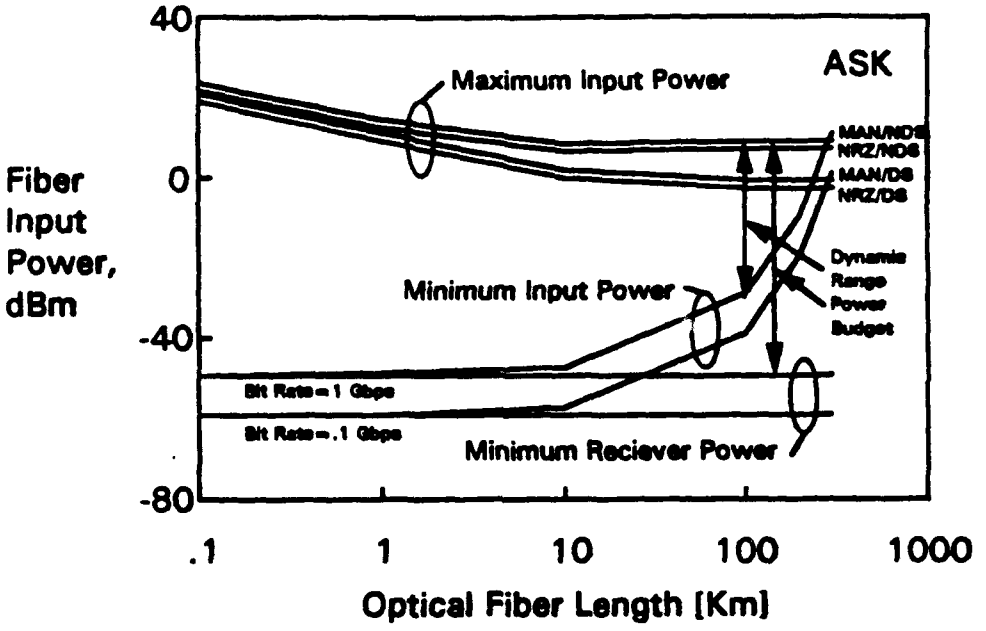

Fig. 3. Maximum input power, minimum input power and system dynamic range and system power budget versus optical fiber length for various fibers and modulation formats.

Impact of four wave mixing on Manchester Coded optical WDM communication systems

Hojoon Lee and Leonid G. Kazovsky

Stanford University, Department of Electrical Engineering
Durand Building 202, Stanford, CA 94305-4055

ABSTRACT

The performance of Manchester-coded optical wavelength division multiplexing (WDM) systems is evaluated taking into account the shot noise and the four wave mixing (FWM) caused by fiber nonlinearities. The result is compared to conventional non-return-to-zero (NRZ) systems for ASK and DPSK modulation formats. Further, the dynamic range, defined as the ratio of the maximum transmitter power (limited by the FWM) to the minimum transmitter power (limited by receiver sensitivity) is evaluated. For 1.55 μm 16 channel WDM systems, the dynamic range of Manchester coded systems shows a 2 dB improvement with respect to the NRZ; DPSK systems outperform ASK systems by 5.5 dB. This result holds true for both dispersion-shifted fiber and conventional fiber; it has been obtained for 10 GHz channel spacing, 1 Gbps/channel bit rate and 100 Km transmission length.

1. INTRODUCTION

Future multichannel optical transmission systems will utilize the large bandwidth of single mode fibers using wavelength division multiplexing (WDM). The performance of optical WDM systems may be degraded by the nonlinearities of optical fibers[1,2]. One important fiber nonlinearity is four wave mixing (FWM). This effect occurs when two or more optical waves at different wavelengths mix to produce new optical waves at other wavelengths. The new optical waves may lead to crosstalk[3,4].

Several studies of four wave mixing in WDM communication systems have been published[5,6]. These studies showed that the FWM crosstalk limits the number of channels, the maximum allowed input power per channel and the channel frequency separation. The allowed power per channel, for a given number of channels and a given frequency separation, depends on the fiber dispersion and attenuation. Previous studies took into account FWM only, and neglected other noise sources, such as shot noise. In addition, the bit error rate in previous studies was calculated under the assumption that the entire power of the interference due to FWM falls into the signal bandwidth.

In this paper, the performance of optical Manchester coded WDM systems is evaluated. Our analysis takes into account the shot noise originating from the light detection process and FWM noise resulting from the optical fiber nonlinearity. These two effects limit the transmission distance as follows: the nonlinearity of the optical fiber limits the maximum transmission power, and the shot noise originating from the detection process limits the minimum receiver power. The ratio of the maximum transmitter power launched into the fiber to the minimum receiver power limits the acceptable attenuation and, therefore, the maximum transmission length. We show that Manchester coding reduces the impact of FWM on WDM systems. Our analysis does take into account the spectral distribution of FWM, and so is believed to be more accurate than previous studies.

The rest of this paper is organized as follows. The system block diagram and the FWM are discussed in Section II. Receiver output signal and noises are described in Section III. Section IV deals with autocorrelation functions for NRZ and Manchester codes and the signal-to-noise ratio. Bit error rate is evaluated in Section V. Numerical results and discussion are contained in Section VI. Finally, Section VII contains the conclusions of this paper.

2. WAVELENGTH DIVISION MULTIPLEXING SYSTEM AND FOUR WAVE MIXING

The block diagram of an optical WDM system employing Manchester coding is shown in Fig. 1. Encoders are used to convert NRZ data to Manchester-coded data. The matched filter is used as a decoder in the receiver. We assume that all transmitters use the same modulation format.

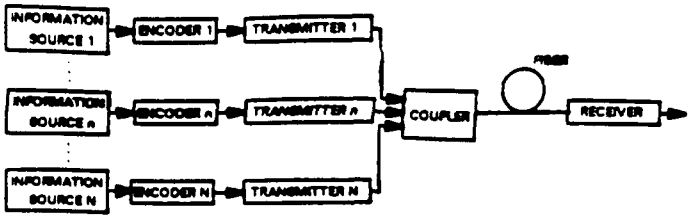

Fig. 1. Block diagram of an optical wavelength division multiplexing system.

To investigate the impact of FWM on the N-channel optical WDM system, we use the first order nonlinear differential equation that governs the optical wave propagation in a nonlinear medium. For the case of light with a finite spectral width, this equation looks as follows[1]:

$$\frac{d}{dz}E_\rho(\omega,z)=-\frac{1}{2}\alpha E_\rho(\omega,z)+\sum_{\mu,\nu}j\frac{2\pi\omega_c}{nc}(D\chi_{1111})\exp(j\Delta kz)$$

$$\cdot\exp(-\frac{3}{2}\alpha z)\int_{-\infty}^{\infty}d\omega'\int_{-\infty}^{\infty}d\omega''E^*_{\mu+\nu-\rho}(\omega'+\omega''-\omega)\cdot E_\mu(\omega')\cdot E_\nu(\omega'') \tag{1}$$

where it is assumed that the light propagates along the z axis, E is electric field in the optical fiber, ω is angular light frequency, n is fiber core refractive index, c is the velocity of light in vacuum, α is the fiber power attenuation constant, χ_{1111} is third order nonlinear susceptibility, D is the degeneracy factor, μ,ν and $\rho = 1,2\cdots N$ and Δk is the phase mismatch given by[2]

$$\Delta k=2\pi\lambda^2C(f_\mu-f_{\mu+\nu-\rho})(f_\nu-f_{\mu+\nu-\rho})/c \tag{2}$$

where C is the group velocity dispersion (G.V.D.). In the derivation of (1), it is assumed that the field depletion due to FWM is small, so that the field amplitude is reduced solely by fiber attenuation. This assumption is valid when the field amplitude of the incident light at the fiber input is much larger than that of the converted wave at the fiber end. Nonlinear term due to four wave mixing is represented by the double convolution of the electric fields of three channels. Expression (1) is a first order nonhomogeneous differential equation. We can obtain the solution at z=L:

$$E_\rho(\omega,L)=u[E_\rho(\omega,0)+\sum_{\mu,\nu}j\frac{2\pi\omega_c}{nc}D\chi_{1111}L_e\cdot\int_{-\infty}^{\infty}d\omega'\int_{-\infty}^{\infty}d\omega''E^*_{\mu+\nu-\rho}(\omega'+\omega''-\omega)\cdot E_\mu(\omega')\cdot E_\nu(\omega'') \tag{3}$$

where the fiber attenuation u and the effective length in the presence of dispersion L_e are given by

$$u=\exp(-\alpha\cdot L/2) \tag{4}$$

$$L_e=\frac{1-u^2\exp(j\Delta kL)}{\alpha-j\Delta k} \tag{5}$$

Taking the inverse Fourier transform of (3), we obtain the complex amplitude of the electric field in the time domain:

$$E_\rho(t,L)=u'\left\{\sqrt{P_\rho(t)}\exp[j\phi_\rho(t)]+\sum_{\mu,\nu}\sqrt{P_n(t)}\exp[j\phi_n(t)]\right\} \tag{6}$$

where u' is defined by

$$u'=u/d \tag{7}$$

where d, the conversion factor between power and electric field, is defined by[1]

$$d^2 = \frac{nc}{8\pi} A_{eff} \tag{8}$$

where A_{eff} is the effective core area of the optical fiber. In equation (6), $P_\rho(t)$ and $\phi_\rho(t)$ are the signal power and phase at the fiber input, and $P_n(t)$ and $\phi_n(t)$ are the power and phase of the optical noise process due to FWM given by

$$P_n(t) = \kappa^2 D^2 \eta P_{\mu+\nu-\rho}(t) P_\mu(t) P_\nu(t) \tag{9}$$

$$\phi_n(t) = \phi_\mu(t) + \phi_\nu(t) - \phi_{\mu+\nu-\rho}(t) + Arg(L_e) - \frac{\pi}{2} \tag{10}$$

where the phase mismatch factor η denotes the ratio of the power of the generated waves without phase matching to their power with phase matching. The parameters κ and η are given by

$$\kappa = \frac{32\pi^3}{n^2 c\lambda} \frac{L_{eff}}{A_{eff}} \chi_{1111} \tag{11}$$

$$\eta = \frac{\alpha^2}{\alpha^2 + \Delta k^2} \left[1 + \frac{4\exp(-\alpha L)\sin^2(\Delta k L/2)}{\{1-\exp(-\alpha L)\}^2} \right] \tag{12}$$

where L_{eff} is the fiber effective length.

III. RECEIVER DESCRIPTION

We consider ASK and DPSK modulation formats in this paper. The block diagrams of ASK and DPSK receivers are shown in Fig. 2. We assume the lowpass filter just removes the second harmonic components resulting from the delay-and-multiply demodulator without changing the baseband components in the DPSK receiver of Fig. 2 b.

In a multichannel system, complex amplitudes of the received optical signal and local oscillator field are given by[7]

$$E_s = \sum_{\rho=1}^{N} E_\rho(t, L) \qquad \rho = 1, 2 \cdots\cdots N \tag{13}$$

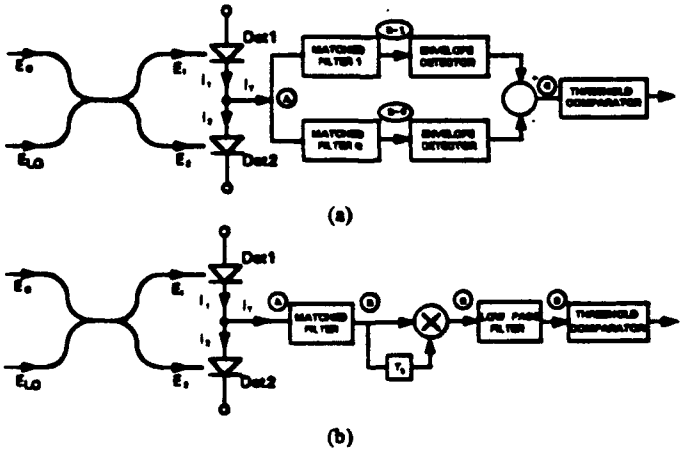

(a)

(b)

Fig. 2. (a) A Heterodyne ASK Receiver, (b) A Heterodyne DPSK Receiver.

$$E_{LO} = \sqrt{P_{LO}} / d \tag{14}$$

where $E_\rho(t,L)$ is the complex amplitude of channel ρ, N is the total number of optical channels, P_{LO} is the local oscillator power, d was defined in expression (8) and E_{LO} is the electric field of the local oscillator. We assume that the channel separation is large enough to neglect the inter-channel crosstalk[7]. The directional coupler output amplitudes are then:

$$E_1(t) = \frac{1}{\sqrt{2}}[E_\rho(t,L) + E_{LO}] \tag{15}$$

$$E_2(t) = \frac{1}{\sqrt{2}}[E_\rho(t,L) - E_{LO}] \tag{16}$$

The resulting photocurrents are

$$\begin{aligned} i_1(t) = \frac{R}{2}\{&u^2 P_\rho(t) + u^2 \sum_{\mu,\nu} P_n(t) + P_{LO} + 2u^2 \sum_{\mu,\nu} \sqrt{P_\rho(t) P_n(t)} \cos[\phi_\rho(t) - \phi_n(t)] \\ &+ 2u^2 \sum_{\mu',\nu'} \sum_{\mu\neq\mu',\nu\neq\nu'} \sqrt{P_n'(t) P_n(t)} \cos[\phi_n'(t) - \phi_n(t)] \\ &+ 2u\sqrt{P_{LO}} \left\{ \left[\sqrt{P_\rho(t)} + n_c(t) \right] \cos[\omega_{IF} t + \phi_\rho(t)] + n_s(t) \sin[\omega_{IF} t + \phi_\rho(t)] \right\} \} + n_1(t) \end{aligned} \tag{17}$$

$$\begin{aligned} i_2(t) = \frac{R}{2}\{&u^2 P_\rho(t) + u^2 \sum_{\mu,\nu} P_n(t) + P_{LO} + 2u^2 \sum_{\mu,\nu} \sqrt{P_\rho(t) P_n(t)} \cos[\phi_\rho(t) - \phi_n(t)] \\ &+ 2u^2 \sum_{\mu',\nu'} \sum_{\mu\neq\mu',\nu\neq\nu'} \sqrt{P_n'(t) P_n(t)} \cos[\phi_n'(t) - \phi_n(t)] \\ &- 2u\sqrt{P_{LO}} \left\{ \left[\sqrt{P_\rho(t)} + n_c(t) \right] \cos[\omega_{IF} t + \phi_\rho(t)] + n_s(t) \sin[\omega_{IF} t + \phi_\rho(t)] \right\} \} + n_2(t) \end{aligned} \tag{18}$$

where $P_n(t)$ and $P_n'(t)$ are the noise powers of ρ-th channel corresponding to μ,ν and μ',ν', respectively, R is the photodetector responsivity, $n_1(t)$ and $n_2(t)$ are shot noises originating from the detection process, and the in-phase and the quadrature components of noise are given by

$$n_c(t) = \sum_{\mu,\nu} \sqrt{P_n(t)} \sin\phi_{\mu\nu\rho}(t) \tag{19}$$

$$n_s(t) = \sum_{\mu,\nu} \sqrt{P_n(t)} \cos\phi_{\mu\nu\rho}(t) \tag{20}$$

The phase change due to FWM is given by

$$\phi_{\mu\nu\rho}(t) = \phi_\mu(t) + \phi_\nu(t) - \phi_\rho(t) - \phi_{\mu\nu\rho}(t) + Arg(L_e) \tag{21}$$

The phases $\phi_{\mu\nu\rho}(t)$ are regarded as independent random variables to simplify the analysis. The resulting output voltage is

$$V_T(t) = A\left\{ \left[\sqrt{P_\rho(t)} + n_c(t) \right] \cos[\omega_{IF} t + \phi_\rho(t)] + n_s(t) \sin[\omega_{IF} t + \phi_\rho(t)] \right\} + n(t) \tag{22}$$

where the amplitude A and the shot noise n(t) are given by

$$A = 2Ru\sqrt{P_{LO}} \tag{23}$$

$$n(t) = n_1(t) - n_2(t) \tag{24}$$

4. CODING METHODS AND SIGNAL-TO-NOISE RATIO

4.1. Power Spectral Density of Coded Signals

The signal-to-noise ratio for conventional NRZ coded signals and Manchester coded signals are given in this section. In the case of unipolar NRZ, the binary 1 is represented by a higher level (+A) and the binary 0 is represented by a zero level (0). In the Manchester code, the binary 1 is represented by a positive pulse occupying 50% of a bit slot followed by a negative pulse of the same duration. Similarly, a binary 0 is represented by a negative pulse followed by a positive pulse.

The baseband power spectral density (PSD) of NRZ signal is given by[8]

$$G_{NRZ}(f) = T_b \operatorname{sinc}^2(fT_b) \tag{25}$$

where T_b is bit period, and the bit rate is $R_b = 1/T_b$; the total signal power is normalized to unity. The autocorrelation function of the baseband NRZ signal is

$$R_{NRZ}(\tau) = \begin{cases} 1 - \dfrac{|\tau|}{T_b} & |\tau| < T_b \\ 0 & |\tau| > T_b \end{cases} \tag{26}$$

The baseband power spectral density of the Manchester-coded baseband signal is given by[8]

$$G_{MAN}(f) = T_b \operatorname{sinc}^2(fT_b/2) \cdot \sin^2(\pi f T_b/2) \tag{27}$$

The bandwidth of the Manchester-coded signal measured to the first null is twice that of the NRZ bandwidth. The Manchester-coded signal has a zero dc level on the bit by bit basis. Moreover, long strings of zeros do not cause a loss of the clocking signal. The Manchester-coded signal is generated by multiplying frequency-doubled bit clock with the NRZ-coded signal. The autocorrelation function of the Manchester-coded baseband signal is given by

$$R_{MAN}(\tau) = \begin{cases} 1 - 3\dfrac{|\tau|}{T_b} & |\tau| < \dfrac{T_b}{2} \\ \dfrac{|\tau|}{T_b} - 1 & \dfrac{T_b}{2} < |\tau| < T_b \\ 0 & |\tau| > T_b \end{cases} \tag{28}$$

4.2. Signal-to-Noise Ratio

The matched filter output voltage at the terminal B of Fig. 2 is given by

$$V_O(T_b) = \int_0^{T_b} V_T(t) \cdot h(T_b - t)dt = \int_0^{T_b} S(t) \cdot h(T_b - t)dt + \int_0^{T_b} n(t) \cdot h(T_b - t)dt \tag{29}$$

where h(t) is impulse response of the matched filter. The first term gives the signal, and the second term is a zero-mean Gaussian random variable; its variance is given by

$$\sigma^2 = \int_0^{T_b} \int_0^{T_b} R_n(t_1 - t_2)h(T_b - t_1)h(T_b - t_2)dt_1 dt_2 \tag{30}$$

where $R_n(t_1\text{-}t_2)=E[n(t_1)n(t_2)]$ is the autocorrelation function of the noise.

Assume that all channels use the same modulation format and have the same power. Then, from expressions (19) and (20), the autocorrelation function of the noise due to FWM is given by

$$R_{n,FWM}(\tau) = \frac{A^2}{2}\kappa^2 P_\rho^3 R'(\tau)\sum_{\mu,\nu} D^2\eta \tag{31}$$

where $R'(\tau)$ is given by

$$R'(\tau) = R^3(\tau)\cos\omega_{IF}\tau \tag{32}$$

where $R(\tau)$ is the autocorrelation function of each signal. An explicit expression for $R(\tau)$ will be given in Section V for each modulation and coding format investigated in this paper. Substituting (31) into (30), we obtain the variance of FWM noise:

$$\sigma_{FWM}^2 = \frac{A^2}{2}\kappa^2 P_\rho^3 V^2 S^2 T_b^2 \tag{33}$$

where V^2 and S^2 are defined by

$$V^2 = \frac{1}{T_b^2}\int_0^{T_b} \int_0^{T_b} R'(t_1 - t_2)h(T_b - t_1)h(T_b - t_2)dt_1 dt_2 \tag{34}$$

$$S^2 = \sum_{\mu,\nu} D^2\eta \tag{35}$$

The autocorrelation function of the shot noise is given by

$$R_{n,SN}(\tau) = qRP_{LO}\delta(\tau) \tag{36}$$

Substituting (36) into (30) we obtain the variance of the shot noise;

$$\sigma_{SN}^2 = qRP_{LO}T_bW \tag{37}$$

where W is given by

$$W = \frac{1}{T_b}\int_0^{T_b} h^2(T_b - t)dt \tag{38}$$

Therefore the total signal-to-noise ratio γ defined as the ratio of the signal power to the noise power, is given by

$$\gamma = \frac{A^2 T_b^2 P_\rho}{4k(\sigma_{FWM}^2 + \sigma_{SN}^2)} = \frac{1}{k[2\kappa^2 P_\rho^2 V^2 S^2 + qW / RT_b u^2 P_\rho]} \tag{39}$$

where k=4 for the Manchester-coded ASK system and k=1 for the three other modulation and coding formats considered in this paper. This equation shows that as the input signal power P_ρ increases, the signal-to-noise ratio γ first increases due to the relative suppression of the shot noise, and then decreases due to the FWM. Thus, at some value of P_ρ, a peak value of γ is reached corresponding to the optimum system performance.

5. ASK AND DPSK SYSTEM PERFORMANCE EVALUATION

5.1. Heterodyne ASK System

Bit Error Rate

We consider first the ASK receiver shown in Fig. 2 a. We assume that a matched filter is used in the receiver. The impulse responses of the matched filters for the NRZ and Manchester coded ASK signals are given by

$$h1_{ASK,NRZ}(t) = \begin{cases} \cos\omega_{IF} t & for \quad t \in [0, T_b] \\ 0 & for \quad t \notin [0, T_b] \end{cases} \tag{40}$$

$$h0_{ASK,NRZ}(t) = \{ \quad 0 \quad for \quad all \quad t \tag{41}$$

$$h1_{ASK,MAN}(t) = \begin{cases} \cos\omega_{IF} t & for \quad t \in [T_b/2, T_b] \\ 0 & for \quad t \notin [T_b/2, T_b] \end{cases} \tag{42}$$

$$h0_{ASK,MAN}(t) = \begin{cases} \cos\omega_{IF} t & for \quad t \in [0, T_b/2] \\ 0 & for \quad t \notin [0, T_b/2] \end{cases} \tag{43}$$

To find the noise variance due to four-wave-mixing, we need the autocorrelation function R(τ) of each ASK signal:

$$R_{ASK,NRZ}(\tau) = \frac{1}{4}[1 + R_{NRZ}(\tau)] \tag{44}$$

$$R_{ASK,MAN}(\tau) = \frac{1}{4}[1 + R_{MAN}(\tau)] \tag{45}$$

where the baseband autocorrelation functions $R_{NRZ}(\tau)$ and $R_{MAN}(\tau)$ are given by expressions (26) and (28) respectively. Substituting (44) and (45) into (32), we obtain the autocorrelation function R'(τ). Next, we substitute (32) and (40) into (34) to obtain

$$V_{ASK,NRZ}^2 = 0.01916 \tag{46}$$

Similarly, substituting (32) and (42) into (34), we obtain

$$V_{ASK,MAN}^2 = 0.00385 \tag{47}$$

Substituting (40) and (42) into (38), we obtain $W_{ASK,NRZ} = 0.5$ and $W_{ASK,MAN} = 0.25$.

The bit error ratio of the heterodyne ASK system is given by[9]

$$BER_{ASK,NRZ} = \frac{1}{2}\exp\left[-\frac{\gamma}{8}\right] \tag{48}$$

$$BER_{ASK,MAN} = \frac{1}{2}\exp\left[-\frac{\gamma}{4}\right] \tag{49}$$

Using expressions (48), (49), (46), (47), (39) and (35), we obtain the numerical value of BER of the ASK multichannel system impaired by the shot noise and the four wave mixing.

Fig. 3 shows BER for the 8 th channel* of a 16 channel WDM system using a dispersion shifted (DS) fiber versus the optical fiber input power for several values of the fiber length; the assumed system parameters are given in Table I. Inspection of Fig. 3 shows that an increase of the input power results in a decrease of the BER for small powers and in an increase of the BER for large input powers. The increase of BER at high powers is due to the FWM that is proportional to the cube of the signal power.

Dynamic Range and Maximum Transmission Distance

The system dynamic range is defined as the ratio of the maximum transmitter power to the minimum transmitter power needed to maintain BER below 10^{-9}; a more detailed description is contained in Section VI-B. Fig. 3 shows that at 100 km the dynamic range of a Manchester-coded system is about 2.0 dB larger than that of an NRZ system. The maximum allowable power for the Manchester-coded system is 2.0 dB larger than that for the NRZ coded system, and receiver sensitivity for the Manchester coded system is same as that for the NRZ system. The maximum transmission distance of a system using Manchester code is 220 Km, about 10 Km longer than that of the NRZ system.

5.2. DPSK Heterodyne System

Bit Error Rate

Fig. 2 b shows a block diagram of a DPSK receiver. The impulse responses of the matched filters for NRZ and Manchester coded DPSK signals are given by

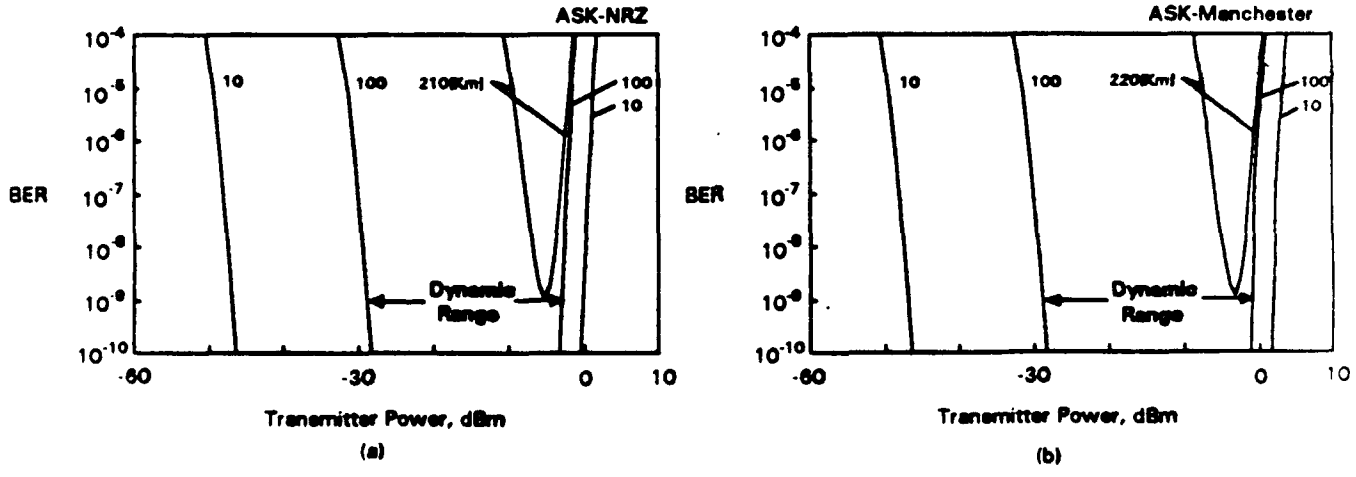

Fig. 3. The bit error rate of a 16 channel ASK coherent WDM system using the DS fiber versus the optical fiber input power; the parameter is the transmission distance. (a) NRZ-coded system, (b) Manchester-coded system.

* Other channels have better BER.

Table I. System parameters

Refractive Index, n		1.47
Wavelength, λ		1.55 μm
Attenuation Coefficient, α		0.2 dB / Km
Channel Spacing		10 GHz
Bit Rate		1 Gbps
Effective Fiber Core Area, A_{eff}	NDS Fiber	$32\pi\ \mu m^2$
	DS Fiber	$16\pi\ \mu m^2$
Group Velocity Dispersion, C	NDS Fiber	15 ps/Km-nm
	DS Fiber	1 ps/Km-nm

$$h_{DPSK,NRZ}(t)=\begin{cases}\cos\omega_{IF}t & for \quad t\in[0,T_b]\\ 0 & for \quad t\notin[0,T_b]\end{cases} \tag{50}$$

$$h_{DPSK,MAN}(t)=\begin{cases}-\cos\omega_{IF}t & for \quad t\in[0,T_b/2]\\ \cos\omega_{IF}t & for \quad t\in[T_b/2,T_b]\\ 0 & for \quad t\notin[0,T_b]\end{cases} \tag{51}$$

To find the noise variance due to four wave mixing we need the autocorrelation function R(τ) of each DPSK signal:

$$R_{DPSK,NRZ}(\tau)=R_{NRZ}(\tau) \tag{52}$$

$$R_{DPSK,MAN}(\tau)=R_{MAN}(\tau) \tag{53}$$

where $R_{NRZ}(\tau)$ and $R_{MAN}(\tau)$ are the autocorrelation functions of the baseband NRZ signal and the baseband Manchester coded signal given by expressions (26) and (28), respectively. Substituting (53) and (54) into (32), we obtain the autocorrelation function R'(τ). Next, we substitute (32) and (50) into (34) to obtain

$$V^2_{DPSK,NRZ}=0.10040 \tag{54}$$

Similarly, substituting (32) and (51) into (34), we obtain

$$V^2_{DPSK,MAN}=0.03889 \tag{55}$$

Substituting expressions (50) and (51) into (38), we obtain $W_{DPSK,NRZ}=0.5$ and $W_{DPSK,MAN}=0.5$. The bit error ratio of the heterodyne DPSK system can now be found as[9]

$$BER_{DPSK}=\frac{1}{2}\exp\left[-\frac{\gamma}{2}\right] \tag{56}$$

Using expressions (56), (54), (55), (39) and (35), we obtain the numerical value of BER of the DPSK optical multichannel system impaired by the shot noise and the four wave mixing. Fig. 4 shows the BER for the 8 th channel* of a

* Other channels have better BER.

16 channel versus the optical fiber input power for several values of the fiber length; the system parameters are shown in Table I.

Dynamic Range and Maximum Transmission Distance

The Manchester code gives a 2.1 dB larger dynamic range than the NRZ. The minimum power due to shot noise is the same for both NRZ and Manchester-coded systems. According to Fig. 4, the maximum transmission distance of Manchester coded systems is 247 Km, 10 Km more than that of NRZ coded system. Table II compares the maximum transmission length of DPSK and ASK systems utilizing NRZ and Manchester coding. The largest transmission distance is achieved using Manchester-coded DPSK systems.

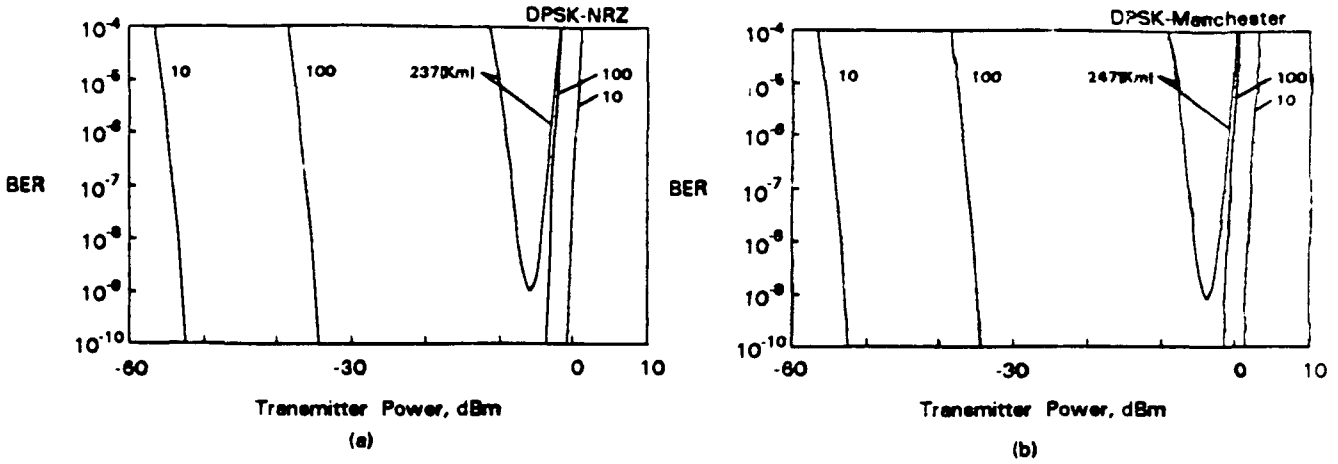

Fig. 4. The bit error rate of a 16 channel DPSK coherent system using DS fiber versus optical fiber input power; the parameteris the transmission distance. (a) NRZ-coded system, (b) Manchester-coded system.

Table II. Maximum transmission length (in Km) for a 16 channel WDM system

Fiber Type	Coding / Modulation Format	ASK	DPSK
DS	MAN	220	247
	NRZ	210	237
NDS	MAN	271	299
	NRZ	261	288

6. NUMERICAL RESULTS AND DISCUSSION

6.1. Maximum Transmission Length

The maximum transmission length of optical WDM systems is limited by the shot noise and the four wave mixing. The optical fiber input power corresponding to the minimum BER is obtained by differentiating expressions (48), (49) and (56) with respect to P_0 and setting the derivative equal to zero. The maximum transmission distance is obtained by substituting that value into expressions (48), (49) and (56) for ASK and DPSK systems, respectively. Fig. 5 shows the maximum transmission length versus the number of channels for various modulation schemes and coding methods; all calculation are for the worst-case channel (i.e. channel N/2). The four-wave-mixing crosstalk is maximum for that channel. The upper four curves are for the non-dispersion shifted (NDS) fiber, while the lower four curves are for the dispersion-shifted (DS) fiber; fiber parameters are shown in Table I. All curves show that the maximum transmission length decreases with the number of channels.

Manchester coded systems have the maximum transmission distance larger than that of NRZ coded system by 10 Km for both DPSK and ASK modulation formats; this conclusion is valid for both kinds of fiber. DPSK systems outperform ASK systems, and, for a large number of channels, NDS fiber outperforms DS fiber. The reason is that the relatively small core area and improved phase matching due to small group velocity dispersion increase the four-wave mixing crosstalk in the DS fiber as compared to the NDS fiber (the transmission length is limited by the FWM rather than by chromatic dispersion in the particular case considered).

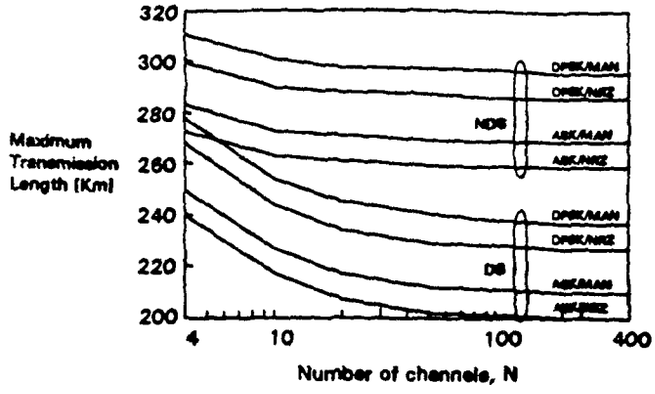

Fig. 5. Maximum transmission length versus number of channels for various modulation schemes and coding methods.

6.2. Dynamic Range and Power Budget

Dynamic Range

The fiber input power must be kept between the minimum value P_{min} and the maximum value P_{max} to maintain BER below 10^{-9}. The maximum input power P_{max} is determined by the four wave mixing, and the minimum value P_{min} is determined by the shot noise. The maximum and minimum input powers for a 16 channels WDM systems are shown in Fig. 6. The upper four curves are the maximum input power for various coding formats and optical fiber types and the lower two curves are the minimum input power for the same coding methods and fiber types. The ratio of the maximum power to the minimum power is defined as the dynamic range, and is an important factor in system design. For example, the dynamic range of a Manchester-coded ASK system with 1 Gbps/channel bit rate and 100 Km non-dispersion sifted fiber is 38 dB, as shown in Fig. 6 a.

Fig. 7 shows the dynamic range of a 16-channel WDM system versus the length of optical fiber for two fiber types and various modulation and coding formats. The fiber parameters are the same as in Table I. The curves show that short-distance systems have a large dynamic range of some 70 dB but as the transmission distance increases, the dynamic range decreases, and falls to some 30 dB at 100 Km. Manchester-coded ASK and DPSK 100 Km systems have some 2.0 dB larger dynamic ranges than the corresponding NRZ systems.

Power Budget

The power budget is defined as the ratio of the maximum input power to the minimum receiver power needed to keep BER below 10^{-9}. For example, the power budget of Manchester coded ASK system for the 8 th channel of a 16 channels WDM system with 1 Gbps and non-dispersion shifted fiber is about 58 dB as shown in Fig. 6 a. The drop of the power budget at long lengths is due to the drop of the maximum allowable input power caused by the four wave mixing. For very long fibers, the maximum power level remains almost the same, and therefore, the power budget remains almost the same. The power budgets of ASK and DPSK systems with various modulation formats and fiber types are given in Table III. The power budget of DPSK is some 5.5 dB larger than that of ASK system. Manchester coded systems show about 2.0 - 2.1 dB improvement with respect to NRZ systems. And power budget of systems using NDS fiber is 10.3 dB larger than that of systems using DS fiber.

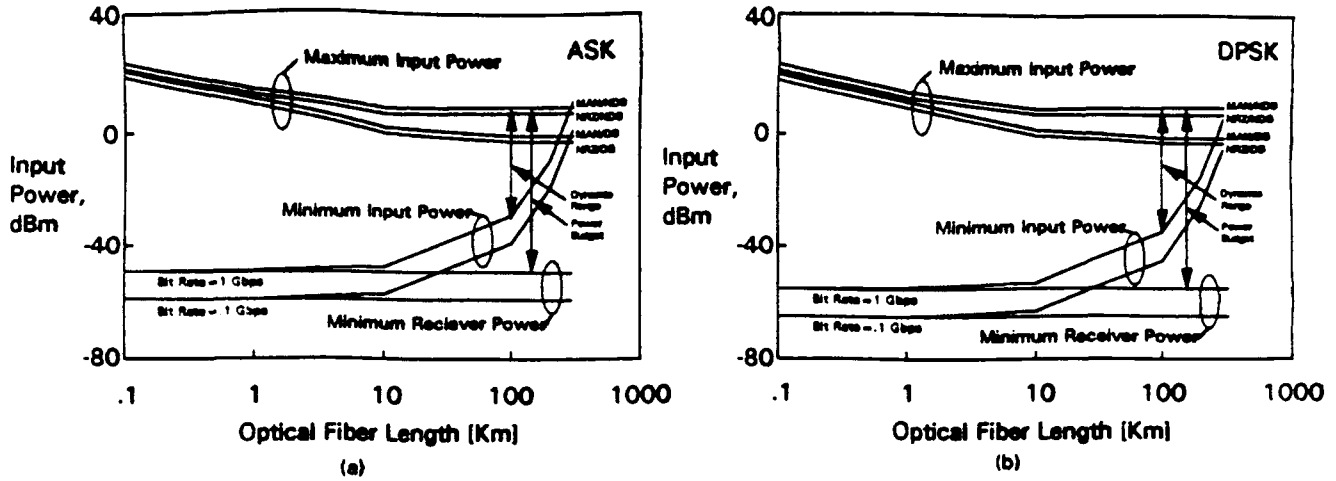

Fig. 6. Maximum input power, minimum input power and system dynamic range and system power budget versus optical fiber length for various fibers and modulation formats. (a) ASK, (b) DPSK.

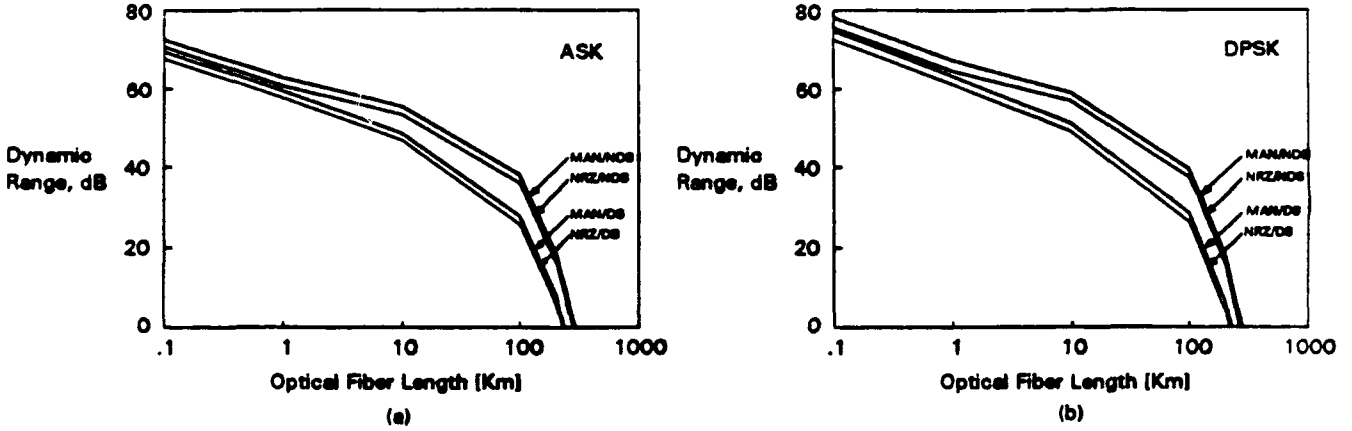

Fig. 7. Dynamic range of a 16 channel WDM system versus optical fiber length for (a) ASK, (b) DPSK systems.

6.3. Polarization, Chromatic Dispersion and Interchannel Interference

The state of polarization of the received wave is random in the optical fiber system without polarization control. As a result, FWM crosstalk is decreased to 5/6 of the value expected for a fixed state of polarization[10]. In this paper, the case of random polarization is considered, so that all our results apply to systems NOT employing polarization-preserving fiber.

The chromatic dispersion can produce distortion in the demodulated waveform resulting in intersymbol interference in the received signal and reduction of transmission system performance. The chromatic dispersion limitations for coherent system were studied by many authors[11,12]. The receiver sensitivity degradation due to chromatic dispersion has been observed in an FSK transmission experiment at more than 4 Gbits/s[11]. However, transmission experiments at 1 to 2 Gbits/s have shown that the influence of chromatic dispersion on FSK systems is less than that on intensity-modulated system[12]. Receiver sensitivity degradation due to chromatic dispersion depends on the modulation and demodulation schemes used. The transmission distance limit due to chromatic dispersion is some 2,000 Km for 1.55 μm non-dispersion shifted ASK and DPSK systems[13]. Since the transmission distance constraints studied in this paper are less than 2,000 Km, the impact of chromatic dispersion can be (and is) neglected.

Table III. Power budget of 100 Km, 16 channel WDM systems (in dB)

Fiber \ Modulation Format / Coding		ASK	DPSK
DS	MAN	48.1	53.6
	NRZ	46.1	51.5
NDS	MAN	58.4	63.9
	NRZ	56.4	61.8

The bandwidth of the Manchester coded signal measured to the first null is twice that of the NRZ bandwidth. If several FDM channels are being transmitted, then a coherent system may suffer a performance degradation stemming from crosstalk generated by intermodulation interference. Prior work showed that balanced receivers are superior to single detector receivers in multichannel environment, and for small penalty (below 1 dB) both time and frequency analysis techniques yield essentially the same results[7]. Based on the results of Ref. 7, the electrical domain channel spacing of ASK and DPSK systems can be set as shown in Table IV. The maximum required electrical channel spacing for the four systems is 5.6. The optical domain channel spacing normalized to bit rate is[7]

$$D_{opt} = D_{nel} + 2 \cdot f_{IF} \cdot T_b \tag{57}$$

where D_{nel} is normalized electrical channel spacing. When the IF frequency for the Manchester-coded system is selected to be $2/T_b$, D_{opt} is less than 10. Thus, for all systems considered in this paper, the optical channel spacing of 10 bit rates is adequate. Thus, we select the optical channel spacing to be 10 GHz for all four 1 Gbits/s systems investigated in this paper.

Table IV. Electrical channel spacing normalized to bit rate of ASK and DPSK systems with 1 dB penalty

Coding \ Modulation Format	ASK	DPSK
Manchester	5.6	4.6
NRZ	3.7	3.0

7. CONCLUSIONS

Wavelength division multiplexing systems are fundamentally limited by the receiver shot noise and by the fiber four wave mixing. In this paper, we analyzed the impact of these limitations on NRZ and Manchester coded systems. The minimum receiver power is determined by the shot noise, and maximum transmitter power is determined by the four wave mixing.

For 1.55 μm dispersion shifted 16 channel ASK systems, having 10 GHz channel spacing and 1 Gbps per channel bit rate, the maximum transmission length is about 210 Km for NRZ and 220 Km for Manchester codes, respectively. The corresponding numbers for DPSK systems are 237 Km and 247 Km, respectively. The maximum transmission length of the ASK system using non-dispersion shifted fiber is 261 Km for NRZ and 271 Km for Manchester codes, respectively.

The corresponding numbers for DPSK systems are 288 Km and 299 Km, respectively. The physical reason is that the transmission length is limited by the FWM rather than by dispersion in this particular case.

To maintain system BER below 10^{-9}, the fiber input power must be kept between the maximum value determined by the fiber four wave mixing and the minimum value determined by the receiver shot noise. The ratio of the maximum input power to the minimum input power is defined as the dynamic range. The dynamic range of 100 Km Manchester coded systems is some 2 dB better than that of NRZ systems for both ASK and DPSK modulation formats.

In summary, Manchester-coded DPSK systems using non-dispersion shifted fiber have the best performance and NRZ-coded ASK system using dispersion shifted fiber have the worst performance.

8. ACKNOWLEDGMENT

This work was supported by ONR under contract number 4148130-01 and by the Korea Science and Engineering Foundation.

9. REFERENCES

1. K. O. Hill, D. C. Johnson, B. S. Kawasaki, R. I. MacDonald,"CW three wave mixing in single-mode optical fiber", *J. of Appl. Phys.*, vol. 49, no. 10, pp. 5098-5106, 1978.

2. N. Shibata, R. P. Braun, R. G. Waarts,"Phase-mismatch dependence of efficiency of wave generation through four-wave mixing in a single-mode optical fiber," *J. of Quantum Elec.*, vol. QE-23, no. 7, pp. 1205-1210, 1987.

3. A. R. Chraplyvy,"Limitations on lightwave communication imposed by optical-fiber nonlinearities," *J. of lightwave Tech.*, vol. , no. 10, pp. 1548-1557, 1990.

4. R. G. Waarts, A. A. Friesem, E. Lichtman, H. H. Yaffe, R. P. Braun, "Nonlinear effects in coherent multichannel transmission through optical fibers," *Proc. IEEE*, vol. 78, no. 8, pp. 1344-1368, 1990.

5. K. Inoue, N. Shibata,"Theoretical evaluation of intermodulation distortion due to four-wave mixing in optical fibers for coherent phase-shift-keying-frequency-division-multiplexing transmission," *Optics Lett.*, vol. 14, no. 11, pp. 584-586, 1989.

6. E. Lichtman,"Performance degradation due to four-wave mixing in multichannel coherent optical communication systems," *J. of Optical Comm.*,vol. 12, no. 2, pp. 53-58, 1991.

7. L.G. Kazovsky, "Sensitivity penalty in multichannel coherent optical communications," *J. of Lightwave Tech.*, vol. 6, no. 9, pp. 1353-1365, 1988.

8. L. Couch, "Digital and analog communication systems," 3rd ed., New York, Macmillan, 1990.

9. T. Okoshi, "Ultimate performance of heterodyne / coherent optical fiber communications," *J. of Lightwave Tech.*, vol. LT-4, no. 10, pp. 1556-1562, 1986.

10. J. Botineau, R. H. Stolen,"Effects of polarization on spectral broadening in optical fibers", *J. Opt. Soc. Am.*, vol. 72, pp. 1592-1596, 1982

11. K. Iwashita and N. Takachio, "Compensation of 202 Km single-mode fibre chromatic dispersion in 4 Gb/s optical CPFSK transmission experiment," *Electron. Lett.*, vol. 24, pp. 759-760, 1988

12. A. Gnauck, R. Linke, B. Kasper, K. pollock, K. Reichmann, R. Valenzuela, and R. Alferness,"Coherent lightwave transmission at 2 Gb/s over 170 Km of optical fiber using phase modulation," *Electron. Lett.*, vol. 23, pp. 286-287, 1987

13. A. Elrefaie, R. Wagner, D. Atlas, and D. Daut,"Chromatic dispersion limitations in coherent lightwave transmission systems," *J. of Lightwave Tech.*, vol. LT-6, no. 5, pp. 704-709, 1988

Future Optical Fiber Communication Systems and Lasers for Their Implementation*

Leonid G. Kazovsky
Stanford University, Durand 202, MC-4055, Stanford, CA 94305-4055

Abstract

We discuss four major directions in optical communication systems research: optical amplifiers; coherent and dense WDM transmission; analog signal transport; and soliton propagation. Then, we focus on laser requirements for the four systems, including reproducible wavelength, high power, narrow linewidth, large side-mode suppression, wide tunability, good amplitude-modulation, frequency-modulation and wavelength-switching characteristics, small frequency- and intensity noise, and narrow spectrum. Finally, we discuss candidates for future laser transmitters including DFB and DBR semiconductor devices, Nd:YAG lasers, and fiber-ring soliton lasers.

1. Introduction

Four major directions in optical fiber communications research are coherent and dense WDM systems; analog systems for CATV distribution and antenna remoting; optical amplifiers; and soliton transmission systems. All foregoing technologies promise major advances in the performance and capabilities of optical fiber communication systems. While some of these technologies are interrelated (for example, soliton systems are impractical without optical amplifiers), each of them offers distinct new features and requires a solution of a unique set of problems. Most of the problems are associated with the need for new lasers, sometimes quite different from those currently available.

In this paper, we review the foregoing four new technologies currently in various stages of R&D, discuss laser requirements for each system, and speculate what lasers might be able to satisfy these requirements. We conclude that no single laser is likely to satisfy all the requirements at once. Rather, a variety of lasers are needed (and are being developed) to operate at the required variety of wavelengths, powers, emission spectra and modulation responses.

The paper is intended as a broad and shallow overview of the issues involved in the R&D of optical communication systems, and has been written for a general electrical engineering audience. Readers

* This work was partially supported by ONR under contract number N00014-91-J-1857.

interested in a more detailed exposition are referred to the many technical papers written on the subject; a small fraction of such papers can be found in the *References* section of this paper.

The rest of this paper is organized as follows. In Section 2, coherent and WDM systems are discussed. In Section 3, analog systems are dealt with. Section 4 is devoted to optical amplifiers while Section 5 is devoted to solitons. Finally, Section 6 contains conclusions of this paper.

2. Coherent and WDM Systems [1]

2.1. Motivation and System Example

Dense wavelength-division-multiplexing (WDM) systems promise larger information bandwidth, more efficient use of the fiber, and, most importantly, flexibility in network design and operation. In particular, WDM allows the logical network topology be independent of and generally different from the physical network topology; in addition, the logical topology can be adjusted to match changing traffic conditions. Further, WDM allows various bit rates and modulation formats to coexist on the same physical network, up to and including mixing digital and analog traffic on the same fiber.

The main obstacle to successful implementation of dense WDM networks is the need for fairly sophisticated lasers and demultiplexers. To appreciate the advantages and the difficulties of WDM, consider a particular example - STARNet - shown in Fig. 1. STARNet is a coherent WDM network proposed and investigated by a group of researchers at Stanford university [1]. Each STARNet node is equipped with one fixed transmitter and two receivers: a main tunable receiver and an auxiliary fixed receiver. Each auxiliary receiver is fixed-tuned to the frequency of the previous transmitter in the frequency comb (see insert in Fig. 1) so that a virtual ring of nodes is formed. That ring is FDDI-compatible and always functioning; through the ring, packet-switched information is exchanged.

Here is what happens in STARNet when a node (say, node A) needs to establish a circuit-switched interconnect (for example, to have a video-conferencing session) with, say, node B. Node A sends a request to node B through the FDDI-compatible ring, and tunes its main tunable receiver to the wavelength of transmitter B. Node B receives the request, and tunes its main tunable receiver to the wavelength of transmitter A. Thus, a circuit-switched interconnect is established between the two stations. Simultaneously, many additional pairs of nodes can "talk" to each other without interference.

A major advantage of that approach is that the network throughput is not limited by the electronics of each node. For example, in the experimental prototype we are currently building, four nodes are planned

to exchange information at 3 GB/s/node, for a total network throughput of 12 GB/s. This is two orders of magnitude larger than the throughput of FDDI.

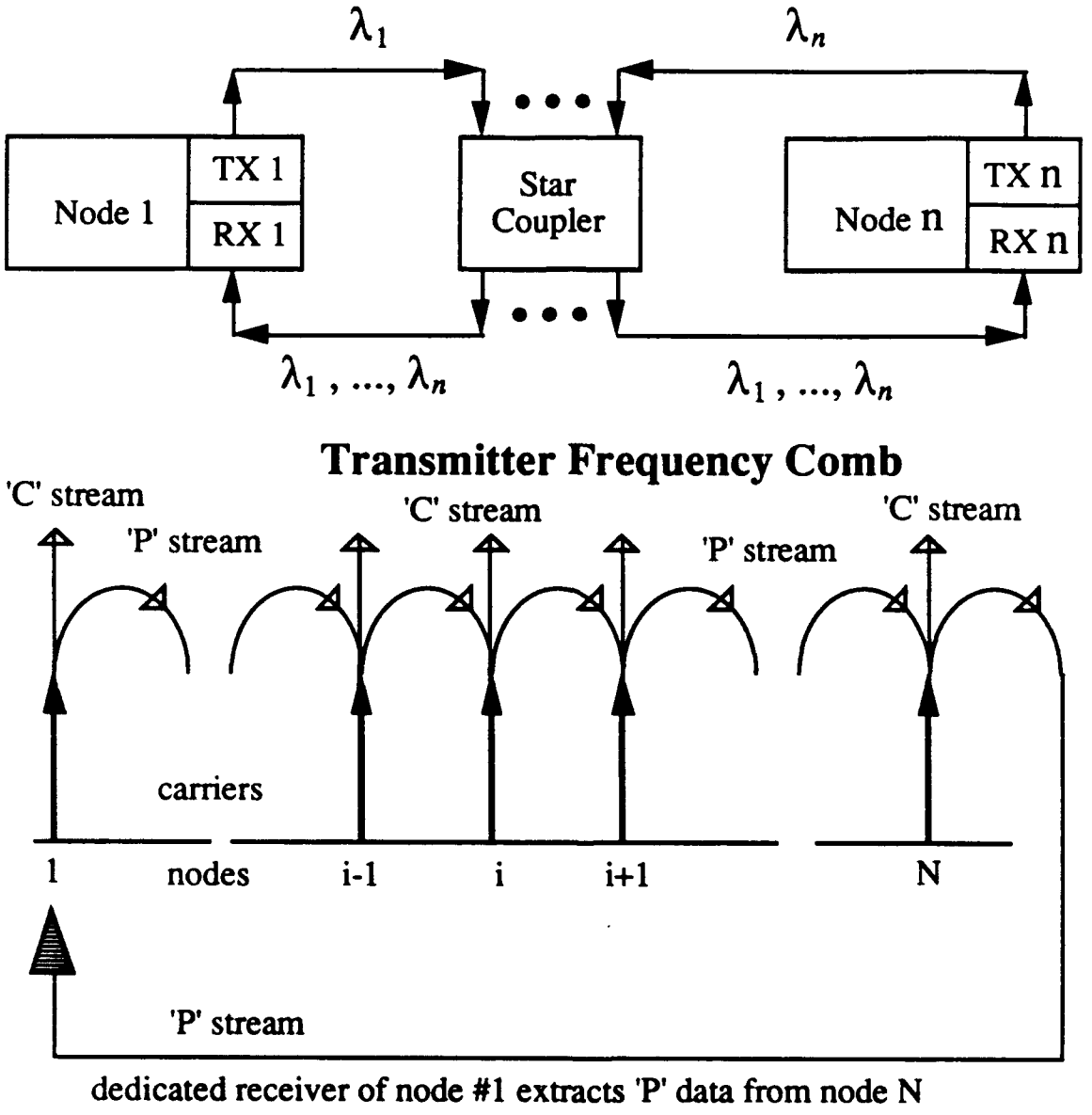

Figure 1. STARNet: a coherent WDM local area network, after Ref. [1].

2.2. Laser Requirements

STARNet and similar networks require tunable optical receivers. Such receivers can be implemented using either coherent technology (with tunable lasers employed to tune coherent receivers to a desired

frequency) or direct-detection technology in conjunction with tunable optical filters. In both cases, lasers have to satisfy the following requirements:

- Wavelength: 1.5 μm (wavelength of minimum attenuation) or, possibly, 1.3 μm (wavelength of minimum dispersion), with 1.5 μm being normally preferable.
- Reproducible wavelength (ideally, within a few GHz).
- Reproducible (preferably - but not necessarily- narrow) linewidth, corresponding to a reproducible phase noise.
- Wide tuning range: for example, tuning over 10,000 GHz is required for a 500-node system with 20 GHz channel spacing.
- Good modulation response extending (ideally) from DC to many GHz.
- Separate and independent control and modulation of frequency (wavelength) and amplitude.
- For local oscillator lasers, very low intensity noise is a must; RIN of -160 dB/Hz is considered to be desirable.
- Though not absolutely necessary, integration with photodiodes and other components is a definite advantage in system design.

2.3. Laser Candidates

Three devices (and their variations) are the main contenders for WDM applications: semiconductor DFB lasers; semiconductor DBR lasers; and diode-pumped Nd:YAG solid-state lasers.

In DFB lasers, a grating guaranteeing a single-frequency operation is etched into the device, and overlaps the active (gain) region. As a result, DFB lasers are relatively easy to make, and are available commercially from a number of vendors. DFB lasers have a reasonably narrow linewidth (a few MHz for outstanding research devices) and a large modulation bandwidth (many GHz). They are small and can be integrated with other semiconductor devices. On the negative side, DFB lasers have a small tuning range (a couple of nanometers) and non-uniform FM response.

Similarly to DFB lasers, DBR lasers have a grating etched into the device to guarantee a single-frequency operation. However, the grating does ***not*** overlap the gain region; instead, it is confined to a separate (passive) section of the device thus allowing an independent control of light amplitude and frequency. DBR lasers are characterized by a reasonable linewidth, very large tuning range (10,000 GHz has been experimentally demonstrated) and flat FM response. Also, DBR lasers can be integrated with other semiconductor devices. On the negative side, the modulation bandwidth of DBR lasers is rather small (less than 1 GHz), and represents a bit-rate bottleneck.

Finally, diode-laser pumped Nd:YAG lasers have high output power, extremely narrow linewidth making them suitable for PSK transmission, and extremely small RIN making them excellent local oscillators and sources for linear transmission. On the negative side, Nd:YAG lasers have a limited tuning range (less than 100 GHz), cannot be modulated at any reasonable communications rate, and cannot be integrated with semiconductor devices.

Review of the advantages and disadvantages of the three devices reveals that no single device satisfies all the requirements. It does, however, appear that DBR lasers satisfy ***most*** requirements, and are a good candidate for WDM applications.

3. Transmission of Analog Signals

3.1. Motivation and System Example

Analog signal transport systems are needed for CATV distribution, antenna remoting, phased-array radar and many other applications. Perhaps the best known applications of analog systems are in the CATV industry where the channel capacity is expected to grow to some 150 channels before the year 2000. That capacity will require fiber optics for transmission. Fiber optic CATV systems are already being manufactured and installed, albeit their current capacity does not reach the 150 channel goal. From the point of view of CATV industry, the link should employ AM to preserve end-to-end compatibility with TV receivers. An example of a trunk CATV system employing an AM fiber optic link is shown in Fig. 2.

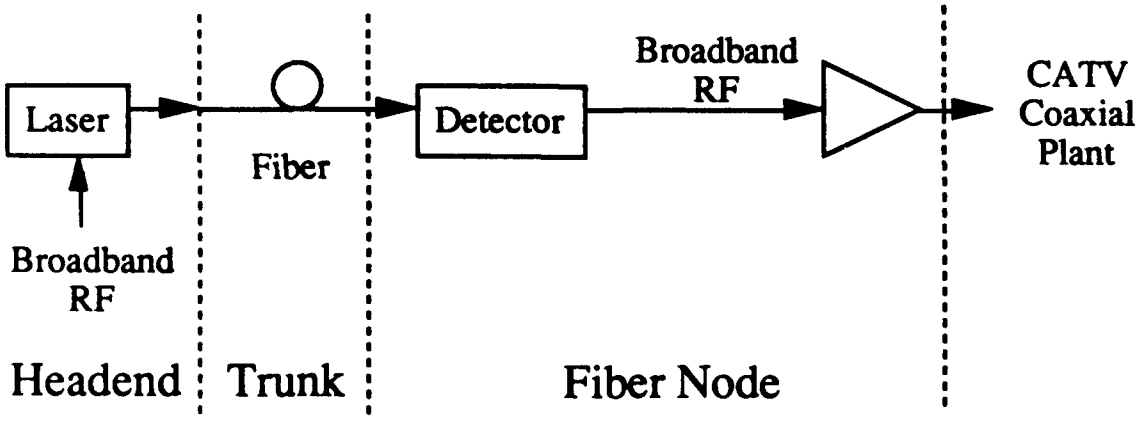

Figure 2. A trunk CATV system employing an analog AM fiber optic link, after Ref.[2].

3.2. Laser Requirements

Lasers for CATV and other analog applications have to satisfy the following requirements:

• High output power to provide a large signal-to-noise-ratio (CNR of some 55 dB is generally required) and a large dynamic range. In distribution systems, high output power helps to increase the number of customers served by a singe transmitter.

• High linearity (both composite triple-beat - CB - and composite second-order - COs - have to be kept below -65 dB).

• Small RIN (below -160 dB/Hz) to keep high SNR.

• Protection against reflections is required as the quality of the outside fiber plant is frequently uneven and unpredictable. For this reason, optical isolators normally have to be built into laser packages.

• Flat modulation response.

• High-frequency capability: The bandwidth of many current CATV systems is 500 MHz, with 1 GHz needed in the near future. For radar systems, a variety of frequencies is needed, up to 10 GHz and beyond.

• Wavelength compatibility with Er-doped fiber amplifiers (1.55 μm) is highly desirable for CATV systems.

• Side modes have to be very small to keep the distortions low.

3.3. Laser Candidates

Two lasers are main contenders for analog applications, and both are in fact used in commercial systems: semiconductor DFB lasers and solid-state diode-pumped Nd:YAG lasers; both are briefly described in Section 2.3.

DFB lasers have important advantages relevant to analog applications: They can be directly intensity-modulated, are available at the 1.5 μm wavelength compatible with Er-doped fiber amplifiers; some (but not all) devices exhibit a low RIN, around -160 dB/Hz. Their output power is modest (a few mW in the fiber for commercial devices), but is improving rapidly.

On the other hand, Nd:YAG lasers have important advantages of very high output power (devices with the output power of 300 mW are commercially available) and extremely low RIN. Most of RIN power in Nd:YAG lasers is concentrated around low frequencies, and is eliminated by feedback loops ("noise-eaters") in many commercial devices. On the negative side, Nd:YAG lasers cannot be directly modulated at any reasonable rate, and thus require external modulation. In addition, their longest wavelength of operation is 1.3 μm, and is incompatible with Er-doped fiber amplifiers.

In summary, DFB-based systems tend to be less costly on a per-system basis, but not necessarily on a per-channel or per-subscriber basis, and are compatible with Er-doped fiber amplifiers. In contrast, Nd:YAG-based systems are incompatible with Er-doped fiber amplifiers, and are more expensive on a per-system basis because of external modulation they must employ. However, the capacity of Nd:YAG-based systems tends to be higher than that of DFB-based systems because of higher output power and lower noise, so that the per-channel and per-subscriber cost is actually lower in many cases.

4. Optical Amplifiers

4.1. Motivation and System Example

Optical amplifiers went from a fairly exotic research topic to an important commercially available device in just a few years. Their main advantages are simplicity, leading to good reliability and potentially low cost; wide optical bandwidth (some 25 nm for Er-doped fiber amplifiers) leading to very high information rates and a possibility of handling several WDM channels simultaneously; and flexibility: optical amplifiers function independently from the bit rate, modulation format, or number of channels, and are compatible with both direct detection and coherent detection.

Two types of optical amplifiers have been developed: semiconductor optical amplifiers, or SOA's (to a first approximation, SOA's are just semiconductor lasers driven below threshold), and Er-doped fiber amplifiers, or EDFA's. The latter type is now preferred in many applications due to very low coupling loss (less than 1 dB), the resulting high gain, polarization-insensitive operation, high saturation power (more than 10 dBm), slow gain dynamics resulting in the lack of saturation-induced crosstalk, and quantum-limited noise figure (around 3.5 dB).

Fig. 3 shows a schematic of EDFA. It is seen to be an exceptionally simple device consisting of a piece of Er-doped fiber (several meters), laser diode pump, and a wavelength-selective coupler (WDM multiplexer) needed to combine the signal and the pump fields. In many practical applications, additional components are needed; optical isolators are required in most cases to keep the system stable.

EDFA's are not free from drawbacks, however: they are currently limited to 1.5 μm applications, require high-power (50-100 mW) pump diodes and a wavelength-selective coupler (instead of direct current pumping), are not integratable, cannot be made small, and cannot be modulated at any reasonable communications rate. Nevertheless, their advantages far outweigh their drawbacks in many important applications including line amplifiers, pre-amplifiers (used in receivers to improve their sensitivity) and power amplifiers used to compensate splitting and components' loss in transmitters and networks.

Examples of recent experiments include 1.2 Gb/s ASK transmission over 900 km using 11 optical amplifiers, and 2.5 Gb/s FSK transmission over 2,223 km using 25 optical amplifiers (Fig. 4). Ever more impressing experiments are being published every few months.

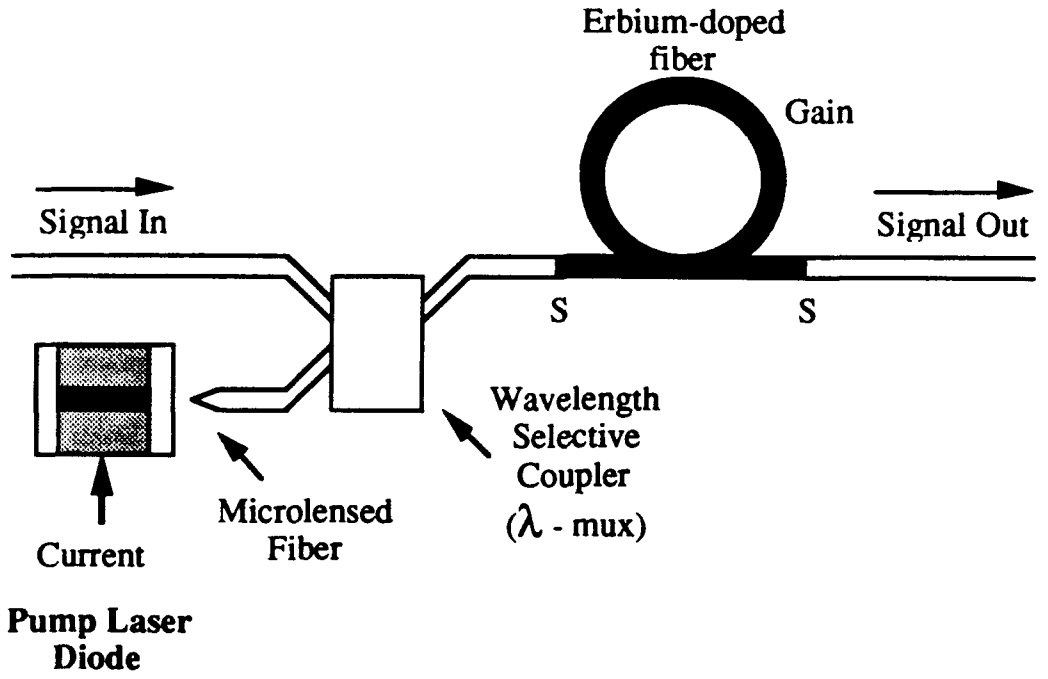

Figure 3. Erbium-doped optical fiber amplifier (EDFA).

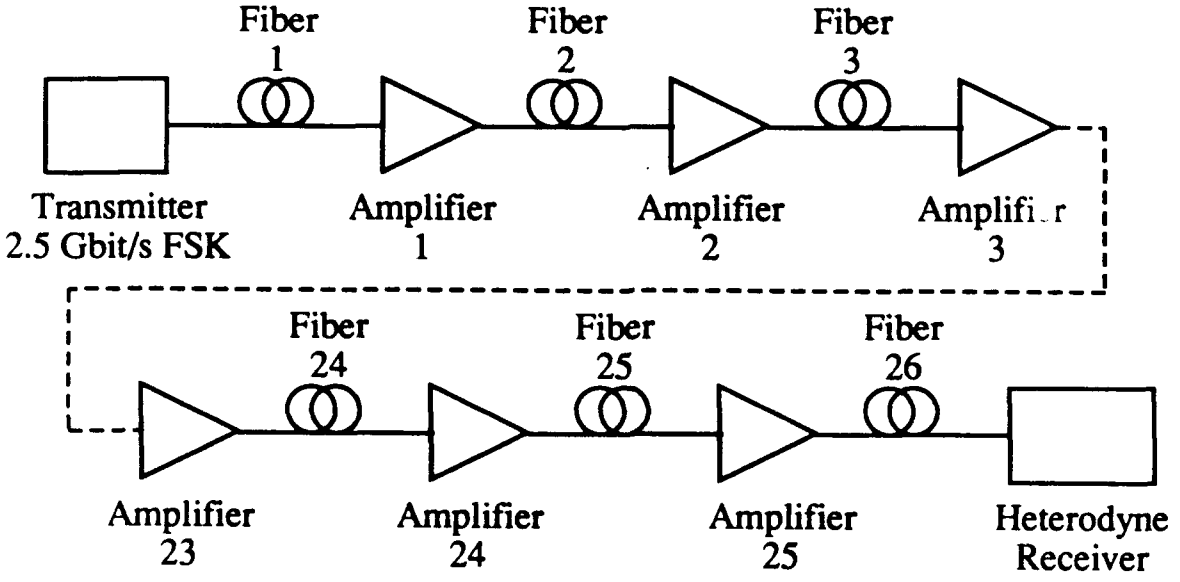

Figure 4. A 2.5 Gb/s FSK transmission experiment over 2,223 km using 25 optical amplifiers, after Ref. [3].

4.2. Laser Pump Requirements

• Wavelength: EDFA's can, in principle, be pumped at a variety of wavelengths including 514 nm, 532 nm, 667 nm, 800 nm, 980 nm, 1.48 μm, and 1.53 μm. However, availability of semiconductor pumps limits the choice of pump wavelengths to the region between 800 nm and 1.53 μm. Though semiconductor laser pumps are readily available at 800 nm, this pump wavelength is not necessarily the best choice: its pumping efficiency is low due to excited-state absorption. Pumping at 1.49 μm and 1.53 μm is less efficient than that at 980 nm (see Fig. 5), pump/signal multiplexing is more difficult, and the noise figure is not as good. Thus, pumping at 980 nm is a reasonable choice leading to pumping efficiencies as good as 10.2 dB/mW [4].

• Wavelength reproducibility: The pumping efficiency remains high as long as the pump wavelength is kept within a window of some 20 nm. Thus, the nominal wavelength has to be guaranteed within +/- 10 nm.

• Output power: The need for high gain and high saturation power leads to a requirement of some 50-100 mW of pump power in the fiber. Even higher powers may be needed for future CATV distribution networks.

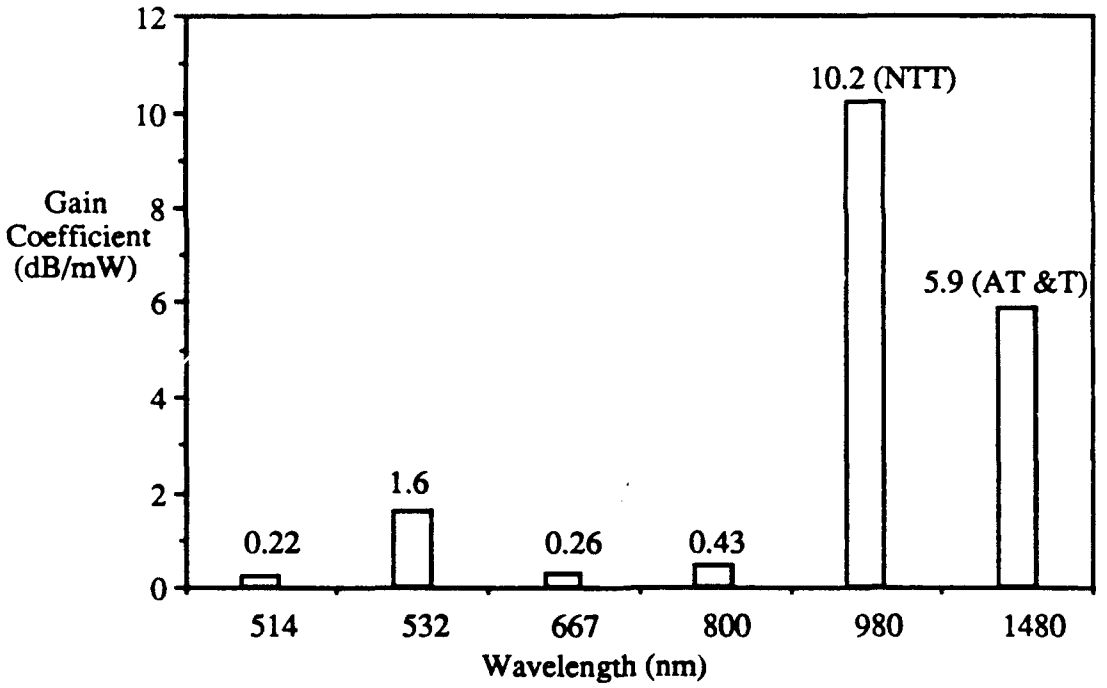

Figure 5. EDFA pumping efficiencies, after Ref. [4].

4.3. Laser Candidates

The obvious choice satisfying the foregoing requirements is a semiconductor AlGaAs Fabry-Perot laser. Such lasers are commercially available at ever increasing powers, and are commonly incorporated into EDFA's.

5. Soliton Systems

5.1. Motivation and System Example

Solitons are pulses for which nonlinear effects and dispersion (which are normally detrimental) cancel each other. Solitons can be explained as the bunching of high-intensity light: the light pulse creates a moving "valley" of higher dielectric constant. A simple physical explanation of solitons ("running on a mattress") is shown in Fig. 6. Runners having different speeds would arrive at different times when running on a flat surface (in fiber, this corresponds to dispersion). However, when running on a soft surface (mattress), their combined weight creates a moving valley (in fiber, this corresponds to a local change of refractive index due to fiber nonlinearity). The moving valley pulls along slower runners (slower photons in the fiber) and retards faster runners (faster photons in the fiber). The net result is that the dispersion is canceled by the nonlinearity, so that short pulses can propagate over extremely long distances without changing their shape as long as their power remains sufficiently high to cause an adequate local change of the refractive index.

The latter condition implies the need for optical amplifiers to compensate for the inevitable light attenuation in the fiber.

Figure 6. A simple physical explanation of solitons: running on a mattress, after Ref. [5].

Fig. 7 illustrates a recent experiment transmitting 70 psec solitons over 10,000 km. To avoid the need to install an actual 10,000 fiber link, the experiment uses a 75 km fiber ring. Solitons "run" around the ring, much like horses on racetrack; three EDFA's are used to compensate fiber losses.

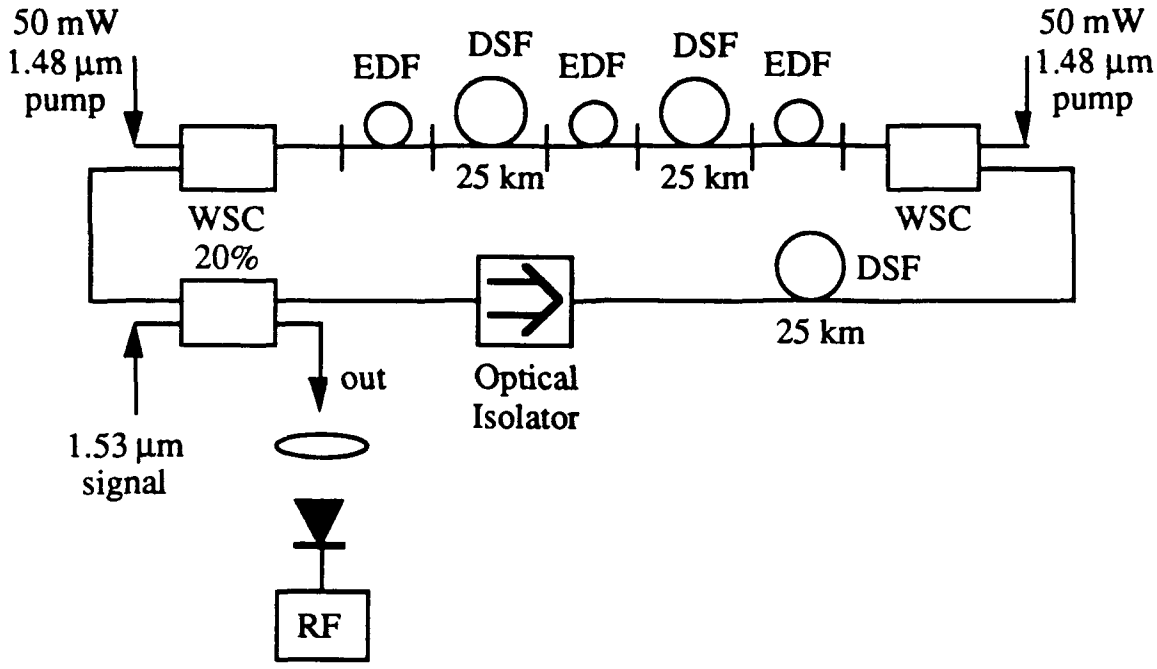

Figure 7. A 10,000 km soliton transmission experiment, after Ref. [5].

Contrary to conventional systems, the bit rate / distance limit in *soliton* systems is ***not*** set by the attenuation or dispersion. Instead, the limit is set by the spontaneous emission noise of optical amplifiers: that noise causes soliton power fluctuations, leading to a arrival time jitter leading, in turn, to a fundamental limit on the bit rate / distance in soliton systems (Gordon-Hause limit). That limit is illustrated in the insert in Fig. 7, and corresponds to 70 psec pulses over 10,000 km. Fortunately, this limit is so high that even most ambitious trans-Pacific and trans-Atlantic links currently on the drawing board are possible - provided, however, that suitable soliton transmitters will be developed.

5.2. Laser Requirements

- Wavelength: Soliton transmitters must operate at 1.55 μm for compatibility with EDFA's.
- They must generate powerful 10-20 psec pulses for multigigabit-per-second transmission rates needed for transoceanic applications.
- The pulses must have extremely narrow transform-limited spectrum to allow exact dispersion compensation.

5.3. Laser Candidates

The lack of a suitable laser is probably the most serious problem in soliton communications. While several approaches have been investigated and appear to work quite satisfactory in the laboratory, it is not clear as yet which one (if any) is a reasonable candidate for practical applications.

One possibility is to take a soliton ring (similar to one shown in Fig. 7) and to provide a net gain larger than unity, as shown in Fig. 8. The resulting device oscillates with the repetition rate set by the free spectral range of the etalon, yields transform-limited sech-shaped pulses and has sufficiently high output power (more than 10 mW average power has been demonstrated). In addition, the pulse width scales inversely with the average power as required for soliton transmission. This device is an excellent laboratory tool for soliton studies. However, it is not clear as yet whether or not practical transmitters can be developed using this approach.

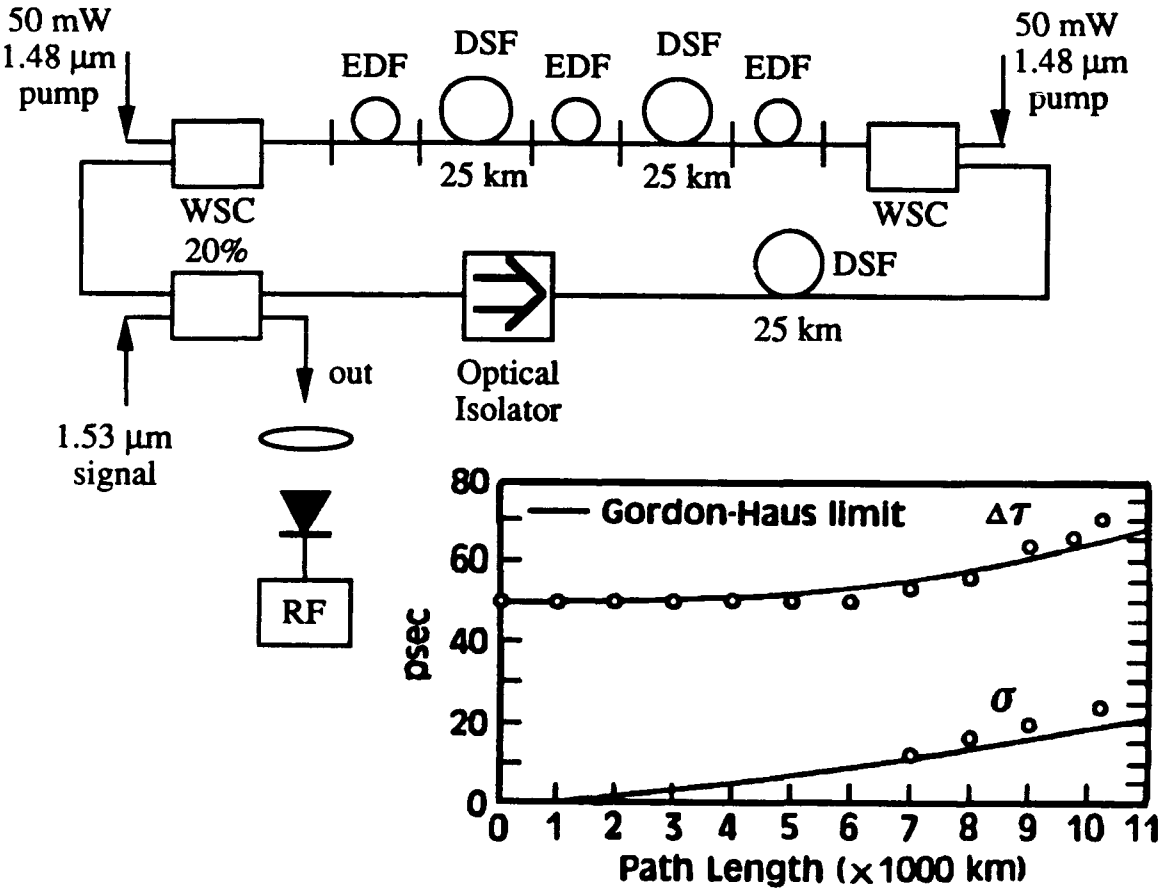

Figure 8. A fiber-ring soliton laser, after Ref. [5].

6. Conclusions

Four exciting system applications will shape the future of optical fiber communications: dense WDM and coherent systems, analog signal transport, optical amplifiers, and solitons. Optical amplifiers and analog systems are "already here", and are commercially available. Dense WDM and soliton systems are further in the future, and depend on the solution to challenging device problems.

All four systems require high-performance lasers, and impose quite different requirements. These requirements are unlikely to be satisfied by any single device, and so "the laser of the future" is, most likely, several quite different devices.

Future coherent and dense WDM systems may operate at 1.5 μm. Lasers for such systems have to have a highly reproducible wavelength, wide tuning range, and good AM, FM and wavelength-switching response; the AM and FM have to be independent from each other. For local oscillators, very low RIN is required. A good candidate for dense WDM and coherent applications is a DBR laser, possibly integrated with an "external" modulator.

Analog signal transport systems require high-power, low RIN lasers with excellent side-mode suppression. Good candidates for 1.5 μm wavelength (desirable for compatibility with Er-doped fiber amplifiers) are DFB lasers while for 1.3 μm wavelength, Nd:YAG lasers are an excellent candidate already used in commercial systems.

High-power semiconductor laser pumps are required for Er-doped fiber amplifiers. The pumps are required to operate within a 20 nm window at 980 nm, and generate 50-100 mW in the fiber (probably even more for future CATV distribution and similar applications). Semiconductor AlGaAs Fabry-Perot lasers are an excellent candidate for that application, and are used in commercially available amplifiers.

Finally, future soliton systems will operate at 1.5 μm for compatibility with EDFA's. They must generate 10-20 psec transform-limited pulses to allow for multigigabit-per-second transmission on trans-Atlantic and trans-Pacific routes. Fiber-ring soliton lasers do have the foregoing desirable properties, and have been successfully used in laboratory experiments. It remains to be seen, however, whether or not laboratory fiber-ring soliton lasers will lead to robust commercial transmitters.

7. References

[1] L.G. Kazovsky, C. Barry, M. Hickey, C. Noronha and P. Poggiolini, "Wavelength Division Multiplexed Local Area Networks," IEEE LTS, May 1992.

[2] J.A. Chiddix, H. Laor, D.M. Pangrac, L.D. Williamson and R.W. Wolfe, "AM Video on Fiber in CATV Systems: Need and Implementation," IEEE Journal on Selected Areas in Communications, Vol. 8, No. 7, September 1990.

[3] S. Saito, et al. "Coherent transmission experiment over 2223 km at 2.5 Gbit/s using erbium-doped fibre amplifiers," Electronics Letters, 1 May 1990, vol.26, no.10, p. 669-71.

[4] E. Desurvire, "Erbium-doped fiber amplifiers," OFC' 91, Tutorial Sessions, pp 206-259, San Diego, CA, 1991.

[5] L.F. Mollenauer, "Solitons in Ultra Long Distance Transmission," OFC' 91, Tutorial Session, pp 164 -205, San Diego, CA, 1991.

Suppression of Four Wave Mixing Crosstalk in WDM Systems Using Manchester Coding and DPSK Modulation

Hojoon Lee and Leonid G. Kazovsky

Stanford University

Department of Electrical Engineering

Durand Building 202

Stanford, CA 94305-4055

Tel.(415) 725-3818, Fax.(415) 723-9251

E-mail leonid@sierra.stanford.edu

Suppression of Four Wave Mixing Crosstalk in WDM Systems Using Manchester Coding and DPSK Modulation

Hojoon Lee and Leonid G. Kazovsky

Stanford University

Department of Electrical Engineering

Durand Building 202

Stanford, CA 94305-4055

Tel.(415) 725-3818, Fax.(415) 723-9251

E-mail leonid@sierra.stanford.edu

Abstract

The detrimental impact of four-wave mixing on WDM systems can be alleviated using Manchester-coding and DPSK modulation. Maximum transmission distance can be extended to 300 Km for 1 Gbps/channel systems with 10 GHz channel spacing.

Suppression of Four Wave Mixing Crosstalk in WDM Systems Using Manchester Coding and DPSK Modulation

Hojoon Lee and Leonid G. Kazovsky

Stanford University

Department of Electrical Engineering

Durand Building 202

Stanford, CA 94305-4055

Tel.(415) 725-3818, Fax.(415) 723-9251

E-mail leonid@sierra.stanford.edu

Introduction: The performance of optical WDM systems may be degraded by four-wave mixing (FWM)[1,2,3,4]. Previous studies investigated FWM in non-return-to zero (NRZ) system only, neglected other noise sources, such as shot noise[5], and did not take into account the spectral distribution of FWM.

In this paper, the performance of optical Manchester-coded WDM systems is evaluated. Our analysis takes into account both shot noise and FWM. We show that Manchester coding reduces the impact of FWM on WDM systems, particularly when used in conjunction with DPSK. Our analysis does take into account the spectral distribution of FWM, and so is more accurate than previous studies.

System Under Study: Fig. 1 shows the block diagram of an optical WDM system employing Manchester coding and block diagram of ASK and DPSK receivers. To investigate the impact of FWM, we use the first order nonlinear differential equation[1]:

$$\frac{d}{dz}E_\rho(\omega,z) = -\frac{1}{2}\alpha E_\rho(\omega,z) + \sum_{\mu,\nu} j\frac{2\pi\omega_c}{nc}(D\chi_{1111})\exp(j\Delta kz)$$

$$\cdot\exp(-\frac{3}{2}\alpha z)\int_{-\infty}^{\infty}d\omega'\int_{-\infty}^{\infty}d\omega'' E^*_{\mu+\nu-\rho}(\omega'+\omega''-\omega)\cdot E_\mu(\omega')\cdot E_\nu(\omega'')$$

The numerical analysis was conducted for the following system parameters: wavelength λ=1.55 μm, fiber attenuation α=0.2 dB/Km, channel spacing 10 GHz, bit rate 1 Gbit/s, effective core area $32\cdot\pi$ μm^2 for non-dispersion shifted fiber (NDS) and $16\cdot\pi$ μm^2 for DS fiber, and group velocity dispersion 15 ps/Km·nm for NDS and 1 ps/Km·nm for DS.

BER Results: Fig. 2 shows BER for the 8th channel (other channels have better BER) of a 16 channel WDM system using a DS fiber versus the optical fiber input power for several values of the fiber length. The decrease of BER at low powers is due to shot noise and the increase of BER at high powers is due to FWM that is proportional to the cube of the signal power. Because the spectral width of Manchester-coded signals is wider than that of NRZ signals, the impact of FWM on Manchester-coded systems is less severe. The maximum transmission distance of Manchester-coded systems is 220 Km for ASK and 247 Km for DPSK; this is 10 Km more than that of NRZ-coded system.

The system dynamic range is defined as the ratio of the maximum fiber input power to minimum fiber input power to maintain BER below 10^{-9}. Manchester-coded 100 Km systems have some 2 dB larger dynamic range than corresponding NRZ systems.

Maximum Transmission Distance: Fig. 3 shows the maximum transmission length versus the number of channels; all calculation are for the worst-case channel. Manchester-coded systems have the maximum transmission distance larger than that of NRZ coded system by 10 Km; DPSK systems outperform ASK systems by some 27 Km, and the NDS fiber outperforms

the DS fiber by some 51 Km. The physical reason for the latter is that the transmission length is limited by the FWM rather than by chromatic dispersion in the case considered.

Conclusions: Fiber-induced FWM limits the maximum transmission distance of WDM systems. Manchester coding used in conjunction with DPSK modulation extends the transmission distance tc 247 Km is compared to 210 Km for NRZ-coded ASK systems. This result refers to dispersion-shifted 16 channel 1 Gbps/channel systems with 10 GHz channel spacing.

REFERENCES

1. K. O. Hill, et. al., J. of Appl. Phys., 49, 5098, (1978).

2. A. R. Chraplyvy, J. of lightwave Tech., 8 , 1548, (1990).

3. R. G. Waarts, et. al., Proc. IEEE, 78, 1344, (1990).

4. K. Inoue, et.al., Optics Lett., 14, 584, (1989).

5. E. Lichtman, J. of Optical Comm., 12, 53, (1991).

FIGURE CAPTIONS

Fig. 1. (a)Block diagram of an optical wavelength-division-multiplexing system.
(b) A Heterodyne ASK Receiver, (c) A Heterodyne DPSK Receiver.

Fig. 2. The bit error rate of a 16 channel ASK and DPSK coherent WDM system using the DS fiber versus the optical fiber input power; the parameter is the transmission distance.

Fig. 3. Maximum transmission length versus number of channels for various modulation formats and coding methods.

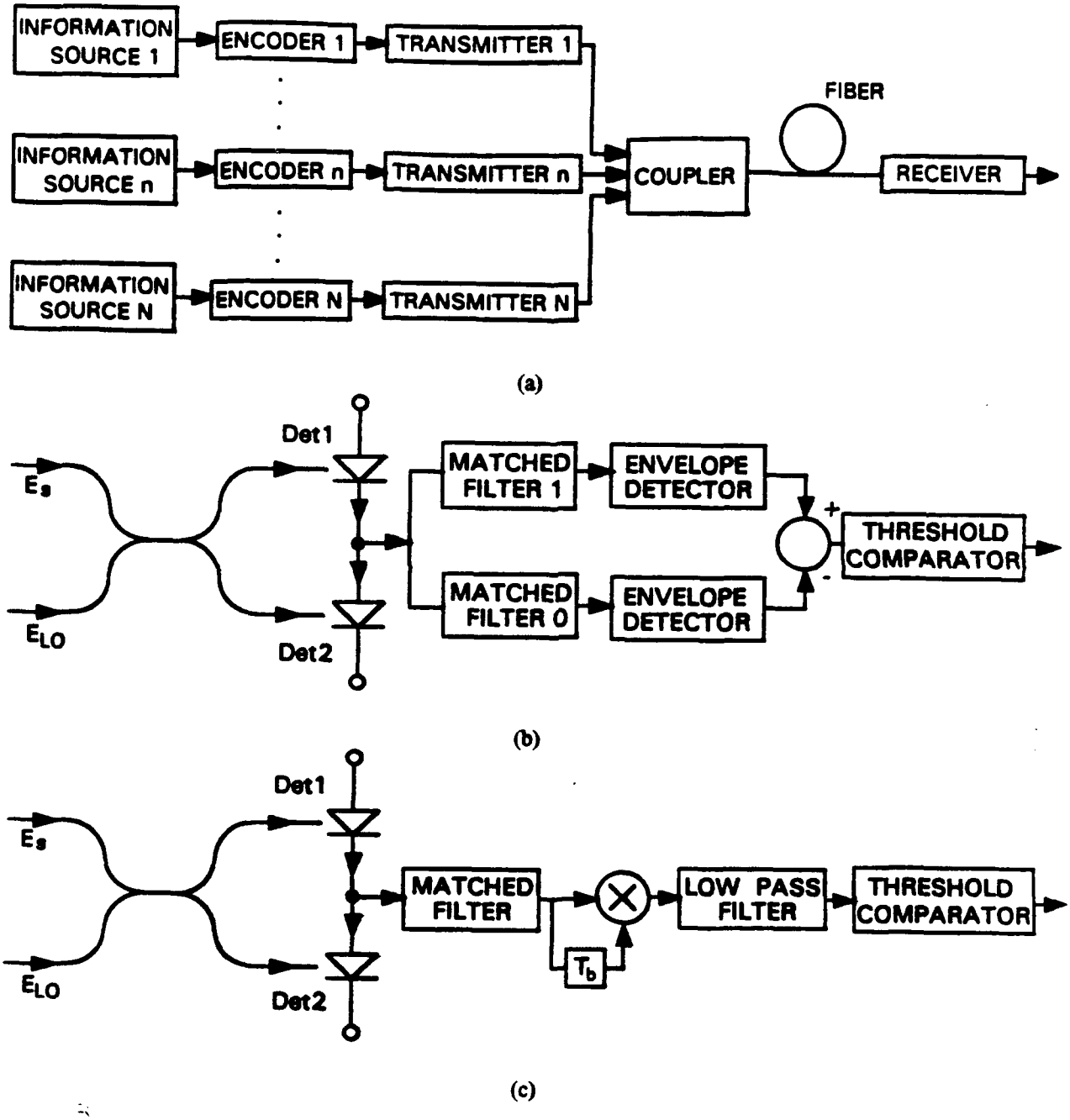

Fig. 1. (a)Block diagram of an optical wavelength division multiplexing system.
(b) A Heterodyne ASK Receiver, (c) A Heterodyne DPSK Receiver.

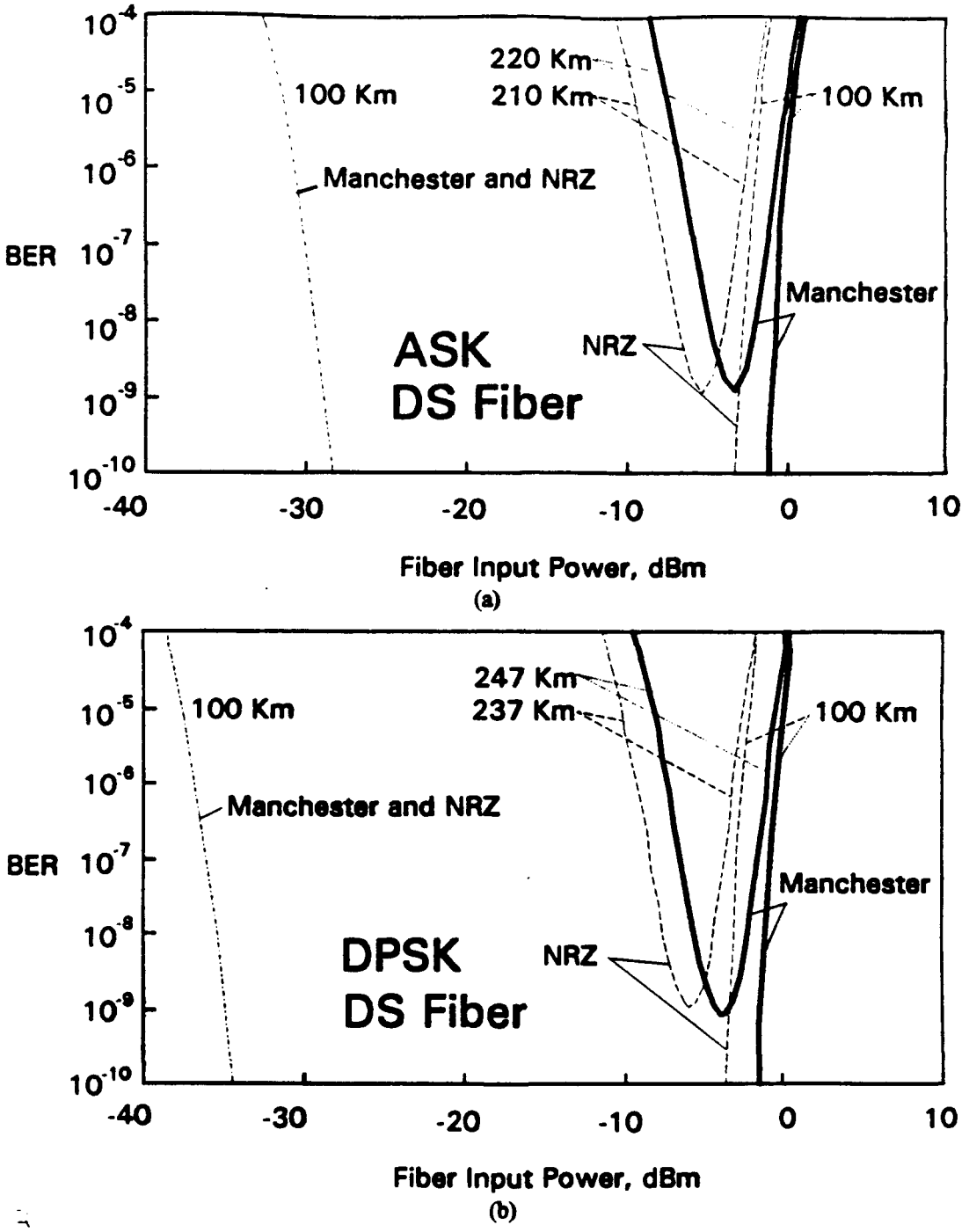

Fig. 2. The bit error rate of a 16 channel ASK and DPSK coherent WDM system using the DS fiber versus the optical fiber input power; the parameter is the transmission distance.

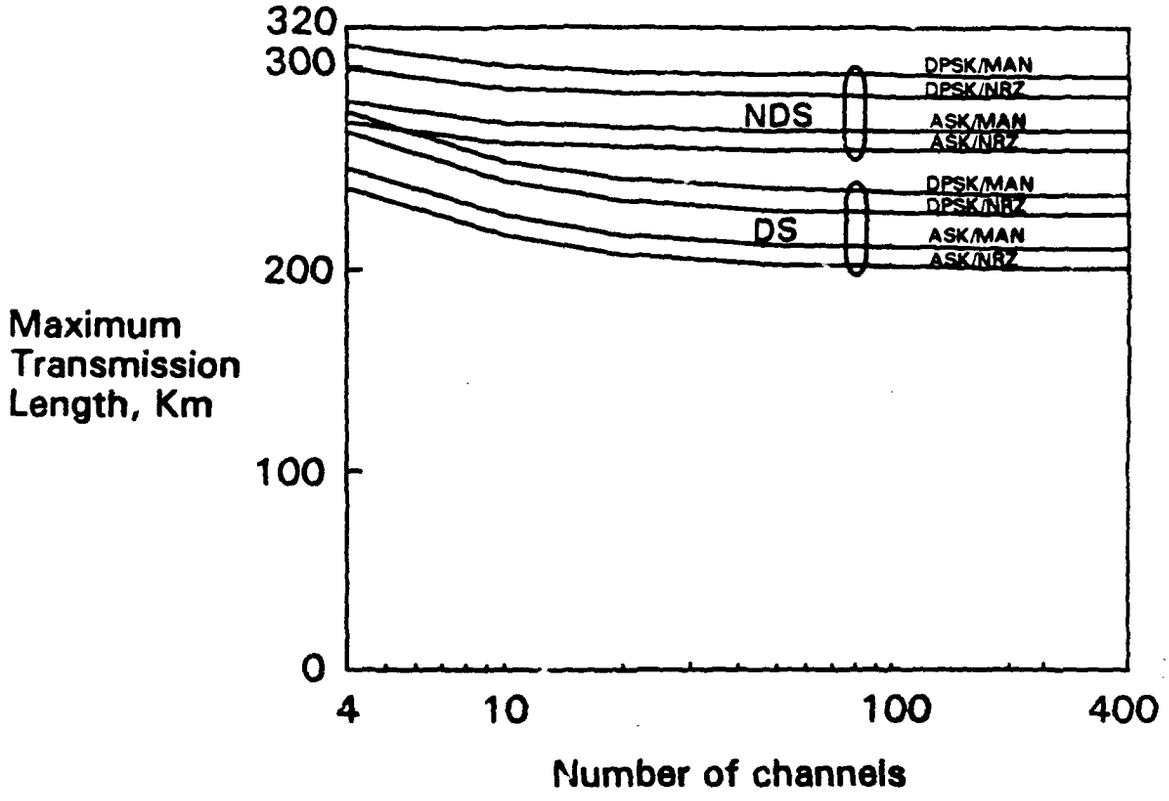

Fig. 3. Maximum transmission length versus number of channels for various modulation formats and coding methods.

Tutorial overview: Multigigabit optical networking

Leonid G. Kazovsky, Karen Liu*, Ciro A. Noronha Jr

Stanford University, Stanford, CA 94305
*IBM T.J. Watson Research Ctr., Yorktown Heights, NY 10598

ABSTRACT

What is multigigabit optical networking? This is a term we are using loosely to refer to the networks with multiple gigabit data channels in order to distinguish them from networks whose aggregate bit rate is on the order of 1 Gbit/s. Current computer networks, such as Ethernet, FDDI and DQDB, suffer from lack of concurrency: at a given time, only a small number (typically one) of computers can transmit new information into the network. Therefore, each computer has to operate at the network aggregate speed, although effectively it has access only to a fraction of that bandwidth. To achieve gigabits/sec throughput, the next generation of computer networks will have to provide multiple high-speed concurrent channels to the nodes. One way to achieve concurrency is to use electronic switching, thereby placing the burden on the switch rather than each computer. Another direction is to place the burden on the optical hardware. Optical transport facilities have been recognized as an excellent choice for gigabits/sec networks due to the high bandwidths and long distances that can be reached. Moreover, WDM optical techniques allow multiple concurrent channels to be created in the same fiber, and with tunable transceivers one can potentially create networks whose topology changes dynamically in response to changing traffic patterns. In this paper, we will review a few current implementations of very high-speed networks as a background context, and then describe several prototype optical networks.

1. INTRODUCTION

Point-to-point link speeds are now in the several hundred Mb/s to 1 Gb/s range. Such high speeds mean that the functional bottlenecks are now elsewhere in the network. Gigabit networks are considered a revolutionary step in data communications because, for the first time, propagation delay as measured in bits in transit dominates over delay due to the limited bandwidth of the communications link. In other words, as far as the recipient of the data is concerned, increasing the transmission speed of the link will not bring him his data any sooner. The optical communications community can be proud of their part in the fiber optics revolution which has enabled this step.

However, now the ball is back in our court to define our next contribution to data communications. Simply adding yet more transmission speed is unlikely to be as widely appreciated as before since it will mean an incremental change. Also, few applications require more than 1 Gb/s especially in view of progress in data compression. There does exist a problem to be solved despite the existence of gigabit links. How can a large number of high speed links be set up, switched, and otherwise controlled efficiently? Since the problem is now not so much to provide more raw bandwidth, as to deal with the multiplicity of data streams, we call the next generation MULTI-gigabit (e.g. rather than Tbit) networks. For this function, new architectures and approaches are necessary.

Let us first look at the desired functions. In addition to existing services (remote logins, file transfer, voice), future networks will be required to support broadband services. Broadband interactive services have been classified by CCITT Recommendation I.121[1] into the following categories:

- Conversational Services: real-time end-to-end information transfer, such as video- telephony, high-definition image transfer, high-speed data transfer;
- Messaging Services: communication via store-and-forward, such as multimedia mail;
- Retrieval Services: retrieval of information stored in databases, such as video on demand, or high-fidelity audio.

To provide the services described above, a network will have to handle both stream traffic (i.e., uncompressed video and audio) and bursty traffic (i.e., variable bit rate video, bursty data, etc.), at a range of data rates which spans several orders of magnitude. Some data rates required to provide broadband services are shown in Fig. 1.

Current network topologies, such as Ethernet, FDDI (Fiber-Distributed Data Interface) and DQDB (Distributed-Queue Dual Bus) provide connectivity between the nodes by means of a small number of shared channels (one, or two, in the case of DQDB). This has two consequences: (i) all the nodes have to operate at network aggregate speed, and (ii) on the average, the capacity available per node is no more than C/N, where C is the aggregate network capacity, and N is the number of nodes.

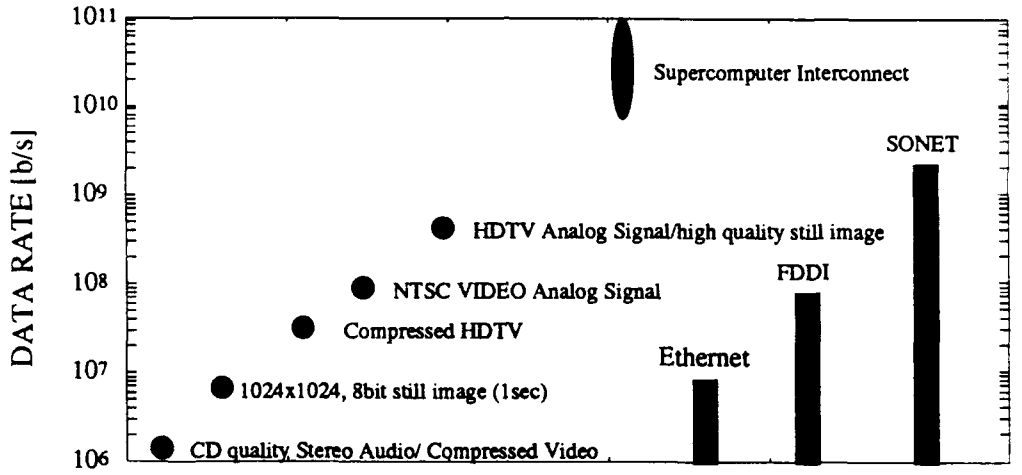

Figure 1: Data rate requirements for broadband services[2]

Due to the high data rate requirements, single channel networks will be unable to provide the required level of service because each node would have to operate at the network aggregate speed, which is neither possible (due to the high speeds involved) nor desirable (due to the low efficiency). Multiple-channel topologies, capable of concurrent transmission, are needed, and optical transport mechanisms are an excellent choice.

In a network composed of multiple channels, some sort of switching between them is needed, except in the trivial case of a fully connected mesh. Two approaches have been proposed and used to provide this switching function:

a. Centralized *electronic* switching: switching is provided by one or more electronic switches, which transfer data from channel to channel; and

b. Distributed *optical* switching: switching is performed at the periphery of the network by optical means.

In the remainder of this paper, we will discuss some examples of practical implementations of these two approaches.

2. MULTIGIGABIT NETWORKS BASED ON ELECTRONIC SWITCHING

In this section we will consider networks where the optical medium is used only convey point-to-point data. Switching between channels is done electronically, at the center of the network, as illustrated in figure 2, where we have shown the transmit and receive sides of each node separately for the sake of clarity. The modules marked "E-O" and "O-E" perform the electrical-to-optical and optical-to-electrical conversions respectively.

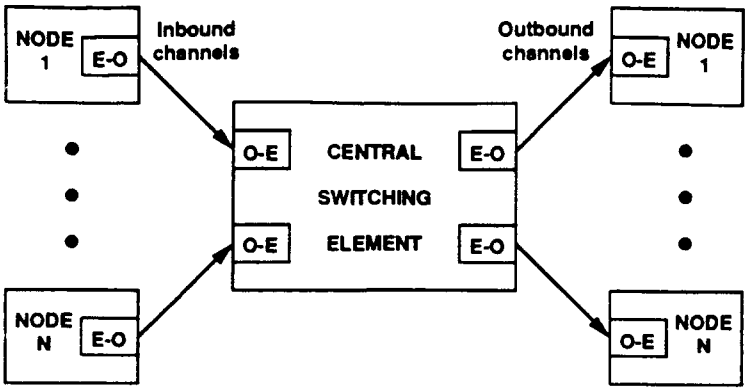

Figure 2: General model model for networks with central switching

2.1 HIPPI and the Fiber Channel

HIPPI (High-Performance Parallel Interface) was started at the Los Alamos National Laboratory in 1987 as an effort to standardize the physical interconnection between supercomputers[3]; it is now under the responsibility of ANSI Task Group X3T9.3. HIPPI provides a simplex (i.e., unidirectional) point-to-point parallel data path, operating at either 800 Mb/s or 1.6 Gb/s; the latter requires two physical connections. A full-duplex link is built by having two simplex links, one on each direction. The original HIPPI standard specified a parallel metallic cable, reaching a maximum distance of 25 m; latter, an extension called "serial HIPPI"[4] was proposed to increase the distance. Serial HIPPI uses 9-μm single-mode fiber and a pigtailed laser operating between 1285 and 1330 nm, with a mean launch power of -9 to -6 dBm, to reach a distance of up to 10 km.

The HIPPI standard also specifies a protocol to interact with a switch and open/close a "connection"; the physical structure is the one shown in figure 2. This is a circuit switch, i.e., a physical path is established between the source and the destination and is kept in place during the life of the connection.

Two flavors of HIPPI switches, both full cross-point switches handling parallel data, are currently commercially available. The 8×8 switch is dumber but faster, with circuit set up times under 1 microsecond and latency through the switch of 160 nsec (4 clock cycles). The fast set-up is possible because source-routing is used, where the switch needs only to examine a specific part of the header field to see how it should configure itself. The 32×32 switch is somewhat slower because it incorporates a microprocessor to allow more complex routing functions including destination routing where the switch has to first determine the routing before performing it. Latency is still only 240 nsec. Since the switch handles parallel data, scaling the switch size up will involve significant increases in hardware complexity. Also, a small amount of additional delay and complexity is required to use the switch with serial HIPPI due to the need to de-serialize and serialize at the output[5].

The Fiber Channel (FC)[3,6] is a follow-on to HIPPI, also being developed at the X3T9.3 Task Group. It is also a point-to-point interface, but with more capabilities. FC supports four data transfer rates: 100, 200, 400 and 800 Mb/s. The physical media can be single or multimode fiber, or even coaxial cable for short distances. The transmitter can either be a light-emitting diode (LED) or a laser.

The physical model for FC is shown in figure 3. The N_Port is the host interface; it has a transmitter and a receiver, which together form a full-duplex path. N_Ports may be interconnected together in point-to-point applications. A fabric interconnects the N_Ports, and is used to route frames between the hosts. Three classes of service have been defined, which determine the way the fabric routes the frames:

- **Class 1: Dedicated Connection.** This is a circuit connection. Once established, a dedicated connection is guaranteed by the fabric. Frames from the source N_Port are delivered to the destination

N_Port in order. Flow control is also provided. This class is intended for applications such as movie-quality animation and distributed computation.

- **Class 2: Multiplex**. This is a connectionless service; in other words, a path is not necessarily reserved for this kind of traffic inside the switch. The fabric may not guarantee in-order delivery of the frames, but in the absence of link errors, notification of delivery (or failure to deliver) is guaranteed. This class is intended to be used in applications such as communication with devices.
- **Class 3: Datagram**. This is also a connectionless service, like class 2, but the fabric does not guarantee in-order delivery nor notification of success/failure. In other words, the fabric will try to deliver the frames, but no guaranties are given, and no confirmations will be sent. This class is viewed as the data link layer for connectionless protocols like IP.

The first commercially available FC switch has been implemented as a dynamically non-blocking switch composed of 16-channel modules which accept serial data. Four such modules can be stacked together to yield a 64 × 64 port switch. In principle, a 4096 × 4096 statically non-blocking switch can be built from the modules with the addition of additional cross-connect hardware. So far, the 256 Mb/s links and switches have been delivered, with the 1 Gb/s version due at the end of the year. Switching latencies are on the order of 200 microseconds for all classes of services on the current 256 Mb/s version but an order of magnitude decrease is expected with a faster processor. Travel time delay through the switch, once the connection is set up, is less than 1 microsecond. The present links are designed for 2 km distances, but 10 km will be available as well[7].

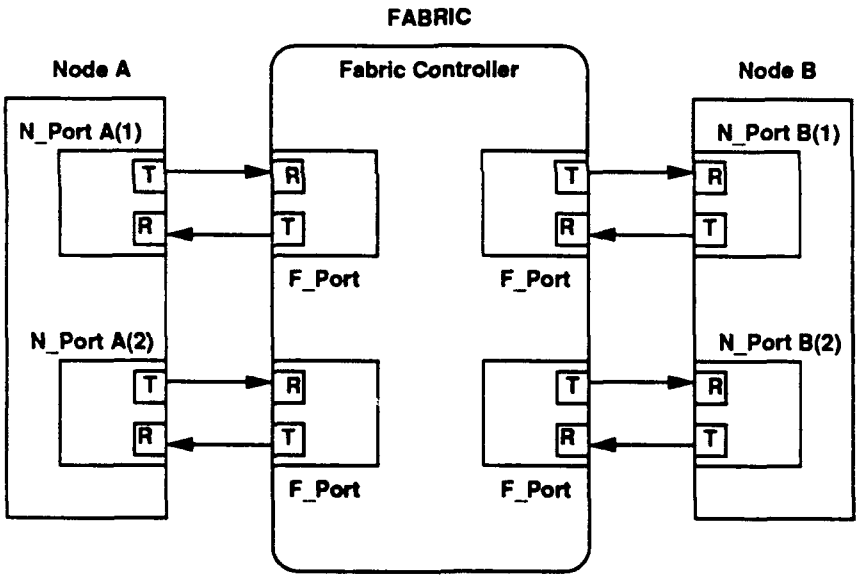

Figure 3: Physical model for a fiber channel interconnection

2.2 The plaNET/ORBIT High-Speed Network

The plaNET/Orbit is a gigabit networking system being developed at IBM[8]. It has two components: a Wide-Area Network (WAN) consisting of fast packet plaNET switches connected by point-to-point links forming a backbone connecting multiple local area networks (LANs) in the form of ORBIT (Optical Ring with Buffer Insertion Technology) rings. Both ORBIT and plaNET use the same protocols, to ease the interoperability between them. The topology is illustrated in figure 4.

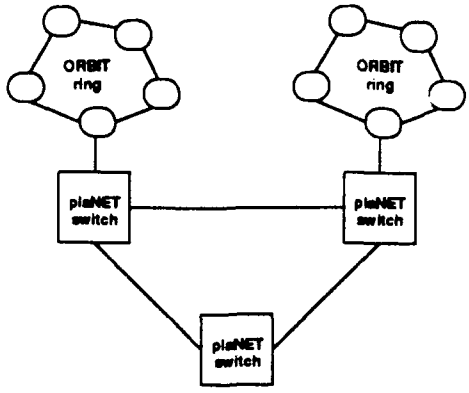

Figure 4: plaNET/ORBIT network model

The ORBIT network can be seen as the local access to the plaNET switch. As indicated by the name, it operates as an insertion ring (i.e., a ring where data is inserted by the sender and retrieved by the destination; a node must "save" enough empty slots before it is allowed to transmit). The ring speed is 1 Gb/s, but since concurrent transmission in different parts of the ring is allowed, the aggregate throghput can be higher, depending on the traffic patterns. The plaNET switch is a shared-medium switch capable of switching both fixed-size ATM cells and variable-size packets, and performing additional functions like multicasting. The design philosophy behind the fast packet switch is to provide a "transparent" transport mechanism, where the network manipulation of the data is minimized, and all packet handling is done in hardware. The purpose is to be able to handle heterogeneous traffic (different priorities, loss requirements, packet lengths, routing methods) in a fast, simple way. Currently, the shared medium is a 64-bit wide bus with a total speed of 6 Gb/s, leading to a maximum switch size is 8×8 for 800 Mb/s on each adaptor. The next generation will use shared memory, and is expected to support 32×32 ports, each slightly over 1 Gb/s. plaNET will initially support three interfaces:

(a) 155 and 622 Mb/s SONET interfaces;

(b) a 1 Gb/s point-to-point optical interface (over "dark" fiber); and

(c) the ORBIT interface.

IBM and Rogers Cable Co. are currently conducting a joint field trial of ORBIT and plaNET in Toronto. Field deployments with other partners are planned. In addition, ORBIT and plaNET will be used in the AURORA testbed, described in the next section.

2.3 The AURORA Testbed

The AURORA testbed[9] is one of five gigabit testbeds currently underway as part of a national effort in high-speed networking. AURORA is a collaboration between Bellcore, IBM, MIT and the University of Pennsylvania, to evaluate technologies supporting network operation at or near gigabit speeds in a wide-area network. It will support both fixed-size ATM packets (cells) and variable-size packets. The four sites will be interconnected by three OC-12 (622 Mb/s) SONET links. Bellcore's Sunshine ATM switch and IBM's plaNET switch (for variable-size packets) will be tested in this environment. The topology is depicted in figure 5.

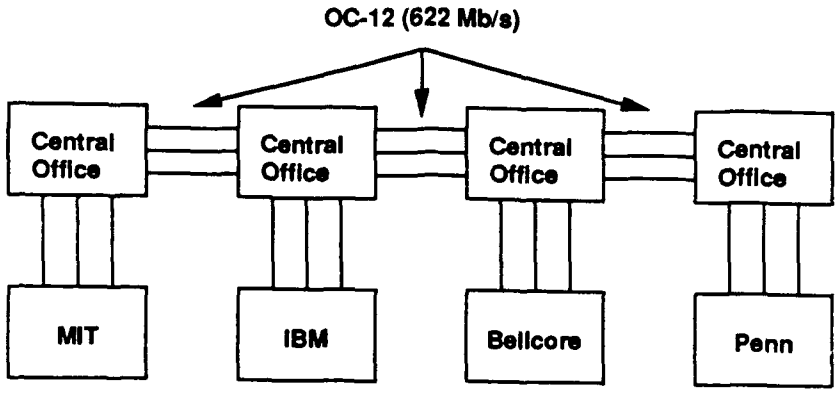

Figure 5: AURORA testbed topology

Two separate networks will be provided: one based on plaNET, supporting variable-size packets, and the other based on Sunshine, supporting fixed-size ATM cells. The central offices have the ability of independently cross-connect the OC-12 links, making it possible to create a large number of *logical topologies* over the *physical topology* of the the network. With this setup, the bandwidth between any two nodes on each of the two networks is at least 622 Mb/s. Deployment is planned for early 1993.

The physical testbed will also be used to test concepts in network protocols, network control and management, and applications that use gigabit capabilities such as video conferencing and multimedia services.

3. MULTIGIGABIT NETWORKS BASED ON OPTICAL SWITCHING

Another way to implement the switching function between the channels is to perform it in the periphery of the network, in a distributed fashion. In an optical network, a natural way to create multiple channels is through the use of Wavelength-Division Multiplexing (WDM). The switching function is then performed by tunable receivers and/or transmitters that select between the available channels (wavelengths), and superimpose a generic *logical topology* over the *physical topology*. The physical topology can be arbitrary, as long as all receivers can access the combined light signal from all transmitters. From a power distribution point of view, the optimum topology is the passive star, as depicted in figure 6 (note the similarity between figure 6 and figure 2; both represent star topologies at the physical level).

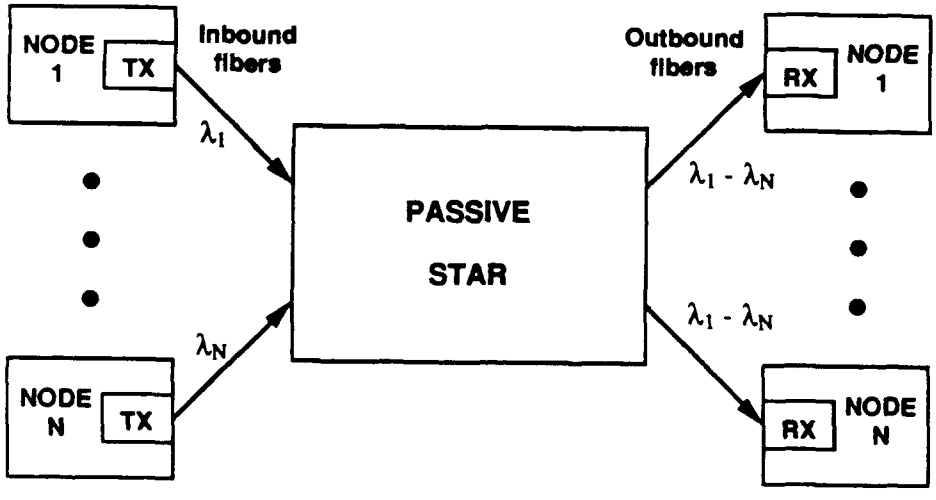

Figure 6: The WDM star topology

The last five years have seen a steady transition of WDM experiments from proof of concepts to experimental networks, with field trials planned in the near future. We will describe here some recent experimental demonstrations of WDM optical metropolitan and local area networks[10].

3.1 TeraNet

TeraNet[11] is a experimental network being developed to study all seven layers of the OSI standard. The network provides either 1 Gb/s ATM packet-switched or 1 Gb/s circuit-switched access using a passive star topology, as shown in figure 7. A hybrid multiple access scheme combines wavelength-division-multiplexing and subcarrier frequency division multiplexing to divide the available optical bandwidth. This method of multiple access reduces the bandwidth requirements on the optical filters but still allows the use of additional channels through electronic means. Each user is assigned a unique address consisting of a specific wavelength and a subcarrier multiplexed frequency. Wavelength channels are spaced by 1.5 nm, or 187 times the bit rate. Each wavelength supports 4-6 subcarrier channels. The receivers use fiber-optic Fabry-Perot (FFP) tunable filters to select wavelengths. Subcarriers are selected by electronic filtering. A packet-switched network, conforming to the ATM standard[12], is being implemented through a multihop architecture. The network can be configured to support up to 64 users. Interfaces are also being developed for SONET and HIPPI. A limited campus field trial is planned for 1992.

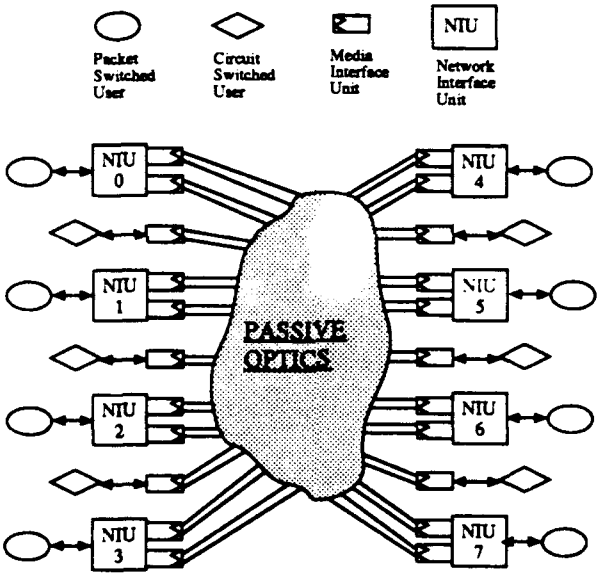

Figure 7: The TeraNet WDM network (adapted from ref. 11)

3.2 RAINBOW

The RAINBOW network[13] is a metropolitan area network designed to cover a diameter of 25 km. This network connects up to 32 IBM PS/2's through a 32 x 32 passive star coupler and allows the computers to communicate circuit-switched data at a rate of 300 Mb/s/node, yielding an aggregate throughput of up to 9.6 Gb/s. The network's physical topology is the passive star shown in figure 6. Each computer is equipped with its own fixed frequency optical transmitter and tunable optical receiver. The optical transmitters utilize directly modulated distributed feedback (DFB) laser diodes. Wavelength selection at the receiver is accomplished with a tunable fiber Fabry-Perot filter whose cavity spacing is varied piezoelectrically. The time for the receiver to identify and lock to a channel is 10 ms. The signalling protocol to coordinate the retuning of the optical receivers is a simple in-band polling procedure. This method is simpler than a faster out-of-band protocol, which would require a separate signalling channel. The transmitter, receiver and

associated electronics are implemented on a single adaptor circuit board, much like an FDDI or token-ring adaptor card. The current version of Rainbow has been prototyped and demonstrated at Telecom '91 and other trade shows. New versions of Rainbow, supporting 1 Gb/s/node, are planned for the future[14].

3.3 UCOL

UCOL is being developed as an ultra-wideband coherent optical local area network[15]. This network has network interface units/access control units (NIU/ACU's) that communicate on 20 wavelength division multiplexed optical channels over a passive star topology, as indicated in figure 8. The user can access each channel through a time division multiplexing access mode (UCOL ATM SWITCH). This technique supports data rates from a fraction of a Mb/s up to 155 Mb/s. The frequency reference for all transmitters and receivers is provided over a separate star coupler by a reference generator block (RGB). The transmit power is set for operation with a Bit Error Ratio (BER) of 10^{-6}. Error-correcting codes are then used to decrease the BER to a value less than 10^{-13}.

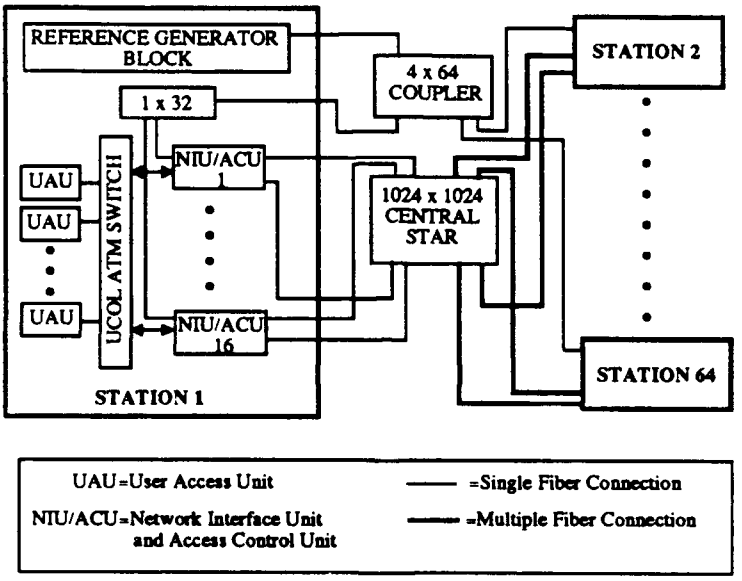

Figure 8: UCOL block diagram (adapted from ref. 15)

3.4 STARNET: a coherent broadband optical network

STARNET[16] is a broadband optical local area network architecture. The STARNET architecture offers all users both a high-speed packet switched network and a multi-gigabit broadband circuit interconnect based on a WDM transport facility, as shown in figure 9. As a result, the STARNET architecture efficiently supports diverse types of traffic. An experimental demonstration of STARNET is currently under development in the Optical Communications Research Laboratory at Stanford University. The initial STARNET experiment will interconnect four workstations through a 4 x 4 passive star coupler. The data rate for the broadband circuit switched network is 2.5 Gb/s/station. The packet switched network data rate is 100 Mb/s.

STARNET's physical topology is the passive star shown in figure 6. However, each node transmitter transmits two independent data streams, stream 'C' (Circuit data) and stream 'P' (Packet data). This is accomplished by phase-modulating the transmitter laser with the 'C' stream, and amplitude-modulating the 'P' stream, with low modulation index. Each node has a tunable receiver that can be tuned to any transmitter and decodes the 'C' stream thus enabling a broadband circuit interconnect among all the nodes. In addition, every node is equipped with a fixed receiver which decodes the 'P' stream of the previous node in the frequency comb. The first node of the chain is equipped with a receiver that decodes the 'P' stream

of the last node: In this manner, a unidirectional logical ring topology similar to that of FDDI is formed, as shown in figure 9.

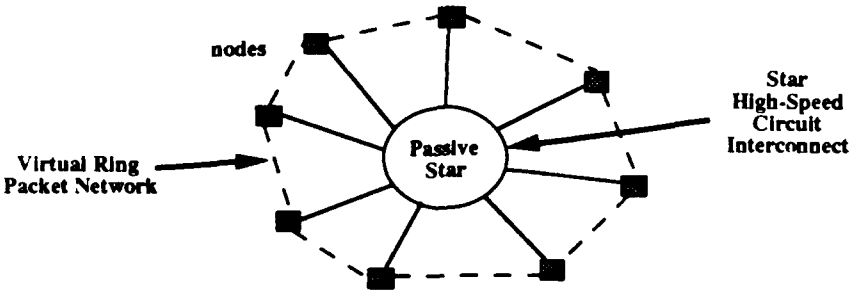

Figure 9: STARNET offers both a packet-switched ring and a circuit interconnection

Each node consists of a transmitter, a 2.5 Gb/s broadband receiver for the circuit interconnect, and a 100 Mb/s receiver for the packet-switched network, which uses off-the-shelf FDDI cards to interface with the workstation. The network operates at a center wavelength of 1319 nm over conventional single mode fiber with a network diameter of 4 km. The system is designed to ensure a BER of 10^{-9} with a 10 dB system margin.

3.5 Comparison of the networks with optical switching

Many challenges are yet to be resolved before multi-Gigabit/s optical networks become practical. Among these challenges are the development of fast tunable and narrow linewidth lasers, tunable filters, automatic frequency selection, frequency stability of the network, design of network protocols efficient for high speed bursty and continuous traffic, and selection of network topologies which optimize both throughput and latency. Table I presents a comparison of the experimental WDM networks discussed in this section.

TABLE I: EXPERIMENTAL WDM NETWORKS

Parameter	TERANET[11]	RAINBOW[13]	UCOL[15]	STARNET[16]
Modulation Format	ASK	ASK	DPSK	PSK
Data Rate	1 Gb/s	300 Mb/s	155 Mb/s	3 Gb/s
Channel Separation	187 Bit rates	1040 Bit rates	23 Bit rates	2.7 Bit rates
Kind of Receiver	Dir. Detection	Dir. Detection	Coherent	Coherent
Tunable Element	Fabry-Perot Filter	Fabry-Perot Filter	Laser	Laser
Frequency Stabilization	Thermal	Thermal	External Reference	Provided by the architecture
Polarization Control	Not needed	Not needed	Polarization Diversity	Manual
Receivers per Node	2/tunable	1/tunable	1/tunable	1/tunable 1/fixed
Transmitters per Node	2/fixed	1/fixed	1/tunable	1/fixed
Extra Features	Multiple subcarrier channels		Wide range of data rates supported	Lower speed packet network embedded

4. CONCLUSIONS

The key to achieving multi-gigabit throughputs in the next generation of networks is concurrency. In the presence of multiple concurrent channels, some sort of switching is needed; this function can be performed either at the center or at the periphery of the network. In both cases, the network assumes a star topology at the physical level.

In the first case, an electronic switch is placed at the center of the network, and it performs most of the routing functions (i.e., the "intelligence" of the network is concentrated at the center). Switching can be done very fast, in a packet-by-packet basis for some switches. Optics is used only for point-to-point connections. However, this kind of network has a single point of failure (the switch). It is generally not easy to upgrade (i.e., to add more nodes the switch has to be upgraded; to increase the access data rate, the switch has to be replaced). While it is simple to route a given message through multiple switches, cascading multiple switches might cause the links between the switches to become bottlenecks.

In the latter case, the center of the network is just a passive star coupler, and is even data-rate independent. The "intelligence" of the network is distributed between the nodes, leading to improved fault-tolerance. Expansion of the network to add more nodes is trivial. The topology need not be restricted to a simple single star. The switching times, however, are not as fast as with electronic switching, and the technology itself is not as mature.

At this point, it is not clear which scheme will prevail in the multigigabit arena, if any. The answer to this question is heavily dependent on how the device technology will evolve (in both fields) on the next few years.

5. ACKNOWLEDGMENTS

C. Noronha is supported by a graduate scholarship from FAPESP.

6. REFERENCES

1. CCITT Recommendation I.121, "Broadband Aspects of ISDN," Blue Book, fascicle III.7, pp. 34-61, Melbourne 1988.
2. F. Tobagi, "High-Speed Networking and B-ISDN," *INFOCOM 1991 Tutorial*, Bal Harbour, Florida, April 9-11, 1991.
3. D. E. Tolmie, "Gigabit Networking," *IEEE LTS*, May 1992, pp 28-36.
4. Serial HIPPI Implementors Group, "Serial-HIPPI Specification, Revision 1.0," May 17, 1991.
5. PS8 HIPPI Switch and PS32 HIPPI Switch, Network Systems Corp., Minneapolis, MN.
6. D. Getchell and P. Rupert, "Fiber Channel in the Local Area Network," *IEEE LTS*, May 1992, pp 38-42.
7. "Ancor CXT 250/1000 Fiber Optic Communications System Specifications", Ancor Communications, Inc., Minnetonka, MN.
8. I. Gopal and R. Guérin, "Network Transparency: The plaNET Approach," *IEEE INFOCOM 92*, Florence, Italy, May 6-8, 1992, pp 590-601.
9. D.D. Clark et al., "An Overview of the AURORA Gigabit Testbed," *IEEE INFOCOM 92*, Florence, Italy, May 6-8, 1992, pp 590-601.
10. L.G. Kazovsky et al., "WDM Local Area Networks," *IEEE LTS*, May 1992, pp 8-15.
11. R. Gidron et al., "TeraNet: A multi gigabit per second hybrid circuit/packet switched lightwave network," *Proc. SPIE Advanced Fiber Communications Technologies*, Boston '91, Sept. 3-4, pp. 40-48.
12. ANSI, "Broadband ISDN ATM Aspects-ATM Layer Functionality and Specification T1S1.5/90-058R2," Aug. 27, 1990.

13. N. R. Dono et al., "A wavelength division multiple access network for computer communication," *IEEE JSAC*, vol. 8, no. 6, pp. 983-994, Aug. 1990.
14. B. Mukherjee, "WDM-Based Local Lightwave Networks Part I: Single-Hop Systems," *IEEE Network*, May 1992, pp 12-27.
15. A. Fioretti et al., "An evolutionary configuration for an optical coherent multichannel network," *GLOBECOM '90*, San Diego, CA, 2-5 Dec. 1990, pp. 779-783.
16. P. T. Poggiolini, L. G. Kazovsky, "STARNET: an Integrated Services Broadband Optical Network with Physical Star Topology," *Advanced Fiber Communications Technologies*, Leonid G. Kazovsky, Editor, Proc. SPIE 1579, pp. 14-29 (1991).

OPTIMIZATION OF DIRECTLY MODULATED FM-SCM SYSTEMS USING AN OPTICAL FREQUENCY DISCRIMINATOR

G.Fiksman, R.Gross, J.Fan*
GTE Laboratories Inc.
40 Sylvan Road, MS 28
Waltham, MA 02254
Tel. (617) 466-4168
FAX. (617) 890-9320

* STAR Laboratory
Stanford University
Stanford, CA 94305-4055

Abstract

A 10 channel direct detection subcarrier multiplexed system using direct frequency modulation of a DFB Laser and a Fabry-Perot filter for frequency discrimination was implemented and optimized. A Bit Error Rate of 10^{-9} was acheived with a detected optical power of -20 dBm.

OPTIMIZATION OF DIRECTLY MODULATED FM-SCM SYSTEMS USING AN OPTICAL FREQUENCY DISCRIMINATOR

G.Fiksman, R.Gross, J.Fan*
GTE Laboratories Inc.
40 Sylvan Road, MS 28
Waltham, MA 02254
Tel. (617) 466-4168
FAX. (617) 890-9320

*STAR Laboratory
Stanford University
Stanford, CA 94305-4055

Direct frequency modulation of a Distributed Feedback (DFB) semiconductor laser is an attractive technique because it can obtain high modulation depths with low drive powers. For direct detection systems an optical frequency discriminator has to precede the photodetector. Systems that use optical filters as frequency discriminators are also well suited for Wavelength Division Multiplexing (WDM) applications with optical amplifiers [1]. Then, the optical filter also reduces the Amplified Spontaneous Emission (ASE) noise and provides wavelength selectivity. In this paper we report the use of a tunable fiber Fabry-Perot (FFP) interferometer as an optical frequency discriminator for a 10 channel FSK-SCM system in the frequency range 2.1-3.9 GHz. Comprehensive models of the FFP response to an optical FM signal have been developed which accurately predict the optimal system parameters and performance. With each channel operating at 100 Mb/s, a BER = 10^{-9} was achieved with a detected optical power of -20 dBm. The experimental data showed excellent agreement with theory.

The system block diagram is shown in Fig. 1. The light source is a 1/4 wave shifted DFB laser diode emitting at 1.54 μm with a

threshold current of 21.5 mA. The laser was biased at 76 mA and modulated by 10 equally spaced channels.

At the receiver the FFP interferometer (bandwidth=10 GHz, finesse=116) is followed by a PIN photodiode and a low noise microwave amplifier. The transmission point and the stability of the FFP were monitored and controlled by a computer-based feedback loop. Channel selection at the receiver is accomplished via electrical tuning and demodulation of the FSK signal is performed by a delay line discriminator followed by a low pass filter.

Theoretical calculations are obtained using the Bessel function method and the asymptotic method of Carson and Fry to predict the signal power and distortion [2]. The FFP response to the FM and AM portions of the signal (both present in direct modulation) along with the phase difference between them are taken into account [3,4]. Thermal noise, shot noise and intermodulation distortion (IMD) are also included. Both methods show good agreement for the FM indices of interest and the Bessel approach was used for calculations in this paper. The effect of phase noise to intensity noise conversion was found experimentally to be insignificant and therefore not addressed in the models.

Experimental (discrete points) and calculated (continuous lines) results are shown in Figs. 2 and 3. The optical input power was held constant, which produced a photocurrent I_{dc}=10μA at the half power transmission point. In Fig. 2 the CNR is measured for the single channel case using the positive and negative slope of the FFP for optical discrimination. There is a 6 dB difference between the curves due to the AM presence. For the 10 channel case (Fig. 3), measurements are made on the channel with the worst performance (ch. 6 at 3.1 GHz) for various transmission points on the positive slope of the FFP. It is seen that a maximum CNR of 20 dB is obtained with transmission Tx = 0.5 and the FM index $\beta \approx 0.3$, which is also accurately predicted by theory.

In summary, we have implemented a direct detection FM system which incorporates a fiber Fabry-Perot interferometer as an optical frequency discriminator. Optimal conditions are accurately predicted by the theoretical models and experimentally verified. The

models include the effects of the non-linear Fabry-Perot response to the FM and AM signals, the AM-FM phase difference, and the intermodulation distortion.

References

[1] W.I. Way, et al., "160-Channel FM-Video Transmission Using Optical FM/FDM and Subcarrier Multiplexing and an Erbium Doped Optical Fibre Amplifier," Elec. Letters, Vol.26, No. 2, pp. 139-142, 1990.

[2] P.F. Panter, "Modulation , Noise, and Spectral Analysis," McGraw-Hill, 1965.

[3] K.Petermann, "Laser Diode Modulation and Noise," Kluwer Academic Publishers, 1988.

[4] R.S. Vodhanel, et al., "Ten-to-Twenty Gigabit-per-Second Modulation Performance of 1.5-μm Distributed Feedback Lasers for Frequency-Shift-Keying Systems," Journal of Lightwave Technology, Vol. 7, No. 10, pp. 1454-1459, 1989.

Figure Captions

1. Schematic diagram of the direct FM-SCM system with the Fabry Perot optical discriminator.

2. CNR for a single channel at 3.1 GHz operating on the positive and negative slope of the FFP with transmission point Tx = 0.5 and I_{dc}=10 μA.

3. CNR for Channel 6 at 3.1 GHz for the 10 channel case with various transmission points of the FFP.

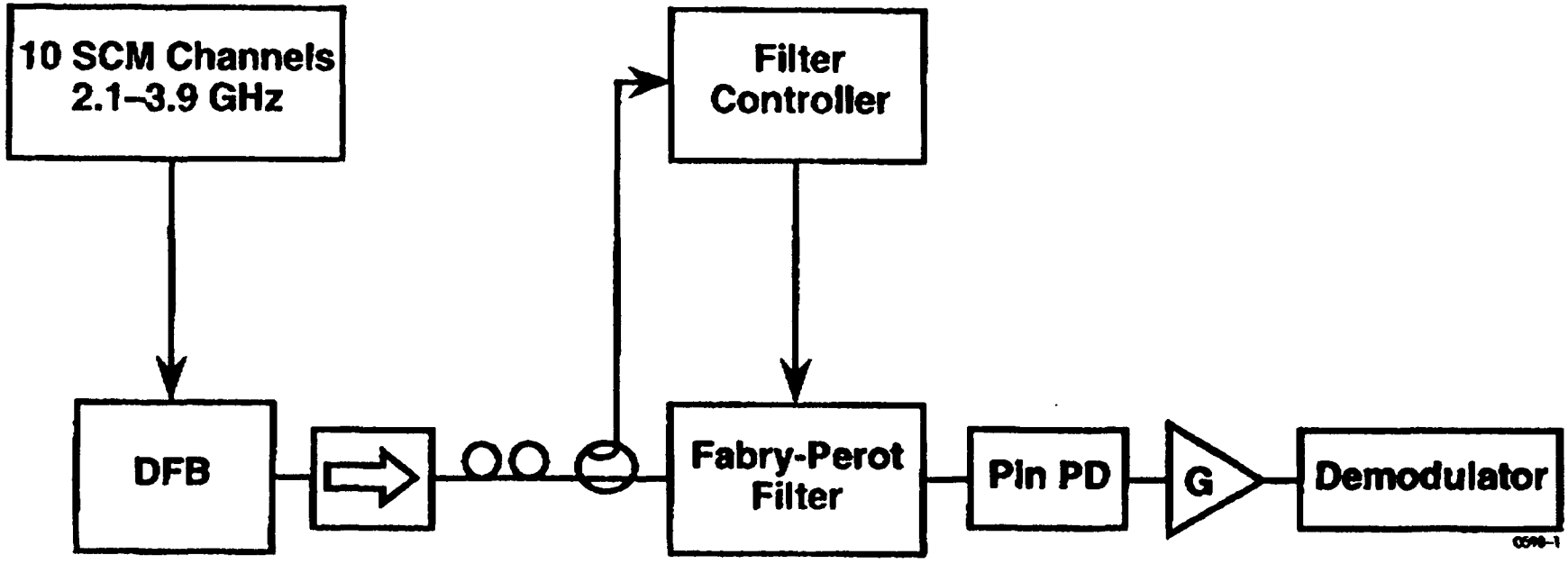
10 SCM Channels
2.1–3.9 GHz
Filter
Controller
DFB
Fabry-Perot
Filter
Pin PD
G
Demodulator

Fig. 1

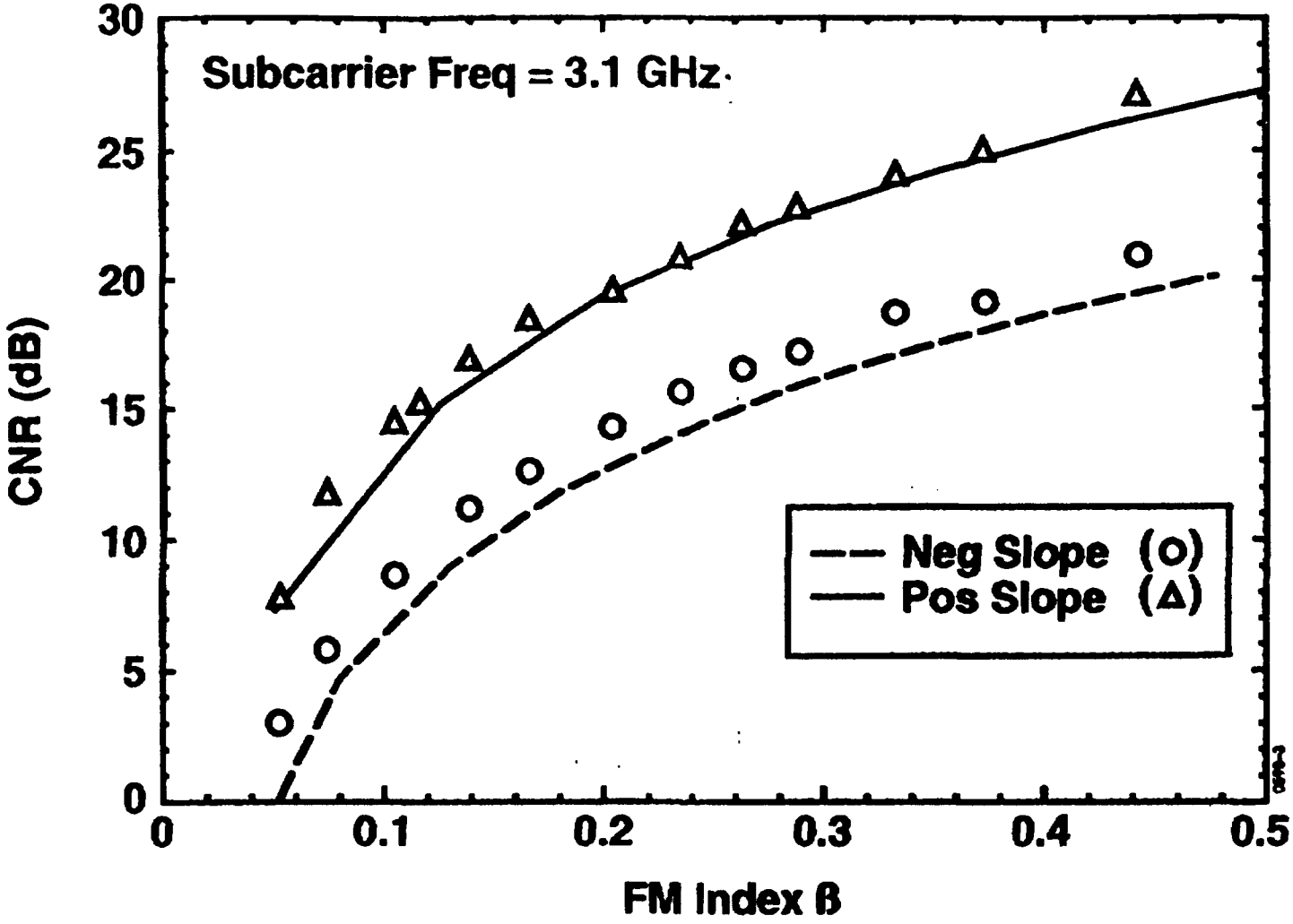
Subcarrier Freq = 3.1 GHz
CNR (dB)
FM Index ß
Neg Slope (o)
Pos Slope (Δ)
0
5
10
15
20
25
30
0
0.1
0.2
0.3
0.4
0.5

Fig. 2

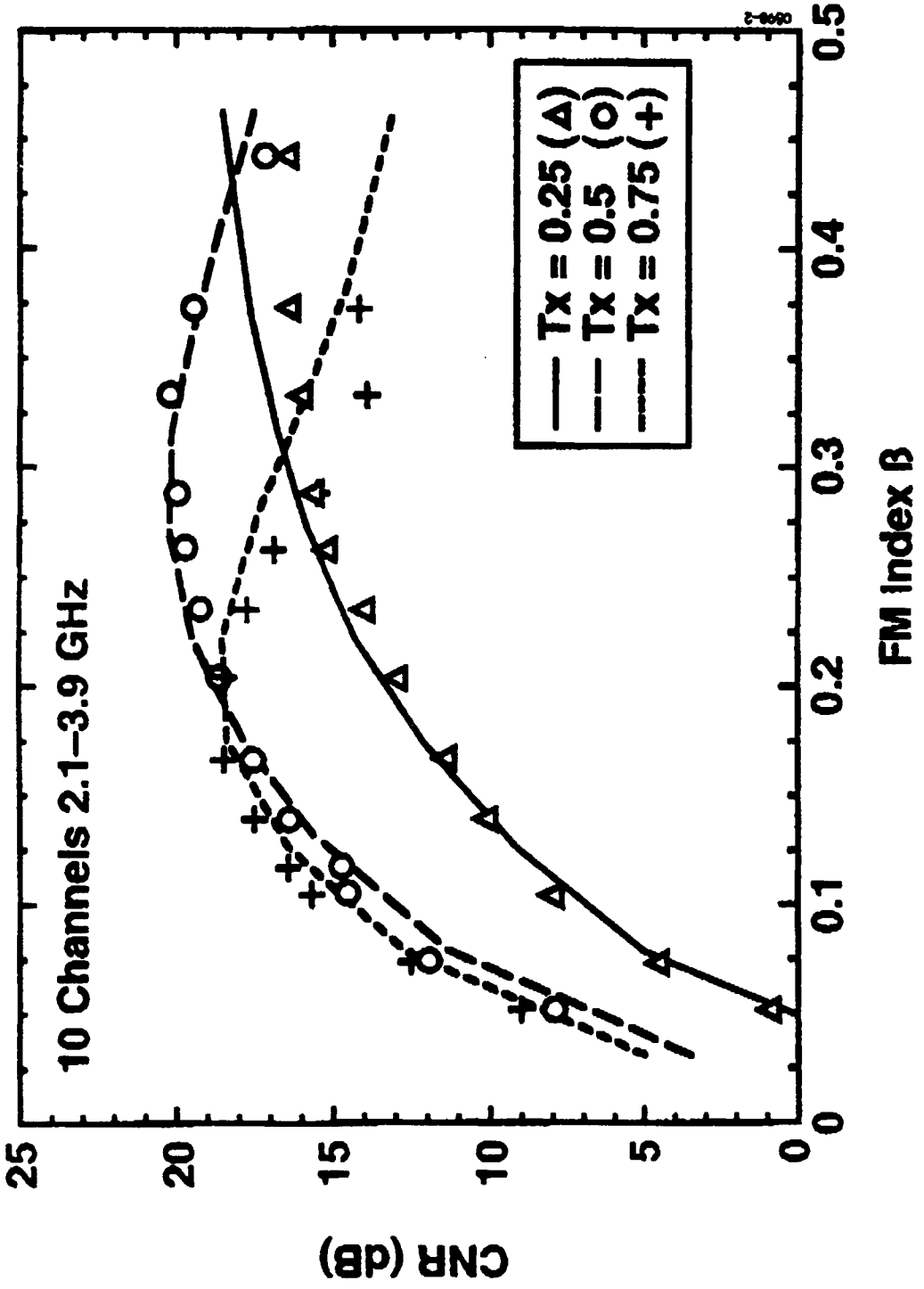

Fig. 3

Scattering from Guided Acoustic Waves in Optical Fiber and Its Influence on DPSK Optical Communication Systems

Ting-Kuang Chiang and Leonid G. Kazovsky

Stanford University
Department of Electrical Engineering
Durand Building 202
Stanford, CA 94305-4055
Tel. (415) 723-1382, Fax. (415) 723-9251
E-mail: tkchiang@leland.stanford.edu

Scattering from Guided Acoustic Waves in Optical Fiber and Its Influence on DPSK Optical Communication Systems

Ting-Kuang Chiang and Leonid G. Kazovsky

Stanford University
Department of Electrical Engineering
Durand Building 202
Stanford, CA 94305-4055
Tel. (415) 723-1382, Fax. (415) 723-9251
E-mail: tkchiang@leland.stanford.edu

Abstract

We experimentally observed optical scattering from thermally excited acoustic waves in single-mode fibers. Theoretical analysis shows that the performance of optical DPSK communication systems can be impaired by the resulting phase noise.

Scattering from Guided Acoustic Waves in Optical Fiber and Its Influence on DPSK Optical Communication Systems

Ting-Kuang Chiang and Leonid G. Kazovsky

Stanford University
Department of Electrical Engineering
Durand Building 202
Stanford, CA 94305-4055
Tel. (415) 723-1382, Fax. (415) 723-9251
E-mail: tkchiang@leland.stanford.edu

Introduction: Optical fiber is usually modeled as a linear attenuating dispersive medium. In a real fiber, thermally excited acoustic waves phase-modulate the propagating light[1]. Thermal vibrations of atoms cause fiber density fluctuations and consequent refractive index fluctuations that induce phase noise in the transmitted light. Due to acoustic waveguiding provided by the optical fiber, the acoustic waves form a series of eigenmodes with discrete natural frequencies. Therefore, optical fiber can be modeled as a phase modulator with modulating signals corresponding to discrete acoustic modes.

In this paper, we present the results of our experimental measurements of the fiber-induced optical phase fluctuations in a fiber link. The result is applied to a performance analysis of DPSK receivers considering both laser phase noise and fiber-induced phase noise.

Experiment: Fig. 1 shows the configuration of the experimental setup used to measure fiber-induced phase modulation. The lasers used in the experiment are Lightwave Electronics LW122 1310 nm single-frequency diode pumped Nd:YAG lasers. 9.9 km of Corning SMF 28 single-mode optical fiber was used in the experiment. Laser 1 operated at a frequency 8 GHz higher than laser 2.

Fig. 2 shows the heterodyned light spectrum for two cases: (a) when there is no fiber in the system, and (b) when there is 9.9 km of single-mode fiber. In both cases, the central peak is the IF component with the difference frequency of the two lasers. After propagating through 9.9 km of fiber, the signal has more than 30 phase modulated spectral components from 20 MHz to 850 MHz. For the 130.0 MHz component, the measured relative amplitude is -34 dB at a transmission distance of 9.9 km. The measured relative amplitude increases 3 dB when the fiber length is increased from 2.2 km to 9.9 km, and can be approximately expressed as $1.3 \cdot 10^{-4} \cdot \sqrt{L(km)}$. This relationship agrees well with the guided acoustic field theory[2,3].

The phase modulation index changes less than 1 dB when the optical power is varied by 10 dB. This shows that this effect is essentially linear and can be treated by linear phase modulation theory. The experimental data actually show that the relative amplitude decreases as the optical power increases. This effect is not completely understood and needs to be further investigated.

BER floor: The phase noise caused by the thermal acoustic waves in optical fiber may affect receiver performance, especially in phase-modulated systems. We used the theory of Ref. 4 to calculate the worst case BER floor. Fig. 3 shows the theoretically predicted BER floor of a 1 Gb/s DPSK receiver versus laser linewidth for several fiber lengths in presence of fiber-induced phase noise. For a laser linewidth of 10 MHz, prior analysis[5] predicts a BER floor of $2\text{x}10^{-14}$ in the absence of fiber-induced phase noise. It is evident from Fig. 3 that the fiber-induced phase noise increases the BER floor to $3\text{x}10^{-13}$, $7\text{x}10^{-12}$, and $7\text{x}10^{-11}$ for transmission distances of 100 km, 500 km, and 1000 km, respectively.

Conclusions: Thermal acoustic waves in optical fibers form discrete eigenmodes. These modes modulate the phase of the light propagating in the fiber. We investigated this effect experimentally and showed that the optical field at the fiber output has discrete spectral components ranging from 20 MHz to 850 MHz. The relative amplitude of the phase-modulated terms is proportional to the square root of the fiber length, and is almost independent of the optical intensity.

The theoretical analysis of DPSK system in the presence of fiber-induced phase noise shows that the BER floor of DPSK systems increases due to the thermal phase noise. For example, in a 1 Gb/s, 500 km system with laser linewidth of 10 MHz, the fiber-induced phase noise increases the BER floor by more than two orders of magnitude.

References

[1] R. M. Shelby, M. D. Levenson, and P. W. Bayer, "Guided acoustic-wave Brillouin scattering," *Phys. Rev. B* , vol. 31, pp. 5244-5252, 1985.

[2] R. N. Thurston, "Elastic waves in rods and clad rods," *J. Acoust. Soc. Am.*, vol. 64, pp. 1-37, 1978.

[3] E. K. Sittig and G. A. Coquin, "Visualization of plane-strain vibration modes of a long cylinder capable of producing sound radiation," *J. Acoust. Soc. Am.*, vol. 48, pp. 1150-1159, 1970.

[4] L. G. Kazovsky, "Impact of laser phase noise on optical heterodyne communication systems," *J. Opt. Commun.*, vol. 7, pp. 66-78, 1986.

[5] J. R. Barry and E. A. Lee, "Performance of coherent optical receivers," *Proc. IEEE*, vol. 78, pp. 1369-1394, 1990.

Figure Captions

Figure 1. Experimental setup for measuring scattered light spectrum resulting from thermal acoustic modulation.

Figure 2. Heterodyned spectrum of the transmitted light modulated by thermal acoustic waves. Laser 1: P_{out} = 7.7 dBm. Laser 2: P_{out} = 11.6 dBm. (a) with no fiber, (b) with 9.9 km of fiber.

Figure 3. Calculated BER floor of a 1 Gb/s DPSK heterodyne receiver.

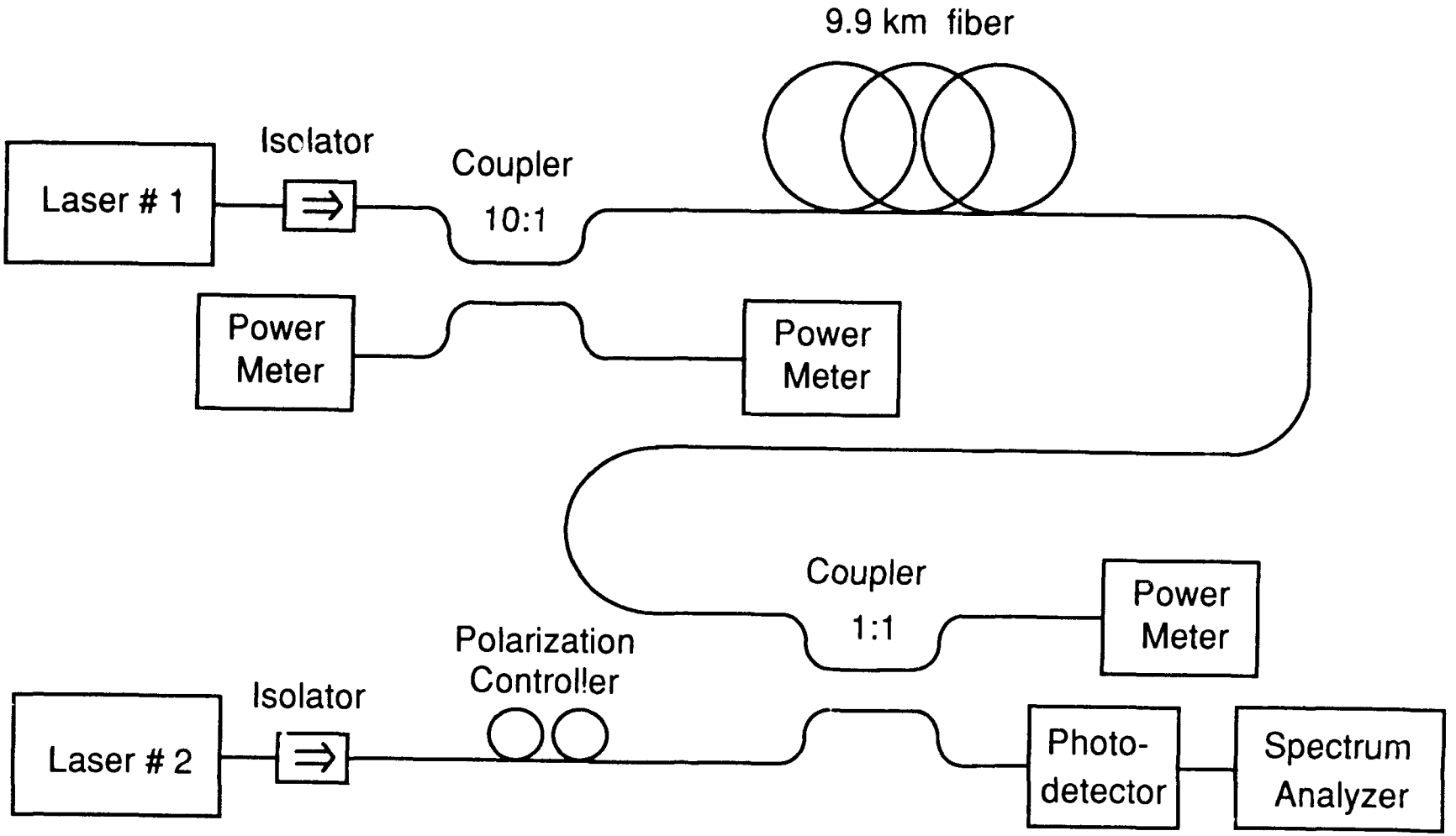

Fig. 1. Experimental setup for measuring scattered light spectrum resulting from thermal acoustic modulation..

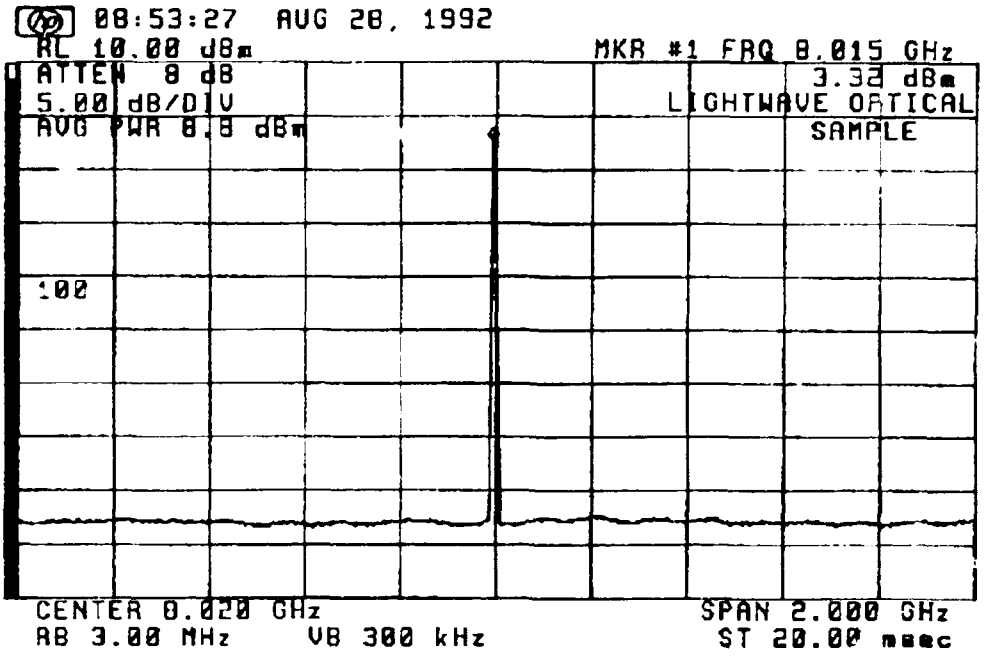

(a)

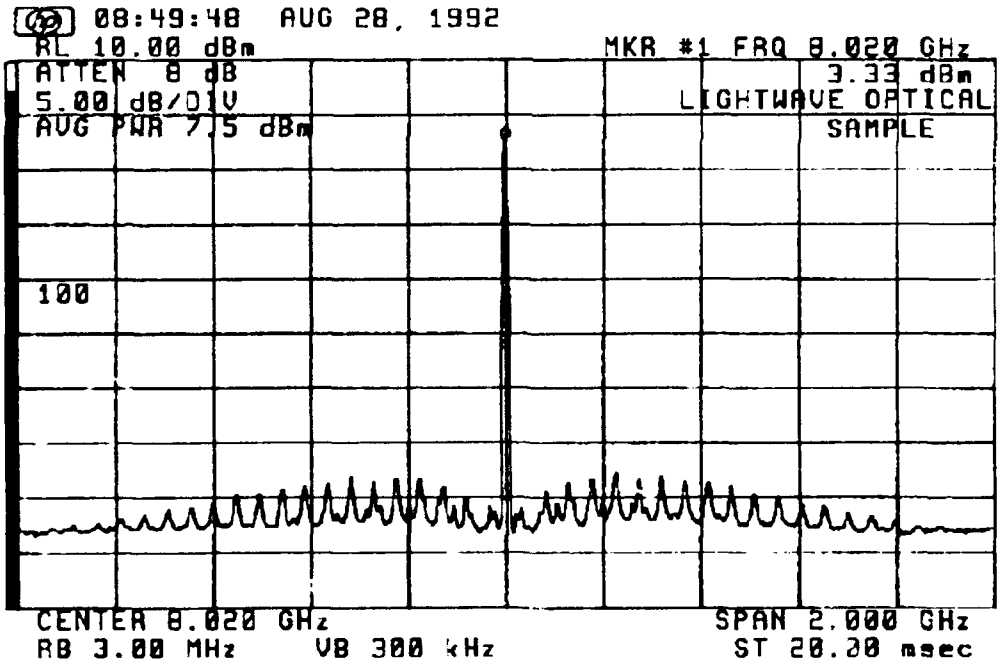

(b)

Fig. 2. Heterodyned spectrum of the transmitted light modulated by thermal acoustic waves. Laser P_{out} = 7.7 dBm. Laser 2: P_{out} = 11.5 dBm. (a) with no fiber, (b) with 9.9 km of fiber.

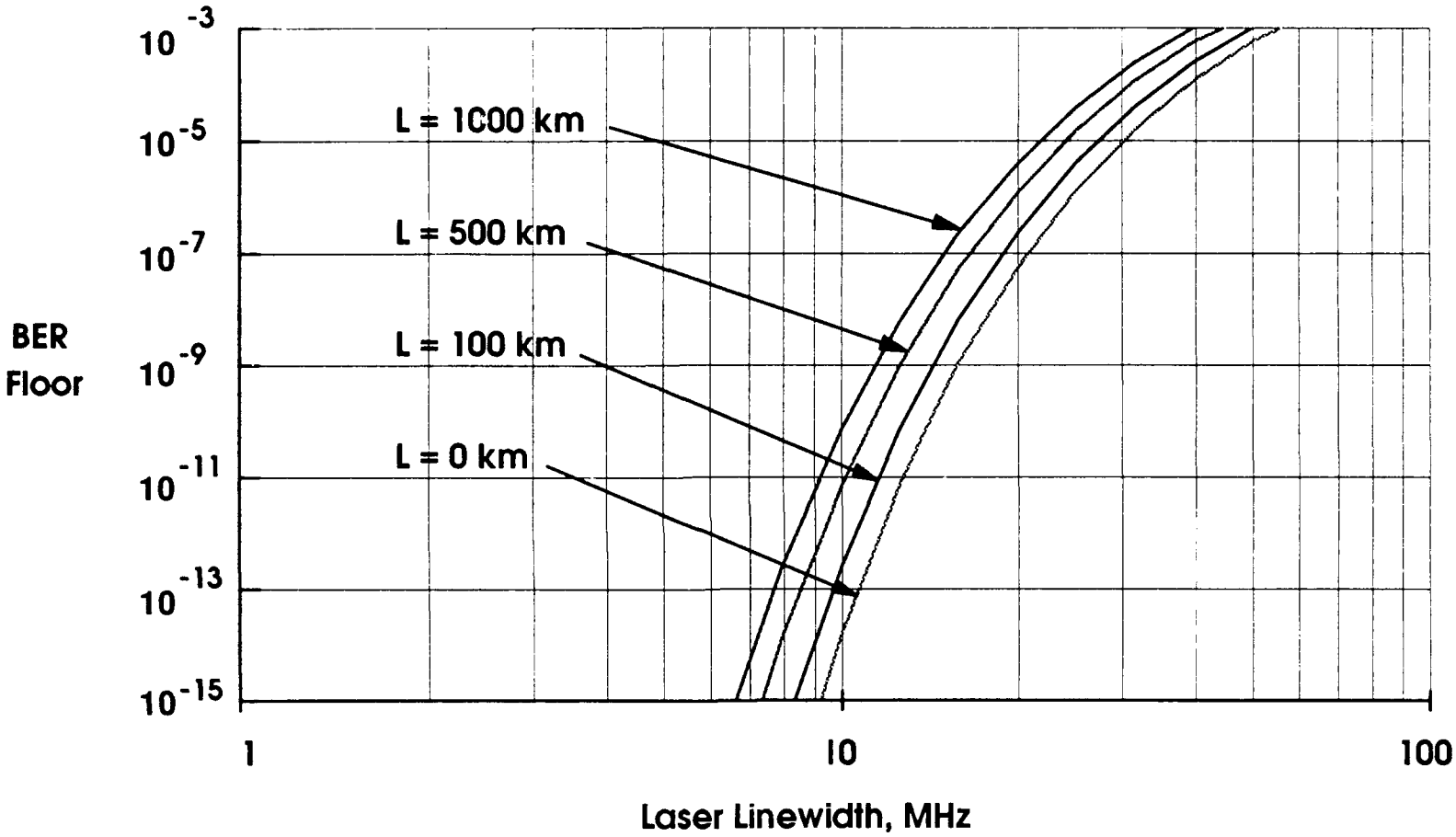

Fig. 3. Calculated BER floor of a 1 Gb/s DPSK heterodyne receiver.